LAPLACIAN EIGENSTRUCTURE OF THE EQUILATERAL TRIANGLE

Brian J. McCartin

Applied Mathematics
Kettering University

HIKARI LTD

HIKARI LTD

Hikari Ltd is a publisher of international scientific journals and books.

www.m-hikari.com

Brian J. McCartin, LAPLACIAN EIGENSTRUCTURE OF THE EQUILATERAL TRIANGLE, First published 2011.

No part of this publication may be reproduced, stored in a retrieval system, or transmitted, in any form or by any means, without the prior permission of the publisher Hikari Ltd.

ISBN 978-954-91999-6-3

Copyright © 2011 by Brian J. McCartin

Typeset using LaTeX.

Mathematics Subject Classification: 34B24, 34L05, 34M25, 35C05, 35J05, 35P05, 35P10

Keywords: Laplacian eigenvalues/eigenvectors, equilateral triangle, Dirichlet problem, Neumann problem, Robin problem, radiation boundary condition, absorbing boundary condition, impedance boundary condition, polygonal domains, trigonometric eigenfunctions, cylindrical waveguides, modal degeneracy, Eisenstein primes, Sturm-Liouville boundary value problem, non-self-adjoint boundary value problem

Published by Hikari Ltd

Dedicated to my soul-mate

Barbara Ann (Rowe) McCartin

for making Life worth living.

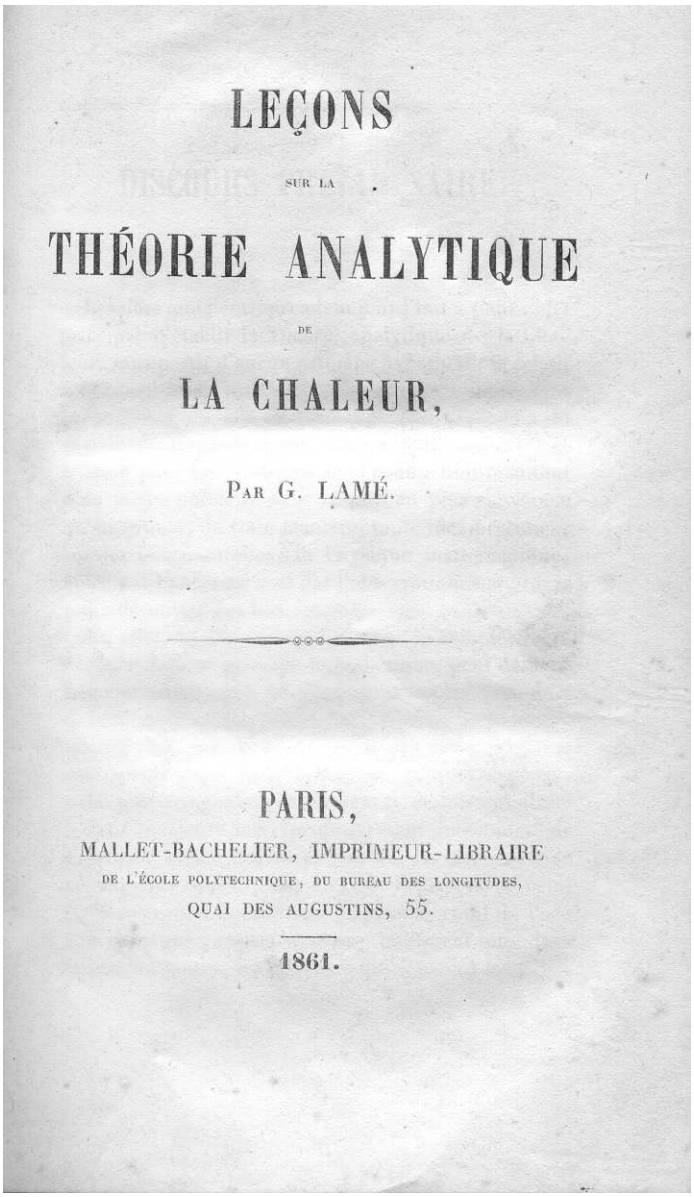

LEÇONS

SUR LA

THÉORIE ANALYTIQUE

DE

LA CHALEUR,

PAR G. LAMÉ.

PARIS,

MALLET-BACHELIER, IMPRIMEUR-LIBRAIRE

DE L'ÉCOLE POLYTECHNIQUE, DU BUREAU DES LONGITUDES,

QUAI DES AUGUSTINS, 55.

1861.

Lamé's *pièce de résistance* [40]

PREFACE

Mathematical analysis of problems of diffusion and wave propagation frequently requires knowledge of the eigenvalues and eigenfunctions of the Laplacian on two-dimensional domains under various boundary conditions. For general regions, this eigenstructure must be numerically approximated. However, for certain simple shapes the eigenstructure of the Laplacian is known analytically. (An advantage of analytical expressions for the eigenstructure over numerical approximations is that they permit parametric differentiation and, consequently, sensitivity and optimization studies.) The simplest and most widely known such domain is the rectangle. Being the cartesian product of two intervals, its eigenstructure is expressible in terms of the corresponding one-dimensional eigenstructure which in turn is comprised of sines and cosines.

Not nearly as well known, in 1833, Gabriel Lamé discovered analytical formulae for the complete eigenstructure of the Laplacian on the equilateral triangle under either Dirichlet or Neumann boundary conditions and a portion of the corresponding eigenstructure under a Robin boundary condition. Surprisingly, the associated eigenfunctions are also trigonometric. The physical context for his pioneering investigation was the propagation of heat throughout polyhedral bodies. For the better part of the last decade, the present author has sought to explicate, extend and apply these ingenious results of Lamé.

The present book narrates this mathematical journey by providing a complete and self-contained treatment of the eigenstructure of the Laplacian on an equilateral triangle. The historical context and practical significance of the problem is carefully traced. The separate cases of Dirichlet, Neumann, radiation, absorbing and impedance boundary conditions are individually and exhaustively treated with the Dirichlet and Neumann cases also extended from the continuous to the discrete Laplacian. Corresponding results for the Sturm-Liouville boundary value problem under an impedance boundary condition are reviewed and applied to the parallel plate waveguide. Polygons with trigonometric eigenfunctions receive comprehensive study. Application to modal degeneracy in equilateral triangular waveguides has also been included.

Mysteries of the Equilateral Triangle [62] surveys the mathematical properties of the equilateral triangle while *Lore & Lure of the Laplacian* [63] explores the same for the Laplacian. Consequently, Chapter 1 commences with but a brief résumé of those facets of the equilateral triangle and the Laplacian which are most germane to the present study. Chapters 2 and 3 present Lamé's analysis of the eigenstructure of the Laplacian on an equilateral triangle under Dirichlet and Neumann boundary conditions, respectively. Chapter 4 develops a complete classification of those polygonal domains possessing trigonometric eigenfunctions under these same boundary conditions while Chapter 5 applies

Lamé's analysis to the investigation of modal degeneracy in acoustic and electromagnetic waveguides of equilateral triangular cross-section.

In the remaining chapters, Lamé's analysis is extended to Robin boundary conditions. Chapter 6 considers the radiation boundary condition while Chapter 7 is devoted to the absorbing boundary condition. The next two chapters are devoted to the important practical case of the impedance boundary condition. Chapter 8 reviews the case of the one-dimensional analysis of the Sturm-Liouville boundary value problem and Chapter 9 then generalizes this analysis to the case of the two-dimensional equilateral triangle. Chapter 10 surveys some alternative approaches to the equilateral triangular eigenproblem from the literature. Finally, Appendix A presents the extension of the analysis of the eigenstructure of the equilateral triangle from the continuous to the discrete Laplacian with Dirichlet or Neumann boundary conditions.

Some moderate redundancy has been incorporated into the presentation so as to endow each chapter with a modicum of independence. Throughout the exposition, enough background material is provided so as to make this monograph accessible to a wide scientific audience. Unless otherwise attributed, the source material for the biographical vignettes sprinkled throughout the text was drawn from *Biographical Dictionary of Mathematicians* [23], *MacTutor History of Mathematics* [71] and *Wikipedia, The Free Encyclopedia* [91].

The target audience for the book consists of practicing Engineers, Scientists and Applied Mathematicians. Particular emphasis has been placed upon including sufficient prerequisites to make the book accessible to graduate students in these same fields. In point of fact, the bulk of the subject matter has been developed at a mathematical level that should be accessible to advanced undergraduates studying Applied Mathematics. The goal of the book has been not only to provide its readership with an understanding of the theory but also to give an appreciation for the context of this problem within the corpus of Applied Mathematics as well as to include sufficient applications for them to apply the results in their own work.

I owe a debt of gratitude to a succession of highly professional Interlibrary Loan Coordinators at Kettering University: Joyce Keys, Meg Wickman and Bruce Deitz. Quite frankly, without their tireless efforts in tracking down many times sketchy citations, whatever scholarly value may be attached to the present work would be substantially diminished. Also, I would like to warmly thank my Professors: Oved Shisha, Ghasi Verma and Antony Jameson. Each of them has played a significant role in my mathematical development and for that I am truly grateful. As always, my loving wife Barbara A. (Rowe) McCartin bears responsibility for the high quality of the mathematical illustrations.

Brian J. McCartin
Fellow of the Electromagnetics Academy
Editorial Board, *Applied Mathematical Sciences*

Contents

Chapter 1

Prolegomenon

It is well known that the collection of two dimensional domains for which the eigenstructure of the Laplacian is explicitly available contains rectangles and ellipses. It is not nearly so widely recognized that the equilateral triangle also belongs to this select class of regions. The eigenvalues and eigenfunctions of the Laplacian on an equilateral triangle were first presented by G. Lamé [39, 40, 41] and then further explored by F. Pockels [75] .

However, Lamé did not provide a complete derivation of his formulas but rather simply stated them and then proceeded to show that they satisfied the relevant equation and associated boundary conditions. Most subsequent authors have either simply made reference to the work of Lamé [79, p. 318] or reproduced his formulas without derivation [75], [84, pp. 393-396]. One notable exception is the work of M. Pinsky [73] where Lamé's formulas are derived using the functional analytic technique of reflection operators due to V. Arnold. Another is the more recent work of Práger [77] wherein these eigenfunctions are derived via an indirect procedure based upon prolongation/folding transformations relating the equilateral triangle and an associated rectangle. Thus, there is presently a lacuna in the applied mathematical literature as concerns a direct elementary treatment of the eigenstructure of the equilateral triangle.

perimeter (p)	$3h$
altitude (a)	$h\frac{\sqrt{3}}{2}$
area (A)	$h^2\frac{\sqrt{3}}{4}$
inradius (r)	$h\frac{\sqrt{3}}{6}$
circumradius (R)	$h\frac{\sqrt{3}}{3}$
incircle area (A_r)	$h^2\frac{\pi}{12}$
circumcircle area (A_R)	$h^2\frac{\pi}{3}$

Table 1.1: Basic Properties of the Equilateral Triangle

1.1 The Equilateral Triangle

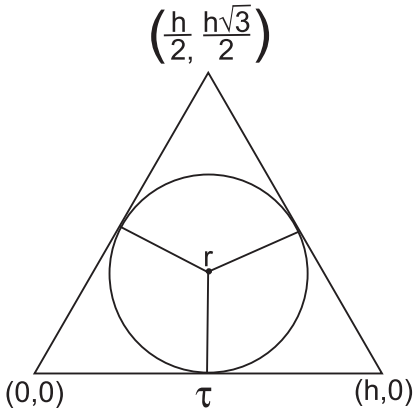

Figure 1.1: Equilateral Triangle with Incircle

With reference to Figure 1.1, an equilateral triangle of side h possesses the basic properties summarized in Table 1.1 [62, p. 29].

1.1.1 Triangular Coordinates

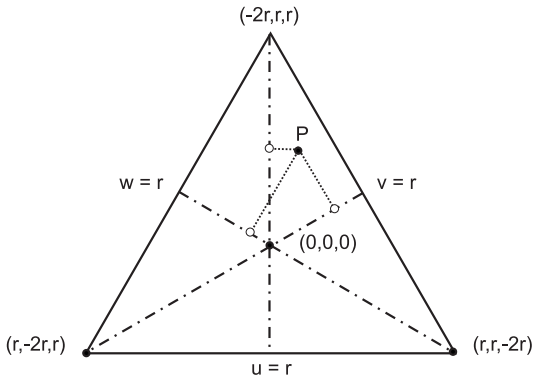

Figure 1.2: Triangular Coordinate System

Consider the equilateral triangle of side h in standard position in Cartesian coordinates (x, y) (Figure 1.1) and define Lamé's triangular coordinates (u, v, w) of a point P (Figure 1.2) by

$$\begin{aligned} u &= r - y \\ v &= \frac{\sqrt{3}}{2} \cdot (x - \frac{h}{2}) + \frac{1}{2} \cdot (y - r) \\ w &= \frac{\sqrt{3}}{2} \cdot (\frac{h}{2} - x) + \frac{1}{2} \cdot (y - r) \end{aligned} \tag{1.1}$$

where $r = h/(2\sqrt{3})$ is the inradius of the triangle. The coordinates u, v, w may be described as the distances of the triangle center to the projections of the point onto the altitudes, measured positively toward a side and negatively toward a vertex.

Note that Lamé's triangular coordinates satisfy the relation

$$u + v + w = 0. \tag{1.2}$$

Moreover, the center of the triangle has coordinates $(0, 0, 0)$ and the three sides of the triangle are given by $u = r$, $v = r$, and $w = r$, thus simplifying the application of boundary conditions. They are closely related to the barycentric coordinates (U, V, W) introduced by his contemporary A. F. Möbius in 1827 [25]:

$$\begin{aligned} U &= \frac{r-u}{3r} \\ V &= \frac{r-v}{3r} \\ W &= \frac{r-w}{3r} \end{aligned} \tag{1.3}$$

satisfying $U + V + W = 1$. This latter coordinate system was destined to become the darling of finite element practitioners in the 20th Century.

1.1.2 Symmetric-Antisymmetric Decomposition

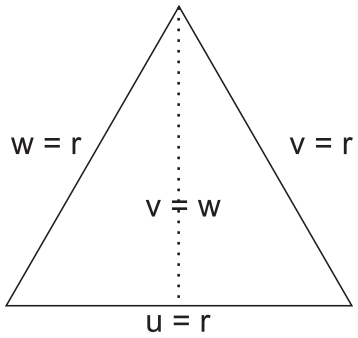

Figure 1.3: Modal Line of Symmetry/Antisymmetry

We may borrow the even-odd decomposition of a function from signal processing [30, p. 73] and decompose any function f whose domain is the equilateral triangle into parts symmetric and antisymmetric about the altitude $v = w$ (see Figure 1.3)

$$f(u, v, w) = f_s(u, v, w) + f_a(u, v, w), \tag{1.4}$$

where

$$f_s(u,v,w) = \frac{f(u,v,w) + f(u,w,v)}{2};\ f_a(u,v,w) = \frac{f(u,v,w) - f(u,w,v)}{2}, \tag{1.5}$$

henceforth to be dubbed the symmetric/antisymmetric part of f, respectively.

1.2 The Laplacian

The two-dimensional Laplacian in rectangular coordinates is given by

$$\Delta = \nabla^2 = \nabla \cdot \nabla = \frac{\partial^2}{\partial x^2} + \frac{\partial^2}{\partial y^2}. \tag{1.6}$$

This fundamental differential operator of Applied Mathematics [63] was introduced by Laplace in his 1782 study of the force of gravitational attraction exerted by spheroids and was named after him by Maxwell in his 1873 treatise on electromagnetism. The notation Δ for the Laplacian was first introduced by Robert Murphy in his 1833 book on electricity and the del or nabla notation, $\nabla = (\frac{\partial}{\partial x}, \frac{\partial}{\partial y})$, was later introduced by Hamilton in his 1853 lectures on quaternions.

Further physical insight may be gleaned from the coordinate-free representation of the Laplacian [63]:

$$\Delta\phi = \lim_{A \to 0} \frac{1}{A} \oint_{\partial D} \frac{\partial \phi}{\partial \nu}\, dl;\ A = \text{area}(D), \tag{1.7}$$

which is a direct consequence of the planar Divergence Theorem. The Laplacian of any scalar field is thereby seen to be interpretable as the limit of the net outward flux per unit enclosed area of this field through a closed contour surrounding the point of evaluation. This viewpoint is particularly fruitful when deriving discrete approximations to the Laplacian [49].

1.2.1 Eigenstructure

Separation of temporal from spatial variables [63] in either the (nondimensional) wave equation

$$\frac{\partial^2 \phi}{\partial t^2} = \Delta\phi, \tag{1.8}$$

or the (nondimensional) heat equation

$$\frac{\partial \phi}{\partial t} = \Delta\phi, \tag{1.9}$$

leads directly to the spatial Helmholtz equation

$$\Delta\psi(x,y) + k^2\psi(x,y) = 0. \tag{1.10}$$

Thus, $\psi(x,y)$ is an eigenfunction of the Laplacian corresponding to the eigenvalue $-k^2$.

For the complete specification of the eigenstructure of the Laplacian on the equilateral triangle τ, the Helmholtz equation must be supplemented by a boundary condition along $(x,y) \in \partial\tau$. This assumes the form of $\psi(x,y) = 0$ for the Dirichlet boundary condition (Chapter 2) and $\frac{\partial\psi}{\partial\nu}(x,y) = 0$ for the Neumann boundary condition (Chapter 3), where ν denotes the direction of the outward pointing normal to $\partial\tau$. The Robin boundary condition is comprised of a linear combination of the above: $\frac{\partial\psi}{\partial\nu}(x,y) + \sigma\psi(x,y) = 0$. This becomes a radiation boundary condition (Chapter 6) if $\sigma > 0$ and an absorbing boundary condition (Chapter 7) if $\sigma < 0$. If the boundary parameter σ is complex then the Robin boundary condition becomes an impedance boundary condition (Chapter 9).

1.2.2 Separation of Variables

We now introduce the orthogonal coordinates (ξ,η) given by

$$\xi = u,\ \eta = v - w. \tag{1.11}$$

The Helmholtz equation, $\Delta\psi(x,y) + k^2\psi(x,y) = 0$, thereby becomes

$$\frac{\partial^2\psi}{\partial\xi^2} + 3\frac{\partial^2\psi}{\partial\eta^2} + k^2\psi = 0. \tag{1.12}$$

Hence, if we seek a spatially separated solution of the form

$$\psi(\xi,\eta) = f(\xi)\cdot g(\eta) \tag{1.13}$$

then we immediately arrive at

$$f'' + \alpha^2 f = 0;\ g'' + \beta^2 g = 0;\ \alpha^2 + 3\beta^2 = k^2. \tag{1.14}$$

Thus, there exist spatially separated solutions of the form

$$\psi(u,v,w) = f(u)\cdot g(v-w), \tag{1.15}$$

where f and g are (possibly complex) trigonometric functions.

1.3 Gabriel Lamé

Figure 1.4: Gabriel Lamé

Of considerable interest, Gabriel Lamé (1795-1870) was the quintessential Applied Mathematician, equally comfortable in settling Fermat's Last Theorem for $n = 7$ as he was in laying the foundations of elasticity theory where two elastic constants bear his name [23, 24, 71].

He was born in Tours and, like most French mathematicians of his time, was educated at l'École Polytechnique, graduating in 1817. He continued his applied studies at l'École des Mines from which he graduated in 1820. As a student, he published papers in geometry and crystallography thus displaying at this early stage his dual interest in pure and applied topics.

Upon graduation, he moved to St. Petersburg and was appointed director of the School of Highways and Transportation. In this position, he not only taught courses in Mathematics, physics and chemistry, but also was deeply involved in the design of roads, highways and bridges. During this time, his subsequent interest in railway development was kindled.

Almost immediately upon his return to Paris in 1832, he completed his work, begun in Russia, on the equilateral triangle [39] which is central to the present work. Contemporaneously, he was offered and accepted the Chair in Physics at l'École Polytechnique. He retained this position until 1844 while simultaneously serving as Chief Engineer of Mines and also participating in the building of the first two railroads from Paris to Versailles and St.-Germain.

In 1844, he moved to Université de Paris where he eventually became Professor of Mathematical Physics until deafness forced him into retirement in

1862. He died in Paris, aged 74. During his long and productive career, he made original contributions to many areas of pure and Applied Mathematics. For example, in addition to the pragmatic studies alluded to above, he established that the number of divisions necessary in the Euclidean algorithm for finding the greatest common divisor of two integers is never greater than five times the number of decimal digits in the smaller number.

In spite of the fact that he has a Parisian street named after him and is commemorated on the Eiffel Tower, he was more revered outside of France than within. (Gauss considered him the foremost French mathematician of his generation.) French mathematicians considered him too practical and French scientists thought him too theoretical!

Chapter 2

The Dirichlet Problem

It is the express purpose of the present chapter to fill the previously alluded to gap in the literature for the case of the Dirichlet boundary condition [51]. Later chapters will present a corresponding treatment of the Neumann and Robin problems. Not only will we supply a derivation of Lamé's formulas from first principles but we will also endeavor to provide an extensive account of modal properties. Many of these properties are simply stated by Lamé and Pockels but herein receive full derivation. Other properties that are clearly identified below are new and appear here for the first time in book form.

Knowing the eigenstructure permits us to construct the Green's function, and we do so. The implications for related geometries are also explored. The primarily pedagogical and historical exposition to follow gladly trades off mathematical elegance for brute-force, yet straightforward, computation in the hope that these interesting results will find their natural place in introductory treatments of boundary value problems.

2.1 The Dirichlet Eigenproblem for the Equilateral Triangle

During his investigations into the cooling of a right prism with equilateral triangular base [40], Lamé was lead to consider the eigenvalue problem

$$\Delta T(x,y) + k^2 T(x,y) = 0,\ (x,y) \in \tau;\ T(x,y) = 0,\ (x,y) \in \partial\tau \tag{2.1}$$

where Δ is the two-dimensional Laplacian, $\frac{\partial^2}{\partial x^2} + \frac{\partial^2}{\partial y^2}$, and τ is the equilateral triangle shown in Figure 1.1. Remarkably, he was able to show that the eigenfunctions satisfying Equation (2.1) could be expressed in terms of combinations of sines and cosines, which are typically the province of rectangular geometries [44].

Lamé later encountered the same eigenproblem when considering the vibrational modes of an elastic membrane stretched over an equilateral triangle [41]. Likewise, it appears again in the vibrational analysis of a simply supported plate in the shape of an equilateral triangle [13]. The identical problem occurs also in acoustic ducts with soft walls and in the propagation of transverse magnetic (TM- or E-) modes in electromagnetic waveguides [37]. Lamé's solution of this problem actually proceeds from quite general considerations about precisely which geometries will give rise to eigenfunctions composed of sines and cosines. These matters we now take up.

2.2 Lamé's Fundamental Theorem I

Let us begin by stating that we will make some alterations to Lamé's presentation of his General Law of a Nodal Plane. First of all, rather than being concerned with three-dimensional problems, we will restrict attention to two dimensions and hence will consider instead nodal lines (i.e. lines along which an eigenfunction vanishes) and antinodal lines (along which the normal derivative vanishes). Secondly, since we are not specifically interested in heat transfer but rather in the eigenproblem, Equation (2.1), in its own right, we will replace his notions of inverse/direct calorific symmetry by the less application-specific concepts of antisymmetry/symmetry, respectively.

Motivated by his earlier work in crystallography, Lamé made the following observations the cornerstone of his work on heat transfer in right prisms.

Theorem 2.2.1 (Fundamental Theorem). *Suppose that $T(x, y)$ can be represented by the trigonometric series*

$$T(x,y) = \sum_i A_i \sin(\lambda_i x + \mu_i y + \alpha_i) + B_i \cos(\lambda_i x + \mu_i y + \beta_i) \tag{2.2}$$

with $\lambda_i^2 + \mu_i^2 = k^2$, then

1. *$T(x, y)$ is antisymmetric about any line along which it vanishes.*
2. *$T(x, y)$ is symmetric about any line along which its normal derivative, $\frac{\partial T}{\partial \nu}$, vanishes.*

Proof. 1. If T vanishes along L then we may transform, via a translation and a rotation by an angle $\pi/2 - \theta$, to an orthogonal coordinate system (x', y') where L corresponds to $x' = 0$ (see Figure 2.1). In these transformed coordinates, Equation (2.2) may be rewritten (using trigonometric identities) as

$$T(x',y') = \sum_i v_i(y') \sin(\lambda_i' x') + \sum_i w_i(y') \cos(\lambda_i' x'), \tag{2.3}$$

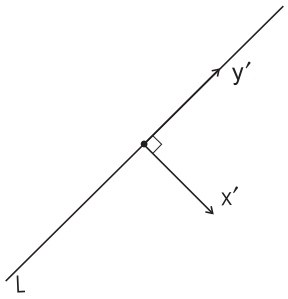

Figure 2.1: Line of Antisymmetry/Symmetry

where $\lambda_i' = \lambda_i \sin\theta - \mu_i \cos\theta$, $\mu_i' = \lambda_i \cos\theta + \mu_i \sin\theta$, $v_i(y') = C_i \cdot \cos(\mu_i' y' + \phi_i)$, $w_i(y') = C_i \cdot \sin(\mu_i' y' + \phi_i)$, for appropriate amplitudes C_i and phase angles ϕ_i. Observe that $(\lambda_i')^2 + (\mu_i')^2 = k^2$. Applying now the condition $T = 0$ along $x' = 0$ yields $\sum_i w_i(y') = 0$ which is possible only if those $w_i(y') \neq 0$ cancel in groups comprised of terms whose corresponding μ_i' all have the same absolute value. Within such a group (say $i \in I$), the λ_i' must also have the same absolute value (say λ'). Thus the corresponding terms of the second series of Equation (2.3) may be collected together as

$$\sum_{i \in I} w_i(y') \cos(\lambda_i' x') = \cos(\lambda' x') \sum_{i \in I} w_i(y') = 0. \tag{2.4}$$

This effectively eliminates the second series of Equation (2.3) leaving us with

$$T(x', y') = \sum_i v_i(y') \sin(\lambda_i' x'). \tag{2.5}$$

Antisymmetry about $x' = 0$ now follows immediately from the oddness of sine.

2. In an entirely analogous fashion, if instead we apply $\frac{\partial T}{\partial \nu} = 0$ then it is the first series of Equation (2.3) which is eliminated, leaving only

$$T(x', y') = \sum_i w_i(y') \cos(\lambda_i' x'). \tag{2.6}$$

Symmetry about $x' = 0$ now follows immediately from the evenness of cosine.

□

The Fundamental Theorem has the following immediate consequences.

Corollary 2.2.1. *With $T(x, y)$ as defined by Equation (2.2),*

1. *If $T = 0$ along the boundary of a polygon then $T = 0$ along the boundaries of the family of congruent and symmetrically placed polygons obtained by reflection about its sides.*

2. *If $\frac{\partial T}{\partial \nu} = 0$ along the boundary of a polygon then $\frac{\partial T}{\partial \nu} = 0$ along the boundaries of the likewise defined family of polygons.*

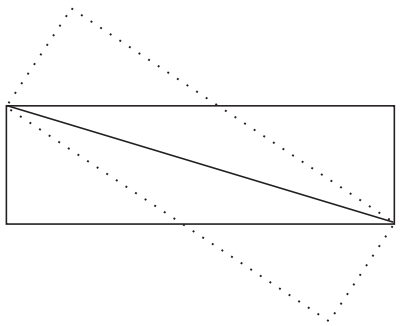

Figure 2.2: Rectangular Reflection

This corollary has far reaching implications for the determination of those domains which possess eigenfunctions expressible in terms of sines and cosines (henceforth referred to as "trigonometric eigenfunctions"). For example, Figure 2.2 illustrates that the diagonal of a rectangle cannot ordinarily be a nodal line, nor for that matter an antinodal line, since the rectangle has a complete orthonormal system of trigonometric eigenfunctions yet does not possess the requisite symmetry unless it is either a square or has aspect ratio $\sqrt{3}$ (see Figures 2.8-9). Here and below, solid lines denote lines of antisymmetry while dashed lines denote lines of symmetry. Furthermore, as illustrated in Figure 2.3, an isosceles right triangle may be repeatedly anti-reflected about its edges to produce the antisymmetry (denoted by $\pm$) required by the Fundamental Theorem and in fact possesses trigonometric eigenfunctions obtained from the restriction of those of a square with a nodal line along a fixed diagonal.

Next consider the equilateral triangular lattice of Figure 2.4 together with its supporting antisymmetric structure. It suggests that the equilateral triangle might possess trigonometric eigenfunctions since the Fundamental Theorem supplies necessary but not sufficient conditions. By devices unknown, Lamé was in fact able to construct such a family of eigenfunctions. We next present an original derivation of this eigenstructure by employing his natural triangular coordinate system (Section 1.1.1). We will return to consider other regions with and without trigonometric eigenfunctions in a later section.

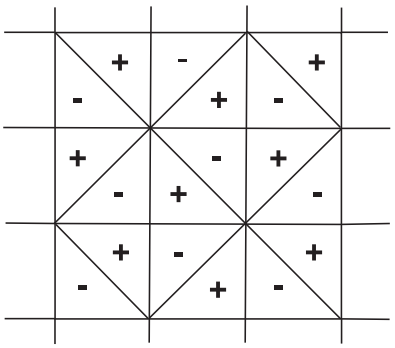

Figure 2.3: Antisymmetry of Isosceles Right Triangle

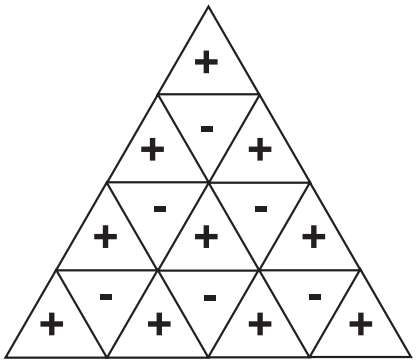

Figure 2.4: Antisymmetry of Equilateral Triangular Lattice

2.3 Construction of Modes

Before proceeding any further, we will decompose the sought after eigenfunction into parts symmetric and antisymmetric about the altitude $v = w$ (see Figure 1.3)

$$T(u, v, w) = T_s(u, v, w) + T_a(u, v, w), \tag{2.7}$$

where

$$T_s(u, v, w) = \frac{T(u, v, w) + T(u, w, v)}{2};\ T_a(u, v, w) = \frac{T(u, v, w) - T(u, w, v)}{2}, \tag{2.8}$$

henceforth to be dubbed a symmetric/antisymmetric mode, respectively. We next take up the determination of T_s and T_a separately.

2.3.1 Symmetric Modes

In light of the fact that T_s must vanish when $u = -2r$ and $u = r$ while

being even as a function of $v - w$, we seek a solution of the form

$$\sin[\frac{\pi l}{3r}(u + 2r)] \cdot \cos[\beta_1(v - w)], \tag{2.9}$$

where l is an integer and $[\frac{\pi l}{3r}]^2+3\beta_1^2 = k^2$. We will show that, by itself, this form cannot satisfy the Dirichlet boundary condition along $v = r$. Observe that if it could then, by symmetry, it would automatically satisfy the corresponding boundary condition along $w = r$.

Moreover, we will show that the sum of two such terms also does not suffice for the satisfaction of the remaining boundary conditions. However, the sum of three appropriately chosen terms of the form Equation (2.9) does indeed satisfy said boundary conditions and thus constitutes the sought after symmetric mode. In the course of this demonstration, the expression for the eigenvalues k^2 will emerge.

Along $v = r$, we have $v-w = u+2r$ where we have invoked the fundamental relation of triangular coordinates given by Equation (1.2). Insertion into Equation (2.9) immediately produces

$$\sin[\frac{\pi l}{3r}(u + 2r)] \cdot \cos[\beta_1(u + 2r)], \tag{2.10}$$

which cannot be identically equal to zero for $-2r \leq u \leq r$. Thus, one such term does not suffice.

Hence, let us try instead a sum of the form

$$\sin[\frac{\pi l}{3r}(u + 2r)] \cdot \cos[\beta_1(v - w)] + \sin[\frac{\pi m}{3r}(u + 2r)] \cdot \cos[\beta_2(v - w)], \tag{2.11}$$

with $[\frac{\pi l}{3r}]^2 + 3\beta_1^2 = [\frac{\pi m}{3r}]^2 + 3\beta_2^2 = k^2$. Along $v = r$, this becomes

$$\sin[\frac{\pi l}{3r}(u + 2r)] \cdot \cos[\beta_1(u + 2r)] + \sin[\frac{\pi m}{3r}(u + 2r)] \cdot \cos[\beta_2(u + 2r)], \tag{2.12}$$

which, by invoking trigonometric identities, may be recast as

$$\begin{aligned}\frac{1}{2}\{ \quad & \sin[(\tfrac{\pi l}{3r} + \beta_1)(u + 2r)] + \sin[(\tfrac{\pi l}{3r} - \beta_1)(u + 2r)] \\ & + \sin[(\tfrac{\pi m}{3r} + \beta_2)(u + 2r)] + \sin[(\tfrac{\pi m}{3r} - \beta_2)(u + 2r)] \quad \}.\end{aligned} \tag{2.13}$$

In order for this to be identically zero for $-2r \leq u \leq r$, we must have either

$$\frac{\pi l}{3r} + \beta_1 = -\frac{\pi m}{3r} - \beta_2;\ \frac{\pi l}{3r} - \beta_1 = -\frac{\pi m}{3r} + \beta_2, \tag{2.14}$$

or

$$\frac{\pi l}{3r} + \beta_1 = -\frac{\pi m}{3r} + \beta_2;\ \frac{\pi l}{3r} - \beta_1 = -\frac{\pi m}{3r} - \beta_2. \tag{2.15}$$

In either event, we have $l = -m$ and $\beta_1 = -\beta_2$ which implies that Equation (2.11) vanishes everywhere and hence is not a valid eigenfunction. Thus, two such terms do not suffice.

Undaunted, we persevere to consider a sum of the form

$$\begin{aligned} T_s &= \sin[\frac{\pi l}{3r}(u+2r)] \cdot \cos[\beta_1(v-w)] \\ &+ \sin[\frac{\pi m}{3r}(u+2r)] \cdot \cos[\beta_2(v-w)] \\ &+ \sin[\frac{\pi n}{3r}(u+2r)] \cdot \cos[\beta_3(v-w)], \end{aligned} \tag{2.16}$$

with

$$[\frac{\pi l}{3r}]^2 + 3\beta_1^2 = [\frac{\pi m}{3r}]^2 + 3\beta_2^2 = [\frac{\pi n}{3r}]^2 + 3\beta_3^2 = k^2. \tag{2.17}$$

Along $v = r$, this becomes

$$\begin{aligned} \sin[\frac{\pi l}{3r}(u+2r)] \cdot \cos[\beta_1(u+2r)] \quad &+ \sin[\tfrac{\pi m}{3r}(u+2r)] \cdot \cos[\beta_2(u+2r)] \\ &+ \sin[\tfrac{\pi n}{3r}(u+2r)] \cdot \cos[\beta_3(u+2r)], \end{aligned} \tag{2.18}$$

which, by invoking trigonometric identities, may be recast as

$$\begin{aligned} \frac{1}{2}\{ \quad & \sin[(\tfrac{\pi l}{3r} + \beta_1)(u+2r)] + \sin[(\tfrac{\pi l}{3r} - \beta_1)(u+2r)] \\ & + \sin[(\tfrac{\pi m}{3r} + \beta_2)(u+2r)] + \sin[(\tfrac{\pi m}{3r} - \beta_2)(u+2r)] \\ & + \sin[(\tfrac{\pi n}{3r} + \beta_3)(u+2r)] + \sin[(\tfrac{\pi n}{3r} - \beta_3)(u+2r)] \quad \}. \end{aligned} \tag{2.19}$$

There are now eight possible ways that cancellation may occur that all lead to essentially the same conclusion. Hence, we pursue in detail only

$$\frac{\pi l}{3r} + \beta_1 = -\frac{\pi n}{3r} + \beta_3; \ \frac{\pi l}{3r} - \beta_1 = -\frac{\pi m}{3r} - \beta_2; \ \frac{\pi m}{3r} - \beta_2 = -\frac{\pi n}{3r} - \beta_3. \tag{2.20}$$

When added together, these three equations yield the important relation

$$l + m + n = 0. \tag{2.21}$$

With this consistency condition satisfied, we may add the first and last of Equations (2.20) to obtain

$$\beta_1 - \beta_2 = \frac{\pi}{3r}(l+m), \tag{2.22}$$

which, when combined with the identity

$$3(\beta_1 - \beta_2)(\beta_1 + \beta_2) = (\frac{\pi}{3r})^2(m-l)(m+l) \tag{2.23}$$

obtained by rearranging the first of Equations (2.17), yields

$$\beta_1 + \beta_2 = \frac{\pi}{9r}(m - l) \tag{2.24}$$

and, finally,

$$\beta_1 = \frac{\pi(m-n)}{9r};\ \beta_2 = \frac{\pi(n-l)}{9r};\ \beta_3 = \frac{\pi(l-m)}{9r}. \tag{2.25}$$

The eigenvalue may now be calculated as

$$k^2 = \frac{2}{27}(\frac{\pi}{r})^2[l^2 + m^2 + n^2] = \frac{4}{27}(\frac{\pi}{r})^2[m^2 + mn + n^2], \tag{2.26}$$

with the corresponding symmetric mode given by

$$\begin{aligned} T_s^{m,n} &= \sin[\frac{\pi l}{3r}(u+2r)] \cdot \cos[\frac{\pi(m-n)}{9r}(v-w)] \\ &+ \sin[\frac{\pi m}{3r}(u+2r)] \cdot \cos[\frac{\pi(n-l)}{9r}(v-w)] \\ &+ \sin[\frac{\pi n}{3r}(u+2r)] \cdot \cos[\frac{\pi(l-m)}{9r}(v-w)], \end{aligned} \tag{2.27}$$

which will vanish identically if and only if any one of $l,\ m,\ n$ is equal to zero.

2.3.2 Antisymmetric Modes

A parallel development is possible for the determination of an antisymmetric mode. In light of the oddness of T_a as a function of $v - w$, we commence with an Ansatz of the form

$$\begin{aligned} T_a &= \sin[\frac{\pi l}{3r}(u+2r)] \cdot \sin[\beta_1(v-w)] \\ &+ \sin[\frac{\pi m}{3r}(u+2r)] \cdot \sin[\beta_2(v-w)] \\ &+ \sin[\frac{\pi n}{3r}(u+2r)] \cdot \sin[\beta_3(v-w)]. \end{aligned} \tag{2.28}$$

As for the symmetric mode, one can establish that all three terms are in fact necessary for the satisfaction of the Dirichlet boundary conditions. Both the symmetric and antisymmetric modes were discovered by Lamé [39] with the antisymmetric modes being rediscovered by Lee and Crandall [42].

Once again we are lead to the conditions $l + m + n = 0$, $k^2 = \frac{2}{27}(\frac{\pi}{r})^2[l^2 + m^2 + n^2] = \frac{4}{27}(\frac{\pi}{r})^2[m^2 + mn + n^2]$, and $\beta_1 = \frac{\pi(m-n)}{9r},\ \beta_2 = \frac{\pi(n-l)}{9r},\ \beta_3 = \frac{\pi(l-m)}{9r}$.

Therefore, we arrive at the antisymmetric mode

$$\begin{aligned} T_a^{m,n} &= \sin[\frac{\pi l}{3r}(u+2r)]\cdot\sin[\frac{\pi(m-n)}{9r}(v-w)] \\ &+ \sin[\frac{\pi m}{3r}(u+2r)]\cdot\sin[\frac{\pi(n-l)}{9r}(v-w)] \\ &+ \sin[\frac{\pi n}{3r}(u+2r)]\cdot\sin[\frac{\pi(l-m)}{9r}(v-w)], \end{aligned} \tag{2.29}$$

which may be identically zero.

2.4 Modal Properties

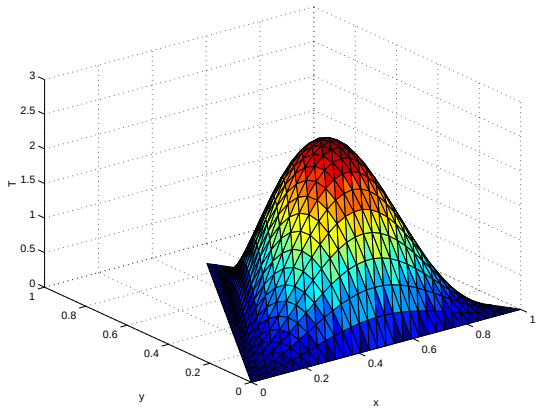

Figure 2.5: Fundamental Mode

In what follows, it will be convenient to have the following alternative representations

$$\begin{aligned} T_s^{m,n} = \frac{1}{2} \quad \{ \quad & \sin[\frac{2\pi}{9r}(lu+mv+nw+3lr)] + \sin[\frac{2\pi}{9r}(nu+mv+lw+3nr)] \\ + \quad & \sin[\frac{2\pi}{9r}(mu+nv+lw+3mr)] + \sin[\frac{2\pi}{9r}(mu+lv+nw+3mr)] \\ + \quad & \sin[\frac{2\pi}{9r}(nu+lv+mw+3nr)] + \sin[\frac{2\pi}{9r}(lu+nv+mw+3lr)]\}; \end{aligned} \tag{2.30}$$

$$\begin{aligned} T_a^{m,n} = \frac{1}{2} \quad \{ \quad & \cos[\frac{2\pi}{9r}(lu+mv+nw+3lr)] - \cos[\frac{2\pi}{9r}(nu+mv+lw+3nr)] \\ + \quad & \cos[\frac{2\pi}{9r}(mu+nv+lw+3mr)] - \cos[\frac{2\pi}{9r}(mu+lv+nw+3mr)] \\ + \quad & \cos[\frac{2\pi}{9r}(nu+lv+mw+3nr)] - \cos[\frac{2\pi}{9r}(lu+nv+mw+3lr)]\}, \end{aligned} \tag{2.31}$$

obtained from Equation (2.27) and Equation (2.29), respectively, by the application of appropriate trigonometric identities.

It is clear from these formulas that both $T_s^{m,n}$ and $T_a^{m,n}$ are invariant under a cyclic permutation of (l, m, n), while $T_s^{n,m} = T_s^{m,n}$ and $T_a^{n,m} = -T_a^{m,n}$ (which are essentially the same since modes are only determined up to a nonzero constant factor). Thus, we need only consider $n \geq m$. Moreover, since $T_{s,a}^{m,n}$, $T_{s,a}^{-n,m+n}$, $T_{s,a}^{-m-n,m}$, $T_{s,a}^{-m,m+n}$, $T_{s,a}^{-m-n,n}$, and $T_{s,a}^{-n,-m}$ all produce equivalent modes, we may also neglect negative m and n. Furthermore, if either m or n is equal to zero then, in both Equations (2.27) and (2.29), one of the terms vanishes while the other two cancel, so that both $T_s^{m,n}$ and $T_a^{m,n}$ vanish identically. Hence, we need only consider the collection $\{T_s^{m,n};\ T_a^{m,n},\ n \geq m > 0\}$.

We may pare this collection further through the following observation due to Lamé [40].

Theorem 2.4.1. *1. $T_s^{m,n}$ vanishes identically if and only if at least one of $l,\ m,\ n$ is equal to zero.*

2. $T_a^{m,n}$ vanishes identically if and only if either at least one of $l,\ m,\ n$ is equal to zero or if two of them are equal.

Proof. 1. We have already noted that $T_s^{m,n}$ vanishes identically if at least one of $l,\ m,\ n$ is equal to zero. But, note further that a symmetric mode is identically zero iff it vanishes along the line of symmetry $v = w$, since the only function both symmetric and antisymmetric is the zero function. Along $v = w$,

$$T_s^{m,n} = -\sin[\frac{\pi(m+n)}{3r}(u+2r)] + \sin[\frac{\pi m}{3r}(u+2r)] + \sin[\frac{\pi n}{3r}(u+2r)], \tag{2.32}$$

which may be trigonometrically recast as

$$\begin{aligned} T_s^{m,n} = \quad & 2\sin[\tfrac{\pi(m+n)}{6r}(u+2r)] \cdot \\ & \{\cos[\tfrac{\pi(m-n)}{6r}(u+2r)] - \cos[\tfrac{\pi(m+n)}{6r}(u+2r)]\}. \end{aligned} \tag{2.33}$$

The first factor equals zero iff $m = -n$ (i.e. $l = 0$) and the second factor vanishes iff $m = 0$ or $n = 0$.

2. We have already noted that $T_a^{m,n}$ vanishes identically if at least one of $l,\ m,\ n$ is equal to zero. But, note further that an antisymmetric mode is identically zero iff its normal derivative vanishes along the line of symmetry $v = w$, since the only function both antisymmetric and symmetric is the zero function. Along $v = w$,

$$\begin{aligned} \frac{\partial T_a^{m,n}}{\partial(v-w)} &= \frac{\pi(m-n)}{9r}\sin[\frac{\pi l}{3r}(u+2r)] + \frac{\pi(n-l)}{9r}\sin[\frac{\pi m}{3r}(u+2r)] \\ &+ \frac{\pi(l-m)}{9r}\sin[\frac{\pi n}{3r}(u+2r)], \end{aligned} \tag{2.34}$$

which may be trigonometrically recast as

$$\begin{aligned}\frac{9r}{\pi}\cdot\frac{\partial T_a^{m,n}}{\partial(v-w)} &= (n-m)\cdot\sin\left[\frac{\pi(m+n)}{3r}(u+2r)\right] \\ &+ (m+n)\cdot\left\{\sin\left[\frac{\pi m}{3r}(u+2r)\right]-\sin\left[\frac{\pi n}{3r}(u+2r)\right]\right\} \\ &+ n\cdot\sin\left[\frac{\pi m}{3r}(u+2r)\right]-m\cdot\sin\left[\frac{\pi n}{3r}(u+2r)\right].\end{aligned} \tag{2.35}$$

This equals zero iff $m=0$ or $n=0$ or $m=-n$ (i.e. $l=0$) or $m=n$ or $m=-2n$ (i.e. $l=n$) or $n=-2m$ (i.e. $l=m$).

□

Hence, our system of eigenfunctions is $\{T_s^{m,n}\ (n\geq m);\ T_a^{m,n}\ (n>m)\}$. Figure 2.5 shows the $(1,1)$ (fundamental) mode whereas the symmetric and antisymmetric $(1,2)$ modes are displayed in Figures 2.6 and 2.7, respectively. We next show that this is a complete orthonormal set of eigenfunctions and then go on to explore some features of these modes.

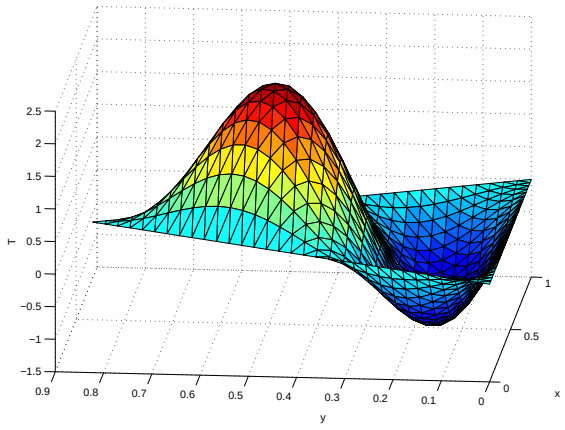

Figure 2.6: (1,2) Symmetric Mode

2.4.1 Orthonormality

By Rellich's Theorem [44], eigenfunctions corresponding to distinct eigenvalues are guaranteed to be orthogonal. However, as we shall eventually discover, the multiplicity of the eigenvalues given by Equation (2.26) is quite a complicated matter. Thus, direct integrations employing Equations (2.30) and (2.31) confirm the orthogonality of our collection of eigenfunctions $\{T_s^{m,n}\ (n\geq m);\ T_a^{m,n}\ (n>m)\}$.

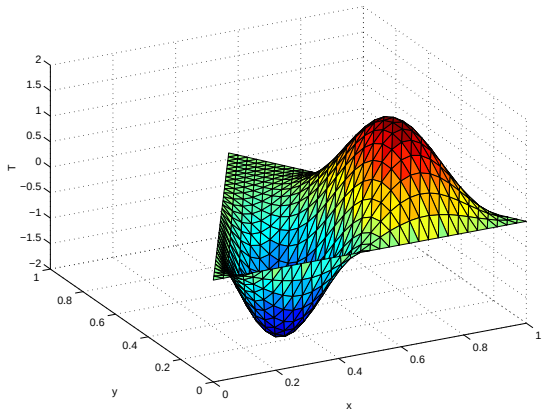

Figure 2.7: (1,2) Antisymmetric Mode

Furthermore, they may be normalized using

$$||T_s^{m,n}||^2 = \frac{9r^2\sqrt{3}}{4} = ||T_a^{m,n}||^2 \ (m \neq n) \tag{2.36}$$

and

$$||T_s^{m,m}||^2 = \frac{9r^2\sqrt{3}}{2} \tag{2.37}$$

by employing the inner product $\langle f, g\rangle = \int\int_\tau fg \ dA$.

2.4.2 Completeness

It is not *a priori* certain that the collection of eigenfunctions $\{T_s^{m,n},\ T_a^{m,n}\}$ constructed above is complete. For domains which are the Cartesian product of intervals in an orthogonal coordinate system, such as rectangles and annuli, completeness of the eigenfunctions formed from products of one-dimensional counterparts has been established [88]. Since the equilateral triangle is not such a domain, we must employ other devices in order to establish completeness.

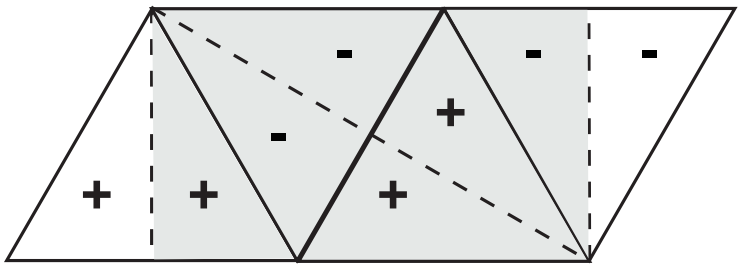

Figure 2.8: Triangle-to-Rectangle Transformation (Symmetric Mode)

M. Pinsky [74] has established completeness of the eigenfunctions under Dirichlet boundary conditions by employing the method of reflections from the spectral theory of the Laplacian invariant with respect to symmetries which in turn is based upon group theoretical arguments. In keeping with the intent of the present work to employ the simplest mathematical tools, we follow the lead of Práger [77] and appeal to the well-known completeness of the corresponding eigenfunctions of the rectangle.

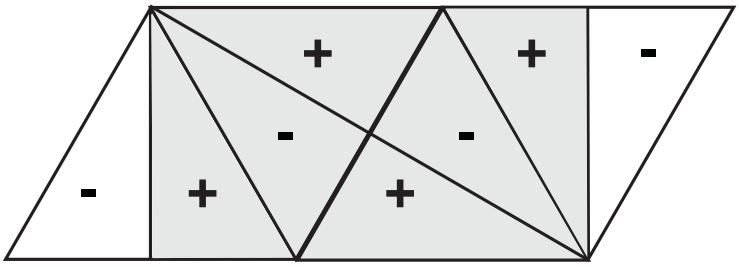

Figure 2.9: Triangle-to-Rectangle Transformation (Antisymmetric Mode)

For this purpose, we introduce the triangle-to-rectangle (TTR) transformation pictorialized in Figure 2.8 for symmetric modes and in Figure 2.9 for antisymmetric modes. There, a solid line represents a Dirichlet condition ($T = 0$) and a dashed line a Neumann condition ($\frac{\partial T}{\partial \nu} = 0$). Restricting attention to the right half of the equilateral triangle, this coincides with the prolongation transformation of Práger [77].

Commencing with the equilateral triangle in the southwest corner of each diagram, we construct the remainder of each figure by performing three antisymmetric reflections across triangle edges as specified by the Fundamental Theorem. In both cases, this leaves us with a (shaded) rectangle of dimensions $\frac{3h}{2} \times \frac{\sqrt{3}h}{2}$.

For the symmetric mode (Figure 2.8), this rectangle has Dirichlet boundary conditions along the top and bottom and Neumann boundary conditions on the sides, while, for the antisymmetric mode (Figure 2.9), there are strictly Dirichlet boundary conditions. In both cases, the corresponding eigenfunctions of the rectangle are known to be complete. By our construction procedure for the modes of the equilateral triangle, they are seen to be precisely the restriction of the corresponding modes of the associated rectangle possessing the indicated pattern of nodal and antinodal lines.

For example, in order to construct a mode of the rectangle $[\sqrt{3}r, 4\sqrt{3}r] \times [0, 3r]$ of Figure 2.9 with the displayed nodal lines, we may confine ourselves to making the mode vanish along the indicated diagonal $y = 4r - x/\sqrt{3}$ since the remaining nodal lines would then follow immediately from the Fundamental Theorem. We do this by suitably combining rectangular modes of the form

$\sin[\mu\frac{\pi}{3r}(3r-y)]\sin[\nu\frac{2\pi}{3\sqrt{3}r}(x-3r)]$, where μ and ν are positive integers, which are known to comprise a complete orthonormal system for this rectangle.

Although this process is laborious, it is identical to that outlined in Sections 2.3.1 and 2.3.2 for the construction of T_s and T_a. The end result is that these rectangular modes must be combined in triplets satisfying $\mu_1+\mu_2+\mu_3=0$, $\nu_1=\mu_2-\mu_3$, $\nu_2=\mu_3-\mu_1$, $\nu_3=\mu_1-\mu_2$. Hence, any such mode of the rectangle will be given by a linear combination of the modes $T_a^{m,n}$ of Equation (2.29).

Similar considerations applied to the rectangle of Figure 2.8, whose modes are $\sin[\mu\frac{\pi}{3r}(3r-y)]\cos[\nu\frac{2\pi}{3\sqrt{3}r}(x-3r)]$, yield the one-to-one correspondence between $T_s^{m,n}$ of Equation (2.27) and the modes of this rectangle which are symmetric about the indicated diagonal.

Thus, if the equilateral triangle were to possess either a symmetric or an antisymmetric mode not expressible as a linear combination of those we have found above then the same would be true for its extension to the associated rectangle by the TTR transformation. This contradiction establishes that our collection of equilateral triangular modes is indeed complete.

2.4.3 Nodal Lines

As evidenced by Figure 2.5, the first eigenfunction (fundamental mode) of an eigenvalue problem can have no nodal lines in the interior of the domain and thus must be of the same sign everywhere [11, p. 451]. Hence, every other eigenfunction orthogonal to it must have nodal lines. We next consider some properties related to these nodal lines. (See [90] for a more detailed study of the nodal lines by means of Chladni figures.)

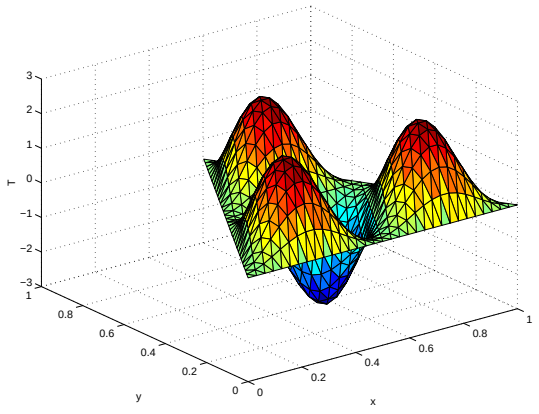

Figure 2.10: (2,2) Mode

We commence by reconsidering the case $m=n$. Recall that we have already determined that $T_a^{m,m}\equiv 0$. Furthermore, in this case, we may combine the

terms of Equation (2.30) to yield

$$T_s^{m,m} = \sin\left[\frac{2\pi m}{3r}(r-u)\right] + \sin\left[\frac{2\pi m}{3r}(r-v)\right] + \sin\left[\frac{2\pi m}{3r}(r-w)\right], \qquad (2.38)$$

which clearly illustrates that any permutation of (u, v, w) leaves $T_s^{m,m}$ invariant. This is manifested geometrically in the invariance of $T_s^{m,m}$ under a 120° rotation about the triangle center (see Figure 2.10). This invariance will henceforth be termed rotational symmetry.

There is in fact an inherent structure to the nodal lines when $m = n$ first noted by Lamé [41]. We see this by rewriting Equation (2.38) as

$$T_s^{m,m} = (-1)^{m+1} \cdot 4 \cdot \sin\left[\frac{\pi m}{3r}(r-u)\right] \cdot \sin\left[\frac{\pi m}{3r}(r-v)\right] \cdot \sin\left[\frac{\pi m}{3r}(r-w)\right]. \quad (2.39)$$

Thus, a nodal line ($T_s^{m,m} = 0$) occurs at

$$u = r - \frac{k}{m} \cdot 3r; \;\; v = r - \frac{k}{m} \cdot 3r; \;\; w = r - \frac{k}{m} \cdot 3r \;\; (k = 0, \ldots, m). \qquad (2.40)$$

That is, there is a network of $m - 1$ equidistant nodal lines parallel to each side of the triangle which subdivides it into m^2 congruent equilateral triangles, each supporting a portion of the mode similar to the fundamental, which may be further partitioned into groups of size $m(m+1)/2$ and $m(m-1)/2$, the members of each group being "in-phase".

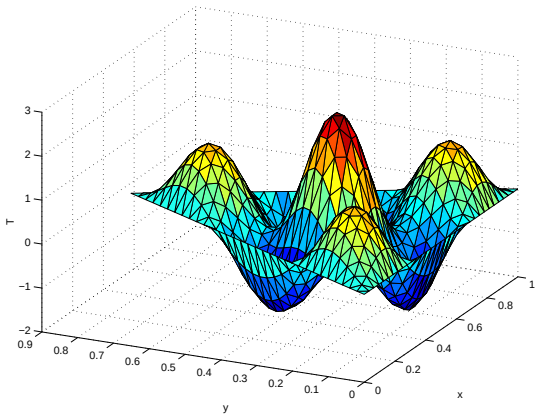

Figure 2.11: (1,4) Symmetric Mode

Surprisingly, consideration of the case $m = n$ has a direct bearing on $T_s^{m,n}$ with $m \neq n$. Specifically, we offer the following new result.

Theorem 2.4.2. *The volume under $T_s^{m,n}$ is equal to zero if and only if $m \neq n$.*

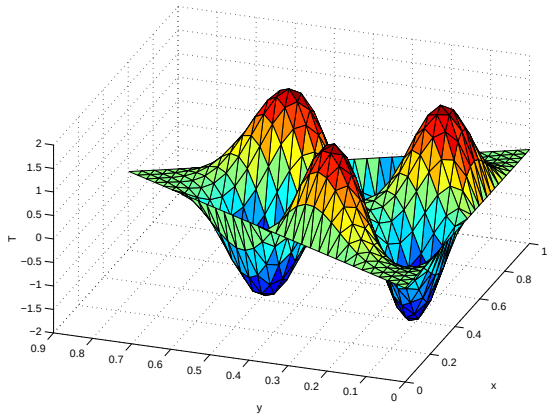

Figure 2.12: (1,4) Antisymmetric Mode

Proof. We will use Parseval's identity [88] . It is clear from the above that the volume under $T_s^{m,m}$ is never equal to zero. A direct calculation establishes that

$$\langle 1, T_s^{m,m} \rangle = \frac{3\sqrt{3}}{4\pi m} \cdot h^2; \ \langle T_s^{m,m}, T_s^{m,m} \rangle = \frac{3\sqrt{3}}{8} \cdot h^2. \tag{2.41}$$

Thus, in projecting the function 1 onto the subspace spanned by $\{T_s^{m,m}\}_{m=1}^{\infty}$, we have the following total "energy" present in the generalized Fourier coefficients:

$$\sum_{m=1}^{\infty} \frac{\langle 1, T_s^{m,m} \rangle^2}{\langle T_s^{m,m}, T_s^{m,m} \rangle} = \frac{\sqrt{3}}{4} \cdot h^2 = ||1||^2. \tag{2.42}$$

Thus, all of the energy is concentrated in these modes, leaving us to conclude that the remaining generalized Fourier coefficients vanish, $\langle 1, T_s^{m,n} \rangle = 0$ for $m \neq n$. □

As first pointed out by Lamé [40], the modes $T_s^{m,m}$ are not the only ones that are rotationally symmetric.

Theorem 2.4.3. *1. $T_s^{m,n}$ is rotationally symmetric if and only if $m \equiv n (\equiv l)$ (mod3).*

2. $T_a^{m,n}$ is rotationally symmetric if and only if $m \equiv n (\equiv l)$ (mod3).

Proof. 1. $T_s^{m,n}$ is rotationally symmetric iff it is symmetric about the line $v = u$. This can occur iff the normal derivative, $\frac{\partial T_s^{m,n}}{\partial \nu}$ vanishes there.

Thus, we require that

$$\begin{aligned}\frac{\partial T_s^{m,n}}{\partial(v-u)}|_{v=u} = \frac{1}{2} \quad \{ \quad & (m-l)\cos[\frac{2\pi}{9r}(lu+mu-2nu+3lr)] \\ + \quad & (m-n)\cos[\frac{2\pi}{9r}(nu+mu-2lu+3nr)] \\ + \quad & (n-m)\cos[\frac{2\pi}{9r}(mu+nu-2lu+3mr)] \\ + \quad & (l-m)\cos[\frac{2\pi}{9r}(mu+lu-2nu+3mr)] \\ + \quad & (l-n)\cos[\frac{2\pi}{9r}(nu+lu-2mu+3nr)] \\ + \quad & (n-l)\cos[\frac{2\pi}{9r}(lu+nu-2mu+3lr)]\} = 0,\end{aligned} \tag{2.43}$$

derived from Equation (2.30). These terms cancel pairwise iff $m \equiv n(\equiv l)\ (\mathrm{mod}3)$.

2. $T_a^{m,n}$ is rotationally symmetric iff it is antisymmetric about the line $v = u$. This can occur iff $T_a^{m,n}$ vanishes there. Thus, we require that

$$\begin{aligned}T_a^{m,n}|_{v=u} = \frac{1}{2} \quad \{ \quad & \cos[\frac{2\pi}{9r}(lu+mu-2nu+3lr)] \\ - \quad & \cos[\frac{2\pi}{9r}(nu+mu-2lu+3nr)] \\ + \quad & \cos[\frac{2\pi}{9r}(mu+nu-2lu+3mr)] \\ - \quad & \cos[\frac{2\pi}{9r}(mu+lu-2nu+3mr)] \\ + \quad & \cos[\frac{2\pi}{9r}(nu+lu-2mu+3nr)] \\ - \quad & \cos[\frac{2\pi}{9r}(lu+nu-2mu+3lr)]\} = 0,\end{aligned} \tag{2.44}$$

derived from Equation (2.31). These terms cancel pairwise iff $m \equiv n(\equiv l)\ (\mathrm{mod}3)$.

□

This is illustrated in Figures 2.11 and 2.12 which display the symmetric and antisymmetric $(1,4)$ modes, respectively.

2.5 Spectral Properties

In those physical problems in which Equation (2.1) arises, the frequency $f_{m,n}$ is proportional to the square root of the eigenvalue. Hence, from Equation

(2.26), we arrive at

$$f_{m,n} \propto \frac{4\pi}{3h}\sqrt{\ell};\ \ell := m^2 + mn + n^2. \tag{2.45}$$

Thus, the spectral structure of the equilateral triangle hinges upon the number theoretic properties of the binary quadratic form $m^2 + mn + n^2$.

Since $T_s^{m,n}$ and $T_a^{m,n}$ both correspond to the same frequency $f_{m,n}$ given by Equation (2.45), it follows that all eigenvalues corresponding to $m \neq n$ have multiplicity equal to at least two. However, this modal degeneracy, as it is known in the engineering literature, extends also to the case $m = n$. For example, the $(7, 7)$ and $(2, 11)$ modes, both corresponding to $\ell = 147$, share the same frequency. In fact, the multiplicity question is quite deep and we defer to [73] and [53] for its definitive treatment.

Turning to the specific application of the vibrating equilateral triangular membrane for the sake of definiteness, the collection of frequencies $\{f_{m,n}\}$ possesses an inherent structure. Specifically, we can partition this collection of frequencies into distinct "harmonic sequences" so that, within such a sequence, all frequencies are integer multiples of a "fundamental frequency". Complete details appear in [53].

2.6 Green's Function

Using Equations (2.27), (2.29), and (2.36-37), we may define the orthonormal system of eigenfunctions

$$\phi_s^{m,n} = \frac{T_s^{m,n}}{\|T_s^{m,n}\|}\ (m = 1, 2, \dots;\ n = m, \dots), \tag{2.46}$$

$$\phi_a^{m,n} = \frac{T_a^{m,n}}{\|T_a^{m,n}\|}\ (m = 1, 2, \dots;\ n = m + 1, \dots), \tag{2.47}$$

together with their corresponding eigenvalues

$$\lambda_{m,n} = \frac{4\pi^2}{27r^2}(m^2 + mn + n^2)\ (m = 1, 2, \dots;\ n = m, \dots). \tag{2.48}$$

The Green's function [82] for the Laplacian with Dirichlet boundary conditions on an equilateral triangle is then constructed as

$$\begin{aligned} G(x, y; x', y') &= \sum_{m=1}^{\infty} \{ \frac{\phi_s^{m,m}(x, y)\phi_s^{m,m}(x', y')}{\lambda_{m,m}} \\ &+ \sum_{n=m+1}^{\infty} \frac{\phi_s^{m,n}(x, y)\phi_s^{m,n}(x', y') + \phi_a^{m,n}(x, y)\phi_a^{m,n}(x', y')}{\lambda_{m,n}} \} \end{aligned} \tag{2.49}$$

This may be employed in the usual fashion to solve the corresponding nonhomogeneous boundary value problem.

2.7 Related Structures

We now turn to structures related to the equilateral triangle in the sense that they share some or all of their eigenfunctions. Of particular interest are symmetry/antisymmetry considerations which show that the eigenfunctions of the equilateral triangle under mixed boundary conditions (i.e. part Dirichlet and part Neumann) are not trigonometric.

2.7.1 Hemiequilateral Triangle

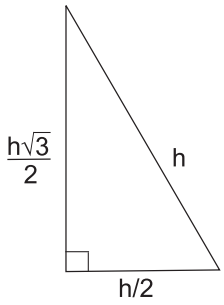

Figure 2.13: Hemiequilateral Triangle

The right triangle obtained by subdividing the equilateral triangle along an altitude is shown in Figure 2.13 and is christened forthwith the **hemiequilateral triangle**. Thus, it may be characterized as a right triangle whose hypotenuse has precisely twice the length of one of its legs. Following Lamé [40], it is immediate that all of its modes (under Dirichlet boundary conditions) are obtained by simply restricting the antisymmetric modes of the equilateral triangle (thereby having a nodal line along said altitude) to this domain. (It is instructive to note that even as great a Mathematician as George Pólya [76] was unfamiliar with Lamé's results and thus mistakenly believed that he had discovered the principal mode of the hemiequilateral triangle.) Rather than subdividing the equilateral triangle to obtain a related structure we may instead consider regions obtainable by combining equilateral triangles. We next consider a couple of examples of this procedure.

2.7.2 Regular Rhombus

For lack of a better term, we will denote a rhombus composed of two equilateral triangles by **regular rhombus**. Thus, a regular rhombus has supplementary angles of 60° and 120°. Any mode of the regular rhombus may be decomposed into the sum of a mode symmetric and a mode antisymmetric about the shorter diagonal. As shown in Figure 2.14 and first observed by

F. Pockels [75], the antisymmetric modes may all be constructed by antisymmetric reflection of the modes of the equilateral triangle. However, as shown by Figure 2.15, the symmetric modes cannot be so constructed by reflections since this always leads to sign conflicts such as that circled (the same sign appearing in positions symmetric about a Dirichlet line and hence positions of antisymmetry). A close inspection of Figure 2.15 reveals the following new underlying principle: *The eigenfunctions of the equilateral triangle with two Dirichlet boundary conditions and one Neumann boundary condition are not trigonometric.*

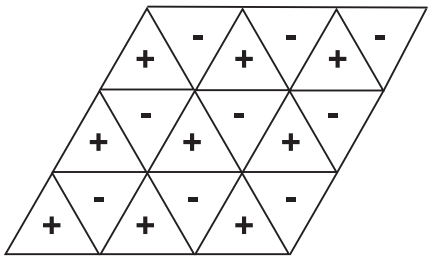

Figure 2.14: Antisymmetric Mode of Regular Rhombus

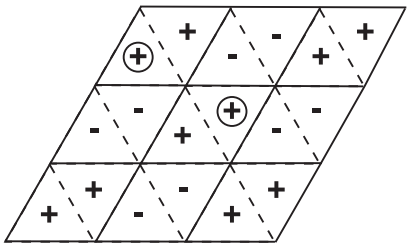

Figure 2.15: Symmetric Mode of Regular Rhombus

2.7.3 Regular Hexagon

A similar situation obtains for a regular hexagon which, of course, can be decomposed into six equilateral triangles. As shown in Figure 2.16 and first observed by F. Pockels [75], any fully antisymmetric mode (i.e. one where all of the edges of the component equilateral triangles are nodal lines) can be constructed by antisymmetric reflection of the modes of the equilateral triangle. Yet, any fully symmetric mode, such as the fundamental, which is composed of symmetric reflections about the interior triangle edges cannot be so constructed due to the inevitable sign conflicts shown circled. A careful perusal of Figure 2.17 reveals the following new underlying principle: *The eigenfunctions of the equilateral triangle with two Neumann boundary conditions and one Dirichlet boundary condition are not trigonometric.*

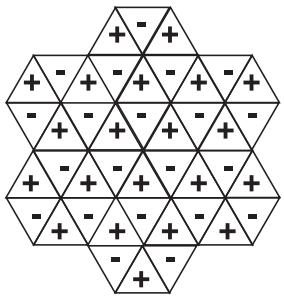

Figure 2.16: Fully Antisymmetric Mode of Regular Hexagon

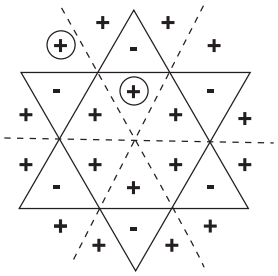

Figure 2.17: Fully Symmetric Mode of Regular Hexagon

2.8 Peter Gustav Lejeune Dirichlet

Peter Gustav Lejeune Dirichlet (1805-1859) was born in Düren, Germany, then part of the French Empire [23]. He was educated at the Gymnasium in Bonn and the Jesuit College in Cologne before studying in Paris from 1822-1825. In 1825, he published his first paper comprising a partial proof of Fermat's Last Theorem for $n = 5$. (He would later produce a complete proof for $n = 14$.) He then returned to Germany where he was awarded an honorary doctorate from University of Cologne and submitted his habilitation thesis on polynomials with a special class of prime divisors to University of Breslau in 1827. He then taught at Breslau and Berlin before being called to fill Gauss' chair at Göttingen in 1855.

He published an early paper inspired by Gauss' work on the Law of Biquadratic Reciprocity. Beginning in 1829, he published a series of papers containing the conditions for the convergence of trigonometric series and the use of the series to represent arbitrary functions [24, pp. 1131-1132]. For this work [6, p. 145-146], he is considered the founder of the theory of Fourier series. In 1837, he proved that in any arithmetic progression, with first term coprime to the difference, there are infinitely many primes. In 1838, he published two papers in analytic number theory which introduced Dirichlet series and determined the formula for the class number of quadratic forms. His work on units in algebraic number theory contains important results on ideals. In

Figure 2.18: Peter Gustav Lejeune Dirichlet

1837, he introduced the modern definition of a function.

In 1846, he produced an analysis of Laplace's problem of proving the stability of the solar system based upon the properties of the energy expression for the system. In 1850, he studied the gravitational attraction of a spheroid by solving what is now known as Dirichlet's problem for the potential function. It was this work in potential theory that led to the naming of the first boundary condition after him. In 1852, he dealt with the motion of a sphere in an incompressible fluid where he performed the first exact integration of the hydrodynamic equations.

Mathematical concepts bearing his name include: Dirichlet boundary condition, Dirichlet problem, Dirichlet tessellation, Dirichlet distribution, Dirichlet series, Dirichlet test [24, p. 725], Dirichlet integral and Dirichlet principle. Gotthold Eisenstein, Leopold Kronecker and Rudolph Lipschitz were his students. He died in Göttingen, aged 54, after suffering a heart attack in Switzerland. After his death, his lectures and other results in number theory were collected, edited and published by his friend Richard Dedkind under the title *Vorlesungen über Zahlentheorie* (1863).

Chapter 3

The Neumann Problem

It is the express purpose of the present chapter to fill the previously alluded to gap in the literature for the case of the Neumann boundary condition [52]. The parallel development for the Dirichlet problem appears in the previous chapter. A subsequent chapter will present a corresponding treatment of the Robin problem. Not only will we supply a derivation of Lamé's formulas from first principles but we will also endeavor to provide an extensive account of modal properties. Many of these properties are simply stated by Lamé and Pockels but herein receive full derivation. Other properties that are clearly identified below are new and appear here for the first time in book form.

Knowing the eigenstructure permits us to construct the Neumann function, and we do so. The implications for related geometries are also explored. The primarily pedagogical and historical exposition to follow gladly trades off mathematical elegance for brute-force, yet straightforward, computation in the hope that these interesting results will thereby find their natural place in introductory treatments of boundary value problems.

3.1 The Neumann Eigenproblem for the Equilateral Triangle

During his investigations into the cooling of a right prism with equilateral triangular base [40], Lamé was lead to consider the eigenvalue problem

$$\Delta T(x,y) + k^2 T(x,y) = 0,\ (x,y) \in \tau;\ \frac{\partial T}{\partial \nu}(x,y) = 0,\ (x,y) \in \partial\tau \qquad (3.1)$$

where Δ is the two-dimensional Laplacian, $\frac{\partial^2}{\partial x^2} + \frac{\partial^2}{\partial y^2}$, τ is the equilateral triangle shown in Figure 1.1, and ν its outward pointing normal. Remarkably, he was able to show that the eigenfunctions satisfying Equation (3.1) could be expressed in terms of combinations of sines and cosines, typically the province of rectangular geometries [44].

Lamé later encountered the same eigenproblem when considering the vibrational modes of a free elastic membrane in the shape of an equilateral triangle [41]. The identical problem occurs also in acoustic ducts with hard walls and in the propagation of transverse electric (TE- or H-) modes in electromagnetic waveguides [37]. Lamé's solution of this problem actually proceeds from quite general considerations about precisely which geometries will give rise to eigenfunctions composed of sines and cosines. These matters we now take up.

3.2 Lamé's Fundamental Theorem II

Let us begin by restating that we will make some alterations to Lamé's presentation of his General Law of a Nodal Plane. First of all, rather than being concerned with three-dimensional problems, we will restrict attention to two dimensions and hence will consider instead nodal lines (i.e. lines along which an eigenfunction vanishes) and antinodal lines (along which the normal derivative vanishes). Secondly, since we are not specifically interested in heat transfer but rather in the eigenproblem, Equation (3.1), in its own right, we will replace his notions of inverse/direct calorific symmetry by the less application-specific concepts of antisymmetry/symmetry, respectively.

Motivated by his earlier work in crystallography, Lamé made the following observations, repeated here for convenience, the cornerstone of his work on heat transfer in right prisms. (See Section 2.2 [51] for a complete elementary proof.)

Theorem 3.2.1 (Fundamental Theorem). *Suppose that $T(x, y)$ can be represented by the double Fourier series*

$$T(x,y) = \sum_i \sum_j A_{ij} \sin(\lambda_i x + \mu_j y + \alpha_{ij}) + B_{ij} \cos(\lambda_i x + \mu_j y + \beta_{ij}) \quad (3.2)$$

with $\lambda_i^2 + \mu_j^2 = k^2$, then

1. *$T(x, y)$ is antisymmetric about any line along which it vanishes.*
2. *$T(x, y)$ is symmetric about any line along which its normal derivative, $\frac{\partial T}{\partial \nu}$, vanishes.*

The Fundamental Theorem has the following immediate consequences.

Corollary 3.2.1. *With $T(x, y)$ as defined by Equation (3.2),*

1. *If $T = 0$ along the boundary of a polygon then $T = 0$ along the boundaries of the family of congruent and symmetrically placed polygons obtained by reflection about its sides.*

2. *If* $\frac{\partial T}{\partial \nu} = 0$ *along the boundary of a polygon then* $\frac{\partial T}{\partial \nu} = 0$ *along the boundaries of the family of congruent and symmetrically placed polygons obtained by reflection about its sides.*

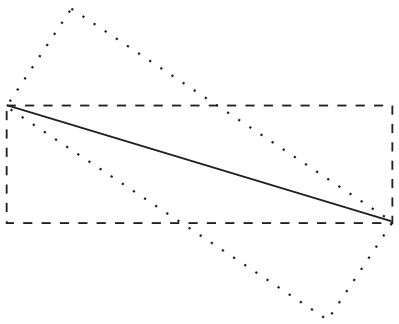

Figure 3.1: Rectangular Reflection

This corollary has far reaching implications for the determination of those domains which possess eigenfunctions expressible in terms of sines and cosines (henceforth referred to as "trigonometric eigenfunctions"). For example, Figure 3.1 illustrates that the diagonal of a rectangle cannot ordinarily be a nodal line, nor for that matter an antinodal line, since the rectangle has a complete orthonormal system of trigonometric eigenfunctions yet does not possess the requisite symmetry unless it is either a square or has aspect ratio $\sqrt{3}$ (see Figures 3.12-13). Here and below, solid lines denote lines of antisymmetry while dashed lines denote lines of symmetry. Furthermore, as illustrated in Figure 3.2, an isosceles right triangle may be repeatedly reflected about its edges to produce the symmetry (denoted by +) required by the Fundamental Theorem and in fact possesses trigonometric eigenfunctions obtained from the restriction of those of a square with an antinodal line along a fixed diagonal.

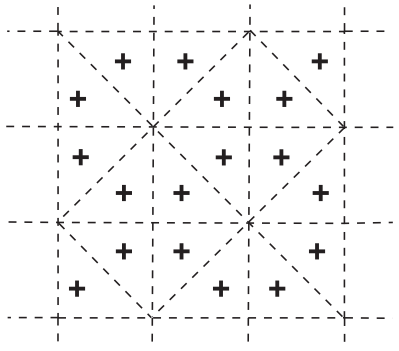

Figure 3.2: Symmetry of Isosceles Right Triangle

Next consider the equilateral triangular lattice of Figure 3.3 together with its supporting symmetric structure. It suggests that the equilateral triangle

might possess trigonometric eigenfunctions since the Fundamental Theorem supplies necessary but not sufficient conditions. By devices unknown, Lamé was in fact able to construct such a family of eigenfunctions. We next present an original derivation of this eigenstructure by employing his natural triangular coordinate system (Section 1.1.1). We will return to consider other regions with and without trigonometric eigenfunctions in a later section.

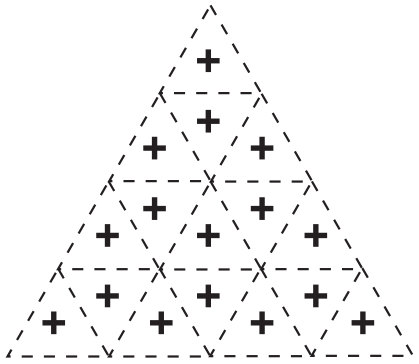

Figure 3.3: Symmetry of Equilateral Triangular Lattice

3.3 Construction of Modes

Before proceeding any further, we will decompose the sought after eigenfunction into parts symmetric and antisymmetric about the altitude $v = w$ (see Figure 1.3)

$$T(u, v, w) = T_s(u, v, w) + T_a(u, v, w), \tag{3.3}$$

where

$$T_s(u, v, w) = \frac{T(u, v, w) + T(u, w, v)}{2};\ T_a(u, v, w) = \frac{T(u, v, w) - T(u, w, v)}{2}, \tag{3.4}$$

henceforth to be dubbed a symmetric/antisymmetric mode, respectively. We next take up the determination of T_s and T_a separately.

3.3.1 Symmetric Modes

We first dispense with the eigenvalue $k^2 = 0$. Its corresponding eigenvector (fundamental mode) is constant and we choose $T_s^{0,0} = 3$ for reasons that will become evident. There is no corresponding antisymmetric mode. Any multiple of this symmetric mode, shown in Figure 3.4, is called a plane wave. We next search for symmetric modes which are not plane waves.

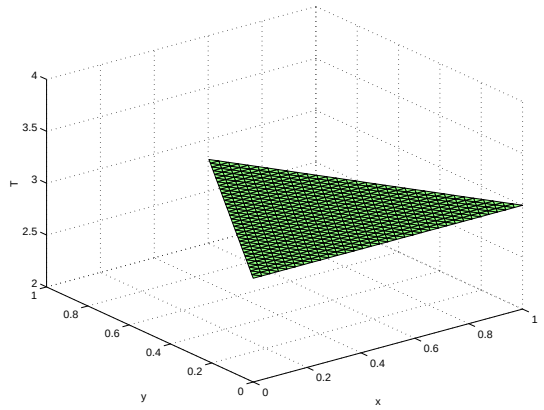

Figure 3.4: Plane Wave

In light of the fact that $\frac{\partial T_s}{\partial u}$ must vanish when $u = -2r$ and $u = r$ while being even as a function of $v - w$, we seek a solution of the form

$$T_s = \cos[\frac{\pi l}{3r}(u + 2r)] \cdot \cos[\beta_1(v - w)], \tag{3.5}$$

where l is an integer and $[\frac{\pi l}{3r}]^2 + 3\beta_1^2 = k^2$. We will show that, by itself, this form cannot satisfy the Neumann boundary condition along $v = r$. Observe that if it could then, by symmetry, it would automatically satisfy the corresponding boundary condition along $w = r$.

Moreover, we will show that the sum of two such terms also does not suffice for the satisfaction of the remaining boundary conditions. However, the sum of three appropriately chosen terms of the form Equation (3.5) does indeed satisfy said boundary conditions and thus constitutes the sought after symmetric mode. In the course of this demonstration, the expression for the eigenvalues k^2 will emerge.

Along $v = r$, we have $v - w = u + 2r$ where we have invoked the fundamental relation of triangular coordinates given by Equation (1.2). In order to facilitate the calculation of the normal derivative along $v = r$, we will utilize the coordinate system $(w - u, w + u)$. In terms of these coordinates, $u = -\frac{1}{2}(w - u) + \frac{1}{2}(w + u)$, $v = -(w + u)$, $w = \frac{1}{2}(w - u) + \frac{1}{2}(w + u)$, and $v - w = -\frac{1}{2}(w - u) - \frac{3}{2}(w + u)$ so that

$$\begin{aligned} \frac{\partial T_s}{\partial(w + u)}|_{v=r} &= (\frac{3}{4}\beta_1 - \frac{\pi l}{12r}) \cdot \sin[(\frac{\pi l}{3r} + \beta_1)(u + 2r)] \\ &+ (\frac{3}{4}\beta_1 + \frac{\pi l}{12r}) \cdot \sin[(-\frac{\pi l}{3r} + \beta_1)(u + 2r)], \end{aligned} \tag{3.6}$$

which cannot be identically equal to zero for $-2r \leq u \leq r$ unless $l = 0$ and $\beta_1 = 0$ in which case Equation (3.5) degenerates to a plane wave. Thus, one such term does not suffice.

Hence, let us try instead a sum of the form

$$T_s = \cos[\frac{\pi l}{3r}(u+2r)] \cdot \cos[\beta_1(v-w)] + \cos[\frac{\pi m}{3r}(u+2r)] \cdot \cos[\beta_2(v-w)], \quad (3.7)$$

with $[\frac{\pi l}{3r}]^2 + 3\beta_1^2 = [\frac{\pi m}{3r}]^2 + 3\beta_2^2 = k^2$. Along $v = r$, we now have

$$\begin{aligned} \frac{\partial T_s}{\partial(w+u)}|_{v=r} &= (\frac{3}{4}\beta_1 - \frac{\pi l}{12r}) \cdot \sin[(\frac{\pi l}{3r} + \beta_1)(u+2r)] \\ &+ (\frac{3}{4}\beta_1 + \frac{\pi l}{12r}) \cdot \sin[(-\frac{\pi l}{3r} + \beta_1)(u+2r)] \\ &+ (\frac{3}{4}\beta_2 - \frac{\pi m}{12r}) \cdot \sin[(\frac{\pi m}{3r} + \beta_2)(u+2r)] \\ &+ (\frac{3}{4}\beta_2 + \frac{\pi m}{12r}) \cdot \sin[(-\frac{\pi m}{3r} + \beta_2)(u+2r)], \end{aligned} \quad (3.8)$$

and the only way to get these terms to cancel pairwise is to choose $l = m = \beta_1 = \beta_2 = 0$ which once again produces only a plane wave. Thus, two such terms do not suffice.

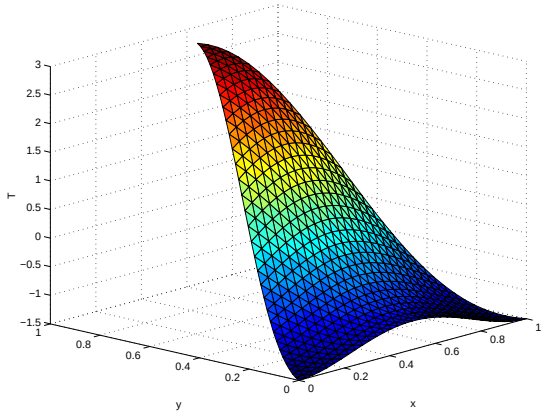

Figure 3.5: $(0, 1)$ Symmetric Mode

Undaunted, we persevere to consider a sum of the form

$$\begin{aligned} T_s &= \cos[\frac{\pi l}{3r}(u+2r)] \cdot \cos[\beta_1(v-w)] \\ &+ \cos[\frac{\pi m}{3r}(u+2r)] \cdot \cos[\beta_2(v-w)] \\ &+ \cos[\frac{\pi n}{3r}(u+2r)] \cdot \cos[\beta_3(v-w)], \end{aligned} \quad (3.9)$$

with

$$[\frac{\pi l}{3r}]^2 + 3\beta_1^2 = [\frac{\pi m}{3r}]^2 + 3\beta_2^2 = [\frac{\pi n}{3r}]^2 + 3\beta_3^2 = k^2. \quad (3.10)$$

Along $v = r$, we now have

$$\begin{aligned}
\frac{\partial T_s}{\partial(w+u)}|_{v=r} &= (\frac{3}{4}\beta_1 - \frac{\pi l}{12r}) \cdot \sin[(\frac{\pi l}{3r} + \beta_1)(u+2r)] \\
&+ (\frac{3}{4}\beta_1 + \frac{\pi l}{12r}) \cdot \sin[(-\frac{\pi l}{3r} + \beta_1)(u+2r)] \\
&+ (\frac{3}{4}\beta_2 - \frac{\pi m}{12r}) \cdot \sin[(\frac{\pi m}{3r} + \beta_2)(u+2r)] \\
&+ (\frac{3}{4}\beta_2 + \frac{\pi m}{12r}) \cdot \sin[(-\frac{\pi m}{3r} + \beta_2)(u+2r)] \\
&+ (\frac{3}{4}\beta_3 - \frac{\pi n}{12r}) \cdot \sin[(\frac{\pi n}{3r} + \beta_3)(u+2r)] \\
&+ (\frac{3}{4}\beta_3 + \frac{\pi n}{12r}) \cdot \sin[(-\frac{\pi n}{3r} + \beta_3)(u+2r)],
\end{aligned} \tag{3.11}$$

There are now eight possible ways that cancellation may occur that all lead to essentially the same conclusion. Hence, we pursue in detail only

$$\frac{\pi l}{3r} + \beta_1 = -\frac{\pi n}{3r} + \beta_3;\ \frac{\pi l}{3r} - \beta_1 = -\frac{\pi m}{3r} - \beta_2;\ \frac{\pi m}{3r} - \beta_2 = -\frac{\pi n}{3r} - \beta_3. \tag{3.12}$$

When added together, these three equations yield the important relation

$$l + m + n = 0. \tag{3.13}$$

With this consistency condition satisfied, we may add the first and last of Equations (3.12) to obtain

$$\beta_1 - \beta_2 = \frac{\pi}{3r}(l+m), \tag{3.14}$$

which, when combined with the identity

$$3(\beta_1 - \beta_2)(\beta_1 + \beta_2) = (\frac{\pi}{3r})^2(m-l)(m+l) \tag{3.15}$$

obtained by rearranging the first of Equations (3.10), yields

$$\beta_1 + \beta_2 = \frac{\pi}{9r}(m-l) \tag{3.16}$$

and, finally,

$$\beta_1 = \frac{\pi(m-n)}{9r};\ \beta_2 = \frac{\pi(n-l)}{9r};\ \beta_3 = \frac{\pi(l-m)}{9r}. \tag{3.17}$$

The eigenvalue may now be calculated as

$$k^2 = \frac{2}{27}(\frac{\pi}{r})^2[l^2 + m^2 + n^2] = \frac{4}{27}(\frac{\pi}{r})^2[m^2 + mn + n^2], \tag{3.18}$$

with the corresponding symmetric mode given by

$$\begin{aligned} T_s^{m,n} &= \cos[\frac{\pi l}{3r}(u+2r)] \cdot \cos[\frac{\pi(m-n)}{9r}(v-w)] \\ &+ \cos[\frac{\pi m}{3r}(u+2r)] \cdot \cos[\frac{\pi(n-l)}{9r}(v-w)] \\ &+ \cos[\frac{\pi n}{3r}(u+2r)] \cdot \cos[\frac{\pi(l-m)}{9r}(v-w)], \end{aligned} \tag{3.19}$$

which never vanishes identically. Figure 3.5 displays the $(0,1)$ symmetric mode.

3.3.2 Antisymmetric Modes

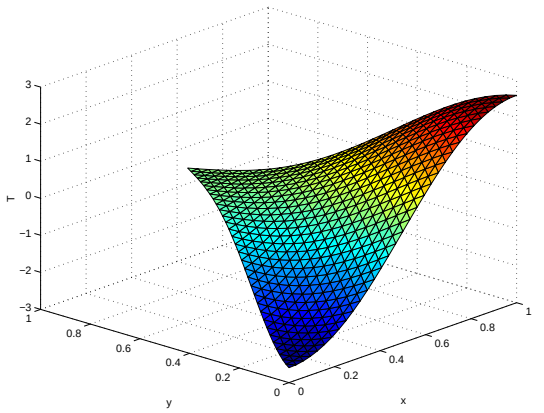

Figure 3.6: $(0,1)$ Antisymmetric Mode

A parallel development is possible for the determination of an antisymmetric mode. In light of the oddness of T_a as a function of $v-w$, we commence with an Ansatz of the form

$$\begin{aligned} T_a &= \cos[\frac{\pi l}{3r}(u+2r)] \cdot \sin[\beta_1(v-w)] \\ &+ \cos[\frac{\pi m}{3r}(u+2r)] \cdot \sin[\beta_2(v-w)] \\ &+ \cos[\frac{\pi n}{3r}(u+2r)] \cdot \sin[\beta_3(v-w)]. \end{aligned} \tag{3.20}$$

As for the symmetric mode, one can establish that all three terms are in fact necessary for the satisfaction of the Neumann boundary conditions.

Once again we are lead to the conditions $l+m+n=0$, $k^2 = \frac{2}{27}(\frac{\pi}{r})^2[l^2+m^2+n^2] = \frac{4}{27}(\frac{\pi}{r})^2[m^2+mn+n^2]$, and $\beta_1 = \frac{\pi(m-n)}{9r}$, $\beta_2 = \frac{\pi(n-l)}{9r}$, $\beta_3 = \frac{\pi(l-m)}{9r}$.

Therefore, we arrive at the antisymmetric mode

$$\begin{aligned} T_a^{m,n} &= \cos[\frac{\pi l}{3r}(u+2r)] \cdot \sin[\frac{\pi(m-n)}{9r}(v-w)] \\ &+ \cos[\frac{\pi m}{3r}(u+2r)] \cdot \sin[\frac{\pi(n-l)}{9r}(v-w)] \\ &+ \cos[\frac{\pi n}{3r}(u+2r)] \cdot \sin[\frac{\pi(l-m)}{9r}(v-w)], \end{aligned} \tag{3.21}$$

which may be identically zero. Figure 3.6 displays the $(0,1)$ antisymmetric mode.

3.4 Modal Properties

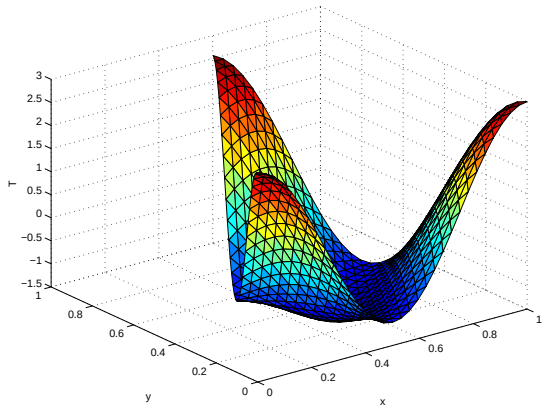

Figure 3.7: $(1,1)$ Mode

In what follows, it will be convenient to have the following alternative representations

$$\begin{aligned} T_s^{m,n} = \frac{1}{2} \quad \{ \quad & \cos[\frac{2\pi}{9r}(lu+mv+nw+3lr)] + \cos[\frac{2\pi}{9r}(nu+mv+lw+3nr)] \\ + \quad & \cos[\frac{2\pi}{9r}(mu+nv+lw+3mr)] + \cos[\frac{2\pi}{9r}(mu+lv+nw+3mr)] \\ + \quad & \cos[\frac{2\pi}{9r}(nu+lv+mw+3nr)] + \cos[\frac{2\pi}{9r}(lu+nv+mw+3lr)]\}; \end{aligned} \tag{3.22}$$

$$T_a^{m,n} = \frac{1}{2} \quad \{ \quad \sin[\frac{2\pi}{9r}(lu+mv+nw+3lr)] - \sin[\frac{2\pi}{9r}(nu+mv+lw+3nr)]$$
$$+ \quad \sin[\frac{2\pi}{9r}(mu+nv+lw+3mr)] - \sin[\frac{2\pi}{9r}(mu+lv+nw+3mr)]$$
$$+ \quad \sin[\frac{2\pi}{9r}(nu+lv+mw+3nr)] - \sin[\frac{2\pi}{9r}(lu+nv+mw+3lr)]\}, \tag{3.23}$$

obtained from Equation (3.19) and Equation (3.21), respectively, by the application of appropriate trigonometric identities.

It is clear from these formulas that both $T_s^{m,n}$ and $T_a^{m,n}$ are invariant under a cyclic permutation of (l, m, n), while $T_s^{n,m} = T_s^{m,n}$ and $T_a^{n,m} = -T_a^{m,n}$ (which are essentially the same since modes are only determined up to a nonzero constant factor). Thus, we need only consider $n \geq m$. Moreover, since $T_{s,a}^{m,n}$, $T_{s,a}^{-n,m+n}$, $T_{s,a}^{-m-n,m}$, $T_{s,a}^{-m,m+n}$, $T_{s,a}^{-m-n,n}$, and $T_{s,a}^{-n,-m}$ all produce equivalent modes, we may also neglect negative m and n.

We may pare this collection further through the following observation due to Lamé [40].

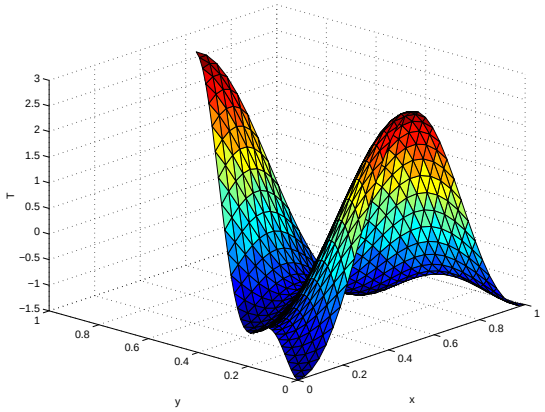

Figure 3.8: $(0, 2)$ Symmetric Mode

Theorem 3.4.1. *1. $T_s^{m,n}$ never vanishes identically.*

2. $T_a^{m,n}$ vanishes identically if and only if two of l, m, n are equal.

Proof. 1. Note that a symmetric mode is identically zero iff it vanishes along the line of symmetry $v = w$, since the only function both symmetric and antisymmetric is the zero function. Along $v = w$,

$$T_s^{m,n} = \cos[\frac{\pi(m+n)}{3r}(u+2r)] + \cos[\frac{\pi m}{3r}(u+2r)] + \cos[\frac{\pi n}{3r}(u+2r)], \tag{3.24}$$

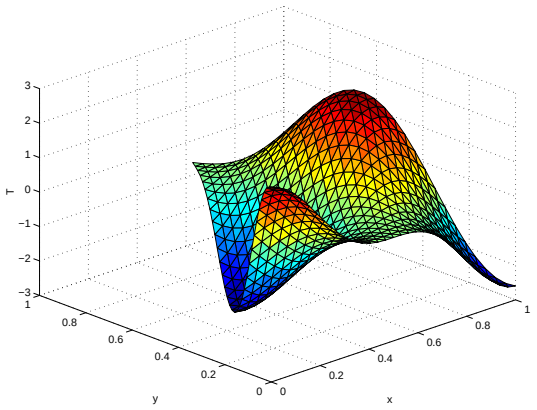

Figure 3.9: $(0, 2)$ Antisymmetric Mode

which may be trigonometrically recast as

$$T_s^{m,n} = 4\cos[\frac{\pi(m+n)}{6r}(u+2r)]\cdot\cos[\frac{\pi m}{6r}(u+2r)]\cdot\cos[\frac{\pi n}{6r}(u+2r)] - 1, \tag{3.25}$$

which cannot vanish identically for $-2r \leq u \leq r$.

2. Note that an antisymmetric mode is identically zero iff its normal derivative vanishes along the line of symmetry $v = w$, since the only function both antisymmetric and symmetric is the zero function. Along $v = w$,

$$\begin{aligned}\frac{\partial T_a^{m,n}}{\partial(v-w)} &= \frac{\pi(m-n)}{9r}\cos[\frac{\pi l}{3r}(u+2r)] + \frac{\pi(n-l)}{9r}\cos[\frac{\pi m}{3r}(u+2r)] \\ &+ \frac{\pi(l-m)}{9r}\cos[\frac{\pi n}{3r}(u+2r)],\end{aligned} \tag{3.26}$$

which may be trigonometrically recast as

$$\begin{aligned}\frac{9r}{\pi}\cdot\frac{\partial T_a^{m,n}}{\partial(v-w)} &= (m-n)\cdot\cos[\frac{\pi(m+n)}{3r}(u+2r)] \\ &+ (m+n)\cdot\{\cos[\frac{\pi m}{3r}(u+2r)] - \cos[\frac{\pi n}{3r}(u+2r)]\} \\ &+ n\cdot\cos[\frac{\pi m}{3r}(u+2r)] - m\cdot\cos[\frac{\pi n}{3r}(u+2r)].\end{aligned} \tag{3.27}$$

This equals zero iff $m = n$ or $m = -2n$ (i.e. $l = n$) or $n = -2m$ (i.e. $l = m$).

□

Hence, our system of eigenfunctions is $\{T_s^{m,n}\ (n \geq m);\ T_a^{m,n}\ (n > m)\}$. Figure 3.7 shows the $(1, 1)$ mode whereas the symmetric and antisymmetric

$(0, 2)$ modes are displayed in Figures 3.8 and 3.9 while the symmetric and antisymmetric $(1, 2)$ modes are displayed in Figures 3.10 and 3.11, respectively. We next show that this is a complete orthonormal set of eigenfunctions and then go on to explore some features of these modes.

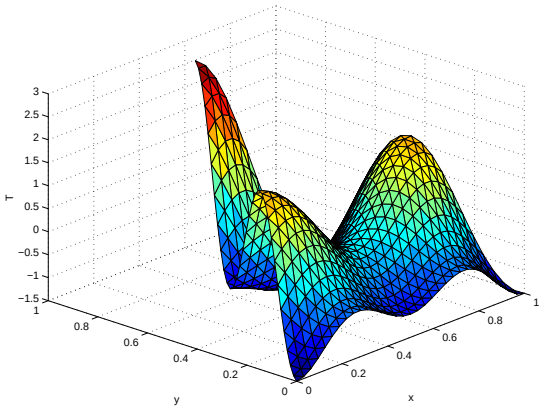

Figure 3.10: $(1, 2)$ Symmetric Mode

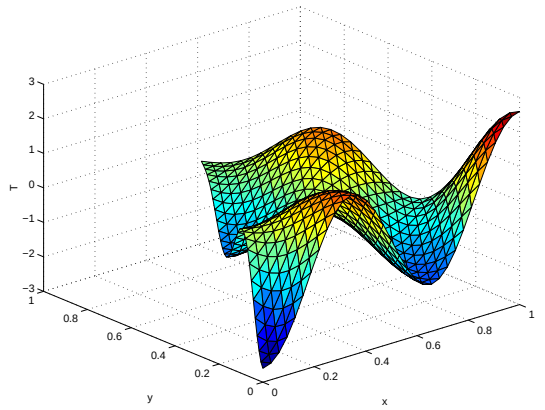

Figure 3.11: $(1, 2)$ Antisymmetric Mode

3.4.1 Orthonormality

By Rellich's Theorem [44], eigenfunctions corresponding to distinct eigenvalues are guaranteed to be orthogonal. However, as we shall eventually discover, the multiplicity of the eigenvalues given by Equation (3.18) is quite a complicated matter. Thus, direct integrations employing Equations (3.22) and (3.23) confirm the orthogonality of our collection of eigenfunctions $\{T_s^{m,n}\ (n \geq m);\ T_a^{m,n}\ (n > m)\}$.

Furthermore, they may be normalized using

$$||T_s^{m,n}||^2 = \frac{9r^2\sqrt{3}}{4} = ||T_a^{m,n}||^2 \ (m \neq n), \tag{3.28}$$

$$||T_s^{m,m}||^2 = \frac{9r^2\sqrt{3}}{2} \ (m^2 + n^2 \neq 0), \tag{3.29}$$

and

$$||T_s^{0,0}||^2 = 27r^2\sqrt{3}, \tag{3.30}$$

by employing the inner product $\langle f, g\rangle = \int\int_\tau fg \ dA$.

3.4.2 Completeness

It is not *a priori* certain that the collection of eigenfunctions $\{T_s^{m,n},\ T_a^{m,n}\}$ constructed above is complete. For domains which are the Cartesian product of intervals in an orthogonal coordinate system, such as rectangles and annuli, completeness of the eigenfunctions formed from products of one-dimensional counterparts has been established [88]. Since the equilateral triangle is not such a domain, we must employ other devices in order to establish completeness. We follow the lead of Práger [77] and appeal to the well-known completeness of the corresponding eigenfunctions of the rectangle.

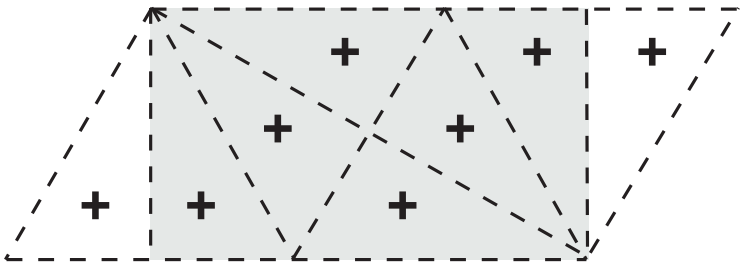

Figure 3.12: Triangle-to-Rectangle Transformation (Symmetric Mode)

For this purpose, we now introduce the triangle-to-rectangle (TTR) transformation pictorialized in Figure 3.12 for symmetric modes and in Figure 3.13 for antisymmetric modes. In these figures, a solid line represents a Dirichlet condition ($T = 0$) and a dashed line a Neumann condition ($\frac{\partial T}{\partial \nu} = 0$), while the patterns of $\pm$ signify symmetry/antisymmetry. Restricting attention to the right half of the equilateral triangle, this coincides with the prolongation transformation of Práger [77].

Commencing with the equilateral triangle in the southwest corner of each diagram, we construct the remainder of each figure by performing three symmetric reflections across triangle edges as specified by the Fundamental Theorem. In both cases, this leaves us with a (shaded) rectangle of dimensions $\frac{3h}{2} \times \frac{\sqrt{3}h}{2}$.

For the symmetric mode (Figure 3.12), this rectangle has strictly Neumann boundary conditions, while, for the antisymmetric mode (Figure 3.13), there are Neumann boundary conditions along the top and bottom and Dirichlet boundary conditions on the sides. In both cases, the corresponding eigenfunctions of the rectangle are known to be complete. By our construction procedure for the modes of the equilateral triangle, they are seen to be precisely the restriction of the corresponding modes of the associated rectangle possessing the indicated pattern of nodal and antinodal lines.

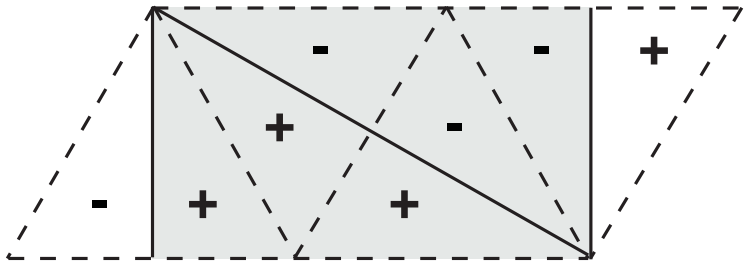

Figure 3.13: Triangle-to-Rectangle Transformation (Antisymmetric Mode)

For example, to construct a mode of the rectangle $[\sqrt{3}r, 4\sqrt{3}r] \times [0, 3r]$ of Figure 3.12 with the displayed antinodal lines, we may confine ourselves to making the mode symmetric about the indicated diagonal $y = 4r - x/\sqrt{3}$ since the remaining antinodal lines would then follow immediately from the Fundamental Theorem. We do this by suitably combining the known complete orthogonal rectangular modes of the form $\cos[\mu\frac{\pi}{3r}(3r - y)]\cos[\nu\frac{2\pi}{3\sqrt{3}r}(x - 3r)]$, where μ and ν are positive integers.

Although this process is laborious, it is identical to that outlined in Sections 3.3.1 and 3.3.2 for the construction of T_s and T_a. The end result is that these rectangular modes must be combined in triplets satisfying $\mu_1 + \mu_2 + \mu_3 = 0$, $\nu_1 = \mu_2 - \mu_3$, $\nu_2 = \mu_3 - \mu_1$, $\nu_3 = \mu_1 - \mu_2$. Hence, any such mode of the rectangle will be given by a linear combination of the modes $T_s^{m,n}$ of Equation (3.19).

Similar considerations applied to the rectangle of Figure 3.13, whose modes are $\cos[\mu\frac{\pi}{3r}(3r - y)]\sin[\nu\frac{2\pi}{3\sqrt{3}r}(x - 3r)]$, yield the one-to-one correspondence between $T_a^{m,n}$ of Equation (3.21) and the modes of this rectangle which vanish along the indicated diagonal.

Thus, if the equilateral triangle were to possess either a symmetric or an antisymmetric mode not expressible as a linear combination of those we have found above then the same would be true for its extension to the associated rectangle by the TTR transformation. This contradiction establishes that our collection of equilateral triangular modes is indeed complete.

3.4.3 Nodal / Antinodal Lines

As evidenced by Figure 3.4, the first eigenfunction (fundamental mode) of an eigenvalue problem can have no nodal lines in the interior of the domain and thus must be of the same sign everywhere [11, p. 451]. Hence, every other eigenfunction orthogonal to it must have nodal lines.

The structure of the nodal lines is nontrivial. For example, based upon the picture of the $(1,1)$ mode displayed in Figure 3.7, one might posit that the line segments connecting the midpoints of the triangle sides are nodal lines. However, this cannot be the case since it clearly does not possess the antisymmetry required by the Fundamental Theorem. We next consider some properties of nodal/antinodal lines. (See [90] for a more detailed study of the nodal/antinodal lines by means of Chladni figures.)

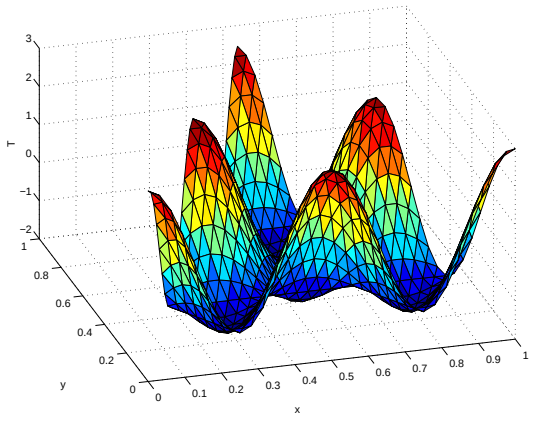

Figure 3.14: $(2,2)$ Mode

We commence by reconsidering the case $m = n$. Recall that we have already determined that $T_a^{m,m} \equiv 0$. Furthermore, in this case, we may combine the terms of Equation (3.22) to yield

$$T_s^{m,m} = \cos\left[\frac{2\pi m}{3r}(r-u)\right] + \cos\left[\frac{2\pi m}{3r}(r-v)\right] + \cos\left[\frac{2\pi m}{3r}(r-w)\right], \qquad (3.31)$$

which clearly illustrates that any permutation of (u, v, w) leaves $T_s^{m,m}$ invariant. This is manifested geometrically in the invariance of $T_s^{m,m}$ under a 120° rotation about the triangle center (see Figure 3.14). This invariance will henceforth be termed rotational symmetry.

We next rewrite Equation (3.31) as

$$T_s^{m,m} = (-1)^m \cdot 4 \cdot \cos\left[\frac{\pi m}{3r}(r-u)\right] \cdot \cos\left[\frac{\pi m}{3r}(r-v)\right] \cdot \cos\left[\frac{\pi m}{3r}(r-w)\right] - 1. \qquad (3.32)$$

Thus, the nodal lines even in this special case are given by the transcendental equation obtained by setting this expression to zero.

In spite of this, there is in fact an inherent structure to the antinodal lines when $m = n$. Straightforward differentiation of Equation (3.31) establishes that $\frac{\partial T_s^{m,m}}{\partial u}\big|_{u=r-\frac{k}{m}\cdot 3r\ (k=0,\ldots,m)} = 0$. Thus, by invoking rotational symmetry, an antinodal line ($\frac{\partial T_s^{m,m}}{\partial \nu} = 0$) occurs at

$$u = r - \frac{k}{m}\cdot 3r;\ v = r - \frac{k}{m}\cdot 3r;\ w = r - \frac{k}{m}\cdot 3r\ (k = 0, \ldots, m). \tag{3.33}$$

That is, there is a network of $m-1$ equidistant antinodal lines parallel to each side of the triangle which subdivides it into m^2 congruent equilateral triangles, each supporting a portion of the mode similar to the $(1,1)$ mode and "in-phase" with one another. This is in evidence in Figure 3.14.

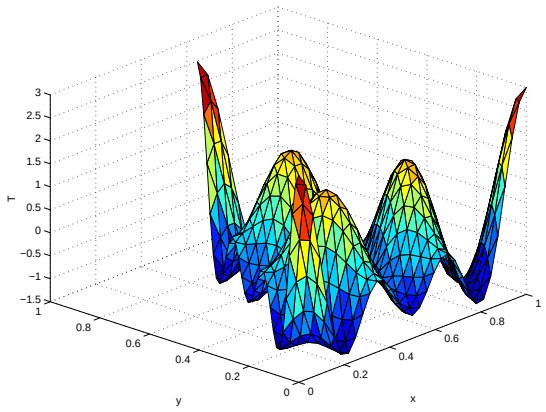

Figure 3.15: $(1,4)$ Symmetric Mode

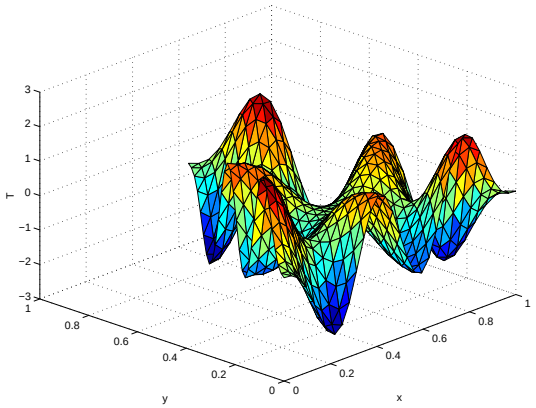

Figure 3.16: $(1,4)$ Antisymmetric Mode

As first pointed out by Lamé [40], the modes $T_s^{m,m}$ are not the only ones that are rotationally symmetric.

Theorem 3.4.2. *1. $T_s^{m,n}$ is rotationally symmetric if and only if $m \equiv n(\equiv l)$ (mod3).*

2. $T_a^{m,n}$ is rotationally symmetric if and only if $m \equiv n(\equiv l)$ (mod3).

Proof. 1. $T_s^{m,n}$ is rotationally symmetric iff it is symmetric about the line $v = u$. This can occur iff the normal derivative, $\frac{\partial T_s^{m,n}}{\partial \nu}$ vanishes there. Thus, we require that

$$\begin{aligned}\frac{\partial T_s^{m,n}}{\partial(v-u)}|_{v=u} = -\frac{1}{2} \quad \{ \quad & (m-l)\sin[\frac{2\pi}{9r}(lu+mu-2nu+3lr)] \\ + \quad & (m-n)\sin[\frac{2\pi}{9r}(nu+mu-2lu+3nr)] \\ + \quad & (n-m)\sin[\frac{2\pi}{9r}(mu+nu-2lu+3mr)] \\ + \quad & (l-m)\sin[\frac{2\pi}{9r}(mu+lu-2nu+3mr)] \\ + \quad & (l-n)\sin[\frac{2\pi}{9r}(nu+lu-2mu+3nr)] \\ + \quad & (n-l)\sin[\frac{2\pi}{9r}(lu+nu-2mu+3lr)]\} = 0,\end{aligned} \tag{3.34}$$

derived from Equation (3.22). These terms cancel pairwise iff $m \equiv n(\equiv l)$ (mod3).

2. $T_a^{m,n}$ is rotationally symmetric iff it is antisymmetric about the line $v = u$. This can occur iff $T_a^{m,n}$ vanishes there. Thus, we require that

$$\begin{aligned}T_a^{m,n}|_{v=u} = \frac{1}{2} \quad \{ \quad & \sin[\frac{2\pi}{9r}(lu+mu-2nu+3lr)] \\ - \quad & \sin[\frac{2\pi}{9r}(nu+mu-2lu+3nr)] \\ + \quad & \sin[\frac{2\pi}{9r}(mu+nu-2lu+3mr)] \\ - \quad & \sin[\frac{2\pi}{9r}(mu+lu-2nu+3mr)] \\ + \quad & \sin[\frac{2\pi}{9r}(nu+lu-2mu+3nr)] \\ - \quad & \sin[\frac{2\pi}{9r}(lu+nu-2mu+3lr)]\} = 0,\end{aligned} \tag{3.35}$$

derived from Equation (3.23). These terms cancel pairwise iff $m \equiv n(\equiv l)$ (mod3).

□

This is illustrated in Figures 3.15 and 3.16 which display the symmetric and antisymmetric $(1, 4)$ modes, respectively.

Finally, we offer the following new result.

Theorem 3.4.3. *The volume under $T_s^{m,n}$ is equal to zero if and only if $m^2 + n^2 \neq 0$.*

Proof. The volume under $T_s^{0,0}$ is obviously nonzero. Also, by Rellich's Theorem [44], eigenfunctions corresponding to distinct eigenvalues are orthogonal. Hence, all of the other modes $T_s^{m,n}$ $(m^2 + n^2 \neq 0)$ are orthogonal to $T_s^{0,0} = 3$ and thus the volume under these modes is equal to zero. □

3.5 Spectral Properties

In those physical problems in which Equation (3.1) arises, the frequency $f_{m,n}$ is proportional to the square root of the eigenvalue. Hence, from Equation (3.18), we arrive at

$$f_{m,n} \propto \frac{4\pi}{3h}\sqrt{\ell};\ \ell := m^2 + mn + n^2. \tag{3.36}$$

Thus, the spectral structure of the equilateral triangle hinges upon the number theoretic properties of the binary quadratic form $m^2 + mn + n^2$.

Since $T_s^{m,n}$ and $T_a^{m,n}$ both correspond to the same frequency $f_{m,n}$ given by Equation (3.36), it follows that all eigenvalues corresponding to $m \neq n$ have multiplicity equal to at least two. However, this modal degeneracy, as it is known in the engineering literature, extends also to the case $m = n$. For example, the $(7, 7)$ and $(2, 11)$ modes, both corresponding to $\ell = 147$, share the same frequency. In fact, the multiplicity question is quite deep and we defer to [53] for its definitive treatment.

Turning to the specific application of the vibrating equilateral triangular membrane for the sake of definiteness, the collection of frequencies $\{f_{m,n}\}$ possesses an inherent structure. Specifically, we can partition this collection of frequencies into distinct "harmonic sequences" so that, within such a sequence, all frequencies are integer multiples of a "fundamental frequency". Complete details appear in [53].

3.6 Neumann Function

Using Equations (3.19), (2.21), and (3.28-30), we may define the orthonormal system of eigenfunctions

$$\phi_s^{m,n} = \frac{T_s^{m,n}}{\|T_s^{m,n}\|}\ (m = 0, 1, 2, \dots;\ n = m, \dots), \tag{3.37}$$

$$\phi_a^{m,n} = \frac{T_a^{m,n}}{\|T_a^{m,n}\|} \ (m = 0, 1, 2, \dots ; \ n = m + 1, \dots), \tag{3.38}$$

together with their corresponding eigenvalues

$$\lambda_{m,n} = \frac{4\pi^2}{27r^2}(m^2 + mn + n^2) \ (m = 0, 1, 2, \dots ; \ n = m, \dots). \tag{3.39}$$

The Neumann function [82] (variously called the modified, generalized, or pseudo Green's function) for the Laplacian with Neumann boundary conditions on an equilateral triangle is then constructed as

$$\begin{aligned} G(x, y; x', y') &= \sum_{m=1}^{\infty} \frac{\phi_s^{m,m}(x, y)\phi_s^{m,m}(x', y')}{\lambda_{m,m}} \\ &+ \sum_{m=0}^{\infty} \sum_{n=m+1}^{\infty} \frac{\phi_s^{m,n}(x, y)\phi_s^{m,n}(x', y') + \phi_a^{m,n}(x, y)\phi_a^{m,n}(x', y')}{\lambda_{m,n}} \end{aligned} \tag{3.40}$$

This may be employed in the usual fashion to solve the corresponding nonhomogeneous boundary value problem, assuming that it is consistent.

3.7 Related Structures

We now turn to structures related to the equilateral triangle in the sense that they share some or all of their eigenfunctions. Of particular interest are symmetry/antisymmetry considerations which show that the eigenfunctions of the equilateral triangle under mixed boundary conditions (i.e. part Dirichlet and part Neumann) are <u>not</u> trigonometric.

3.7.1 Hemiequilateral Triangle

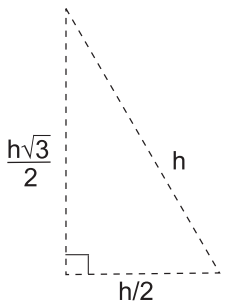

Figure 3.17: Hemiequilateral Triangle

The right triangle obtained by subdividing the equilateral triangle along an altitude is shown in Figure 3.17 and is christened forthwith the **hemiequilateral triangle**. Thus, it may be characterized as a right triangle whose

hypotenuse has precisely twice the length of one of its legs. Following Lamé [40] it is immediate that all of its modes (under Neumann boundary conditions) are obtained by simply restricting the symmetric modes of the equilateral triangle (thereby having an antinodal line along said altitude) to this domain. Rather than subdividing the equilateral triangle to obtain a related structure we may instead consider regions obtainable by combining equilateral triangles. We next consider a couple of examples of this procedure.

3.7.2 Regular Rhombus

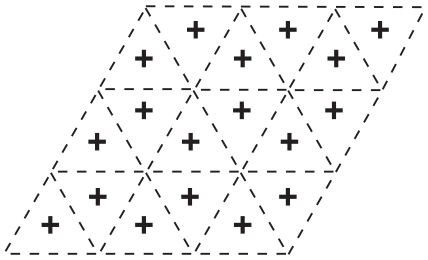

Figure 3.18: Symmetric Mode of Regular Rhombus

Lacking a better term, we will denote a rhombus composed of two equilateral triangles by **regular rhombus**. Thus, a regular rhombus has supplementary angles of 60° and 120°. Any mode of the regular rhombus may be decomposed into the sum of a mode symmetric and a mode antisymmetric about the shorter diagonal. As shown in Figure 3.18 and first observed by F. Pockels [75], the symmetric modes may all be constructed by symmetric reflection of the modes of the equilateral triangle. However, as shown by Figure 3.19, the antisymmetric modes cannot be so constructed by reflections since this always leads to sign conflicts such as that circled (different signs appearing in positions symmetric about a Neumann line and hence positions of symmetry. A close inspection of Figure 3.19 reveals the following new underlying principle: *The eigenfunctions of the equilateral triangle with two Neumann boundary conditions and one Dirichlet boundary condition are not trigonometric.*

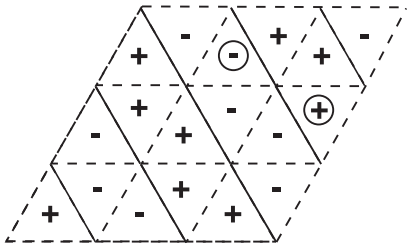

Figure 3.19: Antiymmetric Mode of Regular Rhombus

3.7.3 Regular Hexagon

A similar situation obtains for a regular hexagon which, of course, can be decomposed into six equilateral triangles. As shown in Figure 3.20 and first observed by F. Pockels [75], any fully symmetric mode (i.e. one where all of the edges of the component equilateral triangles are antinodal lines) can be constructed by symmetric reflection of the modes of the equilateral triangle. Yet, any fully antisymmetric mode, which is composed of antisymmetric reflections about the interior triangle edges cannot be so constructed due to the inevitable sign conflicts shown circled. A careful perusal of Figure 3.21 reveals

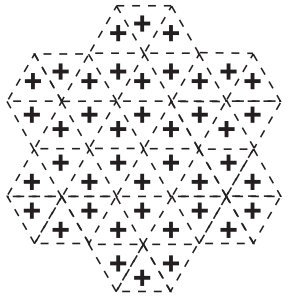

Figure 3.20: Fully Symmetric Mode of Regular Hexagon

the following new underlying principle: *The eigenfunctions of the equilateral triangle with two Dirichlet boundary conditions and one Neumann boundary condition are not trigonometric.*

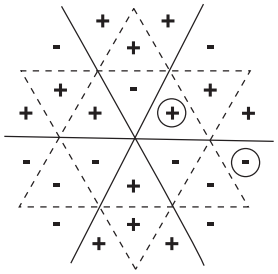

Figure 3.21: Fully Antisymmetric Mode of Regular Hexagon

3.8 Carl Gottfried Neumann

Carl Gottfried Neumann (1832-1925) was born in Königsberg, Prussia, the son of Franz Ernst Neumann, Professor of Physics at University of Königsberg [23]. He completed his doctorate at University of Königsberg in 1855 and his habilitation at University of Halle in 1858. He taught at Halle, Basel and Tübingen before settling at University of Leipzig in 1868.

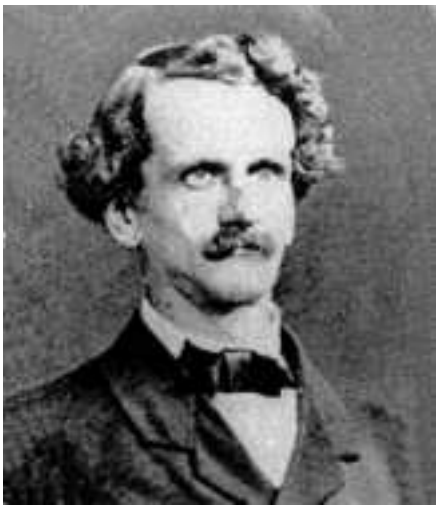

Figure 3.22: Carl Gottfried Neumann

He worked on the Dirichlet principle, studied the order of connectivity of Riemann surfaces and helped initiate the theory of integral equations. He also developed the method of the arithmetic mean for the solution of boundary value problems. However, his most enduring work was in potential theory where he introduced the logarithmic potential and the Neumann series. His contributions to potential theory led to his name being attached to the second boundary condition. Together with Alfred Clebsch, Neumann founded the influential mathematical research journal *Mathematische Annalen* for which he also served as an editor. He died in Leipzig, aged 92.

Chapter 4

Polygons with Trigonometric Eigenfunctions

The Dirichlet/Neumann eigenvalue problems are defined, respectively, by

$$\Delta u(x,y) + k^2 u(x,y) = 0,\ (x,y) \in \mathcal{D};\ u(x,y)\ /\ \frac{\partial u}{\partial \nu}(x,y) = 0,\ (x,y) \in \partial\mathcal{D} \tag{4.1}$$

where Δ is the two-dimensional Laplacian, $\frac{\partial^2}{\partial x^2} + \frac{\partial^2}{\partial y^2}$, $\mathcal{D}$ is a planar domain with outward pointing normal ν, and k^2 is an eigenvalue with corresponding eigenfunction $u(x,y)$. The physical contexts in which these eigenvalue problems arise are many and diverse.

At the outset, we assume that either exclusively Dirichlet or exclusively Neumann boundary conditions are specified on the periphery of $\mathcal{D}$ with no mixing of the two allowed. It is known that the eigenfunctions so defined are all finite trigonometric sums of the form

$$u(x,y) = \sum_i A_i \sin(\lambda_i x + \mu_i y + \alpha_i) + B_i \cos(\lambda_i x + \mu_i y + \beta_i); \lambda_i^2 + \mu_i^2 = k^2 \tag{4.2}$$

for the rectangle (including the important special case of the square) [21], the isosceles right triangle [75], the equilateral triangle [40], and the $30^\circ - 60^\circ - 90^\circ$ "hemiequilateral" triangle [51, 52] (see Figure 1).

In what follows, it will be proven in an essentially geometric fashion that the polygons shown in Figure 1 and listed above are in fact the only ones possessing a complete set of eigenfunctions of the trigonometric form of Equation (4.2) [58]. Coincidentally, this is the same collection of polygons which are admissible for the image method [38]. Those polygonal domains which possess a partial set of such trigonometric eigenfunctions are then completely characterized. Finally, consideration is given to such trigonometric eigenfunctions for the case of a mixture of Dirichlet and Neumann boundary conditions.

Figure 4.1: Polygons with All Trigonometric Eigenfunctions

4.1 Complete Set of Trigonometric Eigenfunctions

Motivated by earlier work in crystallography, Lamé [40] made the following (unproven) result, again repeated here for convenience, the cornerstone for his study of heat transfer in right prisms.

Theorem 4.1.1 (Lamé's Fundamental Theorem). *Suppose that $u(x, y)$ can be represented by the finite trigonometric series given by Equation (4.2), then*

1. *$u(x, y)$ is antisymmetric about any ("nodal") line along which it vanishes.*

2. *$u(x, y)$ is symmetric about any ("antinodal") line along which its normal derivative, $\frac{\partial u}{\partial \nu}$, vanishes.*

Proof: See Section 2.2 [51, p. 269]. □
The Fundamental Theorem has the following immediate consequences.

Corollary 4.1.1. *With $u(x, y)$ as defined by Equation (4.2),*

1. *If $u = 0$ along the boundary of a polygon $\mathcal{D}$ then $u = 0$ along the boundaries of the family of congruent and symmetrically placed polygons obtained by reflection about its sides.*

2. *If $\frac{\partial u}{\partial \nu} = 0$ along the boundary of a polygon $\mathcal{D}$ then $\frac{\partial u}{\partial \nu} = 0$ along the boundaries of the likewise defined family of polygons.*

Proof:

1. For the Dirichlet problem, use Part 1 of Theorem 4.1.1 to reflect antisymmetrically about any side of $\mathcal{D}$.

2. For the Neumann problem, use Part 2 of Theorem 4.1.1 to reflect symmetrically about any side of $\mathcal{D}$. □

This corollary has far-reaching implications for determining those polygonal domains possessing trigonometric eigenfunctions of the form of Equation (4.2).

Corollary 4.1.2. *With nonconstant $u(x, y)$ defined by Equation (4.2), if u / $\frac{\partial u}{\partial \nu} = 0$ along the boundary of a polygon $\mathcal{D}'$ but u / $\frac{\partial u}{\partial \nu}$ does not vanish along any line segment lying in the interior of the polygon, then $\mathcal{D}'$ must be one of the eight prototiles admitting the monohedral tilings [26, p. 20] of the plane displayed in Figure 4.2. Moreover, if u / $\frac{\partial u}{\partial \nu} = 0$ along the boundary of a polygon $\mathcal{D}$, then $\mathcal{D}$ must be composed of a patch [26, p. 19] of these tiles.*

Proof: We will prove this for the case of the Dirichlet boundary condition. The proof for the case of the Neumann boundary condition may be obtained by simply replacing antisymmetric reflection by symmetric reflection and nodal line by antinodal line.

Repeated antisymmetric reflections (Corollary 4.1.1) about the sides of $\mathcal{D}'$ tile the entire plane. This requires that $\mathcal{D}'$ be convex since otherwise reflection about one of the sides forming an obtuse angle would produce an overlap and *ipso facto* an interior line segment along which u would vanish.

By definition, the resulting tiling of the plane with prototile $\mathcal{D}'$ must be isohedral [26, p. 31]. There are precisely 107 types of such convex tilings [26, p. 474] and they have been tabulated and displayed in [26, p. 475-478]. Of these, the 8 tilings displayed in Figure 4.2 are the only ones displaying the requisite reflectional symmetries about the sides of the prototile. Since a domain may have only finitely many nodal lines [75], any polygon $\mathcal{D}$ along whose boundary u vanishes may be dissected into reflections of some such $\mathcal{D}'$. □

The difficulty with Lamé's Fundamental Theorem and its corollaries is that they supply necessary but not sufficient conditions for a complete set of trigonometric eigenfunctions. For example, it is known that the eigenfunctions of the regular hexagon ($P_6 - 13$) are not all trigonometric [14]. In order to completely characterize those polygonal domains possessing a complete set of trigonometric eigenfunctions, we make the following fundamental observations.

Lemma 4.1.1. *Suppose that $u(x, y)$ can be represented by the finite trigonometric series given by Equation (4.2), then*

1. *If $u(x, y)$ vanishes along a line segment L' then it vanishes along the entire line L containing L'.*

2. *If $\frac{\partial u}{\partial \nu}(x, y)$ vanishes along a line segment L' then it vanishes along the entire line L containing L'.*

Proof:

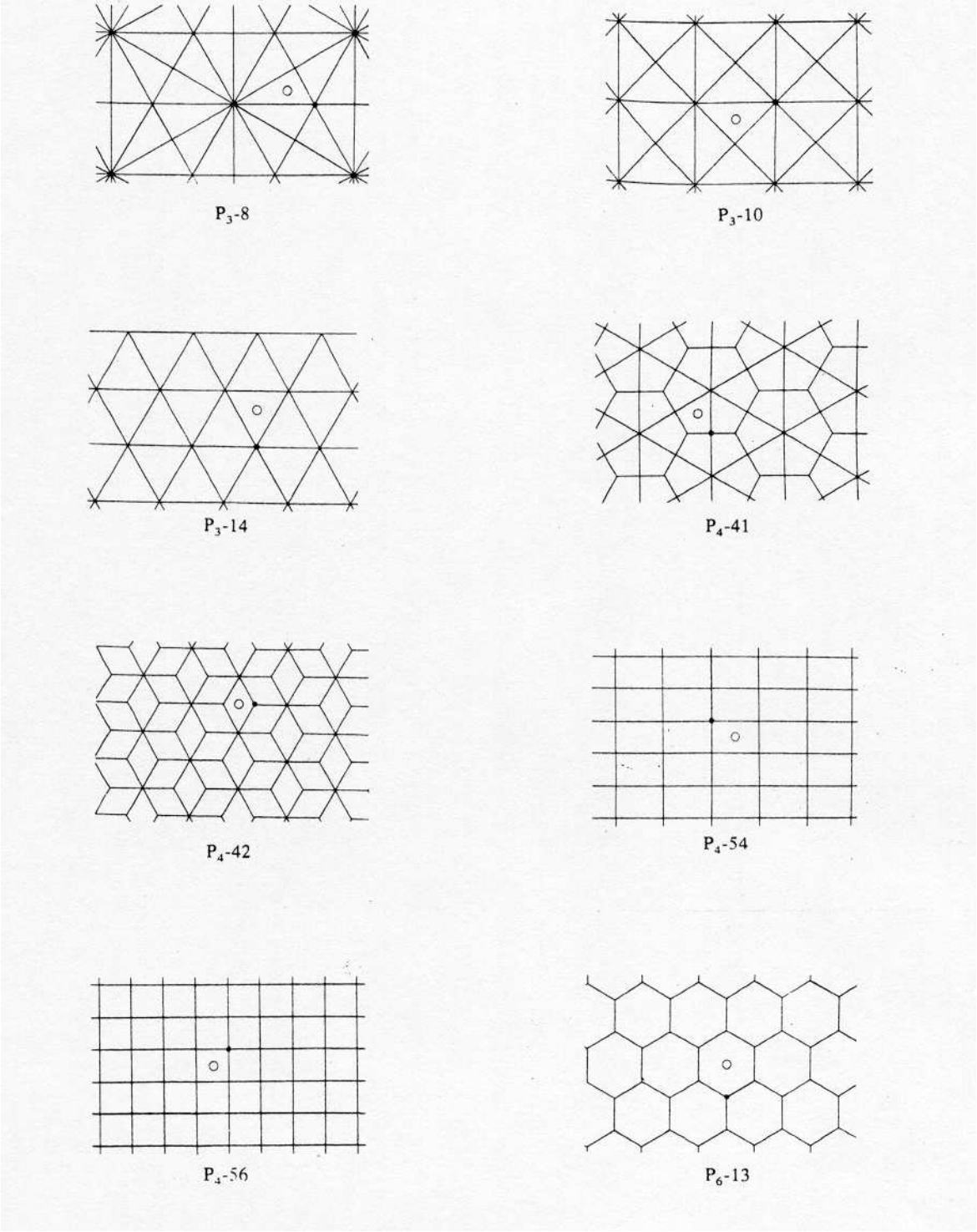

Figure 4.2: Isohedral Tilings Generated by Repeated Reflection [26]

1. If u vanishes along $L' \subset L$ then we may transform, via a translation and a rotation by an angle $\pi/2-\theta$, to an orthogonal coordinate system (x', y') where L corresponds to $x' = 0$ (see Figure 2.1). In these transformed coordinates, Equation (4.2) may be rewritten (using trigonometric identities) as

$$u(x', y') = \sum_i v_i(y') \sin(\lambda_i' x') + \sum_i w_i(y') \cos(\lambda_i' x'), \tag{4.3}$$

where $\lambda_i' = \lambda_i \sin\theta - \mu_i \cos\theta$, $\mu_i' = \lambda_i \cos\theta + \mu_i \sin\theta$, $v_i(y') = C_i \cdot \cos(\mu_i' y' + \phi_i)$, $w_i(y') = C_i \cdot \sin(\mu_i' y' + \phi_i)$, for appropriate amplitudes C_i and phase angles ϕ_i. Observe that $(\lambda_i')^2 + (\mu_i')^2 = k^2$. Applying now the condition $u = 0$ along $x' = 0$, $\epsilon_1 \leq y' \leq \epsilon_2$ yields $\sum_i w_i(y') = 0$ which is possible only if those $w_i(y') \neq 0$ cancel in groups comprised of terms whose corresponding μ_i' all have the same absolute value. Within such a group (say $i \in I$), the λ_i' must also have the same absolute value (say λ'). Thus the corresponding terms of the second series of Equation (4.3) may be collected together as

$$\sum_{i \in I} w_i(y') \cos(\lambda_i' x') = \cos(\lambda' x') \sum_{i \in I} w_i(y') = 0. \tag{4.4}$$

This effectively eliminates the second series of Equation (4.3) leaving us with only

$$u(x', y') = \sum_i v_i(y') \sin(\lambda_i' x'). \tag{4.5}$$

Clearly, u vanishes for $x' = 0$, i.e. along the entire line L.

2. In an entirely analogous fashion, if instead we apply $\frac{\partial u}{\partial \nu} = 0$ along $x' = 0$, $\epsilon_1 \leq y' \leq \epsilon_2$ then it is the first series of Equation (4.3) which is eliminated, leaving only

$$u(x', y') = \sum_i w_i(y') \cos(\lambda_i' x'). \tag{4.6}$$

Clearly, $\frac{\partial u}{\partial \nu}$ vanishes for $x' = 0$, i.e. along the entire line L. □

This lemma may now be combined with Corollary 4.1.2 in order to provide the sought-after characterization of those polygonal domains possessing a complete set of trigonometric eigenfunctions.

Theorem 4.1.2 (Classification Theorem). *The only polygonal domains possessing a complete set of trigonometric eigenfunctions of the form of Equation (4.2) are those shown in Figure 1: the rectangle, the square, the isosceles right triangle, the equilateral triangle and the hemiequilateral triangle.*

Proof: We will prove this for the case of the Dirichlet boundary condition. The proof for the case of the Neumann boundary condition may likewise be obtained by simply replacing nodal line by antinodal line.

By Corollary 4.1.2, if $u(x, y)$ as defined by Equation (4.2) vanishes on the boundary of a polygon $\mathcal{D}'$ but has no nodal lines in its interior, then $\mathcal{D}'$ must be one of the prototiles displayed in Figure 4.2. Furthermore, by Lemma 4.1.1, $u(x, y)$ must vanish along the extensions of the sides of $\mathcal{D}'$. Thus, $\mathcal{D}'$ cannot be the $60° - 90° - 120°$ kite $(P_4 - 41)$, the $60° - 120°$ "regular" rhombus $(P_4 - 42)$ or the regular hexagon $(P_6 - 13)$. As previously pointed out, complete sets of trigonometric eigenfunctions of the form of Equation (4.2) for the five remaining prototiles are available in the literature. □

Of course, the square is a special case of the rectangle but due to its additional symmetry we choose to list it separately. Also, observe that the eigenfunctions of the isosceles right/hemiequilateral triangle correspond to a subset of the eigenfunctions of the square/equilateral triangle, respectively.

4.2 Partial Set of Trigonometric Eigenfunctions

The Classification Theorem may be refined to produce a complete characterization of those polygonal domains possessing a partial set of trigonometric eigenfunctions of the form of Equation (4.2).

Theorem 4.2.1 (Extended Classification Theorem). *The only polygonal domains possessing a partial set of nonconstant trigonometric eigenfunctions of the form of Equation (4.2) are comprised of a patch of the monohedral tilings of the plane whose prototiles are those polygons shown in Figure 4.1: the rectangle, the square, the isosceles right triangle, the equilateral triangle and the hemiequilateral triangle.*

Proof: We prove this for the case of the Dirichlet boundary condition. The proof for the case of the Neumann boundary condition may likewise be obtained. The extension of the sides of the prototile of the $60° - 90° - 120°$ kite $(P_4 - 41)$ produces the hemiequilateral triangle tiling $(P_3 - 8)$ while the extension of the sides of the prototiles of the $60° - 120°$ "regular" rhombus $(P_4 - 42)$ or the regular hexagon $(P_6 - 13)$ produces the equilateral triangle tiling $(P_3 - 14)$. Thus, by Corollary 4.1.2, if nonconstant $u = 0$ along the boundary of a polygon $\mathcal{D}$ and satisfies Equation (4.2), then $\mathcal{D}$ must composed of a patch of one of the five tilings of the plane by the prototiles appearing in Figure 4.1.□

We next look at some examples of polygonal domains possessing a partial set of trigonometric eigenfunctions formed from patches of the equilateral triangular tiling, $P_3 - 14$ (see Figure 4.3). In this and subsequent figures,

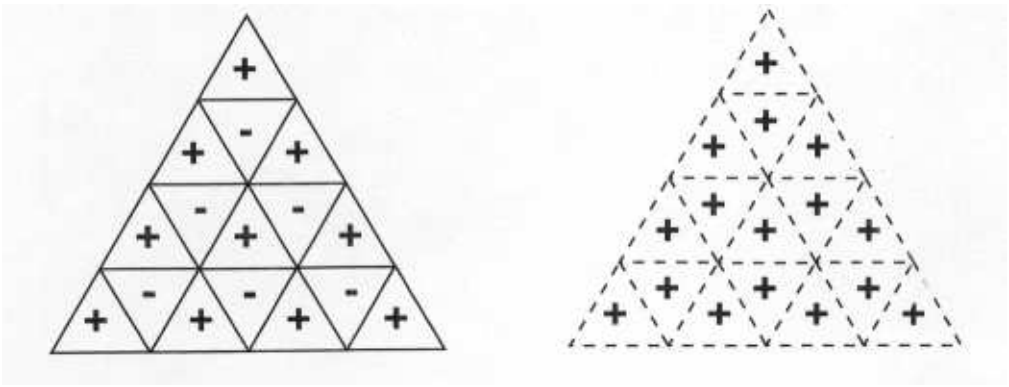

Figure 4.3: Equilateral Triangular Lattices

solid/dashed lines signify nodal/antinodal lines, respectively, while signs of unlike/like parity denote antisymmetric/symmetric reflection.

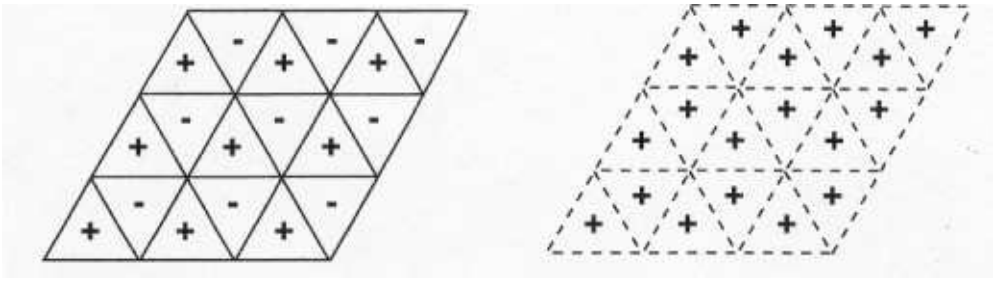

Figure 4.4: Trigonometric Modes of Regular Rhombus

Any mode (i.e. eigenfunction) of the regular rhombus may be decomposed into the sum of a mode symmetric and a mode antisymmetric about the shorter diagonal. As shown in Figure 4.4. and first observed by F. Pockels [75], the antisymmetric/symmetric Dirichlet/Neumann modes may all be constructed by antisymmetric/symmetric reflection of the corresponding modes of the equilateral triangle. However, as shown by Figure 4.5, the symmetric/antisymmetric Dirichlet/Neumann modes cannot be so constructed by such reflections since this always leads to sign conflicts such as those circled (the same/different sign appearing in symmetrical positions about a Dirichlet/Neumann line and hence positions of antisymmetry/symmetry).

A similar situation obtains for a regular hexagon [4] which, of course, can be decomposed into six equilateral triangles. As shown in Figure 4.6 and

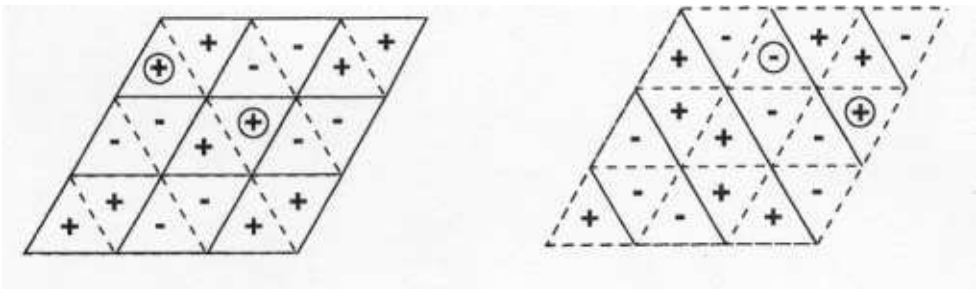

Figure 4.5: Non-Trigonometric Modes of Regular Rhombus

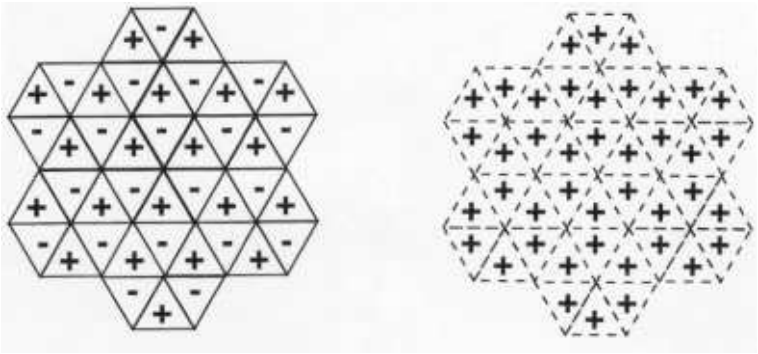

Figure 4.6: Trigonometric Modes of Regular Hexagon

first observed by F. Pockels [75], any fully antisymmetric/symmetric Dirichlet/Neumann mode (i.e. one where all of the edges of the component equilateral triangles are nodal/antinodal lines) can be constructed by antisymmetric/symmetric reflection of the modes of the equilateral triangle. Yet, as shown in Figure 4.7, any fully symmetric/antisymmetric Dirichlet/Neumann mode, which is composed of symmetric/antisymmetric reflections about the interior triangle edges (i.e. the diagonals of the hexagon), cannot be so constructed due to the inevitable sign conflicts shown circled.

A closer inspection of Figures 4.5 and 4.7 reveals the following [51, 52]:

- *Eigenfunctions of the equilateral triangle with two Dirichlet boundary conditions and one Neumann boundary condition are not trigonometric.*

- *Eigenfunctions of the equilateral triangle with two Neumann boundary conditions and one Dirichlet boundary condition are not trigonometric.*

We next extend our classification of polygonal domains with trigonometric eigenfunctions to such mixed Dirichlet/Neumann boundary conditions.

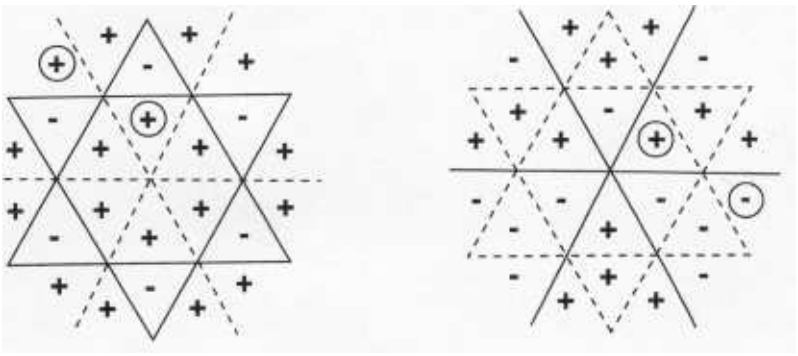

Figure 4.7: Non-Trigonometric Modes of Regular Hexagon

4.3 Trigonometric Eigenfunctions under Mixed Boundary Conditions

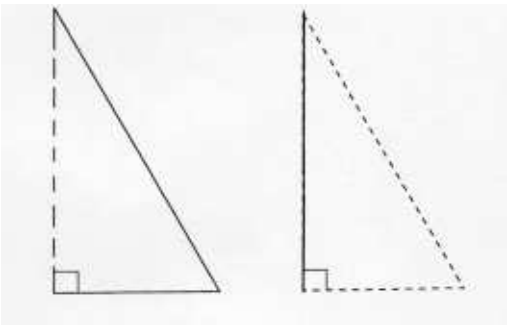

Figure 4.8: Mixed BC Hemiequilateral Triangles: Trigonometric Eigenfunctions

Now consider the case of a mixture of Dirichlet and Neumann boundary conditions (BCs) on a polygonal domain with the restriction that each edge of the boundary be of a single type. In that event, the Classification Theorem becomes:

Theorem 4.3.1 (Mixed BC Classification Theorem). *The only polygonal domains possessing a complete set of trigonometric eigenfunctions of the form of Equation (4.2) under a mixture of Dirichlet and Neumann BCs are:*

- *the rectangle (square) under any combination of BCs,*
- *the isosceles right triangle under any combination of BCs,*
- *the hemiequilateral triangle under the BCs displayed in Figure 4.8 [46].*

The only polygonal domains possessing a partial set of such nonconstant trigonometric eigenfunctions are composed of a patch of the monohedral tilings of the plane with precisely these prototiles.

Proof: As previously noted, the equilateral triangle does not possess trigonometric eigenfunctions under such a mixture of boundary conditions. Similar pictorial constructions reveal that combinations of boundary conditions other than those shown in Figure 4.8 for the hemiequilateral triangle lead to inevitable sign conflicts and consequently must likewise be excluded. The remaining cases listed above lead to tilings of the entire plane by appropriate reflections without sign conflict and thus possess trigonometric eigenfunctions. □

Observe that such trigonometric eigenfunctions for the rectangle (square) are products of their well-known one-dimensional counterparts while those for the isosceles right/hemiequilateral triangle are the restriction of eigenfunctions of the square/equilateral triangle, respectively.

4.4 Friedrich Carl Alwin Pockels

Figure 4.9: Friedrich Pockels

Friedrich Carl Alwin Pockels (1865-1913) was a German physicist who was born in Vincenza, Italy and died in Heidelberg, Germany, aged 48 [91]. His older sister, Agnes, was also a physicist. After studying in Braunschweig and Freiburg, he moved to the University of Göttingen in 1883 where he completed his doctorate (1888) and his habilitation (1892) in theoretical physics under

the supervision of Waldemar Voigt. From 1889 to 1896 he was an Assistant at the Physikalischen Institut and, in 1896, he became Extraordinary Professor at the Technischen Hochschule in Dresden. From 1900 to 1913, he was Professor of Theoretical Physics in the Faculty of Sciences and Mathematics at the University of Heidelberg where he carried out extensive studies on electro-optic properties of crystals. In 1893, he discovered that a steady electric field applied to certain birefringent materials causes the refractive index to vary approximately in proportion to the strength of the field. This phenomenon is now called the Pockels effect and is the basis of many practical electro-optic modulators. In 1906, he published *Lehrbuch der Kristalloptik*. From 1908 to 1913, he was Editor of *Beiblätter zu den Annalen der Physik*. Very early in his career (1891), he published his classic treatise on the Helmholtz equation, *Über die partielle Differentialgleichung* $\Delta u + k^2 u = 0$ [75], with a foreward by Felix Klein. Section II.B.9 of this Meisterwerke contains his contribution to the study of which polygons possess trigonometric eigenfunctions.

Chapter 5

Modal Degeneracy

Expressions for the propagating modes in homogeneously filled cylindrical waveguides of equilateral triangular cross-section were given without derivation in [84, pp. 393-396] and were later derived in [7]. However, their origin dates back to Lamé's fundamental investigations into the cooling of a right prism with equilateral triangular base [40].

As pointed out by F. Pockels [75], most of these modes have multiplicity greater than one. Thus, such structures exhibit modal degeneracy whereby linearly independent modes may share the same cutoff frequency and *ipso facto* the same propagation constant. In fact, Pockels observes that an adequate treatment of such modal degeneracy demands the application of tools from number theory but he only sketches such an approach.

It is the express purpose of the present chapter to provide an essentially complete and self-contained treatment of this problem [53]. We begin by recalling Lamé's formulas for the eigenvalues and corresponding eigenfunctions of the Laplacian on an equilateral triangle under Dirichlet and Neumann boundary conditions. We then give the modal degeneracy problem a succinct statement in the form of four questions. Finally, we proceed to apply factorization into Eisenstein primes, which is developed in an appendix, to provide comprehensive answers to these questions. Representative examples are provided.

The engineering significance of these results lies in their potential application to nearly equilateral triangular waveguides. Within such structures, the propagation of electromagnetic waves may be studied by classical perturbation procedures [48]. However, these approximation techniques require the *a priori* determination of the multiplicity of each eigenvalue together with a basis for the corresponding eigenspace. The treatment to follow in many ways parallels that for square waveguides [50].

5.1 Equilateral Triangular Modes

The transverse magnetic (TM- or E-) modes satisfy the following eigenvalue problem with Dirichlet boundary conditions [37]

$$\Delta\phi(x,y) + k^2\phi(x,y) = 0,\ (x,y) \in \tau;\ \phi(x,y) = 0,\ (x,y) \in \partial\tau \tag{5.1}$$

where Δ is the two-dimensional Laplacian, $\frac{\partial^2}{\partial x^2} + \frac{\partial^2}{\partial y^2}$, and τ is the equilateral triangle shown in Figure 1.1.

We will decompose the sought after eigenfunction into parts symmetric and antisymmetric about the altitude $v = w$ (see Figure 1.3)

$$\phi(u,v,w) = \phi_s(u,v,w) + \phi_a(u,v,w), \tag{5.2}$$

where

$$\phi_s(u,v,w) = \frac{\phi(u,v,w) + \phi(u,w,v)}{2};\ \phi_a(u,v,w) = \frac{\phi(u,v,w) - \phi(u,w,v)}{2}, \tag{5.3}$$

henceforth to be dubbed a symmetric/antisymmetric mode, respectively.

The eigenvalue may now be calculated as [7, 40], [84, pp. 393-396]

$$k^2 = \frac{4}{27}(\frac{\pi}{r})^2[m^2 + mn + n^2]\ (m = 1,2,\dots;n = m,m+1,\dots), \tag{5.4}$$

with the corresponding symmetric mode given by (with $l + m + n = 0$)

$$\begin{aligned}\phi_s^{m,n} &= \sin[\frac{\pi l}{3r}(u+2r)] \cdot \cos[\frac{\pi(m-n)}{9r}(v-w)] \\ &+ \sin[\frac{\pi m}{3r}(u+2r)] \cdot \cos[\frac{\pi(n-l)}{9r}(v-w)] \\ &+ \sin[\frac{\pi n}{3r}(u+2r)] \cdot \cos[\frac{\pi(l-m)}{9r}(v-w)],\end{aligned} \tag{5.5}$$

and antisymmetric mode

$$\begin{aligned}\phi_a^{m,n} &= \sin[\frac{\pi l}{3r}(u+2r)] \cdot \sin[\frac{\pi(m-n)}{9r}(v-w)] \\ &+ \sin[\frac{\pi m}{3r}(u+2r)] \cdot \sin[\frac{\pi(n-l)}{9r}(v-w)] \\ &+ \sin[\frac{\pi n}{3r}(u+2r)] \cdot \sin[\frac{\pi(l-m)}{9r}(v-w)].\end{aligned} \tag{5.6}$$

Hence, our system of TM modes is $\{\phi_s^{m,n}\ (n \geq m > 0);\ \phi_a^{m,n}\ (n > m > 0)\}$.

The transverse electric (TE- or H-) modes satisfy the following eigenvalue problem with Neumann boundary conditions [37]

$$\Delta\psi(x,y) + k^2\psi(x,y) = 0,\ (x,y) \in \tau;\ \frac{\partial\psi}{\partial\nu}(x,y) = 0,\ (x,y) \in \partial\tau \tag{5.7}$$

where Δ is the two-dimensional Laplacian, $\frac{\partial^2}{\partial x^2}+\frac{\partial^2}{\partial y^2}$, τ is the equilateral triangle shown in Figure 1.1, and ν its outward pointing normal.

The eigenvalue may again be calculated as [7, 40], [84, pp. 393-396]

$$k^2 = \frac{4}{27}(\frac{\pi}{r})^2[m^2+mn+n^2] \ (m=0,1,\dots;n=m,m+1,\dots), \tag{5.8}$$

with the corresponding symmetric mode given by

$$\begin{aligned}\psi_s^{m,n} &= \cos[\frac{\pi l}{3r}(u+2r)]\cdot\cos[\frac{\pi(m-n)}{9r}(v-w)] \\ &+ \cos[\frac{\pi m}{3r}(u+2r)]\cdot\cos[\frac{\pi(n-l)}{9r}(v-w)] \\ &+ \cos[\frac{\pi n}{3r}(u+2r)]\cdot\cos[\frac{\pi(l-m)}{9r}(v-w)],\end{aligned} \tag{5.9}$$

and antisymmetric mode

$$\begin{aligned}\psi_a^{m,n} &= \cos[\frac{\pi l}{3r}(u+2r)]\cdot\sin[\frac{\pi(m-n)}{9r}(v-w)] \\ &+ \cos[\frac{\pi m}{3r}(u+2r)]\cdot\sin[\frac{\pi(n-l)}{9r}(v-w)] \\ &+ \cos[\frac{\pi n}{3r}(u+2r)]\cdot\sin[\frac{\pi(l-m)}{9r}(v-w)].\end{aligned} \tag{5.10}$$

Hence, our system of TE modes is $\{\psi_s^{m,n}\ (n\geq m\geq 0);\ \psi_a^{m,n}\ (n>m\geq 0)\}$.

5.2 Modal Degeneracy: Questions

From Equations (5.4) and (5.8), the cutoff frequency for each mode is given by

$$f_{m,n} = \frac{2}{3h}\sqrt{\ell};\ \ell := m^2+mn+n^2. \tag{5.11}$$

Thus, the spectral structure of the equilateral triangular waveguide hinges upon the number theoretic properties of the binary quadratic form m^2+mn+n^2. A complete and exhaustive treatment of this topic is relegated to Section 5.3. See [50] for the corresponding treatment for a square waveguide.

Since $\{\phi_s^{m,n},\phi_a^{m,n}\}$ for the TM case and $\{\psi_s^{m,n},\psi_a^{m,n}\}$ for the TE case both correspond to the same cutoff frequency $f_{m,n}$ given by Equation (5.11) (and thus share the same propagation constant), it follows that all eigenvalues corresponding to $m\neq n$ have multiplicity equal to at least two. However, this modal degeneracy, as it is known in the engineering literature, extends also to the case $m=n$. For example, the $(7,7)$ and $(2,11)$ modes, both corresponding to $\ell=147$, share the same frequency. Thus, the multiplicity question is seen to be quite deep and we now attend to its definitive treatment.

Specifically, we are concerned with the following four interrelated questions concerning modal degeneracy:
1. Which cutoff frequencies emerge from Equation (5.11)?
2. Precisely how many linearly independent modes correspond to each such frequency?
3. Given a permissible cutoff frequency, is there an algorithm to list all (m, n) for which $f_{m,n}$ coincides with it?
4. Can we group all of the allowed cutoff frequencies into disjoint "harmonic sequences" so that those within a group are all integer multiples of a "fundamental frequency"?

5.3 Eisenstein Primes

The specific questions with which we shall be concerned are as follows:

1. Which integers, ℓ, may be written in the form (5.18)? (We call such ℓ **representable**.)

2. In how many ways may this be done?

3. Given ℓ, how may this be done?

4. How may we partition the collection of square roots of all such integers into groups, so that each group is comprised of multiples of a "seed"?

Prior to supplying the answers to these questions, we need to outline the basic number theory supporting them [3, pp. 138-144 & pp. 185-199], [10], [31, Chapter XII].

Whereas many results in elementary number theory hinge upon the prime factorization of an integer $\ell = p_1^{\pi_1} \cdot p_2^{\pi_2} \cdots p_k^{\pi_k}$, the questions raised above are best treated in the complex plane. Thus, we define the **Eisenstein integers** to be the complex numbers $a + b\omega$ where a and b are integers and $\omega = (1 + \imath\sqrt{3})/2$ is the principal cube root of -1. Consequently, they form an equilateral triangular lattice in the complex plane (see Figure 5.1). Mathematically, they constitute a ring. The special values $u = \pm 1, \pm\omega, \pm\bar{\omega}$ are called the **units** and any two Eisenstein integers differing only by a unit factor are called **associates**. The **norm** of an Eisenstein integer is $N(a+b\omega) := (a+b\omega)(a+b\bar{\omega}) = a^2+ab+b^2$. Note that $a + b\bar{\omega} = (a + b) - b\omega$ so that the conjugate of an Eisenstein integer is also an Eisenstein integer.

An Eisenstein integer, E, is said to be an **Eisenstein prime** if its only factorizations are the trivial ones $E = u \cdot e$ involving unit factors, u. We now state, without proof, a characterization of the Eisenstein primes. We begin with the straightforward observation that the usual odd real primes greater

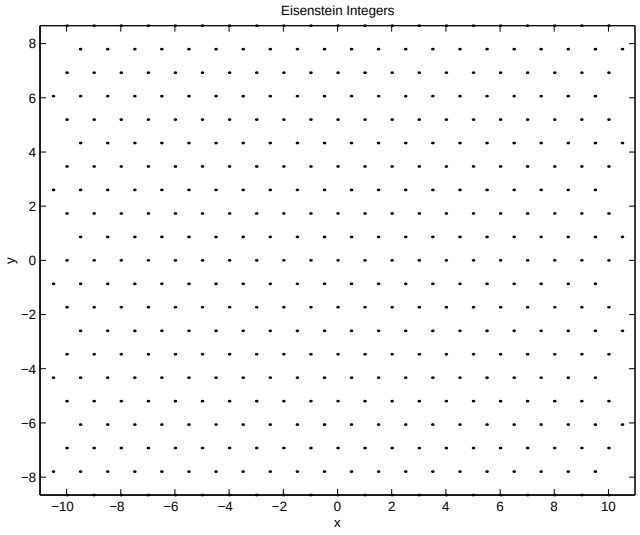

Figure 5.1: The Eisenstein Integers in the Complex Plane

than 3 may all be written as either $6k+1$ or $6k-1$. Then, the Eisenstein primes are given by:

- The real primes 2 and those of the form $6k-1$, and their associates.
- The Eisenstein integers for which $N(a+b\omega) = p$ where p is a real prime of the form $6k+1$,
- The Eisenstein integers for which $N(a+b\omega) = 3$. I.e., $1+\omega,\ -1-\omega,\ -1+2\omega,\ 1-2\omega,\ 2-\omega,\ -2+\omega$.

These are shown with their hexagonal symmetry in Figure 5.2 and are of sufficient visual allure to have inspired floor tilings and tablecloth weavings.

Through this characterization, we may now uncover the connection between Eisenstein primes and our questions concerning representable integers. If we initially restrict our attention to real primes, $\ell = p$, then

$$\ell = p = m^2 + mn + n^2 = (m+n\omega)(m+n\bar{\omega}) \tag{5.12}$$

requires that p either be equal to 3 or be of the form $6k+1$ since real primes equal to 2 or of the form $6k-1$ cannot be factored as Eisenstein integers. Conversely, if $p = 3,\ 6k+1$ then it may be decomposed as in Equation (5.12) and hence is representable in an essentially unique fashion (i.e., up to unit factors and the order of the factors).

Thus, the real primes naturally partition themselves into those that either are or are not (uniquely) representable. This is summarized in Table 5.1. Observe that the first column is essentially a table of Eisenstein primes (other

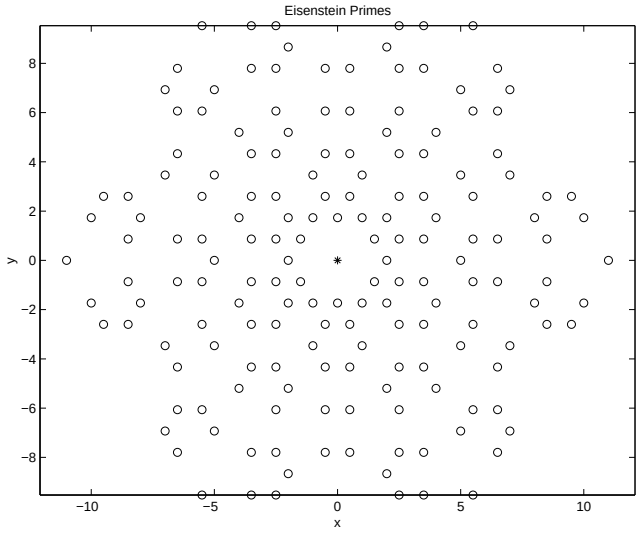

Figure 5.2: The Eisenstein Primes in the Complex Plane

than the real ones appearing in the second column and their associates) since, for example, $7 = 1^2+1\cdot 2+2^2 = (1+2\omega)(1+2\bar{\omega})$ and thus yields the Eisenstein primes $1+2\omega$ and $2+\omega$ together with all of their associates. Using the relations $\bar{\omega} = 1-\omega$ and $\omega^2 = \omega - 1$, these are $2+\omega,\ 3-\omega,\ -2-\omega,\ -3+\omega,\ -1+3\omega,\ 2-3\omega,\ 1-3\omega,\ -2+3\omega,\ 3-2\omega,\ 1+2\omega,\ -3+2\omega,\ -1-2\omega$, all lying on the ellipse $x^2+xy+y^2 = 7$ in the complex plane. In general, we have $a+b\omega,\ -a-b\omega,\ -b+(a+b)\omega,\ b-(a+b)\omega,\ (a+b)-a\omega,\ -(a+b)+a\omega,\ b+a\omega,\ -b-a\omega,\ -a+(a+b)\omega,\ a-(a+b)\omega,\ (a+b)-b\omega,\ -(a+b)+b\omega$ corresponding to each entry in the table. This table is easily constructed by putting all of the Eisenstein integers in order of increasing norm and identifying those with norm $p = 3,\ 6k+1$.

This leads us to the final tool required from number theory, the Prime Factorization Theorem. This fundamental result states that any real integer may be factored as

$$\ell = 3^{\alpha_0} \cdot \prod_{p_i \equiv 1 \pmod 6} p_i^{\alpha_i} \cdot 2^{\beta_0} \prod_{q_j \equiv -1 \pmod 6} q_j^{\beta_j}, \tag{5.13}$$

or in terms of Eisenstein primes

$$\ell = [(1+\omega)(1+\bar{\omega})]^{\alpha_0} \cdot \prod_i [(a+b\omega)(a+b\bar{\omega})]^{\alpha_i} \cdot 2^{\beta_0} \cdot \prod_j q_j^{\beta_j}, \tag{5.14}$$

in a way that is unique up to units and order of factors.

Table 5.1: Partitioning of the Primes

Representable	Non-Representable
$3 = 1^2 + 1 \cdot 1 + 1^2$	2
$7 = 1^2 + 1 \cdot 2 + 2^2$	5
$13 = 1^2 + 1 \cdot 3 + 3^2$	11
$19 = 2^2 + 2 \cdot 3 + 3^2$	17
$31 = 1^2 + 1 \cdot 5 + 5^2$	23
$37 = 3^2 + 3 \cdot 4 + 4^2$	29
$43 = 1^2 + 1 \cdot 6 + 6^2$	41
$61 = 4^2 + 4 \cdot 5 + 5^2$	47
$67 = 2^2 + 2 \cdot 7 + 7^2$	53
$73 = 1^2 + 1 \cdot 8 + 8^2$	59
$79 = 3^2 + 3 \cdot 7 + 7^2$	71
$97 = 3^2 + 3 \cdot 8 + 8^2$	83
$103 = 2^2 + 2 \cdot 9 + 9^2$	89
$109 = 5^2 + 5 \cdot 7 + 7^2$	101
$127 = 6^2 + 6 \cdot 7 + 7^2$	107
$139 = 3^2 + 3 \cdot 10 + 10^2$	113
$151 = 5^2 + 5 \cdot 9 + 9^2$	131
$157 = 1^2 + 1 \cdot 12 + 12^2$	137
$163 = 3^2 + 3 \cdot 11 + 11^2$	149

5.4 Modal Degeneracy: Answers

Armed with the tools from number theory developed in Section 5.3, we may now supply complete answers to our four questions.
1. An integer, ℓ, is representable if and only if each of the β_j (including $j = 0$) of Equation (5.13) is even, since in this and only this case Equation (5.14) may be regrouped as $\ell = (m + n\omega)(m + n\bar{\omega})$ where $m + n\omega$ is given by

$$(1+\omega)^{\gamma_0}(1+\bar{\omega})^{(\alpha_0-\gamma_0)}\prod_i (a+b\omega)^{\gamma_i}(a+b\bar{\omega})^{(\alpha_i-\gamma_i)} \cdot 2^{\beta_0/2}\prod_j q_j^{\beta_j/2}, \qquad (5.15)$$

and $m + n\bar{\omega}$ is given by

$$(1+\omega)^{(\alpha_0-\gamma_0)}(1+\bar{\omega})^{\gamma_0}\prod_i (a+b\omega)^{(\alpha_i-\gamma_i)}(a+b\bar{\omega})^{\gamma_i} \cdot 2^{\beta_0/2}\prod_j q_j^{\beta_j/2}. \qquad (5.16)$$

2. Since $(1+\omega)^{\gamma_0}(1+\bar{\omega})^{(\alpha_0-\gamma_0)}$ and $(1+\omega)^{(\alpha_0-\gamma_0)}(1+\bar{\omega})^{\gamma_0}$ are associates, factors of 3 do not increase the number of possible groupings, Equations (5.15-16). Likewise, so long as all of the β_j are even, they also do not affect the number of such groupings. Thus, it is the middle term of Equation (5.14) which alone

determines the number of ways that l is representable. Specifically, with

$$\alpha := \prod_{i=1}^{k}(\alpha_i + 1), \tag{5.17}$$

the number of essentially distinct groupings is $\alpha/2$ if α is even and $(\alpha+1)/2$ if α is odd (in which case, ℓ is either a perfect square or thrice one). In any event, the number of linearly independent modes is equal to α unless ℓ is a perfect square in which case there are $\alpha - 1$ independent TM modes and $\alpha + 1$ independent TE modes.

3. It is now straightforward to develop a general algorithm to reveal the modal structure corresponding to the frequency, Equation (5.11). Begin by factoring ℓ as in Equation (5.14) with the aid of Table 5.1. Then, perform all of the groupings described by Equations (5.15-16). This process will yield all of the possible representations of ℓ and *ipso facto* all of the modes with the given frequency.

4. From Equation (5.11), we see that there is a harmonic sequence corresponding to every integer ℓ which is representable (so that all prime factors of the form 2 or $6k-1$ must appear to an even power) which is <u>not</u> divisible by a perfect square (and hence must have no factors of the form 2 or $6k-1$ and all of the α_i $(i = 0, 1, \dots)$ in Equation (5.13) must be equal to either 0 or 1). Thus, for every seed, $s = 3^{\alpha_0} \cdot \prod_i p_i^{\alpha_i}$, with the α 's so restricted, we may construct the corresponding harmonic sequence by multiplying s by the sequence of perfect squares. Note that, in the TM case, the seed $s = 1$ is absent from its harmonic sequence which will also be missing any perfect square not divisible by any prime of the form $6k+1$. This is a consequence of $m \cdot n = 0$ which produces $\phi_{s,a}^{m,n} = 0$.

5.5 Modal Degeneracy: Examples

We now illustrate the above procedures on a collection of examples selected so as to display the variety of situations that may arise.

$\ell = \mathbf{4} = 2^2 = \underline{0^2 + 0 \cdot 2 + 2^2}$. $\alpha = 0 + 1 = 1$. Since ℓ is a perfect square, there are $\alpha - 1 = 0$ TM modes and $\alpha + 1 = 2$ TE modes: $[\psi_s^{0,2}$ & $\psi_a^{0,2}]$.

$\ell = \mathbf{21} = 3 \cdot 7 = (1+\omega)(1+\bar{\omega}) \cdot (2+\omega)(2+\bar{\omega}) =$
$(1+\omega)(2+\omega) \cdot (1+\bar{\omega})(2+\bar{\omega}) = (1+4\omega) \cdot (1+4\bar{\omega}) = \underline{1^2 + 1 \cdot 4 + 4^2}$. Thus, there are $\alpha = 1 + 1 = 2$ TM modes: $[\phi_s^{1,4}$ & $\phi_a^{1,4}]$ and 2 TE modes: $[\psi_s^{1,4}$ & $\psi_a^{1,4}]$.

$\ell = \mathbf{12} = 3 \cdot 2^2 = (1+\omega)(1+\bar{\omega}) \cdot 2^2 = (1+\omega)2 \cdot (1+\bar{\omega})2 = (2+2\omega) \cdot (2+2\bar{\omega}) =$
$\underline{2^2 + 2 \cdot 2 + 2^2}$. Thus, there is $\alpha = 0 + 1 = 1$ TM mode: $[\phi_s^{2,2}]$ and 1 TE mode: $[\psi_s^{2,2}]$.

$\ell = \mathbf{49} = 7^2 = (2+\omega)^2 \cdot (2+\bar{\omega})^2 = (3+5\omega) \cdot (3+5\bar{\omega}) = \underline{3^2 + 3 \cdot 5 + 5^2} =$
$(7 + 0\omega) \cdot (7 + 0\bar{\omega}) = \underline{0^2 + 0 \cdot 7 + 7^2}$. $\alpha = 2 + 1 = 3$. Since ℓ is a perfect

square, there are $\alpha - 1 = 2$ TM modes: $[\phi_s^{3,5}$ & $\phi_a^{3,5}]$ and $\alpha + 1 = 4$ TE modes: $[\psi_s^{0,7}$ & $\psi_a^{0,7}$ & $\psi_s^{3,5}$ & $\psi_a^{3,5}]$.

$\ell = \mathbf{189} = 3^3 \cdot 7 = 3^2[3 \cdot 7] = 3^2[1^2 + 1 \cdot 4 + 4^2] = \underline{3^2 + 3 \cdot 12 + 12^2}$. Thus, there are $\alpha = 1 + 1 = 2$ TM modes: $[\phi_s^{3,12}$ & $\phi_a^{3,12}]$ and 2 TE modes: $[\psi_s^{3,12}$ & $\psi_a^{3,12}]$.

$\ell = \mathbf{147} = 3 \cdot 7^2 = (1+\omega)(1+\bar{\omega}) \cdot (2+\omega)^2(2+\bar{\omega})^2 =$
$(1+\bar{\omega})(2+\omega)^2 \cdot (1+\omega)(2+\bar{\omega})^2 = (11+2\omega) \cdot (11+2\bar{\omega}) = \underline{2^2 + 2 \cdot 11 + 11^2} =$
$(1+\omega)(2+\omega)(2+\bar{\omega}) \cdot (1+\bar{\omega})(2+\bar{\omega})(2+\omega) = (7+7\omega) \cdot (7+7\bar{\omega}) = \underline{7^2 + 7 \cdot 7 + 7^2}$. Thus, there are $\alpha = 2 + 1 = 3$ TM modes: $[\phi_s^{7,7}$ & $\phi_s^{2,11}$ & $\phi_a^{2,11}]$ and 3 TE modes: $[\psi_s^{7,7}$ & $\psi_s^{2,11}$ & $\psi_a^{2,11}]$.

$\ell = \mathbf{91} = 7 \cdot 13 = (2+\omega)(2+\bar{\omega}) \cdot (3+\omega)(3+\bar{\omega}) = (2+\omega)(3+\omega) \cdot (2+\bar{\omega})(3+\bar{\omega}) =$
$(5+6\omega) \cdot (5+6\bar{\omega}) = \underline{5^2 + 5 \cdot 6 + 6^2} = (2+\omega)(3+\bar{\omega}) \cdot (2+\bar{\omega})(3+\omega) =$
$(9+\omega) \cdot (9+\bar{\omega}) = \underline{1^2 + 1 \cdot 9 + 9^2}$. Thus, there are $\alpha = (1+1)(1+1) = 4$ TM modes: $[\phi_s^{5,6}$ & $\phi_a^{5,6}$ & $\phi_s^{1,9}$ & $\phi_a^{1,9}]$ and 4 TE modes: $[\psi_s^{5,6}$ & $\psi_a^{5,6}$ & $\psi_s^{1,9}$ & $\psi_a^{1,9}]$.

$\ell = \mathbf{156} = 3 \cdot 13 \cdot 2^2$ belongs to the harmonic sequence sprouting from the seed $s = 3 \cdot 13 = 39$ while $\ell = \mathbf{694,575} = 3^4 \cdot 7^3 \cdot 5^2$ springs forth from $s = 7$. $\ell = \mathbf{441} = 21^2 = 3^2 \cdot 7^2$ produces both TM and TE modes while its seed $s = 1$ and sibling sprout $\ell = \mathbf{225} = 15^2 = 3^2 \cdot 5^2$ have no TM modes.

5.6 Gotthold Eisenstein

Figure 5.3: Gotthold Eisenstein

Diophantine analysis of the binary quadratic form

$$m^2 + mn + n^2 \tag{5.18}$$

has a rich history [17] having attracted the attention of, among others, Euler and Gauss. However, we have approached the problem by following the footsteps of Ferdinand Gotthold Max Eisenstein (1823-1852) [23, 71]. He was the first to use geometrical lattices of points to prove the Law of Quadratic Reciprocity, a technique later refined and further developed by Minkowski (*Geometry of Numbers*), and he made the (still unproven) conjecture that numbers of the form $2^2+1, 2^{2^2}+1, 2^{2^{2^2}}+1, \ldots$ are primes. Perhaps it would be best to simply quote Gauss [8]: "There have been only three epoch-making mathematicians: Archimedes, Newton and Eisenstein."!

Except for a brief hiatus in England, his short life centered around Berlin. When he was seventeen, he began attending the lectures of Dirichlet at the University of Berlin and by age 24 Riemann was attending his lectures on elliptic functions there. In 1845, Kummer and Jacobi arranged that he receive an honorary doctorate from the University of Breslau and, in 1847, he received his habilitation from the University of Berlin. Some idea of his mathematical fecundity is indicated by the fact that he published 25 papers in *Crelle's Journal* in the year 1844 alone. His mathematical precocity was rivaled by his musical talent and he remained an avid composer and pianist throughout his life. Eisenstein died of pulmonary tuberculosis at the age of 29.

Chapter 6

The Radiation Boundary Condition

A complete, direct, and elementary derivation of Lamé's formulas has previously been provided for the Dirichlet problem (Chapter 2 [51]) as well as the Neumann problem (Chapter 3 [52]). It is the express purpose of the present chapter to extend this previous work to the much more difficult case of the radiation (Robin) boundary condition [12, p. 695], [54]. Lamé [39, 40] presented a partial treatment of this problem when he considered eigenfunctions possessing 120° rotational symmetry. In all likelihood, Lamé avoided consideration of the complete set of eigenfunctions with Robin boundary conditions because of the attendant complexity of the transcendental equations which so arise. However, armed with the numerical and graphical capabilities of MATLAB [34, 64], we herein study the complete family of Robin eigenfunctions of the Laplacian on an equilateral triangle.

We commence by employing separation of variables in Lamé's natural triangular coordinate system to derive the eigenvalues and eigenfunctions of the Robin problem. An important feature of this derivation is the decomposition into symmetric and antisymmetric modes (eigenfunctions). The problem is then reduced to the solution of a system of transcendental equations which we treat numerically. Surprisingly, all of the modes so determined are expressible as combinations of sines and cosines.

A natural homotopy between Lamé's Neumann and Dirichlet modes is exploited not only in the derivation of the modes but is also employed to shed light on the properties of these newly derived modes. Prominent among these considerations is rotational symmetry and modal degeneracy [53]. We resort to a continuity argument in order to demonstrate orthogonality of these modes. Completeness is then established via an analytic continuation argument relying on the previously published completeness of the Neumann modes [77]. Knowing the eigenstructure permits us to construct the Robin function [18].

6.1 The Robin Eigenproblem for the Equilateral Triangle

During his investigations into the cooling of a right prism with equilateral triangular base [39, 40], Lamé was lead to consider the eigenvalue problem

$$\Delta T(x,y) + k^2 T(x,y) = 0,\ (x,y) \in \tau;\ \frac{\partial T}{\partial \nu}(x,y) + \sigma T(x,y) = 0,\ (x,y) \in \partial\tau \tag{6.1}$$

where Δ is the two-dimensional Laplacian, $\frac{\partial^2}{\partial x^2} + \frac{\partial^2}{\partial y^2}$, τ is the equilateral triangle shown in Figure 1.1, ν is its outward pointing normal, and $0 \leq \sigma < +\infty$ is a material parameter. However, he was only able to show that an eigenfunction satisfying Equation (6.1) could be expressed in terms of combinations of sines and cosines when it possesses 120° rotational symmetry. We shall find through the ensuing analysis that all of the eigenfunctions (modes) of this problem are so expressible.

The boundary condition in Equation (6.1) with $\sigma > 0$ arises when heat dissipates from a body into a surrounding medium by a combination of convection, radiation and conduction. It also appears in the study of the vibrational modes of an elastic membrane. If σ is allowed to be complex (which is prohibited herein) then the identical problem occurs also in wave propagation in acoustic ducts and electromagnetic waveguides. This is sometimes referred to as a boundary condition of the third kind. However, we will adhere to the more common moniker of Robin boundary condition even though recent researches [28, 29] indicate that this appellation is not historically justified.

Observe that in Equation (6.1) when $\sigma = 0$ we have the Neumann problem [52] while $\sigma \to +\infty$ yields the Dirichlet problem [51]. Thus, we may profitably view σ as a continuation parameter which provides a homotopy between these two well understood problems. Throughout the ensuing development we will avail ourselves of this important observation.

6.2 Construction of Modes

Before proceeding any further, we will decompose the sought after eigenfunction into parts symmetric and antisymmetric about the altitude $v = w$ (see Figure 1.3)

$$T(u,v,w) = T_s(u,v,w) + T_a(u,v,w), \tag{6.2}$$

where

$$T_s(u,v,w) = \tfrac{T(u,v,w)+T(u,w,v)}{2};\ T_a(u,v,w) = \tfrac{T(u,v,w)-T(u,w,v)}{2}, \tag{6.3}$$

henceforth to be dubbed a symmetric/antisymmetric mode, respectively. We next take up the determination of T_s and T_a separately.

6.2.1 Symmetric Modes

As shown previously, a sum of three terms of the form of Equation (1.15) is required to solve either the Neumann (Chapter 3 [52]) or Dirichlet (Chapter 2 [51]) problem. Hence, we make the Ansatz

$$\begin{aligned} T_s &= \cos[\frac{\pi\lambda}{3r}(u+2r)-\delta_1]\cdot\cos[\frac{\pi(\mu-\nu)}{9r}(v-w)] \\ &+ \cos[\frac{\pi\mu}{3r}(u+2r)-\delta_2]\cdot\cos[\frac{\pi(\nu-\lambda)}{9r}(v-w)] \\ &+ \cos[\frac{\pi\nu}{3r}(u+2r)-\delta_3]\cdot\cos[\frac{\pi(\lambda-\mu)}{9r}(v-w)], \end{aligned} \tag{6.4}$$

with

$$\lambda+\nu+\mu=0, \tag{6.5}$$

and eigenvalue

$$k^2=\frac{2}{27}(\frac{\pi}{r})^2[\lambda^2+\mu^2+\nu^2]=\frac{4}{27}(\frac{\pi}{r})^2[\mu^2+\mu\nu+\nu^2]. \tag{6.6}$$

As we shall see, this symmetric mode never vanishes identically.

Careful perusal of Equation (6.4) now reveals that for $\delta_1=\delta_2=\delta_3=0$ it reduces to a symmetric mode of the Neumann problem (Chapter 3 [52]) while for $\delta_1=-3\pi/2,\ \delta_2=\pi/2,\ \delta_3=\pi/2$ it reduces to a symmetric mode of the Dirichlet problem (Chapter 2 [51]). Thus, our task amounts to finding values of $\lambda,\ \mu,\ \nu,\ \delta_1,\ \delta_2,\ \delta_3$ so that the Robin boundary condition is satisfied along the periphery of the equilateral triangle. These values are to satisfy the constraints $-3\pi/2<\delta_1\leq 0,\ 0\leq\delta_2<\pi/2,\ 0\leq\delta_3<\pi/2;\ 0\leq\mu,\ 0\leq\nu$, as well as Equation (6.5).

Imposition of the Robin boundary condition along $u=r$ yields

$$\tan(\lambda-\delta_1)=\frac{3\sigma r}{\pi\lambda},\ \tan(\mu-\delta_2)=\frac{3\sigma r}{\pi\mu},\ \tan(\nu-\delta_3)=\frac{3\sigma r}{\pi\nu}, \tag{6.7}$$

while imposition along $v=r$ yields

$$\tan(-\frac{\delta_2+\delta_3}{2})=\frac{3\sigma r}{\pi\lambda},\ \tan(-\frac{\delta_3+\delta_1}{2})=\frac{3\sigma r}{\pi\mu},\ \tan(-\frac{\delta_1+\delta_2}{2})=\frac{3\sigma r}{\pi\nu}. \tag{6.8}$$

By symmetry, the boundary condition along $w=r$ will thereby be automatically satisfied.

Introducing the auxiliary variables, $L,\ M,\ N$, while collecting together these equations produces

$$\begin{aligned} \tan(\lambda-\delta_1)=\tan(-\frac{\delta_2+\delta_3}{2})=\frac{3\sigma r}{\pi\lambda}=\tan L \quad &, \quad -\frac{\pi}{2}<L\leq 0 \\ \tan(\mu-\delta_2)=\tan(-\frac{\delta_3+\delta_1}{2})=\frac{3\sigma r}{\pi\mu}=\tan M \quad &, \quad 0\leq M<\frac{\pi}{2} \\ \tan(\nu-\delta_3)=\tan(-\frac{\delta_1+\delta_2}{2})=\frac{3\sigma r}{\pi\nu}=\tan N \quad &, \quad 0\leq N<\frac{\pi}{2} \end{aligned} \tag{6.9}$$

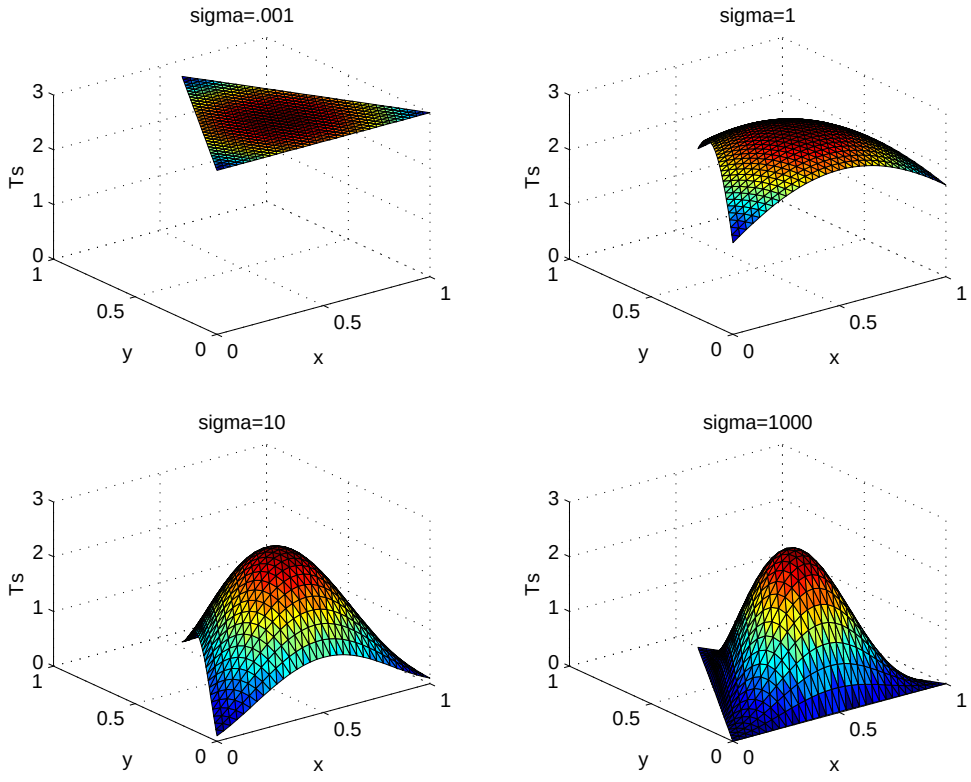

Figure 6.1: $(0,0)$ Symmetric Mode

and these six equations may in turn be reduced to the solution of the system of three transcendental equations for $L,\ M,\ N$

$$\begin{aligned} [2L - M - N - (m+n)\pi] \cdot \tan L &= 3\sigma r \\ [2M - N - L + m\pi] \cdot \tan M &= 3\sigma r \\ [2N - L - M + n\pi] \cdot \tan N &= 3\sigma r \end{aligned} \tag{6.10}$$

where $m = 0, 1, 2, \ldots,\ n = m, m+1, \ldots$.

Once $L,\ M,\ N$ have been numerically approximated, e.g. using MATLAB [34, 64], the parameters of primary interest may then be determined as

$$\delta_1 = L - M - N;\ \delta_2 = -L + M - N;\ \delta_3 = -L - M + N, \tag{6.11}$$

and

$$\lambda = \tfrac{2L-M-N}{\pi} - m - n;\ \mu = \tfrac{2M-N-L}{\pi} + m;\ \nu = \tfrac{2N-L-M}{\pi} + n. \tag{6.12}$$

For future reference, when $m = n$ we have $M = N$, $\delta_2 = \delta_3$, $\mu = \nu$, and $2\pi\mu = \delta_2 - \delta_1 + 2m\pi$.

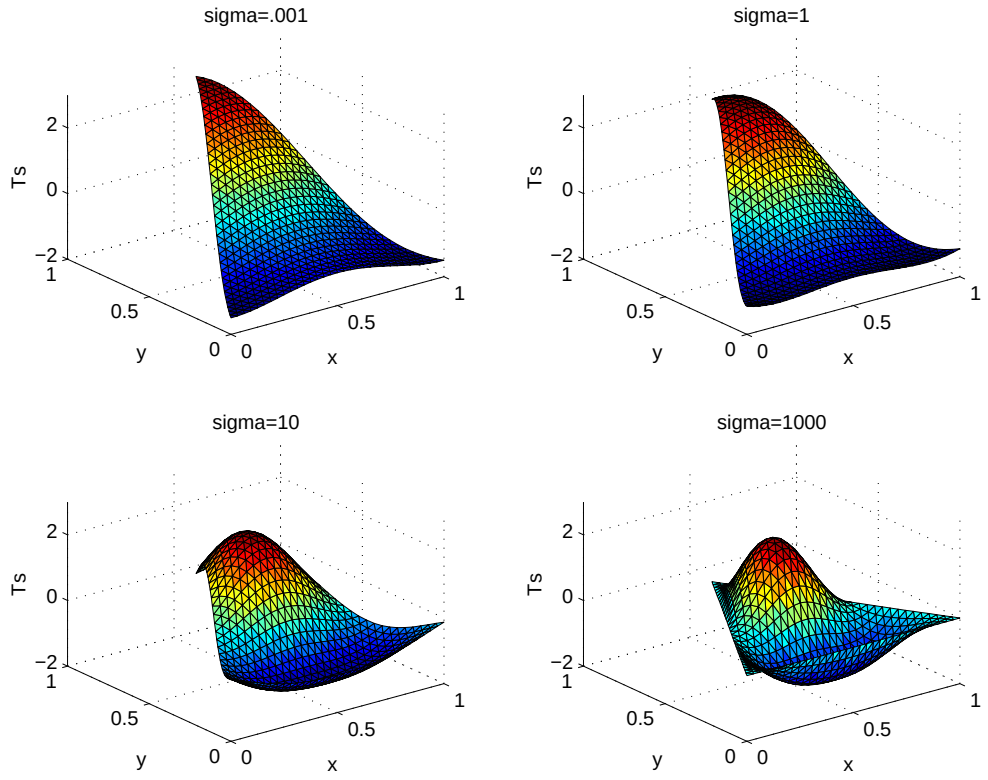

Figure 6.2: $(0, 1)$ Symmetric Mode

Of particular interest are the following limits. As $\sigma \to 0^+$, we find that L, M, N each approach 0, as do $\delta_1, \delta_2, \delta_3$, and, most significantly, $\lambda \to -(m + n), \mu \to m, \nu \to n$. In other words, we recover in this limit the Neumann modes. Furthermore, as $\sigma \to +\infty$, we find that $L \to -\pi/2, M \to \pi/2, N \to \pi/2$ and $\delta_1 \to -3\pi/2, \delta_2 \to \pi/2, \delta_3 \to \pi/2$, and, most significantly, $\lambda \to -2-(m+n), \mu \to m+1, \nu \to n+1$. In other words, we recover in this limit the Dirichlet modes. Thus, we have successfully fulfilled our original Ansatz and thereby constructed a homotopy leading from the symmetric Neumann modes to the symmetric Dirichlet modes. Moreover, we have indexed our symmetric Robin modes, $T_s^{m,n}$, which are given by Equation (6.4) in correspondence with the symmetric Neumann modes with the result that, as σ ranges from 0 to $+\infty$, the (m, n) symmetric Neumann mode "morphs" continuously (in fact, analytically!) into the $(m + 1, n + 1)$ symmetric Dirichlet mode.

Figure 6.1 shows the plane wave $(0, 0)$ mode morphing into the fundamental $(1, 1)$ Dirichlet mode. Figure 6.2 displays the $(0, 1)$ symmetric mode.

6.2.2 Antisymmetric Modes

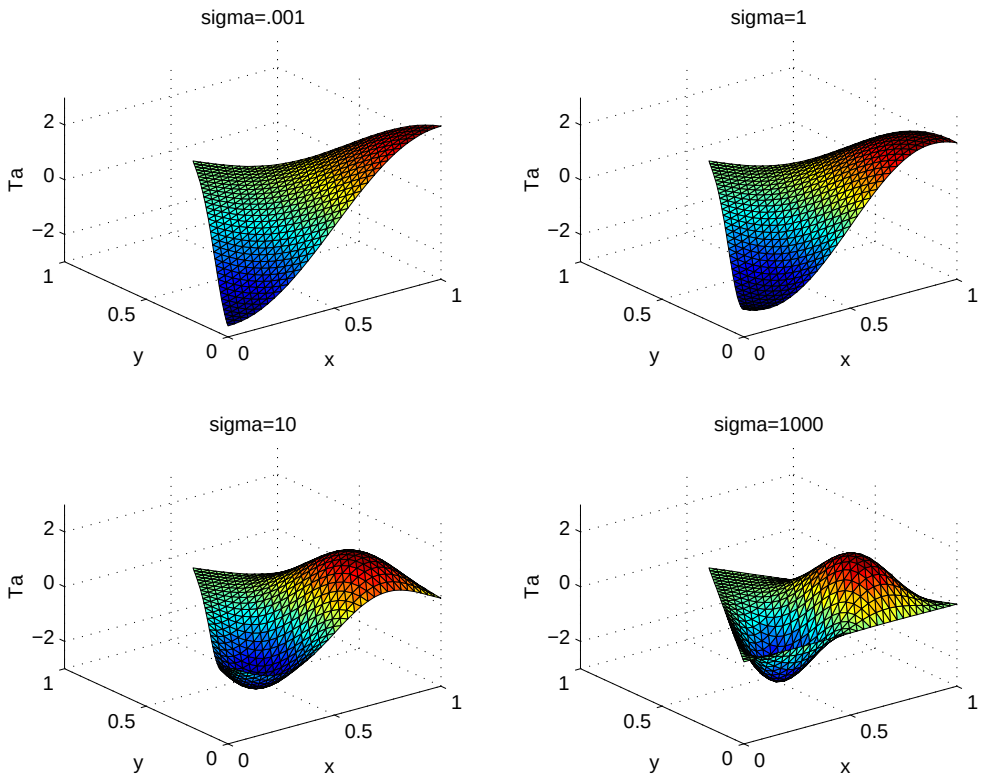

Figure 6.3: $(0, 1)$ Antisymmetric Mode

A parallel development is possible for the determination of an antisymmetric mode. In light of the oddness of T_a as a function of $v - w$, we commence with an Ansatz of the form

$$\begin{aligned} T_a &= \cos[\frac{\pi\lambda}{3r}(u+2r) - \delta_1] \cdot \sin[\frac{\pi(\mu-\nu)}{9r}(v-w)] \\ &+ \cos[\frac{\pi\mu}{3r}(u+2r) - \delta_2] \cdot \sin[\frac{\pi(\nu-\lambda)}{9r}(v-w)] \\ &+ \cos[\frac{\pi\nu}{3r}(u+2r) - \delta_3] \cdot \sin[\frac{\pi(\lambda-\mu)}{9r}(v-w)]. \end{aligned} \tag{6.13}$$

Once again, $\lambda+\mu+\nu = 0$ and $k^2 = \frac{2}{27}(\frac{\pi}{r})^2[\lambda^2+\mu^2+\nu^2] = \frac{4}{27}(\frac{\pi}{r})^2[\mu^2+\mu\nu+\nu^2]$. However, this antisymmetric mode may vanish identically.

Equations (6.7)-(6.12) still obtain so that, for a given m and n, $\{\lambda,\ \mu,\ \nu\}$ and $\{\delta_1,\ \delta_2,\ \delta_3\}$ are the same for the symmetric, $T_s^{m,n}$, and antisymmetric, $T_a^{m,n}$, modes which are given by Equation (6.13). In particular, the comments made above concerning indexing of modes and "mode-morphing" also apply here. Figure 6.3 displays the $(0, 1)$ antisymmetric mode.

6.3 Modal Properties

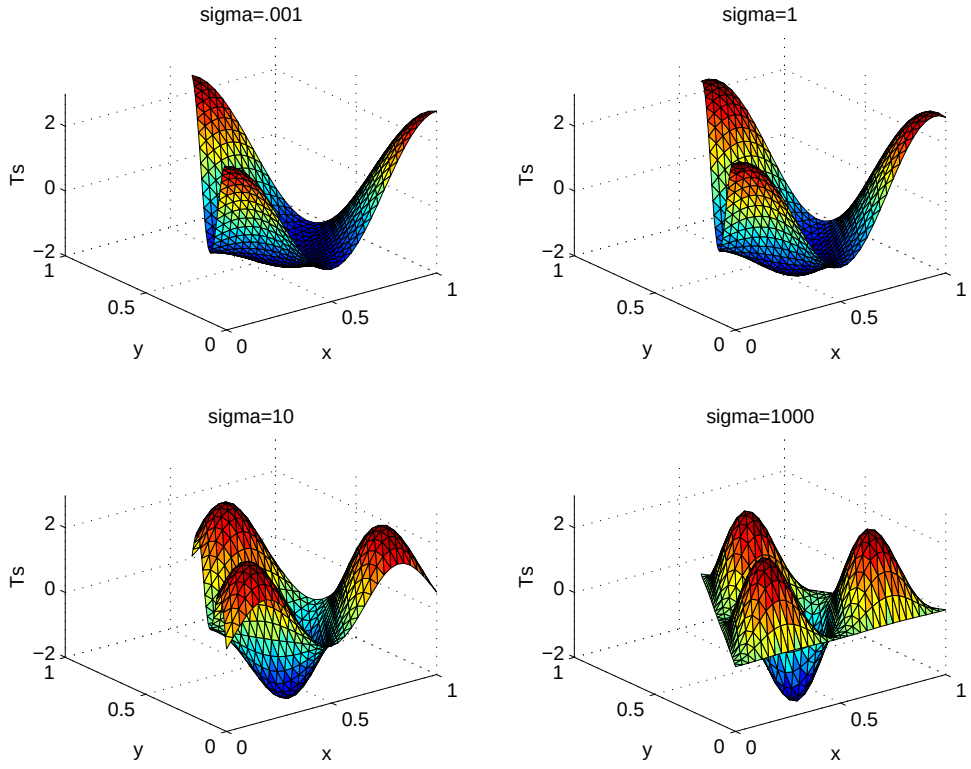

Figure 6.4: $(1,1)$ Symmetric Mode

In what follows, it will be convenient to have the following alternative representations of our Robin modes

$$\begin{aligned} T_s^{m,n} = \frac{1}{2} \quad \{ \quad & \cos\left[\frac{2\pi}{9r}(\lambda u + \mu v + \nu w + 3\lambda r) - \delta_1\right] \\ + \quad & \cos\left[\frac{2\pi}{9r}(\nu u + \mu v + \lambda w + 3\nu r) - \delta_3\right] \\ + \quad & \cos\left[\frac{2\pi}{9r}(\mu u + \nu v + \lambda w + 3\mu r) - \delta_2\right] \\ + \quad & \cos\left[\frac{2\pi}{9r}(\mu u + \lambda v + \nu w + 3\mu r) - \delta_2\right] \\ + \quad & \cos\left[\frac{2\pi}{9r}(\nu u + \lambda v + \mu w + 3\nu r) - \delta_3\right] \\ + \quad & \cos\left[\frac{2\pi}{9r}(\lambda u + \nu v + \mu w + 3\lambda r) - \delta_1\right]\}, \end{aligned} \tag{6.14}$$

$$\begin{aligned} T_a^{m,n} = \frac{1}{2} \quad \{ \quad & \sin[\frac{2\pi}{9r}(\lambda u + \mu v + \nu w + 3\lambda r) - \delta_1] \\ - \quad & \sin[\frac{2\pi}{9r}(\nu u + \mu v + \lambda w + 3\nu r) - \delta_3] \\ + \quad & \sin[\frac{2\pi}{9r}(\mu u + \nu v + \lambda w + 3\mu r) - \delta_2] \\ - \quad & \sin[\frac{2\pi}{9r}(\mu u + \lambda v + \nu w + 3\mu r) - \delta_2] \\ + \quad & \sin[\frac{2\pi}{9r}(\nu u + \lambda v + \mu w + 3\nu r) - \delta_3] \\ - \quad & \sin[\frac{2\pi}{9r}(\lambda u + \nu v + \mu w + 3\lambda r) - \delta_1]\}, \end{aligned} \tag{6.15}$$

obtained from Equation (6.4) and Equation (6.13), respectively, by the application of appropriate trigonometric identities.

We may pare the collection of antisymmetric Robin modes through the following observation.

Theorem 6.3.1. *1. $T_s^{m,n}$ never vanishes identically.*

2. $T_a^{m,n}$ vanishes identically if and only if m=n.

Proof. 1. Note that a symmetric mode is identically zero iff it vanishes along the line of symmetry $v = w$, since the only function both symmetric and antisymmetric is the zero function. Along $v = w$,

$$\begin{aligned} T_s^{m,n} \quad = \quad & \cos[\frac{\pi(\mu+\nu)}{3r}(u+2r) - \delta_1] + \cos[\frac{\pi\mu}{3r}(u+2r) - \delta_2] \\ + \quad & \cos[\frac{\pi\nu}{3r}(u+2r) - \delta_3], \end{aligned} \tag{6.16}$$

which cannot vanish identically for $-2r \leq u \leq r$.

2. Note that an antisymmetric mode is identically zero iff its normal derivative vanishes along the line of symmetry $v = w$, since the only function both antisymmetric and symmetric is the zero function. Along $v = w$,

$$\begin{aligned} \frac{\partial T_a^{m,n}}{\partial(v-w)} \quad = \quad & \frac{\pi(\mu-\nu)}{9r}\cos[\frac{\pi(\mu+\nu)}{3r}(u+2r) + \delta_1] \\ + \quad & \frac{\pi(\mu+2\nu)}{9r}\cos[\frac{\pi\mu}{3r}(u+2r) - \delta_2] \\ - \quad & \frac{\pi(2\mu+\nu)}{9r}\cos[\frac{\pi\nu}{3r}(u+2r) - \delta_3]. \end{aligned} \tag{6.17}$$

This equals zero iff $m = n$.

□

Hence, our system of eigenfunctions is $\{T_s^{m,n}\ (n \geq m);\ T_a^{m,n}\ (n > m)\}$. Figure 6.4 shows the $(1,1)$ mode whereas the symmetric and antisymmetric $(0,2)$ modes are displayed in Figures 6.5 and 6.6, respectively, while the symmetric and antisymmetric $(1,2)$ modes are displayed in Figures 6.7 and 6.8, respectively.

We next give the case $m = n$ further consideration. Recall that we have just determined that $T_a^{m,m} \equiv 0$. Furthermore, in this case, we may combine the terms of Equation (6.14) to yield

$$T_s^{m,m} = \cos[\tfrac{2\pi\mu}{3r}(r-u) - \delta_2] + \cos[\tfrac{2\pi\mu}{3r}(r-v) - \delta_2] + \cos[\tfrac{2\pi\mu}{3r}(r-w) - \delta_2], \tag{6.18}$$

which clearly illustrates that any permutation of (u, v, w) leaves $T_s^{m,m}$ invariant. This is manifested geometrically in the invariance of $T_s^{m,m}$ under a 120° rotation about the triangle center (see Figure 6.4). This invariance will henceforth be termed rotational symmetry.

Moreover, the modes $T_s^{m,m}$ are not the only ones that are rotationally symmetric.

Theorem 6.3.2. *1. $T_s^{m,n}$ is rotationally symmetric if and only if $m \equiv n(\equiv l)$ (mod3).*

2. $T_a^{m,n}$ is rotationally symmetric if and only if $m \equiv n(\equiv l)$ (mod3).

Proof. 1. $T_s^{m,n}$ is rotationally symmetric iff it is symmetric about the line $v = u$. This can occur iff the normal derivative, $\frac{\partial T_s^{m,n}}{\partial \nu}$ vanishes there. Thus, we require that

$$\begin{aligned}
\frac{\partial T_s^{m,n}}{\partial(v-u)}|_{v=u} = -\frac{1}{4} \quad \{ \quad & (2\mu+\nu)\sin[\frac{2\pi}{3r}(-\nu u - (\mu+\nu)r) - \delta_1] \\
+ \quad & (\mu-\nu)\sin[\frac{2\pi}{3r}((\mu+\nu)u + \nu r) - \delta_3] \\
- \quad & (\mu-\nu)\sin[\frac{2\pi}{3r}((\mu+\nu)u + \mu r) - \delta_2] \\
- \quad & (2\mu+\nu)\sin[\frac{2\pi}{3r}(-\nu u + \mu r) - \delta_2] \\
- \quad & (\mu+2\nu)\sin[\frac{2\pi}{3r}(-\mu u + \nu r) - \delta_3] \\
+ \quad & (\mu+2\nu)\sin[\frac{2\pi}{3r}(-\mu u - (\mu+\nu)r) - \delta_1]\} = 0,
\end{aligned} \tag{6.19}$$

derived from Equation (6.14). These terms cancel pairwise iff $m \equiv n(\equiv l)$ (mod3).

2. $T_a^{m,n}$ is rotationally symmetric iff it is antisymmetric about the line $v = u$. This can occur iff $T_a^{m,n}$ vanishes there. Thus, we require that

$$\begin{aligned} T_a^{m,n}|_{v=u} = \frac{1}{2} \quad \{ \quad & \sin[\frac{2\pi}{3r}(-\nu u - (\mu+\nu)r) - \delta_1] \\ - \quad & \sin[\frac{2\pi}{3r}((\mu+\nu)u + \nu r) - \delta_3] \\ + \quad & \sin[\frac{2\pi}{3r}((\mu+\nu)u + \mu r) - \delta_2] \\ - \quad & \sin[\frac{2\pi}{3r}(-\nu u + \mu r) - \delta_2] \\ + \quad & \sin[\frac{2\pi}{3r}(-\mu u + \nu r) - \delta_3] \\ - \quad & \sin[\frac{2\pi}{3r}(-\mu u - (\mu+\nu)r) - \delta_1]\} = 0, \end{aligned} \tag{6.20}$$

derived from Equation (6.15). These terms cancel pairwise iff $m \equiv n(\equiv l)\ (\mathrm{mod} 3)$.

□

This is illustrated in Figures 6.9 and 6.10 which display the symmetric and antisymmetric $(0, 3)$ modes, respectively.

6.4 Spectral Properties

The modal frequencies, $f_{m,n}$, are proportional to the square root of the eigenvalues given by Equation (6.6). Hence, we have

$$f_{m,n} \propto \frac{4\pi}{3h}\chi;\ \chi^2 := \mu^2 + \mu\nu + \nu^2. \tag{6.21}$$

Thus, the spectral structure of the equilateral triangle hinges upon the properties of the spectral parameter χ^2.

This spectral parameter is shown for the first 29 modes in Figure 6.11 as σ ranges from 0 to $+\infty$. The left side corresponds to the Neumann modes ($\sigma = 0$) and the right side corresponds to the Dirichlet modes ($\sigma = +\infty$). Thus, this figure graphically displays the homotopy relating these two well understood eigenvalue problems.

The monotonicity of these curves is apparent and easily established from the identity

$$\frac{d\ \chi^2}{d\ \sigma} = (2\mu+\nu)\frac{d\ \mu}{d\ \sigma} + (\mu+2\nu)\frac{d\ \nu}{d\ \sigma} \geq 0, \tag{6.22}$$

since (μ, ν) increase monotonically from (m, n) to $(m+1, n+1)$ as σ varies from 0 to $+\infty$.

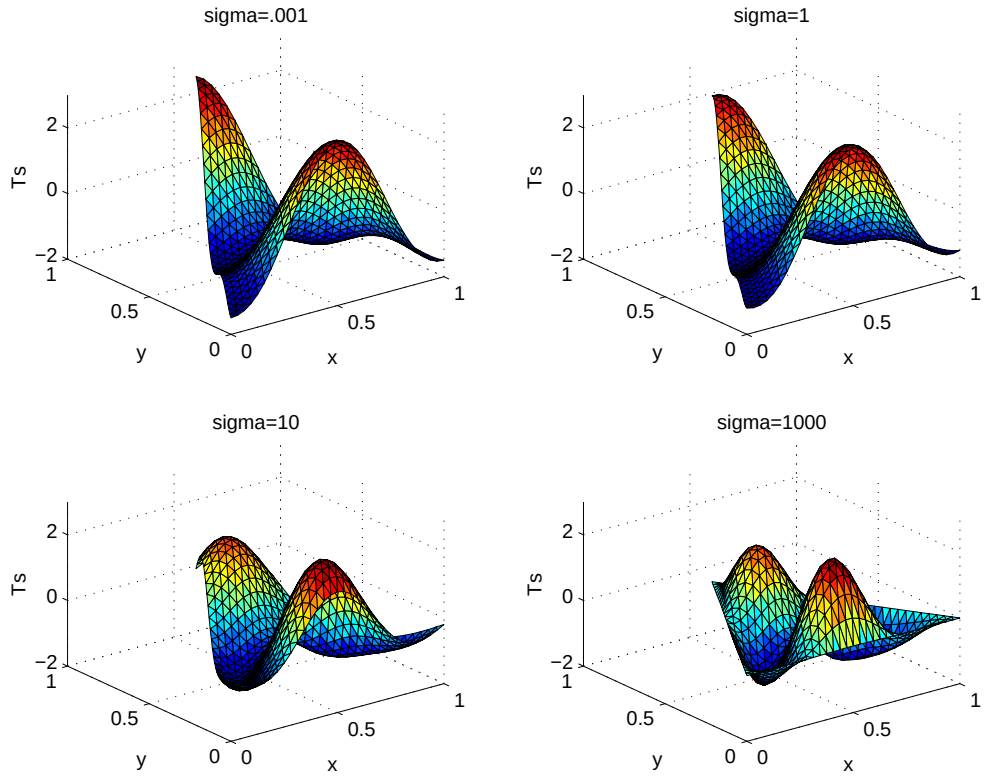

Figure 6.5: $(0, 2)$ Symmetric Mode

Since $T_s^{m,n}$ and $T_a^{m,n}$ both correspond to the same frequency $f_{m,n}$ given by Equation (6.21), it follows that all eigenvalues corresponding to $m \neq n$ have multiplicity equal to at least two. However, this modal degeneracy, as it is known in the engineering literature, extends also to the case $m = n$. Modal degeneracy is manifested in Figure 6.11 as an intersection of two modal curves. For the Dirichlet and Neumann problems, number theoretic techniques permit a comprehensive treatment of such spectral multiplicity (Chapter 5 [53]).

However, for the Robin problem μ and ν are not integers and such techniques fail. At the present time, no general results are available and one must resort to perusal of Figure 6.11 in order to locate modal degeneracies for $0 < \sigma < +\infty$. All one can say with certainty is that if (m_1, n_1) and (m_2, n_2) are modal indices satisfying the inequalities

$$0 < (m_2^2 + m_2 n_2 + n_2^2) - (m_1^2 + m_1 n_1 + n_1^2) < 3[(m_1 + n_1) - (m_2 + n_2)] \quad (6.23)$$

then the corresponding modal curves must intersect for some value of σ which will thereby generate a corresponding modal degeneracy.

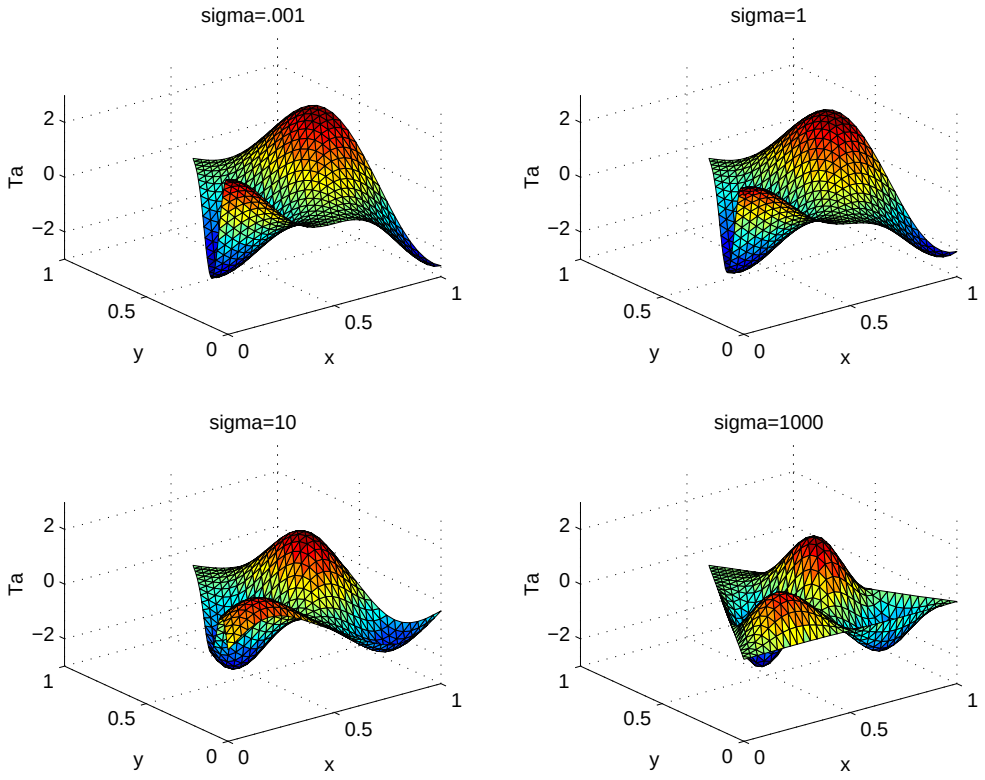

Figure 6.6: $(0, 2)$ Antisymmetric Mode

6.5 Orthogonality

By Rellich's Theorem [44], eigenfunctions corresponding to distinct eigenvalues are guaranteed to be orthogonal. Also, a symmetric mode and an antisymmetric mode are automatically orthogonal. However, as we discovered above, the multiplicity of the eigenvalues given by Equation (6.6) is quite a complicated matter. Thus, we invoke the following continuity argument in order to confirm the orthogonality of our collection of eigenfunctions $\{T_s^{m,n}\ (n \geq m);\ T_a^{m,n}\ (n > m)\}$.

Suppose that f and g are eigenfunctions of like parity that share an eigenvalue, k^2, for some fixed value of $\sigma = \hat{\sigma}$. This corresponds to an intersection of two spectral curves in Figure 8.1. For σ in the neighborhood of $\hat{\sigma}$, Rellich's theorem guarantees that $\langle f, g \rangle = \int \int_\tau fg\ dA = 0$. Thus, by continuity, $\langle f, g \rangle = 0$ for $\sigma = \hat{\sigma}$ and orthogonality of our full collection of Robin modes is assured. Note that this same continuity argument may be employed to demonstrate the orthogonality of the Robin eigenfunctions for other differential operators on other domains.

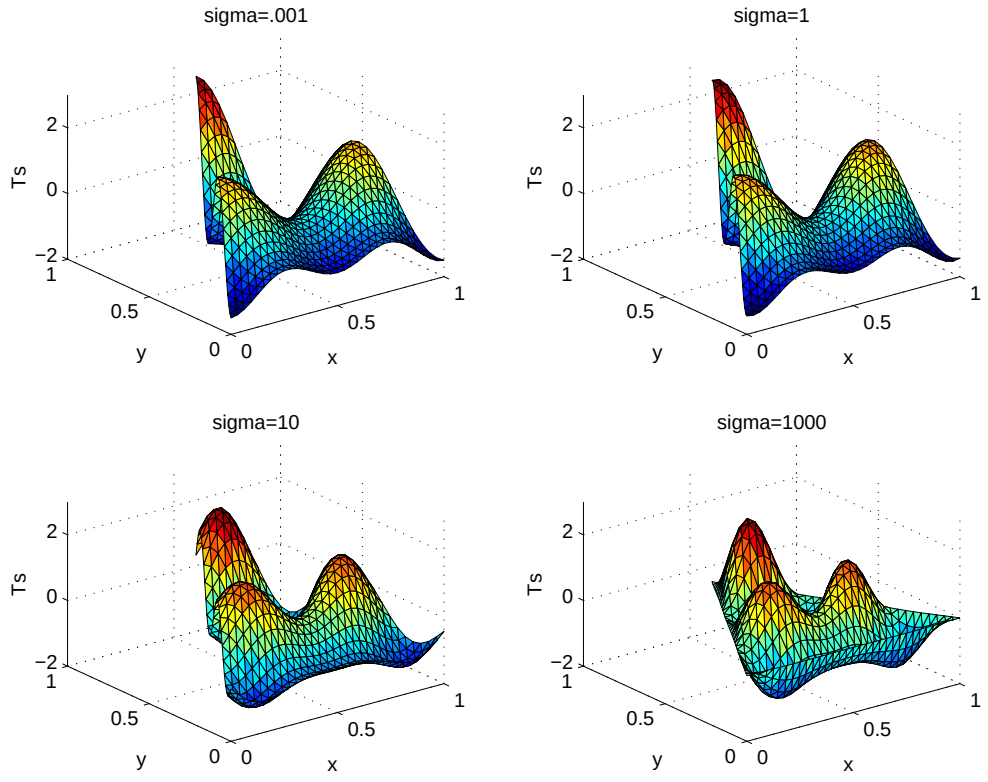

Figure 6.7: $(1, 2)$ Symmetric Mode

6.6 Completeness

It is not *a priori* certain that the collection of eigenfunctions $\{T_s^{m,n},\ T_a^{m,n}\}$ constructed above is complete. For domains which are the Cartesian product of intervals in an orthogonal coordinate system, such as rectangles and annuli, completeness of the eigenfunctions formed from products of one-dimensional counterparts has been established [88]. Since the equilateral triangle is not such a domain, we must employ other devices in order to establish completeness.

We will utilize an analytic continuation argument which hinges upon the previously established completeness of the Neumann modes [77]. The homotopy between the Neumann and Dirichlet modes that we have established above guarantees a unique branch leading from each of the Neumann modes to its corresponding Dirichlet mode. Likewise, for any $0 < \sigma < \infty$ we may trace out a branch from any mode leading back to a Neumann mode as $\sigma \to 0^+$.

Suppose, for the sake of argument, that the collection of Robin modes constructed above is not complete for some $0 < \sigma = \hat{\sigma} < \infty$. Then, let $u(x, y; \hat{\sigma})$ be a mode that is not contained in our collection. As we have a self-adjoint operator, there exist ℓ analytic branches emanating from this point in

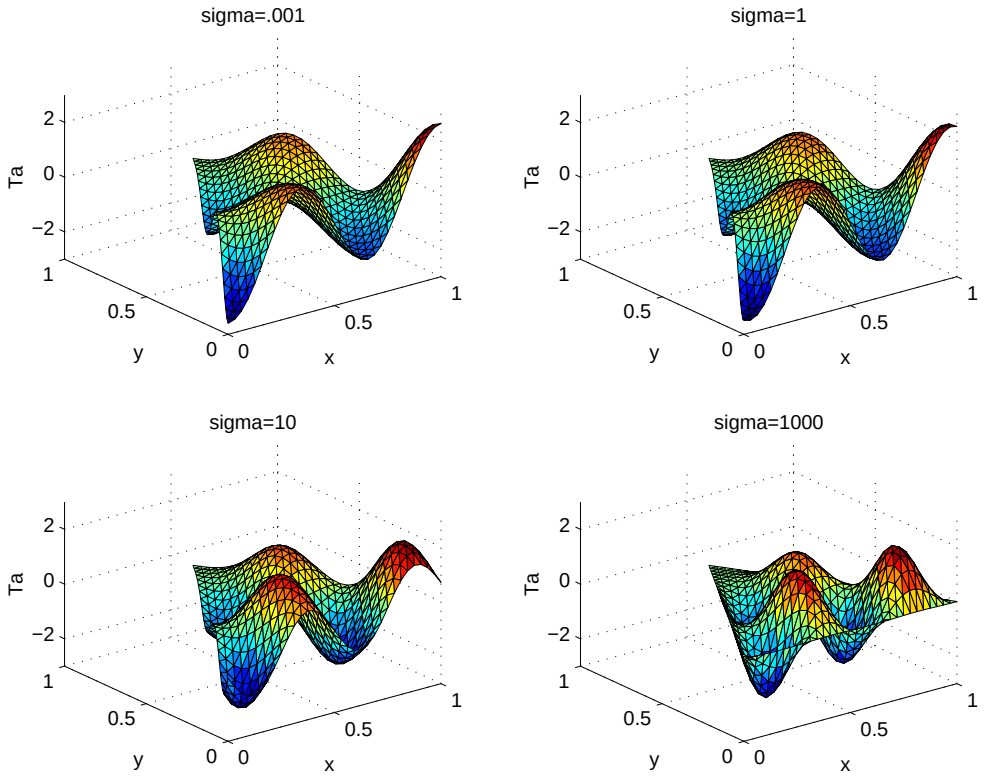

Figure 6.8: $(1,2)$ Antisymmetric Mode

Hilbert space where ℓ is the multiplicity of $k^2(\hat{\sigma})$ [22, pp. 92-94]. Denote any of these branches, analytically continued back to $\sigma = 0$ as $u(x,y;\sigma)$. Since we know that the collection of Neumann modes is complete, this branch must at some point, $\sigma = \sigma^*$, coalesce with a branch emanating from one of our Robin modes.

However, as we now show, the analytic dependence of $u(x,y;\sigma)$ upon σ prohibits such a bifurcation at $\sigma = \sigma^*$. To see this, let

$$\Delta u + k^2 u = 0,\ (x,y) \in \tau;\ \frac{\partial u}{\partial \nu} + \sigma u = 0,\ (x,y) \in \partial\tau. \tag{6.24}$$

Then

$$u(x,y;\sigma) = u(x,y;\sigma^*) + u'(x,y;\sigma^*)\cdot(\sigma-\sigma^*) + u''(x,y;\sigma^*)\cdot\tfrac{(\sigma-\sigma^*)^2}{2} + \cdots, \tag{6.25}$$

where $u' := \frac{\partial\ u}{\partial\ \sigma}$ and each of the correction terms in the Taylor series is orthogonal to the eigenspace of $k^2(\sigma^*)$.

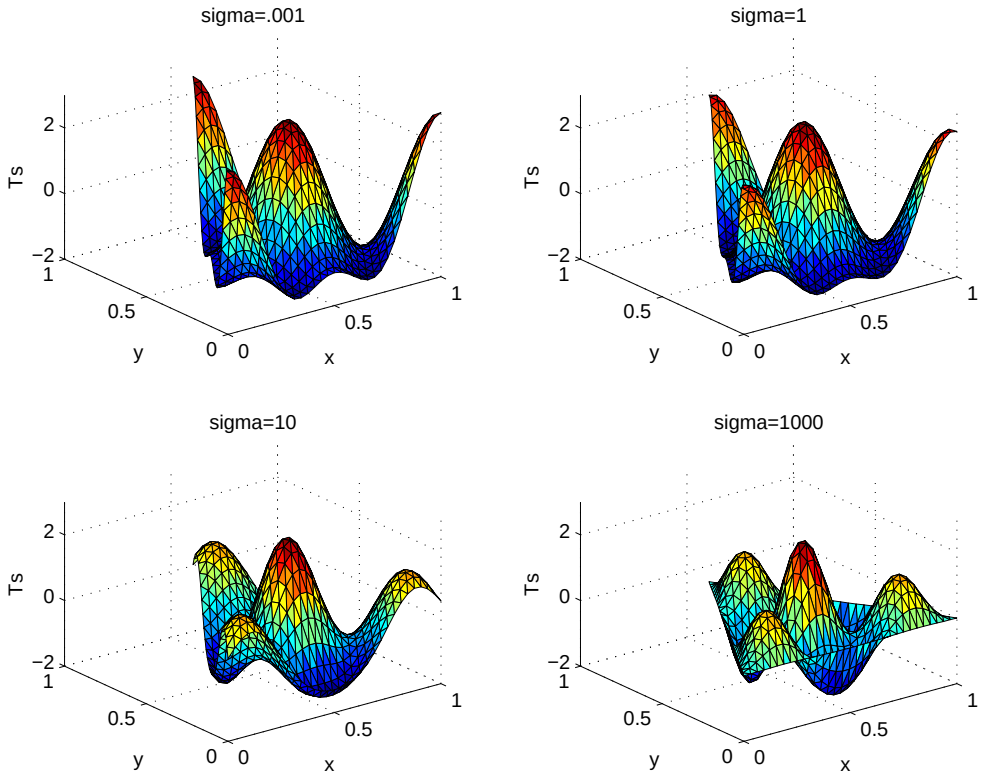

Figure 6.9: $(0,3)$ Symmetric Mode

Each of the Taylor coefficients satisfies the boundary value problem

$$\Delta u^{(n)}(x,y;\sigma^*) + k^2(\sigma^*)u^{(n)}(x,y;\sigma^*) = 0,\ (x,y) \in \tau, \quad (6.26)$$
$$\frac{\partial u^{(n)}}{\partial \nu}(x,y;\sigma^*) + \sigma^* u^{(n)}(x,y;\sigma^*) = -nu^{(n-1)}(x,y;\sigma^*),\ (x,y) \in \partial\tau,$$

which may be solved recursively and uniquely for $u', u'', \ldots, u^{(n)}, \ldots$ since they are each orthogonal to the eigenspace of k^2. Thus, $u(x,y;\sigma)$ is uniquely determined and bifurcation cannot transpire. Consequently, our collection of Robin modes is indeed complete. Note that this same analytic continuation argument may be invoked to establish the completeness of the Robin eigenfunctions for other differential operators on other domains once completeness of the corresponding Neumann eigenfunctions has been certified.

6.7 Robin Function

Using Equations (6.14) and (6.15), we may define the orthonormal system

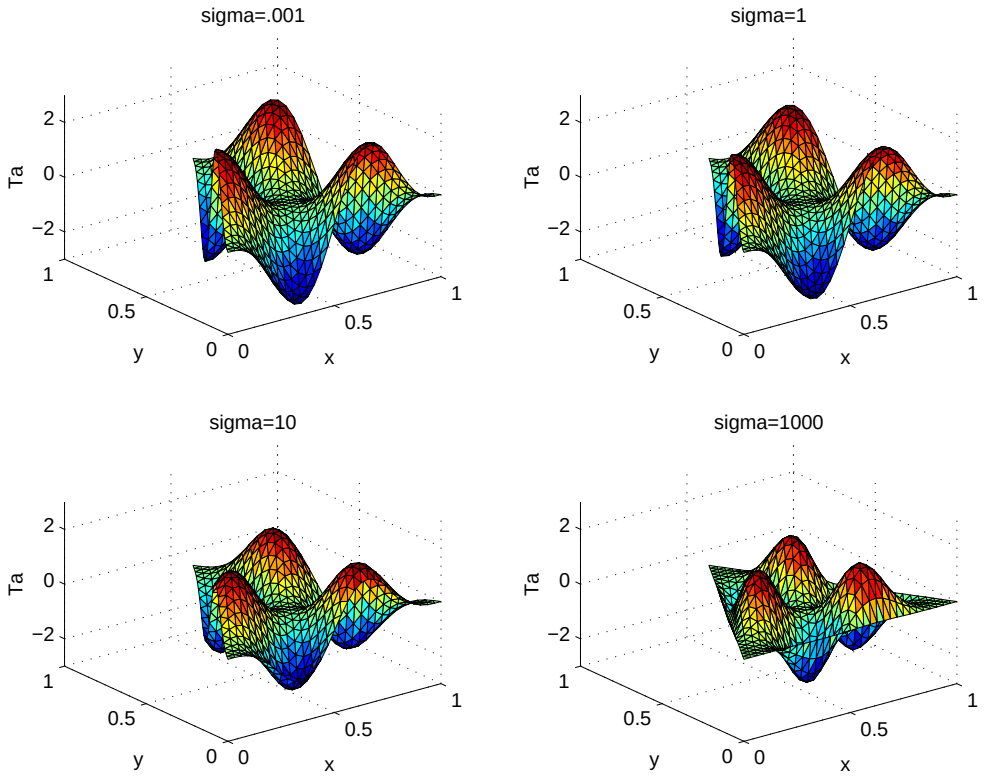

Figure 6.10: $(0,3)$ Antisymmetric Mode

of eigenfunctions

$$\phi_s^{m,n} = \frac{T_s^{m,n}}{\|T_s^{m,n}\|} \ (m = 0, 1, 2, \dots;\ n = m, \dots), \tag{6.27}$$

$$\phi_a^{m,n} = \frac{T_a^{m,n}}{\|T_a^{m,n}\|} \ (m = 0, 1, 2, \dots;\ n = m+1, \dots), \tag{6.28}$$

together with their corresponding eigenvalues

$$\lambda_{m,n} = \frac{4\pi^2}{27r^2}(\mu^2 + \mu\nu + \nu^2) \ (m = 0, 1, 2, \dots;\ n = m, \dots). \tag{6.29}$$

The Green's function [82] for the Laplacian with Robin boundary conditions (the Robin function [18]) on an equilateral triangle is then constructed as

$$\begin{aligned} G(x, y; x', y') &= \sum_{m=1}^{\infty} \frac{\phi_s^{m,m}(x, y)\phi_s^{m,m}(x', y')}{\lambda_{m,m}} \\ &+ \sum_{m=0}^{\infty} \sum_{n=m+1}^{\infty} \frac{\phi_s^{m,n}(x, y)\phi_s^{m,n}(x', y') + \phi_a^{m,n}(x, y)\phi_a^{m,n}(x', y')}{\lambda_{m,n}} \end{aligned} \tag{6.30}$$

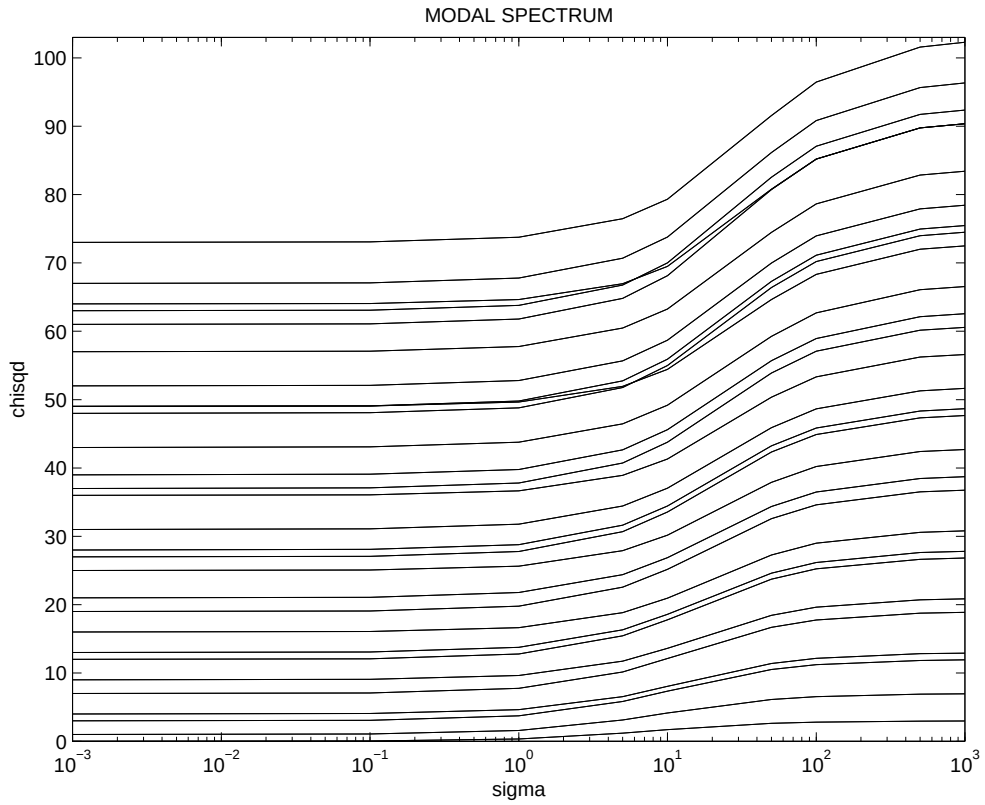

Figure 6.11: Spectral Parameter

This may be employed in the usual fashion to solve the corresponding nonhomogeneous boundary value problem [18].

6.8 Victor Gustave Robin

Victor Gustave Robin (1855-1897), the eponym for the third boundary condition, was a French mathematical analyst and Applied Mathematician who lectured in Mathematics at the Sorbonne in Paris and also worked in the area of thermodynamics [28, 29]. Amazingly, searches through the archives of Paris have turned up absolutely no information about him other than his birthdate, May 17. Historians of Mathematics have been unable to obtain either his obituary or a photograph or portrait of him. His collected works were published in the period 1899-1903 and they clearly indicate that he in fact had no involvement whatsoever with the third boundary condition which is named after him. The first known such reference is by Stefan Bergman in 1948 where the kernel function satisfying the third boundary condition is called Robin's function.

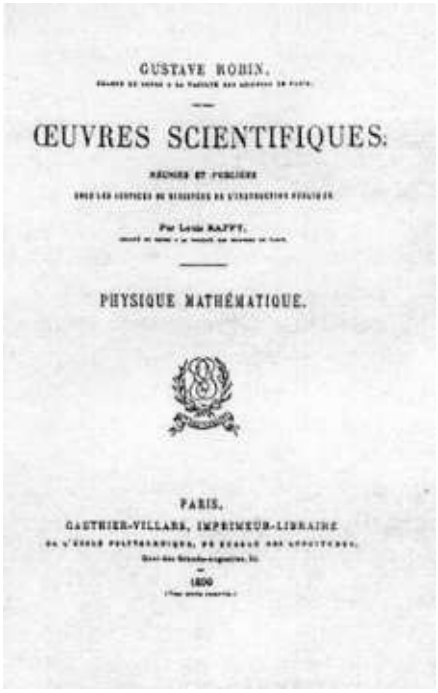
GUSTAVE ROBIN.

ŒUVRES SCIENTIFIQUES.

PHYSIQUE MATHÉMATIQUE.

PARIS.
GAUTHIER-VILLARS, IMPRIMEUR-LIBRAIRE

Figure 6.12: Victor Gustave Robin: Collected Works

His doctoral thesis of 1886 on single- and double-layer potentials for boundary value problems of electrostatics, written under the supervision of Émile Picard, has been his most enduring contribution to Applied Mathematics. (His thesis committee had an all-star cast: Picard, Hermite and Darboux!) It is believed that it was on the basis of this work that Robin's name was later placed on the third boundary condition. He also applied this technique to hydrodynamics and provided some mathematical foundation for thermodynamics which gave rise to Robin's Constant in complex function theory. Idiosyncratically, he also proposed a foundation for analysis utilizing only rational numbers! He died in Paris, aged 42.

Chapter 7

The Absorbing Boundary Condition

A complete, direct, and elementary derivation of Lamé's formulas has previously been provided for the Dirichlet problem (Chapter 2 [51]) as well as the Neumann problem (Chapter 3 [52]). This was subsequently extended to the Robin problem with a radiation boundary condition (Chapter 6 [54]). It is the express purpose of the present chapter to extend this previous work to the much more difficult case of the Robin problem with an absorbing boundary condition [12, p. 698], [55]. (This is sometimes called the Steklov problem [28].) The principal analytical difficulty that must be overcome is that, unlike the case of a radiation boundary condition, the eigenvalues, while still real, may now be negative. The presence of these negative eigenvalues has the unfortunate consequence of destroying the natural homotopy between Lamé's Neumann and Dirichlet modes which was so heavily exploited in the prior investigation of the radiation boundary condition (Chapter 6 [54]).

We commence by employing separation of variables in Lamé's natural triangular coordinate system to derive the eigenvalues and eigenfunctions of the Robin problem with an absorbing boundary condition (ABC). An important feature of this derivation is the decomposition into symmetric and antisymmetric modes (eigenfunctions). The problem is then reduced to the solution of a system of transcendental equations which we treat numerically using MATLAB [34, 64]. Surprisingly, all of the modes so determined (henceforth dubbed ABC modes) are expressible as combinations of either trigonometric or hyperbolic sines and cosines.

A natural homotopy between Lamé's Neumann modes and the ABC modes is exploited not only in the derivation of the modes but is also employed to shed light on the properties of these newly derived modes. Prominent among these considerations is rotational symmetry and modal degeneracy (Chapter 5 [53]). It is observed that the arguments presented in Chapter 6 [54] for

orthogonality and completeness in the case of a radiation boundary condition are likewise applicable in the case of an absorbing boundary condition.

This natural homotopy from Lamé's Neumann modes to the ABC modes possesses a bipartite structure. On the one hand, for ABC modes corresponding to eigenvalues that always remain positive, the homotopy may be extended to approach Lamé's Dirichlet modes. On the other hand, ABC modes corresponding to eigenvalues that eventually become negative do not approach Dirichlet modes. The determination of the precise nature of these latter eigenvalues together with that of their corresponding eigenfunctions is the primary focus of the present study.

7.1 The Absorbing Eigenproblem for the Equilateral Triangle

In the course of his investigations into the cooling of a right prism with equilateral triangular base [39, 40], Lamé was led to consider the eigenvalue problem

$$\Delta T(x,y) + k^2 T(x,y) = 0,\ (x,y) \in \tau;\ \frac{\partial T}{\partial \nu}(x,y) + \sigma T(x,y) = 0,\ (x,y) \in \partial\tau \tag{7.1}$$

where Δ is the two-dimensional Laplacian, $\frac{\partial^2}{\partial x^2} + \frac{\partial^2}{\partial y^2}$, τ is the equilateral triangle shown in Figure 1.1, ν is its outward pointing normal, and σ is a material parameter. Lamé later encountered the same eigenproblem when considering the vibrational modes of an elastic membrane stretched over an equilateral triangle [41]. We shall find through the ensuing analysis that all of the eigenfunctions (modes) of this problem are expressible in terms of either trigonometric or hyperbolic sines and cosines.

The boundary condition in Equation (7.1) with $\sigma > 0$ arises when heat dissipates from a body into a surrounding medium by a combination of convection, radiation and conduction. It also appears in the study of the vibrational modes of an elastic membrane. This case of the so-called radiation boundary condition, which is self-adjoint with k^2 real and nonnegative, received exhaustive treatment in Chapter 6 [54].

When $\sigma < 0$, this boundary condition corresponds to the absorption of energy [88]. It is this case of the so-called absorbing boundary condition (ABC), which is still self-adjoint so that k^2 is again real but may now be negative, that is the subject of the present paper. If σ is allowed to be complex (which is prohibited herein) then the identical problem occurs also in wave propagation in acoustic ducts and electromagnetic waveguides. This problem, which is no

longer self-adjoint so that k^2 may now be complex, will be taken up in Chapter 9 whose subject is the eigenstructure of the equilateral triangle subject to an impedance boundary condition (IBC).

Observe that in Equation (7.1) when $\sigma \to 0^-$ we recover the Neumann problem (Chapter 3 [52]). Thus, we may profitably view σ as a continuation parameter which provides a homotopy extending from this well understood problem to that of the absorbing boundary condition. Throughout the ensuing development we will avail ourselves of this important observation.

Furthermore, note that *if the normal derivative remains bounded* then $\sigma \to -\infty$ yields the Dirichlet problem (Chapter 2 [51]). In that case, the homotopy may be further extended to lead from a Neumann mode to a corresponding Dirichlet mode. For the radiation boundary condition this is always the case (Chapter 6 [54]), while for the absorbing boundary condition only sometimes so.

7.2 Symmetric/Antisymmetric Modes

Before proceeding any further, we will decompose the sought after eigenfunction into parts symmetric and antisymmetric about the altitude $v = w$ (see Figure 1.3)

$$T(u, v, w) = T_s(u, v, w) + T_a(u, v, w), \tag{7.2}$$

where

$$T_s(u, v, w) = \frac{T(u, v, w) + T(u, w, v)}{2};\ T_a(u, v, w) = \frac{T(u, v, w) - T(u, w, v)}{2}, \tag{7.3}$$

henceforth to be dubbed a symmetric/antisymmetric mode, respectively. We next take up the determination of T_s and T_a.

As shown previously, a sum of three terms of the form of Equation (1.15) is required to solve the Robin problem (Chapter 6 [54]). Hence, we make the Ansatz

$$\begin{aligned} T_s &= \cos[\frac{\pi\lambda}{3r}(u + 2r) - \delta_1] \cdot \cos[\frac{\pi(\mu - \nu)}{9r}(v - w)] \\ &+ \cos[\frac{\pi\mu}{3r}(u + 2r) - \delta_2] \cdot \cos[\frac{\pi(\nu - \lambda)}{9r}(v - w)] \\ &+ \cos[\frac{\pi\nu}{3r}(u + 2r) - \delta_3] \cdot \cos[\frac{\pi(\lambda - \mu)}{9r}(v - w)], \end{aligned} \tag{7.4}$$

$$\begin{aligned} T_a &= \cos[\frac{\pi\lambda}{3r}(u+2r)-\delta_1]\cdot\sin[\frac{\pi(\mu-\nu)}{9r}(v-w)] \\ &+ \cos[\frac{\pi\mu}{3r}(u+2r)-\delta_2]\cdot\sin[\frac{\pi(\nu-\lambda)}{9r}(v-w)] \\ &+ \cos[\frac{\pi\nu}{3r}(u+2r)-\delta_3]\cdot\sin[\frac{\pi(\lambda-\mu)}{9r}(v-w)]. \end{aligned} \tag{7.5}$$

with

$$\lambda+\mu+\nu=0, \tag{7.6}$$

and eigenvalue

$$k^2=\frac{2}{27}(\frac{\pi}{r})^2[\lambda^2+\mu^2+\nu^2]=\frac{4}{27}(\frac{\pi}{r})^2[\mu^2+\mu\nu+\nu^2]. \tag{7.7}$$

As we shall see, the symmetric mode never vanishes identically while the antisymmetric mode may.

Careful perusal of Equations (7.4) and (7.5) now reveals that for $\delta_1=\delta_2=\delta_3=0$ they reduce to the symmetric/antisymmetric modes of the Neumann problem (Chapter 3 [52]) while for $\delta_1=3\pi/2,\ \delta_2=-\pi/2,\ \delta_3=-\pi/2$ they reduce to the symmetric/antisymmetric modes of the Dirichlet problem (Chapter 2 [51]). Thus, our task amounts to finding values of $\lambda,\ \mu,\ \nu,\ \delta_1,\ \delta_2,\ \delta_3$ so that the Robin boundary condition is satisfied along the periphery of the equilateral triangle. These values are to satisfy the constraints that k^2, T_s and T_a must be real as well as Equation (7.6).

Imposition of the Robin boundary condition along $u=r$ yields

$$\tan(\pi\lambda-\delta_1)=\frac{3\sigma r}{\pi\lambda},\ \tan(\pi\mu-\delta_2)=\frac{3\sigma r}{\pi\mu},\ \tan(\pi\nu-\delta_3)=\frac{3\sigma r}{\pi\nu}, \tag{7.8}$$

while imposition along $v=r$ yields

$$\tan(-\frac{\delta_2+\delta_3}{2})=\frac{3\sigma r}{\pi\lambda},\ \tan(-\frac{\delta_3+\delta_1}{2})=\frac{3\sigma r}{\pi\mu},\ \tan(-\frac{\delta_1+\delta_2}{2})=\frac{3\sigma r}{\pi\nu}. \tag{7.9}$$

By symmetry/antisymmetry, the boundary condition along $w=r$ will thereby be automatically satisfied.

Introducing the auxiliary variables, $L,\ M,\ N$, while collecting together these equations produces

$$\begin{aligned} \tan(\pi\lambda-\delta_1)=\tan(-\frac{\delta_2+\delta_3}{2})=\frac{3\sigma r}{\pi\lambda}=\tan L \quad &, \quad L:=-\frac{\delta_2+\delta_3}{2} \\ \tan(\pi\mu-\delta_2)=\tan(-\frac{\delta_3+\delta_1}{2})=\frac{3\sigma r}{\pi\mu}=\tan M \quad &, \quad M:=-\frac{\delta_3+\delta_1}{2} \\ \tan(\pi\nu-\delta_3)=\tan(-\frac{\delta_1+\delta_2}{2})=\frac{3\sigma r}{\pi\nu}=\tan N \quad &, \quad N:=-\frac{\delta_1+\delta_2}{2} \end{aligned} \tag{7.10}$$

and these six equations may in turn be reduced to the solution of the system of three transcendental equations for $L,\ M,\ N$

$$\begin{aligned} [2L - M - N - (m+n)\pi] \cdot \tan L &= 3\sigma r, \\ [2M - N - L + m\pi] \cdot \tan M &= 3\sigma r, \\ [2N - L - M + n\pi] \cdot \tan N &= 3\sigma r, \end{aligned} \tag{7.11}$$

where $m = 0, 1, 2, \ldots,\ n = m, m+1, \ldots$.

Once $L,\ M,\ N$ have been numerically approximated, e.g. using MATLAB [34, 64], the parameters of primary interest may then be determined as

$$\delta_1 = L - M - N;\ \delta_2 = -L + M - N;\ \delta_3 = -L - M + N, \tag{7.12}$$

and

$$\lambda = -\mu - \nu;\ \mu = \frac{2M - N - L}{\pi} + m;\ \nu = \frac{2N - L - M}{\pi} + n. \tag{7.13}$$

For future reference, when $m = n$ we have $M = N$, $\delta_2 = \delta_3$, $\mu = \nu$, and $2\pi\mu = \delta_2 - \delta_1 + 2m\pi$.

Of particular interest is the limit $\sigma \to 0^-$, where we find that L, M, N each approach 0, as do $\delta_1, \delta_2, \delta_3$, and, most significantly, $\lambda \to -(m+n), \mu \to m, \nu \to n$. In other words, we recover in this limit the Neumann modes. Thus, we have constructed a homotopy extending from each ABC mode back to the Neumann mode with the same index (m, n) as $\sigma \to 0^-$. The behavior of the ABC modes as $\sigma \to -\infty$ is more subtle and will be addressed once we have established some of their basic properties.

7.3 Modal Properties

Certain properties of the ABC modes follow directly from Equations (7.4) and (7.5). However, these equations are identical to those for the radiation boundary condition [54] except that some quantities may now be complex so long as k^2, T_s and T_a are real. Thus, their proofs are formally identical to those of Chapter 6 [54] and for that reason they are omitted here.

In what follows, it will be convenient to have the following alternative

representations of our ABC modes

$$\begin{aligned} T_s^{m,n} = \frac{1}{2} \quad \{ \quad & \cos[\frac{2\pi}{9r}(\lambda u + \mu v + \nu w + 3\lambda r) - \delta_1] \\ + \quad & \cos[\frac{2\pi}{9r}(\nu u + \mu v + \lambda w + 3\nu r) - \delta_3] \\ + \quad & \cos[\frac{2\pi}{9r}(\mu u + \nu v + \lambda w + 3\mu r) - \delta_2] \\ + \quad & \cos[\frac{2\pi}{9r}(\mu u + \lambda v + \nu w + 3\mu r) - \delta_2] \\ + \quad & \cos[\frac{2\pi}{9r}(\nu u + \lambda v + \mu w + 3\nu r) - \delta_3] \\ + \quad & \cos[\frac{2\pi}{9r}(\lambda u + \nu v + \mu w + 3\lambda r) - \delta_1]\}, \end{aligned} \tag{7.14}$$

$$\begin{aligned} T_a^{m,n} = \frac{1}{2} \quad \{ \quad & \sin[\frac{2\pi}{9r}(\lambda u + \mu v + \nu w + 3\lambda r) - \delta_1] \\ - \quad & \sin[\frac{2\pi}{9r}(\nu u + \mu v + \lambda w + 3\nu r) - \delta_3] \\ + \quad & \sin[\frac{2\pi}{9r}(\mu u + \nu v + \lambda w + 3\mu r) - \delta_2] \\ - \quad & \sin[\frac{2\pi}{9r}(\mu u + \lambda v + \nu w + 3\mu r) - \delta_2] \\ + \quad & \sin[\frac{2\pi}{9r}(\nu u + \lambda v + \mu w + 3\nu r) - \delta_3] \\ - \quad & \sin[\frac{2\pi}{9r}(\lambda u + \nu v + \mu w + 3\lambda r) - \delta_1]\}, \end{aligned} \tag{7.15}$$

obtained from Equation (7.4) and Equation (7.5), respectively, by the application of appropriate trigonometric identities.

We may pare the collection of antisymmetric Robin modes through the following observation.

Theorem 7.3.1. *$T_s^{m,n}$ never vanishes identically while $T_a^{m,n}$ vanishes identically if and only if m=n.*

Hence, our reduced modal system is $\{T_s^{m,n}\ (n \geq m \geq 0);\ T_a^{m,n}\ (n > m \geq 0)\}$.

We next give the case $m = n$ further consideration. Recall that we have just determined that $T_a^{m,m} \equiv 0$. Furthermore, in this case, we may combine the terms of Equation (7.14) to yield

$$T_s^{m,m} = \cos[\frac{2\pi\mu}{3r}(r-u) - \delta_2] + \cos[\frac{2\pi\mu}{3r}(r-v) - \delta_2] + \cos[\frac{2\pi\mu}{3r}(r-w) - \delta_2] \tag{7.16}$$

which clearly illustrates that any permutation of (u, v, w) leaves $T_s^{m,m}$ invariant. This is manifested geometrically in the invariance of $T_s^{m,m}$ under a 120° rotation about the triangle center. This invariance will henceforth be termed rotational symmetry.

Moreover, the modes $T_s^{m,m}$ are not the only ones that are rotationally symmetric.

Theorem 7.3.2. *$T_s^{m,n}$ and $T_a^{m,n}$ are rotationally symmetric if and only if $m \equiv n \pmod 3$.*

7.4 The Limit $\sigma \to -\infty$

In the case of the radiation boundary condition ($\sigma > 0$) (Chapter 6 [54]), the (m, n) Neumann mode (Chapter 3 [52]) "morphs" analytically into the $(m+1, n+1)$ Dirichlet mode (Chapter 2 [51]) as σ ranges from 0 to ∞. This suggests that in the case of the absorbing boundary condition ($\sigma < 0$), the (m, n) Neumann mode might "morph" analytically into the $(m-1, n-1)$ Dirichlet mode as σ ranges from 0 to $-\infty$.

However, the complete set of Neumann modes is given by $\{N_s^{m,n}\ (n \geq m \geq 0);\ N_a^{m,n}\ (n > m \geq 0)\}$ while the complete set of Dirichlet modes is given by $\{D_s^{m,n}\ (n \geq m > 0);\ D_a^{m,n}\ (n > m > 0)\}$. Thus, the above conjectured behavior of the ABC modes, $\{T_s^{m,n}\ (n \geq m \geq 0);\ T_a^{m,n}\ (n > m \geq 0)\}$, as $\sigma \to -\infty$, while feasible for $m \geq 2$ (the "ABC-Dirichlet modes"), is insufficient in the case of $m = 0, 1$ (the "missing modes"). Consequently, we next investigate these cases individually.

7.4.1 ABC-Dirichlet Modes

The case $m \geq 2$ closely parallels that of the radiation boundary condition (Chapter 6 [54]). Specifically, as $\sigma \to -\infty$, we find that $L \to \pi/2, M \to -\pi/2, N \to -\pi/2$ so that $\delta_1 \to 3\pi/2, \delta_2 \to -\pi/2, \delta_3 \to -\pi/2$, and, most significantly, $\lambda \to 2 - (m+n), \mu \to m-1, \nu \to n-1$. In other words, we recover in this limit the Dirichlet modes. Thus, we have successfully constructed a homotopy leading from the ABC-Dirichlet modes to the Dirichlet modes. Moreover, we have indexed our ABC-Dirichlet modes in correspondence with the associated Neumann modes with the result that, as σ ranges from 0 to $-\infty$, the (m, n) ABC-Dirichlet mode "morphs" continuously (in fact, analytically!) from the (m, n) Neumann mode into the $(m-1, n-1)$ Dirichlet mode.

Figure 7.1 shows the $(2, 2)$ Neumann mode morphing into the fundamental $(1, 1)$ Dirichlet mode. In this and all subsequent figures, we set $h = 1$. By Theorem 7.3.1, there is no antisymmetric mode and, by Theorem 7.3.2, the

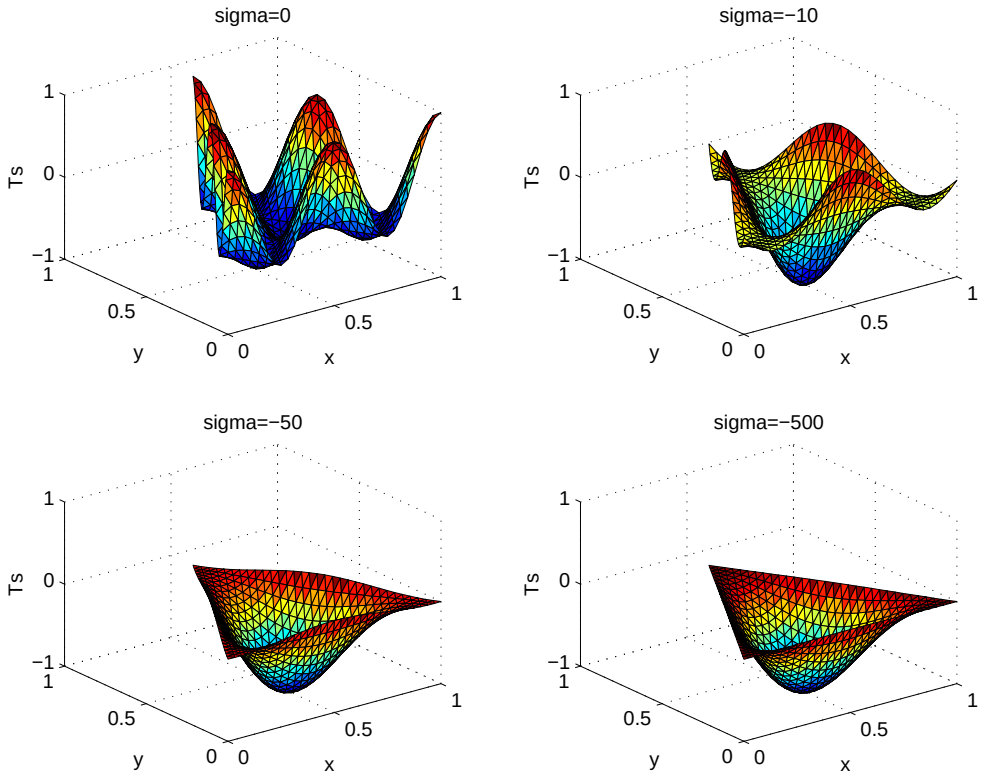

Figure 7.1: $(2, 2)$ Symmetric Mode

symmetric mode is rotationally symmetric. Figures 7.2 and 7.3 correspondingly display the $(2, 3)$ symmetric and antisymmetric modes, respectively. By Theorem 7.3.1, there are indeed both symmetric and antisymmetric modes and, by Theorem 7.3.2, neither of them is rotationally symmetric. In these and all subsequent plots, the modes have been normalized so that their maximum absolute value is unity. This elegant treatment of the ABC-Dirichlet modes begs the question: "What happens to the missing $m = 0, 1$ modes as $\sigma \to -\infty$?"

7.4.2 The Missing Modes

The solution to the mystery of the missing modes naturally decomposes into four special cases each of which we now explore separately.

The $(0, 0)$ Mode

For $\sigma < 0$, all the parameters of Section 7.2 become pure imaginary:

$$\lambda = \lambda^I \cdot \imath, \ \mu = \mu^I \cdot \imath, \ \nu = \nu^I \cdot \imath, \tag{7.17}$$

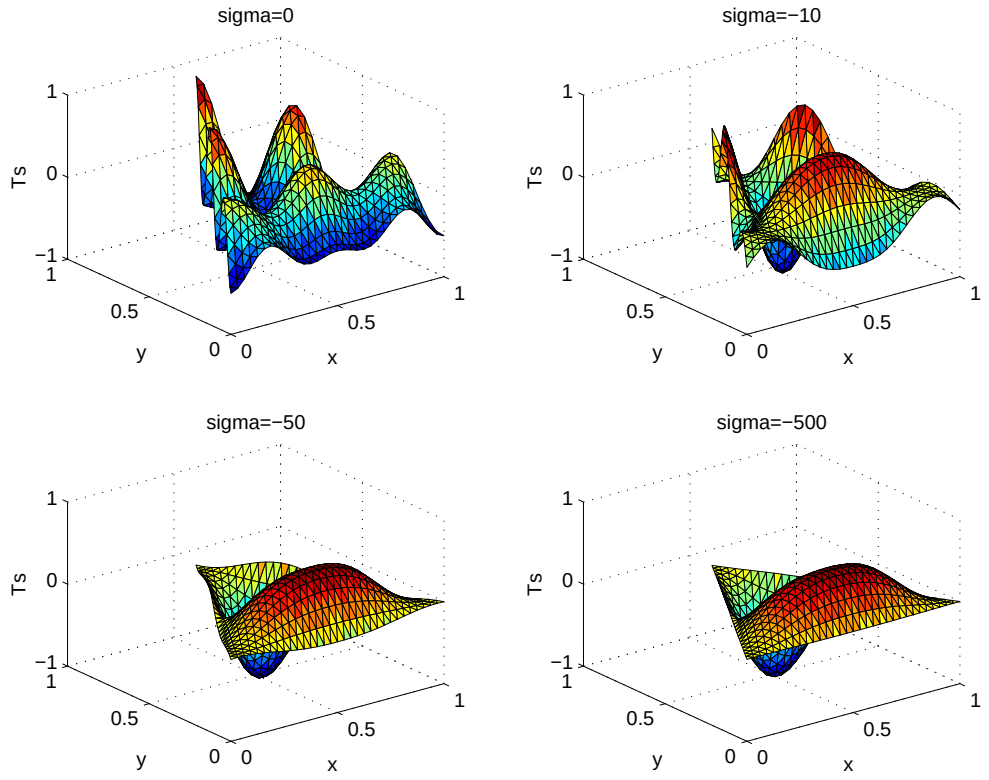

Figure 7.2: $(2,3)$ Symmetric Mode

$$\delta_1 = \delta_1^I \cdot \imath,\ \delta_2 = \delta_2^I \cdot \imath,\ \delta_3 = \delta_3^I \cdot \imath, \tag{7.18}$$

$$L = L^I \cdot \imath,\ M = M^I \cdot \imath,\ N = N^I \cdot \imath. \tag{7.19}$$

Equation (7.4) becomes

$$\begin{aligned} T_s &= \cosh[\frac{\pi\lambda^I}{3r}(u+2r) - \delta_1^I] \cdot \cosh[\frac{\pi(\mu^I - \nu^I)}{9r}(v-w)] \\ &+ \cosh[\frac{\pi\mu^I}{3r}(u+2r) - \delta_2^I] \cdot \cosh[\frac{\pi(\nu^I - \lambda^I)}{9r}(v-w)] \\ &+ \cosh[\frac{\pi\nu^I}{3r}(u+2r) - \delta_3^I] \cdot \cosh[\frac{\pi(\lambda^I - \mu^I)}{9r}(v-w)], \end{aligned} \tag{7.20}$$

with

$$\lambda^I + \mu^I + \nu^I = 0, \tag{7.21}$$

and eigenvalue

$$k^2 = -\frac{2}{27}(\frac{\pi}{r})^2[(\lambda^I)^2 + (\mu^I)^2 + (\nu^I)^2] = -\frac{4}{27}(\frac{\pi}{r})^2[(\mu^I)^2 + \mu^I \cdot \nu^I + (\nu^I)^2]. \tag{7.22}$$

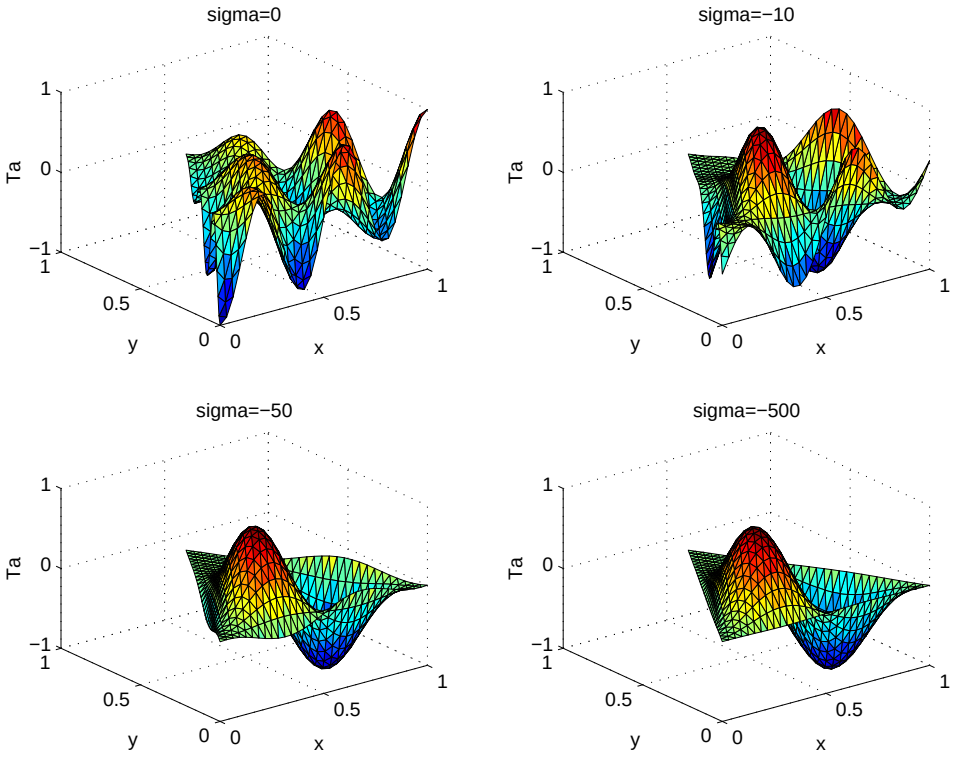

Figure 7.3: $(2,3)$ Antisymmetric Mode

Equations (7.11) become

$$\begin{aligned}[2L^I - M^I - N^I] \cdot \tanh L^I &= -3\sigma r, \\ [2M^I - N^I - L^I] \cdot \tanh M^I &= -3\sigma r, \\ [2N^I - L^I - M^I] \cdot \tanh N^I &= -3\sigma r.\end{aligned} \tag{7.23}$$

Finally, Equations (7.12) become

$$\delta_1^I = L^I - M^I - N^I;\ \delta_2^I = -L^I + M^I - N^I;\ \delta_3^I = -L^I - M^I + N^I, \tag{7.24}$$

and Equations (7.13) become

$$\lambda^I = -\mu^I - \nu^I;\ \mu^I = \frac{2M^I - N^I - L^I}{\pi};\ \nu^I = \frac{2N^I - L^I - M^I}{\pi}. \tag{7.25}$$

Furthermore, we have $M^I = N^I$, $\delta_2^I = \delta_3^I = -L^I$, and $\mu^I = \nu^I$. Asymptotically, as $\sigma \to -\infty$, we have the limiting values:

$$L^I = -\delta_2^I = -\delta_3^I \to \tanh^{-1}(1/2), \tag{7.26}$$

$$M^I = N^I \to \tanh^{-1}(1/2) + 3\sigma r, \tag{7.27}$$

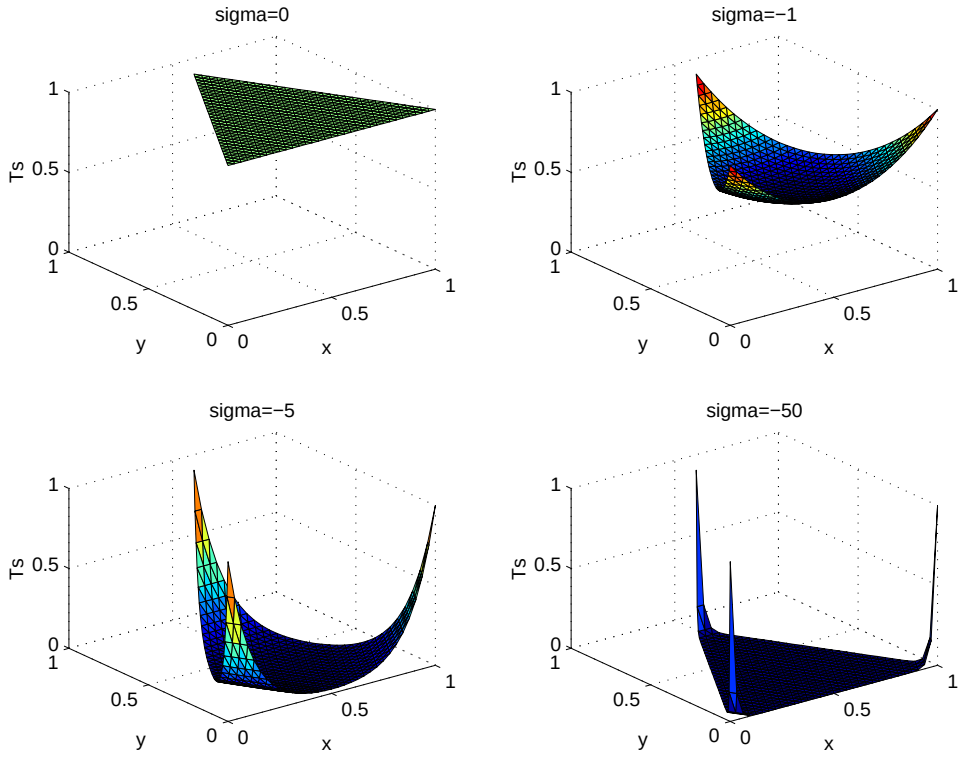

Figure 7.4: $(0,0)$ Symmetric Mode

$$\delta_1^I \to -\tanh^{-1}(1/2) - 6\sigma r, \tag{7.28}$$

$$\mu^I = \nu^I \to \frac{3\sigma r}{\pi} \Rightarrow k^2 \to -4\sigma^2. \tag{7.29}$$

Equation (7.20) for $T_s^{0,0}(u,v,w)$ becomes unbounded as $\sigma \to -\infty$. However, if we first scale it by its value at a vertex, $T_s^{0,0}(r,-2r,r)$, we find that this normalized mode approaches 1 at the three vertices and 0 elsewhere. Such singular limiting behavior, necessary since this mode does not approach a Dirichlet mode, is on display in Figure 7.4.

The $(0, n \geq 1)$ Modes

For $\sigma < 0$, μ becomes pure imaginary, and the remaining parameters of Section 7.2 become complex in such a way so as to guarantee that k^2, T_s and T_a are real:

$$\lambda = -\nu^R - \frac{\mu^I}{2} \cdot \imath,\ \mu = \mu^I \cdot \imath,\ \nu = \nu^R - \frac{\mu^I}{2} \cdot \imath, \tag{7.30}$$

$$\delta_1 = -\delta_3^R + \delta_3^I \cdot \imath,\ \delta_2 = \delta_2^I \cdot \imath,\ \delta_3 = \delta_3^R + \delta_3^I \cdot \imath, \tag{7.31}$$

$$L = -N^R + N^I \cdot \imath,\ M = M^I \cdot \imath,\ N = N^R + N^I \cdot \imath. \tag{7.32}$$

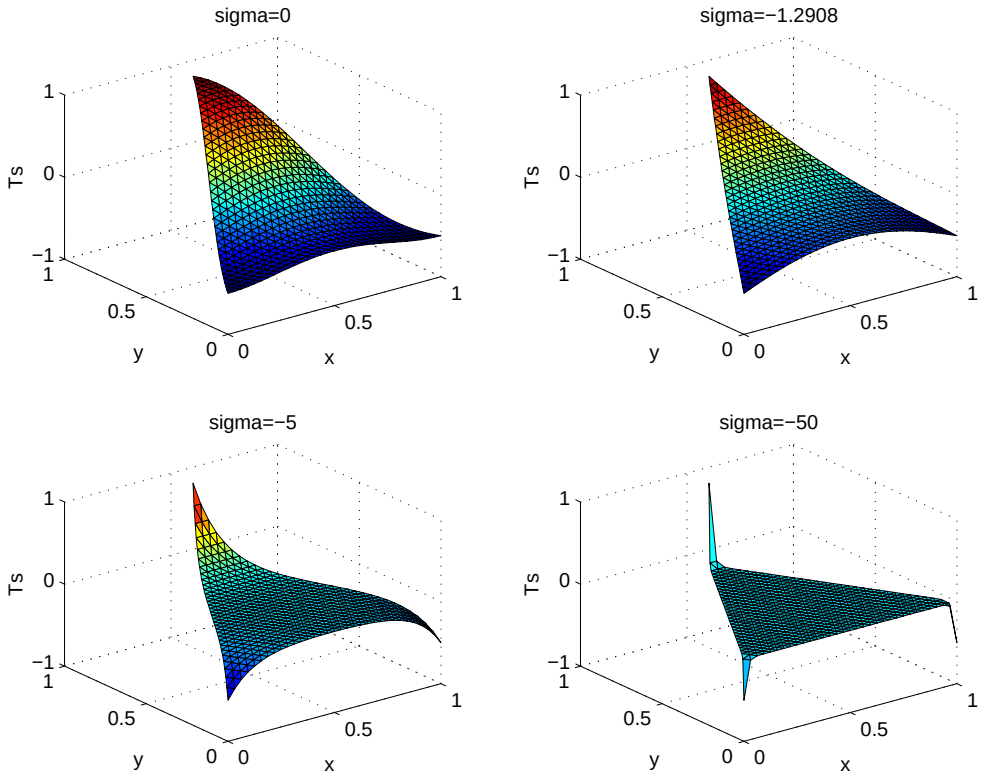

Figure 7.5: $(0, 1)$ Symmetric Mode

Note that

$$\lambda + \mu + \nu = 0. \tag{7.33}$$

Now, the middle term of Equation (7.4)/(7.5) is real while the outer terms are complex conjugates so that these equations may be recast in the real form

$$\begin{aligned} T_s &= \cosh[\frac{\pi\mu^I}{3r}(u+2r) - \delta_2^I] \cdot \cos[\frac{2\pi\nu^R}{9r}(v-w)] \\ &+ 2 \cdot \cosh[\frac{\pi\mu^I}{6r}(u+2r) + \delta_3^I] \cdot \cosh[\frac{\pi\mu^I}{6r}(v-w)] \\ &\quad \cdot \cos[\frac{\pi\nu^R}{3r}(u+2r) - \delta_3^R] \cdot \cos[\frac{\pi\nu^R}{9r}(v-w)] \\ &+ 2 \cdot \sinh[\frac{\pi\mu^I}{6r}(u+2r) + \delta_3^I] \cdot \sinh[\frac{\pi\mu^I}{6r}(v-w)] \\ &\quad \cdot \sin[\frac{\pi\nu^R}{3r}(u+2r) - \delta_3^R] \cdot \sin[\frac{\pi\nu^R}{9r}(v-w)], \end{aligned} \tag{7.34}$$

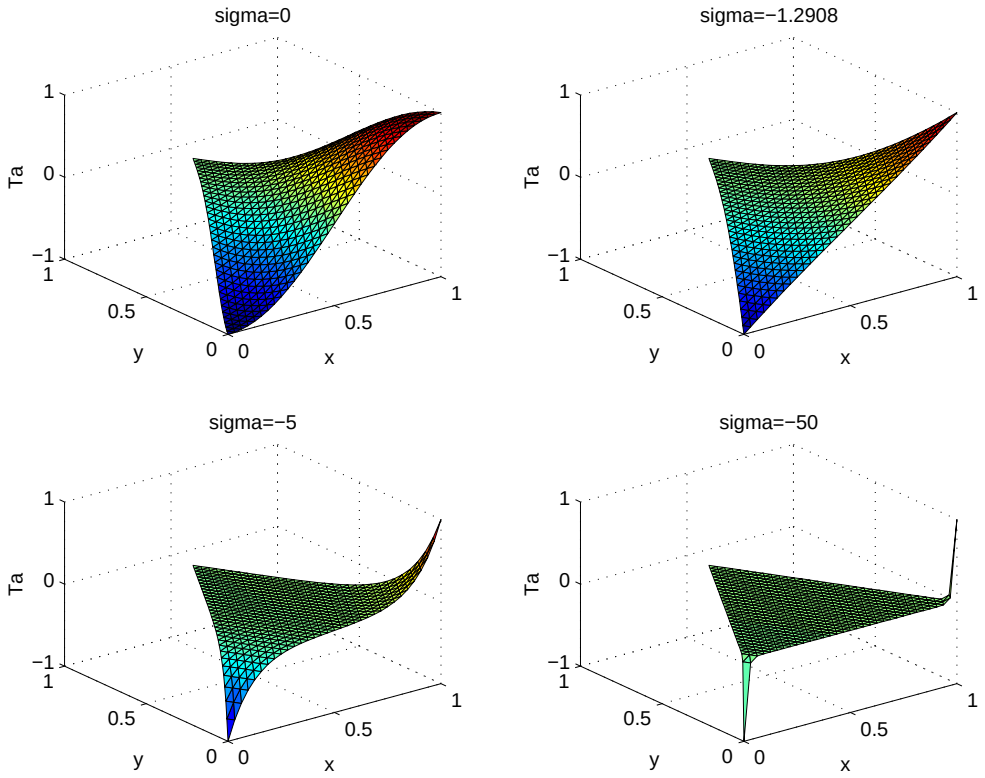

Figure 7.6: $(0,1)$ Antisymmetric Mode

$$\begin{aligned} T_a &= \cosh[\frac{\pi\mu^I}{3r}(u+2r) - \delta_2^I] \cdot \sin[\frac{2\pi\nu^R}{9r}(v-w)] \\ &+ 2 \cdot \cosh[\frac{\pi\mu^I}{6r}(u+2r) + \delta_3^I] \cdot \cosh[\frac{\pi\mu^I}{6r}(v-w)] \\ &\quad \cdot \cos[\frac{\pi\nu^R}{3r}(u+2r) - \delta_3^R] \cdot \sin[\frac{\pi\nu^R}{9r}(v-w)] \\ &- 2 \cdot \sinh[\frac{\pi\mu^I}{6r}(u+2r) + \delta_3^I] \cdot \sinh[\frac{\pi\mu^I}{6r}(v-w)] \\ &\quad \cdot \sin[\frac{\pi\nu^R}{3r}(u+2r) - \delta_3^R] \cdot \cos[\frac{\pi\nu^R}{9r}(v-w)]. \end{aligned} \tag{7.35}$$

with eigenvalue

$$k^2 = \frac{4}{27}(\frac{\pi}{r})^2[(\nu^R)^2 - \frac{3}{4}(\mu^I)^2]. \tag{7.36}$$

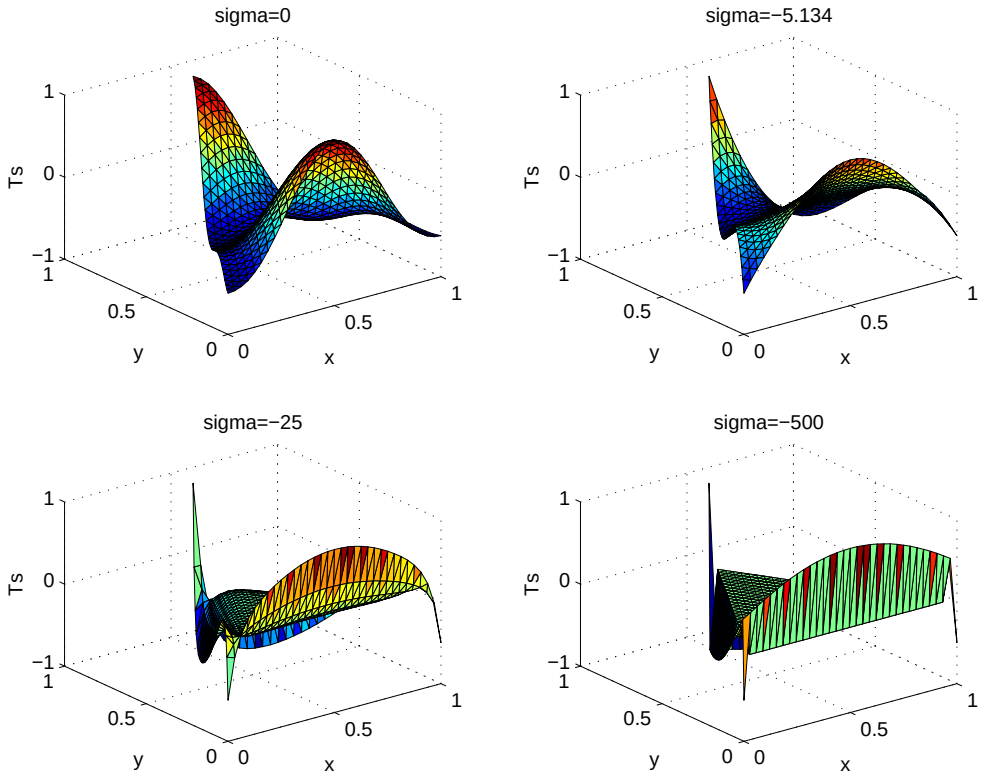

Figure 7.7: $(0, 2)$ Symmetric Mode

Equations (7.11) become

$$\begin{aligned} -2(M^I - N^I) \cdot \tanh M^I &= 3\sigma r, \\ \frac{(3N^R + n\pi)\sin(N^R)\cos(N^R) - (N^I - M^I)\sinh(N^I)\cosh(N^I)}{\cos^2(N^R)\cosh^2(N^I) + \sin^2(N^R)\sinh^2(N^I)} &= 3\sigma r, \\ \frac{(N^I - M^I)\sin(N^R)\cos(N^R) + (3N^R + n\pi)\sinh(N^I)\cosh(N^I)}{\cos^2(N^R)\cosh^2(N^I) + \sin^2(N^R)\sinh^2(N^I)} &= 0 \end{aligned} \quad (7.37)$$

Finally, Equations (7.12) become

$$\delta_1 = -2N^R - M^I \cdot \imath;\ \delta_2 = (M^I - 2N^I) \cdot \imath;\ \delta_3 = 2N^R - M^I \cdot \imath, \quad (7.38)$$

and Equations (7.13) become

$$\lambda = -\mu - \nu;\ \mu = \frac{2(M^I - N^I)}{\pi} \cdot \imath;\ \nu = (\frac{3N^R}{\pi} + n) + \frac{N^I - M^I}{\pi} \cdot \imath. \quad (7.39)$$

For $\sigma = 0$, k^2 is positive and, as σ is decreased, k^2, likewise, decreases. When σ reaches a critical value, $\hat{\sigma}_n$, $k^2(\hat{\sigma}_n) = 0$ and thereafter continues to

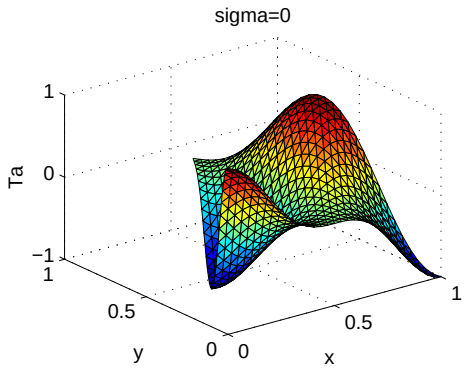
sigma=0
Ta
1
0
−1
1
0.5
y
0
0
0.5
x
1

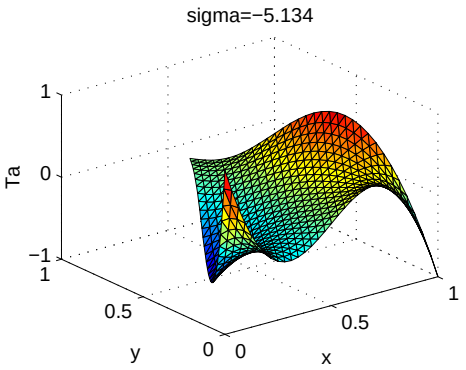
sigma=−5.134
Ta
1
0
−1
1
0.5
y
0
0
0.5
x
1

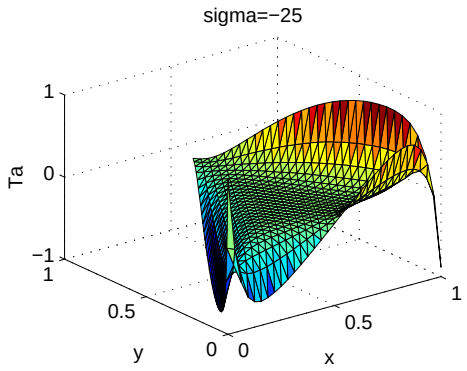
sigma=−25
Ta
1
0
−1
1
0.5
y
0
0
0.5
x
1

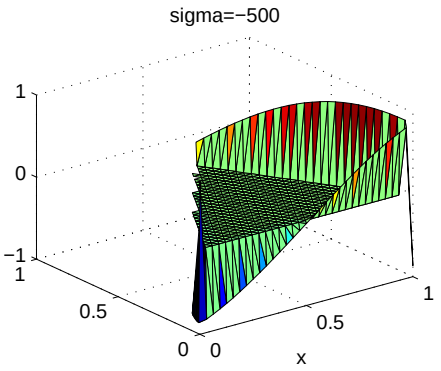
sigma=−500
1
0
−1
1
0.5
0
0
0.5
x
1

$$\mu \to -\frac{3\sigma r}{\pi}\cdot \imath \ \& \ \nu \to (n-\frac{3}{2}) + \frac{3\sigma r}{2\pi}\cdot \imath \Rightarrow k^2 \to -\sigma^2 + \frac{4}{27}[\frac{\pi}{r}(n-\frac{3}{2})]^2. \quad (7.45)$$

Figures 7.7 and 7.8 display $T_s^{0,2}$ and $T_a^{0,2}$, respectively, where $\hat{\sigma}_2 \approx -5.134$. Both plots display prominent corner and edge singularities.

The $(1,1)$ Mode

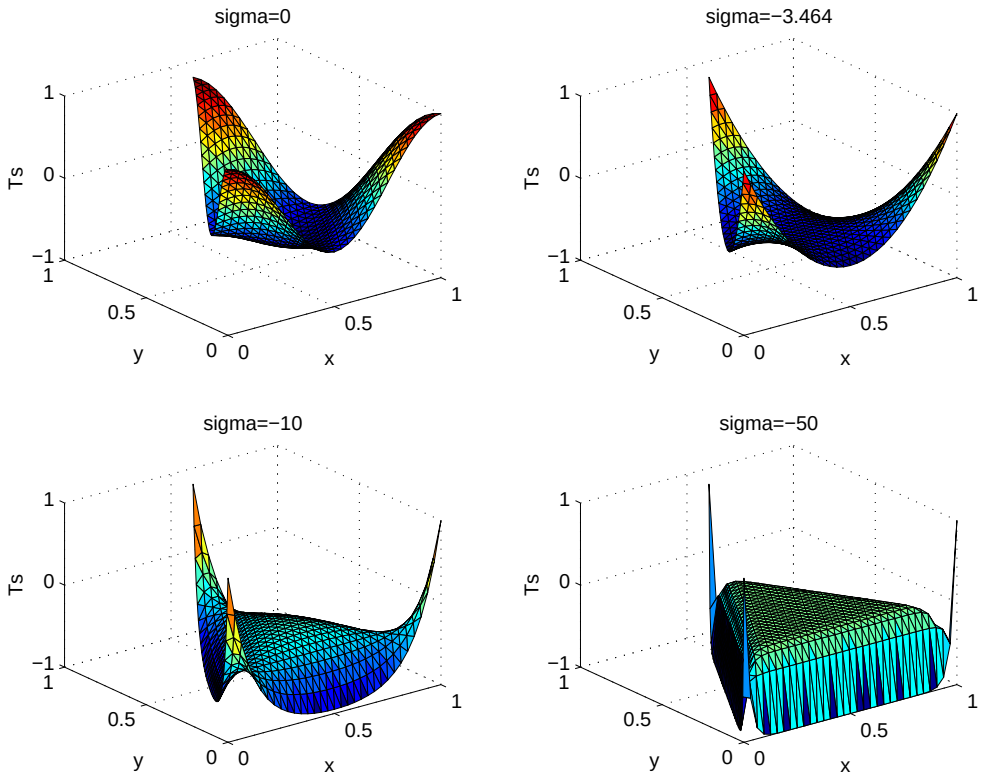

Figure 7.9: $(1,1)$ Symmetric Mode

For $0 > \sigma > \tilde{\sigma} := -1/r$, we have $\mu = \nu > 0$ and the relevant equations are those of Section 7.2 with $m = 1$ and $n = 1$. However, when $\sigma = \tilde{\sigma} = -2\sqrt{3} \approx -3.464$ with the normalization $h = 1$, we have $\mu = \nu = 0 \Rightarrow k^2 = 0$. Also, as $\sigma \to \tilde{\sigma}$, we have $\delta_1 \to 3\pi/2$ and $\delta_2 = \delta_3 \to -\pi/2$ so that $T_s^{1,1}$ of Equation (7.4) approaches zero. However, if we normalize $T_s^{1,1}$ so that its maximum value is one then it approaches the harmonic polynomial

$$\tilde{T}_s^{1,1} = 1 - \frac{2}{9r^3}[(r-u)^2(u+2r) + (r-v)^2(v+2r) + (r-w)^2(w+2r)]. \quad (7.46)$$

For $\sigma < \tilde{\sigma}$, all the parameters of Section 7.2 become complex:

$$\lambda = \lambda^I \cdot \imath, \ \mu = \mu^I \cdot \imath, \ \nu = \nu^I \cdot \imath, \quad (7.47)$$

$$\delta_1 = \frac{3\pi}{2} + \delta_1^I \cdot \imath,\ \delta_2 = \delta_3 = -\frac{\pi}{2} + \delta_2^I \cdot \imath, \tag{7.48}$$

$$L = \frac{\pi}{2} + L^I \cdot \imath,\ M = N = -\frac{\pi}{2} + M^I \cdot \imath. \tag{7.49}$$

Equation (7.4) becomes

$$\begin{aligned} T_s &= \sinh[\frac{\pi\lambda^I}{3r}(u+2r) - \delta_1^I] \cdot \cosh[\frac{\pi(\mu^I - \nu^I)}{9r}(v-w)] \\ &+ \sinh[\frac{\pi\mu^I}{3r}(u+2r) - \delta_2^I] \cdot \cosh[\frac{\pi(\nu^I - \lambda^I)}{9r}(v-w)] \\ &+ \sinh[\frac{\pi\nu^I}{3r}(u+2r) - \delta_3^I] \cdot \cosh[\frac{\pi(\lambda^I - \mu^I)}{9r}(v-w)], \end{aligned} \tag{7.50}$$

with

$$\lambda^I + \mu^I + \nu^I = 0, \tag{7.51}$$

and eigenvalue

$$k^2 = -\frac{2}{27}(\frac{\pi}{r})^2[(\lambda^I)^2 + (\mu^I)^2 + (\nu^I)^2] = -\frac{4}{27}(\frac{\pi}{r})^2[(\mu^I)^2 + \mu^I \cdot \nu^I + (\nu^I)^2]. \tag{7.52}$$

Equations (7.11) become

$$\begin{aligned} [2L^I - M^I - N^I] \cdot \coth L^I &= -3\sigma r, \\ [2M^I - N^I - L^I] \cdot \coth M^I &= -3\sigma r, \\ [2N^I - L^I - M^I] \cdot \coth N^I &= -3\sigma r. \end{aligned} \tag{7.53}$$

Finally, Equations (7.12) become

$$\delta_1^I = L^I - M^I - N^I;\ \delta_2^I = -L^I + M^I - N^I;\ \delta_3^I = -L^I - M^I + N^I, \tag{7.54}$$

and Equations (7.13) become

$$\lambda^I = -\mu^I - \nu^I;\ \mu^I = \frac{2M^I - N^I - L^I}{\pi};\ \nu^I = \frac{2N^I - L^I - M^I}{\pi}. \tag{7.55}$$

Furthermore, we have $M^I = N^I$, $\delta_2^I = \delta_3^I = -L^I$, and $\mu^I = \nu^I$. Asymptotically, as $\sigma \to -\infty$, we have the limiting values:

$$L^I = -\delta_2^I = -\delta_3^I \to \frac{3}{2}\sigma r + \tanh^{-1}(1/2), \tag{7.56}$$

$$M^I = N^I \to \tanh^{-1}(1/2), \tag{7.57}$$

$$\delta_1^I \to \frac{3}{2}\sigma r - \tanh^{-1}(1/2), \tag{7.58}$$

$$\mu^I = \nu^I \to \frac{3\sigma r}{2\pi} \Rightarrow k^2 \to -\sigma^2. \tag{7.59}$$

Equation (7.50) for $T_s^{1,1}(u,v,w)$ becomes unbounded as $\sigma \to -\infty$. However, if we first scale it by its value at a vertex, $T_s^{1,1}(r,-2r,r)$, we find that this normalized mode approaches 1 at the three vertices and 0 in the interior. The resulting edge and corner singularities are on display in Figure 7.9.

The $(1, n > 1)$ Modes

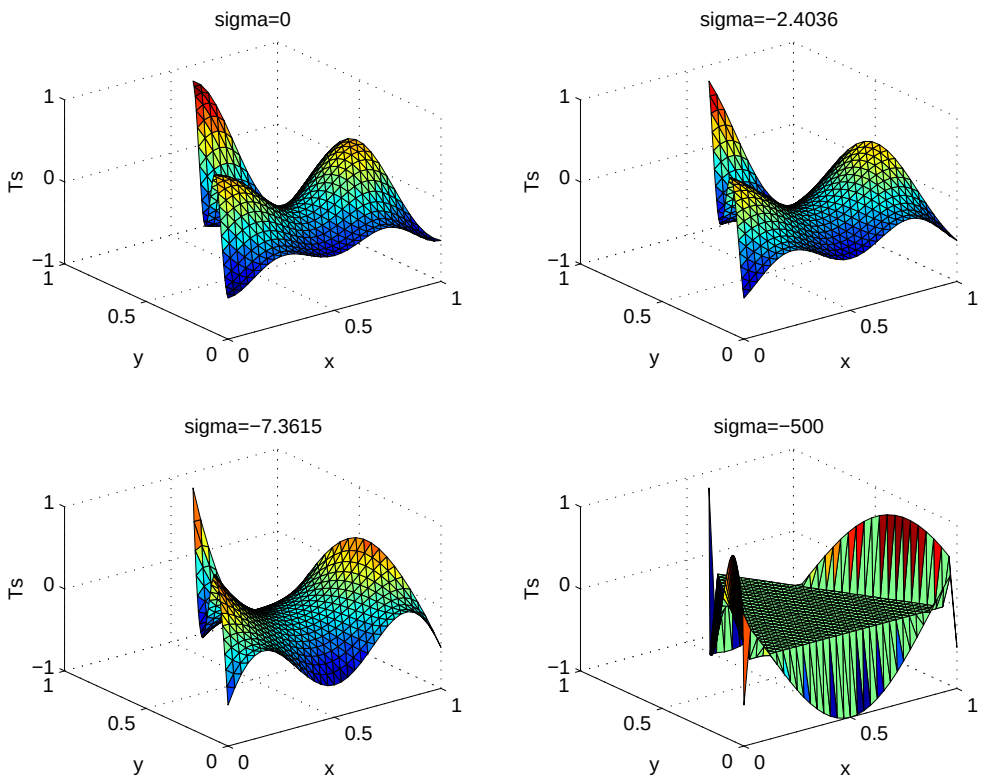

Figure 7.10: $(1, 2)$ Symmetric Mode

For $0 > \sigma > \sigma_n^*$, we have $\mu > 0$ and the relevant equations are those of Section 7.2 with $m = 1$. However, as $\sigma \to \sigma_n^*$ we have $\mu \to 0$ while $\delta_2 \to -\pi/2$ and $\delta_1 \to \delta_3 \to \pi/2$. As σ passes through σ_n^*, T_s and T_a make the transition from purely trigonometric functions to combinations of trigonometric and hyperbolic functions as in the case of the $(0, n \geq 1)$ modes.

For $\sigma < \sigma_n^*$, μ becomes pure imaginary, and the remaining parameters of Section 7.2 become complex in such a way so as to guarantee that k^2, T_s and T_a are real :

$$\lambda = -\nu^R - \frac{\mu^I}{2} \cdot \imath, \ \mu = \mu^I \cdot \imath, \ \nu = \nu^R - \frac{\mu^I}{2} \cdot \imath, \tag{7.60}$$

$$\delta_1 = \pi - \delta_3^R + \delta_3^I \cdot \imath, \ \delta_2 = -\frac{\pi}{2} + \delta_2^I \cdot \imath, \ \delta_3 = \delta_3^R + \delta_3^I \cdot \imath, \tag{7.61}$$

$$L = -N^R + N^I \cdot \imath, \ M = -\frac{\pi}{2} + M^I \cdot \imath, \ N = N^R + N^I \cdot \imath. \tag{7.62}$$

Note that

$$\lambda + \mu + \nu = 0. \tag{7.63}$$

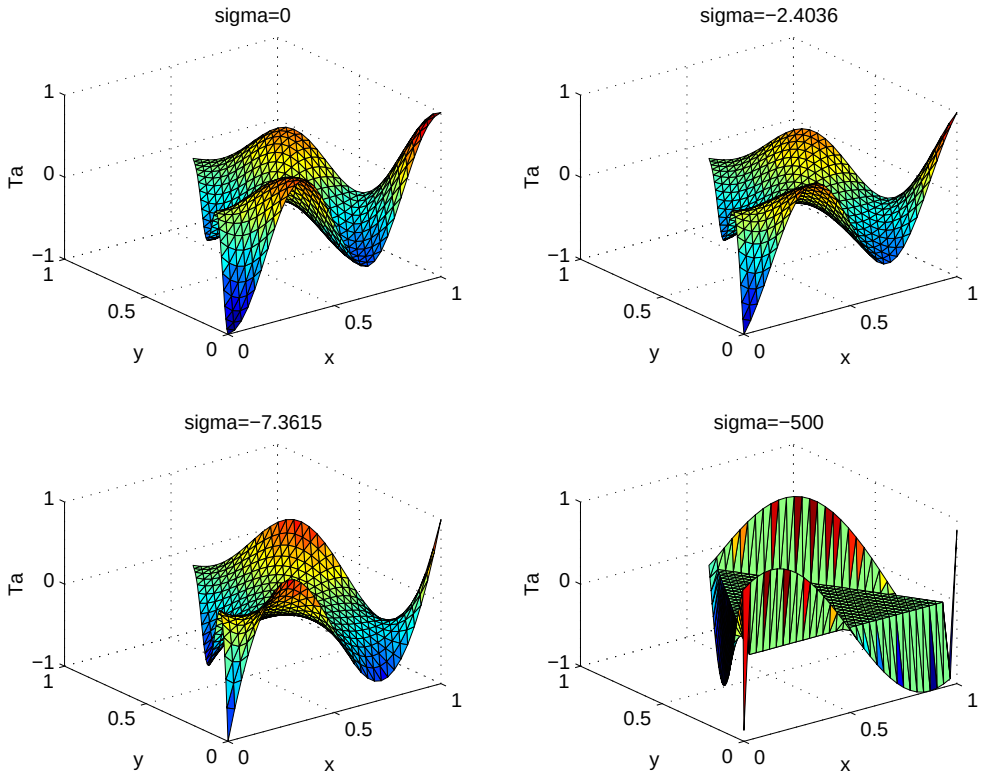

Figure 7.11: $(1, 2)$ Antisymmetric Mode

Now, the middle term of Equation (7.4)/(7.5) is imaginary while the outer terms are negative conjugates so that these equations may be recast in the real form

$$\begin{aligned} T_s &= \sinh[\frac{\pi\mu^I}{3r}(u+2r) - \delta_2^I] \cdot \cos[\frac{2\pi\nu^R}{9r}(v-w)] \\ &+ 2 \cdot \sinh[\frac{\pi\mu^I}{6r}(u+2r) + \delta_3^I] \cdot \cosh[\frac{\pi\mu^I}{6r}(v-w)] \\ &\quad \cdot \sin[\frac{\pi\nu^R}{3r}(u+2r) - \delta_3^R] \cdot \cos[\frac{\pi\nu^R}{9r}(v-w)] \\ &- 2 \cdot \cosh[\frac{\pi\mu^I}{6r}(u+2r) + \delta_3^I] \cdot \sinh[\frac{\pi\mu^I}{6r}(v-w)] \\ &\quad \cdot \cos[\frac{\pi\nu^R}{3r}(u+2r) - \delta_3^R] \cdot \sin[\frac{\pi\nu^R}{9r}(v-w)], \end{aligned} \tag{7.64}$$

$$\begin{aligned} T_a &= \sinh[\frac{\pi\mu^I}{3r}(u+2r)-\delta_2^I]\cdot\sin[\frac{2\pi\nu^R}{9r}(v-w)] \\ &- 2\cdot\sinh[\frac{\pi\mu^I}{6r}(u+2r)+\delta_3^I]\cdot\cosh[\frac{\pi\mu^I}{6r}(v-w)] \\ &\quad\cdot\sin[\frac{\pi\nu^R}{3r}(u+2r)-\delta_3^R]\cdot\sin[\frac{\pi\nu^R}{9r}(v-w)] \\ &- 2\cdot\cosh[\frac{\pi\mu^I}{6r}(u+2r)+\delta_3^I]\cdot\sinh[\frac{\pi\mu^I}{6r}(v-w)] \\ &\quad\cdot\cos[\frac{\pi\nu^R}{3r}(u+2r)-\delta_3^R]\cdot\cos[\frac{\pi\nu^R}{9r}(v-w)], \end{aligned} \tag{7.65}$$

with eigenvalue

$$k^2=\frac{4}{27}(\frac{\pi}{r})^2[(\nu^R)^2-\frac{3}{4}(\mu^I)^2]. \tag{7.66}$$

Equations (7.11) become

$$\begin{aligned} -2(M^I-N^I)\cdot\coth M^I &= 3\sigma r, \\ \frac{(3N^R+(n+\frac{1}{2})\pi)\sin(N^R)\cos(N^R)-(N^I-M^I)\sinh(N^I)\cosh(N^I)}{\cos^2(N^R)\cosh^2(N^I)+\sin^2(N^R)\sinh^2(N^I)} &= 3\sigma r, \\ \frac{(N^I-M^I)\sin(N^R)\cos(N^R)+(3N^R+(n+\frac{1}{2})\pi)\sinh(N^I)\cosh(N^I)}{\cos^2(N^R)\cosh^2(N^I)+\sin^2(N^R)\sinh^2(N^I)} &= 0. \end{aligned} \tag{7.67}$$

Finally, Equations (7.12) become

$$\delta_1=\frac{\pi}{2}-2N^R-M^I\cdot\imath;\ \delta_2=-\frac{\pi}{2}+(M^I-2N^I)\cdot\imath;\ \delta_3=\frac{\pi}{2}+2N^R-M^I\cdot\imath, \tag{7.68}$$

and Equations (7.13) become

$$\lambda=-\mu-\nu;\ \mu=\frac{2(M^I-N^I)}{\pi}\cdot\imath;\ \nu=(\frac{3N^R}{\pi}+n+\frac{1}{2})+\frac{N^I-M^I}{\pi}\cdot\imath. \tag{7.69}$$

For $\sigma=0$, k^2 is positive and, as σ is decreased, k^2, likewise, decreases. When σ reaches a critical value, $\hat{\sigma}_n<\sigma_n^*$, $k^2(\hat{\sigma}_n)=0$ and thereafter continues to decrease without bound. At the critical point, $\hat{\nu}=-\frac{1+\sqrt{3}\imath}{2}\cdot\hat{\mu}$ and $\hat{N}^R=-\frac{1}{3}[\sqrt{3}(\hat{N}^I-\hat{M}^I)+(n+\frac{1}{2})\pi]$.

Asymptotically, as $\sigma\to-\infty$, we have the limiting values:

$$M\to-\frac{\pi}{2}+[\frac{3}{2}\sigma r+\tanh^{-1}(1/2)]\cdot\imath;\ N\to-\frac{\pi}{2}+\tanh^{-1}(1/2)\cdot\imath, \tag{7.70}$$

$$\delta_2\to-\frac{\pi}{2}+[\frac{3}{2}\sigma r-\tanh^{-1}(1/2)]\cdot\imath;\ \delta_3\to-\frac{\pi}{2}-[\frac{3}{2}\sigma r+\tanh^{-1}(1/2)]\cdot\imath, \tag{7.71}$$

$$\mu\to\frac{3\sigma r}{\pi}\cdot\imath\ \&\ \nu\to(n-1)-\frac{3\sigma r}{2\pi}\cdot\imath\Rightarrow k^2\to-\sigma^2+\frac{4}{27}[\frac{\pi}{r}(n-1)]^2. \tag{7.72}$$

Figures 7.10 and 7.11 display $T_s^{1,2}$ and $T_a^{1,2}$, respectively, where $\sigma_2^*\approx-2.4036$ and $\hat{\sigma}_2\approx-7.3615$. Both plots display prominent vertex and edge singularities.

7.5 Spectral Properties

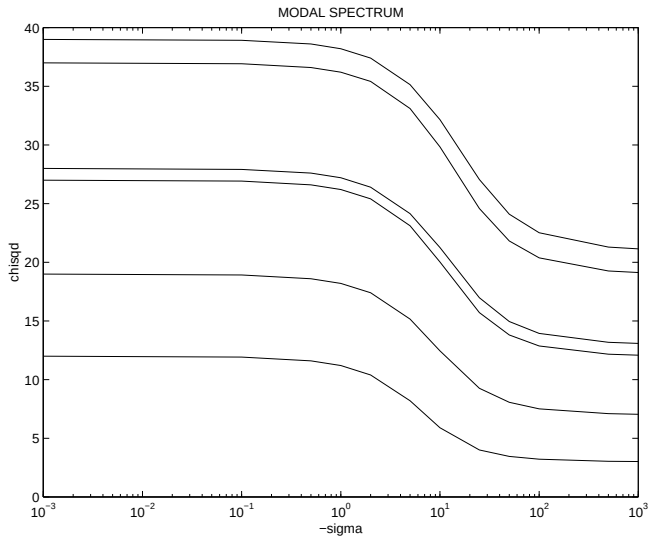

Figure 7.12: Spectral Parameter: ABC-Dirichlet Modes

The modal frequencies, $f_{m,n}$, are proportional to the square root of the eigenvalues given by Equation (7.7). Hence, we have

$$f_{m,n} \propto \frac{4\pi}{3h}\chi;\ \chi^2 := \mu^2 + \mu\nu + \nu^2. \tag{7.73}$$

Thus, the spectral structure, real or imaginary, of the equilateral triangle hinges upon the properties of the spectral parameter χ^2.

This spectral parameter as σ ranges from 0 to $-\infty$ is shown in Figure 7.12 for the first six ABC-Dirichlet modes: the $(2,2)$, $(2,3)$, $(3,3)$, $(2,4)$, $(3,4)$ and $(2,5)$ modes in order of increasing χ^2. The left side corresponds to the Neumann modes ($\sigma = 0$) and the right side corresponds to the Dirichlet modes ($\sigma = -\infty$). Thus, this figure graphically displays the homotopy relating these two well understood eigenvalue problems. Likewise, Figure 7.13 displays the cube root of the spectral parameter for the first six missing modes: the $(0,0)$, $(0,1)$, $(1,1)$, $(0,2)$, $(1,2)$ and $(0,3)$ modes also in order of increasing χ^2. Since $n^2 < 1+n+n^2 < (n+1)^2$ for $n \geq 1$, the interleaving of $(0,n)$ and $(1,n)$ modes present in Figure 7.13 persists as $n \to \infty$.

Since $T_s^{m,n}$ and $T_a^{m,n}$ both correspond to the same frequency $f_{m,n}$ given by Equation (7.73), it follows that all eigenvalues corresponding to $m \neq n$ have multiplicity equal to at least two. However, this modal degeneracy, as it is known in the engineering literature, extends also to the case $m = n$. Additional modal degeneracy is manifested by the intersection of two modal curves. For

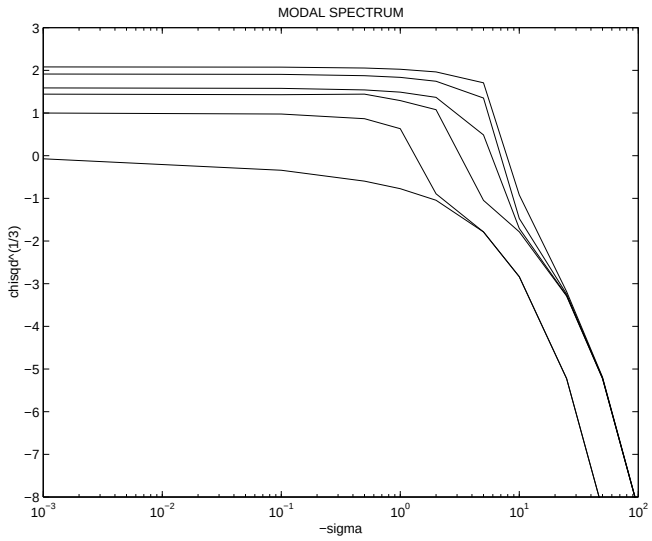

Figure 7.13: Spectral Parameter: Missing Modes

the Dirichlet and Neumann problems, number theoretic techniques permit a comprehensive treatment of such spectral multiplicity (Chapter 5 [53]).

However, for the Robin problem with either radiation or absorbing boundary condition, μ and ν are not integers and such techniques fail. At the present time, no general results are available and one must resort to perusal of Figure 7.12, suitably extended, in order to locate ABC-Dirichlet modal degeneracies for $0 > \sigma > -\infty$. All one can say with certainty is that if $(m_1 \geq 2, n_1)$ and $(m_2 \geq 2, n_2)$ are modal indices satisfying the inequalities

$$0 < (m_2^2 + m_2 n_2 + n_2^2) - (m_1^2 + m_1 n_1 + n_1^2) < 3[(m_2 + n_2) - (m_1 + n_1)] \quad (7.74)$$

then the corresponding modal curves must intersect for some value of σ which will thereby generate a corresponding modal degeneracy. For example, this inequality reveals that the $(2, 11)$ and $(6, 8)$ modes must be degenerate for some intermediate value of σ.

As Figure 7.13 indicates, the modal curves corresponding to missing modes never intersect (except possibly at infinity). However, if we were to superimpose Figure 7.13 upon Figure 7.12 then the $(0, n \geq 4)$ and $(1, n \geq 3)$ modal curves would intersect with those of ABC-Dirichlet modes thereby generating additional degeneracies.

7.6 Orthogonality and Completeness

By Rellich's Theorem [44], eigenfunctions corresponding to distinct eigenvalues are guaranteed to be orthogonal. Also, a symmetric mode and an

antisymmetric mode are automatically orthogonal. However, as we discovered above, the multiplicity of the eigenvalues given by Equation (7.7) is quite a complicated matter. Thus, we invoke the following continuity argument in order to confirm the orthogonality of our collection of eigenfunctions $\{T_s^{m,n}\ (n \geq m \geq 0);\ T_a^{m,n}\ (n > m \geq 0)\}$.

Suppose that f and g are eigenfunctions of like parity that share an eigenvalue, k^2, for some fixed value of $\sigma = \hat{\sigma}$. This corresponds to an intersection of two spectral curves. For σ in the neighborhood of $\hat{\sigma}$, Rellich's theorem guarantees that $\langle f, g \rangle = \int\int_\tau fg\ dA = 0$. Thus, by continuity, $\langle f, g \rangle = 0$ for $\sigma = \hat{\sigma}$ and orthogonality of our full collection of ABC modes is assured.

It is not *a priori* certain that the collection of eigenfunctions $\{T_s^{m,n},\ T_a^{m,n}\}$ constructed above is complete. For domains which are the Cartesian product of intervals in an orthogonal coordinate system, such as rectangles and annuli, completeness of the eigenfunctions formed from products of one-dimensional counterparts has been established [88]. Since the equilateral triangle is not such a domain, we must employ other devices in order to establish completeness.

We will utilize an analytic continuation argument which hinges upon the previously established completeness of the Neumann modes [77]. The homotopy between the Neumann and ABC modes that we have established above guarantees a unique branch leading from each of the Neumann modes to its corresponding ABC mode. Likewise, for any $-\infty < \sigma < 0$ we may trace out a branch from any mode leading back to a Neumann mode as $\sigma \to 0^-$.

Suppose, for the sake of argument, that the collection of ABC modes constructed above is not complete for some $-\infty < \sigma = \hat{\sigma} < 0$. Then, let $u(x, y; \hat{\sigma})$ be a mode that is not contained in our collection. As we have a self-adjoint operator, there exist ℓ analytic branches emanating from this point in Hilbert space where ℓ is the multiplicity of $k^2(\hat{\sigma})$ [22, pp. 92-94]. Denote any of these branches, analytically continued back to $\sigma = 0$ as $u(x, y; \sigma)$. Since we know that the collection of Neumann modes is complete, this branch must at some point, $\sigma = \sigma^*$, coalesce with a branch emanating from one of our ABC modes.

However, as we now show, the analytic dependence of $u(x, y; \sigma)$ upon σ precludes such a bifurcation at $\sigma = \sigma^*$. To see this, let

$$\Delta u + k^2 u = 0,\ (x, y) \in \tau;\ \frac{\partial u}{\partial \nu} + \sigma u = 0,\ (x, y) \in \partial\tau. \tag{7.75}$$

Then

$$u(x, y; \sigma) = u(x, y; \sigma^*) + u'(x, y; \sigma^*) \cdot (\sigma - \sigma^*) + u''(x, y; \sigma^*) \cdot \frac{(\sigma - \sigma^*)^2}{2} + \cdots, \tag{7.76}$$

where $u' := \frac{\partial u}{\partial \sigma}$ and each of the correction terms in the Taylor series is orthogonal to the eigenspace of $k^2(\sigma^*)$.

Each of the Taylor coefficients satisfies the boundary value problem

$$\Delta u^{(n)}(x,y;\sigma^*) + k^2(\sigma^*)u^{(n)}(x,y;\sigma^*) = 0,\ (x,y) \in \tau, \quad (7.77)$$
$$\frac{\partial u^{(n)}}{\partial \nu}(x,y;\sigma^*) + \sigma^* u^{(n)}(x,y;\sigma^*) = -nu^{(n-1)}(x,y;\sigma^*),\ (x,y) \in \partial\tau,$$

which may be solved recursively and uniquely for $u', u'', \ldots, u^{(n)}, \ldots$ since they are each orthogonal to the eigenspace of k^2. Thus, $u(x,y;\sigma)$ is uniquely determined and bifurcation cannot transpire. Consequently, our collection of ABC modes is indeed complete.

7.7 Hilbert and Courant

Figure 7.14: David Hilbert

Figure 7.15: Richard Courant

Methoden der mathematischen Physik [11, 12], affectionately known as Courant-Hilbert, is the most influential treatise on Applied Mathematics written in the 20th Century. (It is still in print in several languages well into the 21st Century!) It had its genesis in Hilbert's bold statement "Physics is much too hard for physicists!" [81, p. 127] and his subsequent fundamental work in mathematical physics. In 1918, Courant, his former assistant, proposed a joint book on methods of mathematical physics based upon Hilbert's Göttingen lecture notes. The main purpose of the text was to be that of reuniting divergent trends in Mathematics and physics. It succeeded in restoring the historically

deep connections between physical intuition and mathematical development and provided a unified approach to mathematical physics.

Due to Hilbert's poor health and focus on the foundations of Mathematics, Volume I (the first edition appeared in 1924 and the second edition, with the aid of K. O. Friedrichs, R. Luneberg and F. Rellich, in 1931) was written completely by Courant. Thus, what was originally envisioned as "Hilbert mit Courant" became "Courant und Hilbert". In addition to that of Hilbert, the influence of Lord Rayleigh's *Theory of Sound* was profoundly felt. This is especially true of its emphasis on vibration and eigenvalue problems. An extensive treatment of orthogonal function systems, integral equations, calculus of variations and special functions is also provided. It was fortuitous timing in that this volume contained much of the Mathematics needed to understand and solve the equations of Schrödinger's quantum wave mechanics of 1926.

Volume II appeared in 1937 and is concerned with the theory of partial differential equations, especially those aspects related to concepts of physics and mechanics. Kurt Friedrichs and Fritz John made substantial contributions to this volume. Essentially the first modern text on partial differential equations, it contains presages of the finite element method on which Courant would subsequently work. The most original part of this volume is the study of hyperbolic equations contained in Chapters 5 & 6. Subsequent German editions are essentially permutations and combinations of the 1931/1937 versions.

In 1943, as a result of its suppression by the Ministry of Culture in Nazi Germany, the U.S. Government licensed the reprinting of both volumes by Interscience Publishers. In 1953, an English translation of Volume I appeared [11] and was followed in 1962 by an English translation of Volume II [12]. Volume I was essentially a transcription from the German with some additions and modifications but Volume II grew from 549 pages to 830 pages. This significant expansion was assisted by Peter Lax, Louis Nirenberg and Lipman Bers. This translation ends with a new 30 page essay on ideal functions such as distributions in place of the last chapter of the German original on existence proofs using variational methods.

In Volume I, Chapter VI, the Robin boundary condition is treated by the calculus of variations [11, p.398]. A more elaborate treatment was contained in the last chapter of the 1937 German edition of Volume II which, unfortunately, was not translated in the 1962 English edition. A projected Volume III was to include it together with a treatment of finite difference methods [12, p. viii, p. 222]. It is lamentable that Volume III never appeared.

7.7.1 David Hilbert

David Hilbert (1862-1943), the most influential Mathematician of the late 19th and early 20th Centuries, was born in Königsberg, Prussia (now Kalin-

ingrad, Russia) [81]. He studied at the University of Königsberg where he received his doctorate in 1885 for a thesis on invariant properties of binary forms written under the supervision of Ferdinand von Lindemann. It was here that he became close life-long friends with his classmate Hermann Minkowski and young teacher Adolf Hurwitz. He remained as a professor at Königsberg from 1886 to 1895.

In 1895, he was recruited by Felix Klein to what would become the center of the Mathematical Universe at University of Göttingen where he would remain for the rest of his life. Among his students, there was a stellar alignment of mathematical talent: Wilhelm Ackermann, Felix Bernstein, Otto Blumenthal, Richard Courant, Haskell Curry, Max Dehn, Erich Hecke, Hellmuth Hecke, Carl Gustav Hempel, future world chess champion Emmanuel Lasker, Erhard Schmidt, Hugo Steinhaus, Hermann Weyl and Ernst Zermelo. As if this were not enough, John von Neumann served as his assistant.

Hilbert first worked in invariant theory before moving on to algebraic number theory. He put geometry in a formal axiomatic setting in his 1899 *Grundlagen der Geometrie*. In 1900, he presented his famous 23 "Problems of Mathematics" to the Second International Congress of Mathematicians in Paris. He then moved on to integral equations and mathematical physics where he introduced the notion of Hilbert space (one of the cornerstones of functional analysis) and made fundamental contributions to the field equations of general relativity, kinetic gas theory, radiation theory and the molecular theory of matter. See the above discussion of *Methoden* by Courant and Hilbert.

In the winter of 1920-21, Hilbert gave a course of public lectures four times weekly at Göttingen on geometry based upon an approach of strictly visual intuition. They were intended by him to popularize Mathematics with the young men returning to the University after the war. The corresponding notes were published in 1932 (with Stephan Cohn-Vossen) as *Anschauliche Geometrie* and translated into English as *Geometry and the Imagination* in 1952. In his own words, "We want to take the reader on a leisurely walk, as it were, in the big garden that is geometry, so that each may pick for himself a bouquet to his liking.". In a 1933 review, the journal *Nature* described it as "surely the most fascinating volume ever offered to the ordinary mathematician".

Also in 1920, he proposed the so-called Hilbert Program to formally axiomatize all of Mathematics. In this direction, he published *Grundzüge der Theoretischen Logik* with Wilhelm Ackermann in 1928 and *Grundlagen der Mathematik* (two volumes) with Paul Bernays in 1934/1938. To a certain extent, this program was undercut by Gödel's Incompleteness Theorem of 1931. Other mathematical concepts which bear his name are the Hilbert Hotel, Hilbert matrix, Hilbert transform, Hilbert-Schmidt operator and Hilbert's Nullstellensatz.

He died in Göttingen in the midst of World War II from complications aris-

ing from a broken arm incurred during a fall in the street, aged 81. Not more than a dozen people attended the funeral service of this Mathematical Titan! Engraved on his tombstone is the immortal epitath: *Wir müssen wissen. Wir werden wissen.* (*We must know. We shall know.*)

7.7.2 Richard Courant

Richard Courant (1888-1972), founder of two great Mathematical Institutes, was born in Lublinitz in Upper Silesia, now part of Poland but then of Germany [80]. He began his studies at University of Breslau, spent a semester at University of Zurich and, in 1907, arrived at the Mecca of Mathematics, University of Göttingen. The following year, Hilbert chose him to be his assistant and supervised his 1910 doctoral thesis on the application of Dirichlet's Principle to conformal mapping. This same topic was the subject of his 1912 habilitation dissertation and also became the basis for his classic 1950 treatise *Dirichlet's Principle, Conformal Mapping, and Minimal Surfaces*. He also achieved considerable notoriety for his soap bubble realizations of such minimal surfaces as recorded in the 1966 *MAA Video Classics #4: Courant in Göttingen and New York*.

After serving in World War I and a brief appointment at Münster, he returned to Göttingen where, in 1922 he founded the Mathematisches Institut, which he directed until his expulsion by the Nazis in 1933. (Figure 7.16 shows a 1995 photo of yours truly visiting the Mathematisches Institut at Göttingen as part of his Gauss Pilgrimage.) During this period, he showed that among all plane domains with prescribed perimeter, the circle has the lowest fundamental frequency. This was followed by his max-min principle that enabled him to determine the asymptotic distribution and lower bounds for the eigenvalues of the Laplacian over any domain. In 1922, his first book (with Adolf Hurwitz) *Function Theory* was published. Also, see the above discussion of Courant-Hilbert's *Methoden* of 1924. In 1927/1929, there appeared his remarkable two-volume text *Differential and Integral Calculus*. In 1928, Courant, Friedrichs and Lewy published their famous paper on the partial difference equations of mathematical physics which introduced the notions of CFL condition and Courant number.

After his expulsion by the Nazis, he joined New York University in 1934. One of his most influential contributions was what became known in the 1960's as the "finite element method". This method first appeared in an existence proof of a version of the Riemann mapping theorem in Hurwitz-Courant in 1922. The idea reappeared as a footnote in Courant-Hilbert in 1924. Its first application as a numerical method was given by Courant in 1943 in his solution of a torsion problem.

In 1941, Courant (with Herbert Robbins) published the classic *What Is*

Figure 7.16: Mathematisches Institut Universität Göttingen

Mathematics? for the general reader. In his own words, "It is possible to proceed on a straight road from the very elements to vantage points from which the substance and driving force of modern Mathematics can be surveyed. The present book is an attempt in this direction.". Courant-Robbins is spectacularly successful in its mission and has fundamentally altered the lives of many young developing Mathematicians, as it did for the present author when he discovered it in high school. It has received uniformly high praise from the likes of Albert Einstein, "A lucid presentation of the fundamental concepts and methods of the whole field of Mathematics. It is an easily understandable introduction for the layman and helps to give the mathematical student a general view of the basic principles and methods.".

During the remaining years of World War II he assembled an all-star cast of Mathematicians and worked on defense-related Mathematics which culminated in the 1948 monograph (with Kurt Otto Friedrichs) *Supersonic Flow and Shock Waves*. He was also charged with the development of a graduate program in Applied Mathematics. This he did with a vengeance, successfully transplanting the mathematical spirit from Göttingen to New York. The net result was the establishment in 1953 of the Institute of Mathematical Sciences at New York University which in 1964 was renamed the Courant Institute of Mathematical Sciences (CIMS). CIMS has become a focal point for the train-

ing of new generations of Applied Mathematicians (present author included). After suffering a stroke, he died in New Rochelle, New York, aged 84. As a testament to his legacy, Figure 7.17 shows CIMS towering above the surrounding Washington Square, a shining beacon for Applied Mathematicians world-wide. In 2010, *U.S. News and World Report* once again ranked the graduate program of the Courant Institute #1 in Applied Mathematics!

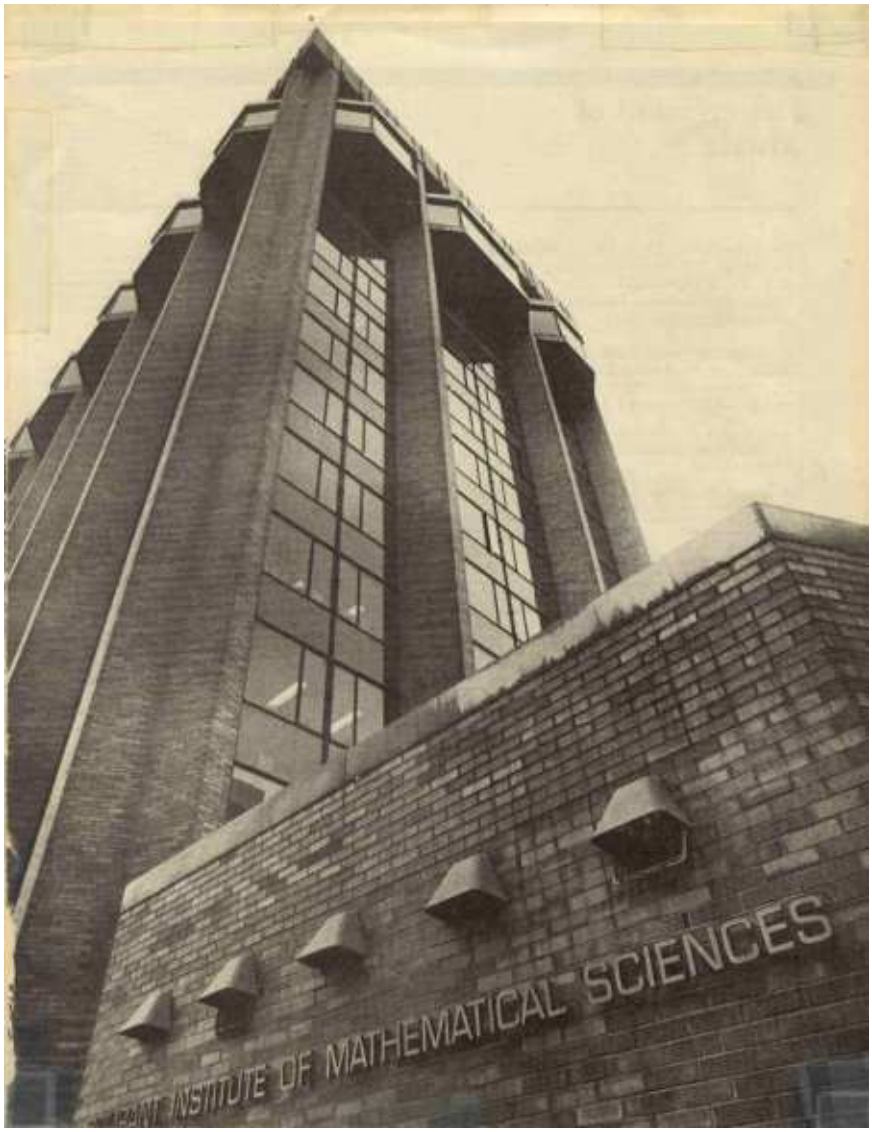

Figure 7.17: Courant Institute of Mathematical Sciences

Chapter 8

The Sturm-Liouville Boundary Value Problem

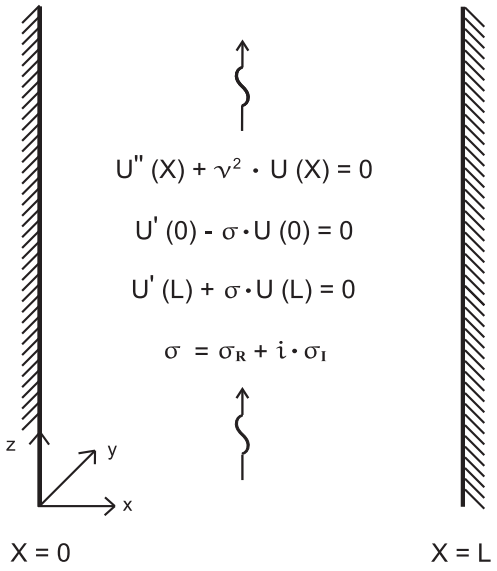

Figure 8.1: Parallel Plate Waveguide

Herein, we explore the eigenstructure of the Sturm-Liouville boundary value problem (SL-BVP) with an impedance boundary condition (IBC)

$$\begin{aligned} u''(x) + \lambda \cdot u(x) &= 0,\ 0 < x < L, \\ u'(0) - \sigma \cdot u(0) &= 0, \\ u'(L) + \sigma \cdot u(L) &= 0. \end{aligned} \tag{8.1}$$

The complex boundary parameter $\sigma = \sigma_R + \imath \cdot \sigma_I$ is assumed to have the same value at both ends of the interval $J = [0, L]$. Attention will be restricted to

this case as it is the one most relevant to the extension of the results for the eigenstructure of the equilateral triangle [54, 55] from real to complex values of σ which furnishes the motivation for the present one-dimensional study.

Figure 8.1 illustrates the parallel plate waveguide problem which gives rise to the SL-BVP, Equation (8.1). Either an acoustic [70, pp. 485-496] or electromagnetic [45, pp. 81-84] time-harmonic wave of angular frequency ω is propagating in the z-direction with no field variation in the y-direction. The complex material parameter σ is related to the wall impedance which accounts for field penetration into the walls of the waveguide. After the SL-BVP has been solved for the eigenvalue λ and the corresponding eigenfunction (mode) $u(x)$, the real physical field may be reconstructed as

$$U(x,z,t) = Re\{u(x) \cdot e^{i(\omega t - \gamma z)}\},\ \gamma := \sqrt{\omega^2 - \lambda}. \tag{8.2}$$

This same SL-BVP arises in the study of the vibrating string with sidewise displacement of the end supports [66, pp. 133-134].

Much of the current mathematical literature devoted to SL-BVPs is concerned primarily with the self-adjoint case [1, 93]. However, the SL-BVP described by Equation (8.1) is non-self-adjoint for complex values of σ. Fortunately, a classic reference on the non-self-adjoint case is provided by [9, pp. 298-305] where it is shown that this problem reduces to the study of the solutions of a single transcendental equation.

In what follows, we will derive and exhaustively study this transcendental equation [56]. The principal focus will be on what happens to the eigenstructure of the Neumann problem ($\sigma = 0$) as σ proceeds along rays emanating from the origin toward the point at infinity in the complex plane. We will find that, for the most part, there is a natural homotopy connecting the Neumann modes to those of a corresponding Dirichlet problem (IBC-Dirichlet modes). However, we will show that, under appropriate conditions, there will be two Neumann eigenvalues that have no Dirichlet counterpart. The determination of the precise nature of these latter eigenvalues together with that of their corresponding eigenfunctions ("missing modes") is the primary concern of the present investigation.

8.1 Solution of the Sturm-Liouville Boundary Value Problem

Ignoring the boundary conditions, the general solution to Equation (8.1) is

$$u(x) = \cos\left(\frac{\nu\pi x}{L} - \delta\right),\ \lambda = \left(\frac{\nu\pi}{L}\right)^2. \tag{8.3}$$

Application of the boundary condition at $x = 0$ yields

$$\tan(\delta) = \frac{\sigma L}{\nu\pi}, \tag{8.4}$$

while imposition of the boundary condition at $x = L$ yields

$$\tan(\nu\pi - \delta) = \frac{\sigma L}{\nu\pi}. \tag{8.5}$$

Equations (8.4) and (8.5) may be combined to produce the transcendental equation

$$(2\delta + n\pi)\tan(\delta) = \sigma L,\ \nu = \frac{2\delta}{\pi} + n, \tag{8.6}$$

with n an integer.

Observe that in Equation (8.1) when $\sigma \to 0$ we recover the Neumann problem, $u'(0) = 0 = u'(L)$, whose solution, $u(x) = N_n(x) := \cos(\frac{n\pi x}{L})$, is obtained from Equation (8.6) with $\delta = 0 \Rightarrow \nu = n$. Thus, we may profitably view σ as a continuation parameter which provides a homotopy extending from this well understood problem to that of the impedance boundary condition. Throughout the ensuing development we will avail ourselves of this important observation.

Furthermore, note that *if the normal derivative remains bounded* then $\sigma \to \infty$ yields the Dirichlet problem, $u(0) = 0 = u(L)$, whose solution, $u(x) = \pm D_{n\pm1}(x) := \pm\sin(\frac{(n\pm1)\pi x}{L})$, is obtained from Equation (8.6) with $\delta = \pm\frac{\pi}{2} \Rightarrow \nu = n \pm 1$. In that case, the homotopy may be further extended to lead from a Neumann mode to a corresponding Dirichlet mode. As will subsequently be shown, for the impedance boundary condition this is usually, although by no means always, the case.

Introduction of $z := \delta + \frac{n\pi}{2}$ into Equation (8.6) reduces it to

$$z\tan(z) = \frac{\sigma L}{2}, \tag{8.7}$$

if n is even and

$$z\cot(z) = -\frac{\sigma L}{2}, \tag{8.8}$$

if n is odd. These two cases may then be separately studied from the graphical representation of their respective complex transformations [70, p. 909].

However, in the case of the equilateral triangle [54, 55] which is our ultimate goal, such a reduction is not available. Thus, Equation (8.6) itself will be numerically approximated using MATLAB [34, 64]. This will permit us to trace out trajectories in the complex δ-plane or, equivalently, in the complex ν-plane as the complex boundary parameter σ is varied.

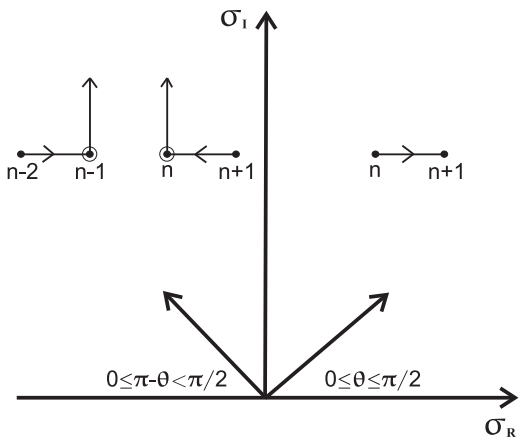

Figure 8.2: Complex Boundary Parameter

As shown in Figure 8.2, beginning with $\sigma = 0$ (the Neumann problem), we will allow σ to move along a ray inclined at an angle θ to the horizontal toward the point at infinity. We may then track the trajectory of each Neumann eigenvalue in order to determine whether it eventually approaches a Dirichlet eigenvalue (in which case it will be called an IBC-Dirichlet mode) or migrates to infinity (in which case it will be called a "missing mode"). We will eventually find that these are the only two possible types of asymptotic behavior.

8.2 S-L BVP Solution Properties

Before constructing a taxonomy of the asymptotic nature of the eigenstructure of our SL-BVP with an IBC as $\sigma \to \infty$ (at which time, the mysterious icons on Figure 8.2 will become intelligible), it behooves us to first catalog some important properties of the eigenvalues and eigenfunctions of Equation (8.1).

We begin with the observation that, without loss of generality, we may restrict our attention to the case $Im(\sigma) \geq 0$ since, by taking complex conjugates in Equation (8.6), we find that $\sigma \mapsto \bar{\sigma} \Rightarrow \delta \mapsto \bar{\delta} \Rightarrow \nu \mapsto \bar{\nu}$. Thus, in the event that $Im(\sigma) < 0$, we can obtain trajectories in either the δ-plane or ν-plane by reflection about the real axis of the corresponding trajectories for $\bar{\sigma}$.

Furthermore, taking complex conjugates in Equation (8.1) itself reveals that $\sigma \mapsto \bar{\sigma} \Rightarrow \lambda \mapsto \bar{\lambda} =: \mu,\ u(x) \mapsto \bar{u}(x) =: v(x)$ where μ and $v(x)$ form the solution to the adjoint boundary value problem

$$\begin{aligned} v''(x) + \mu \cdot v(x) &= 0,\ 0 < x < L, \\ v'(0) - \bar{\sigma} \cdot v(0) &= 0, \\ v'(L) + \bar{\sigma} \cdot v(L) &= 0. \end{aligned} \tag{8.9}$$

Since the SL-BVP is non-self-adjoint for complex σ, the eigenvalues and eigenfunctions can be complex and, most importantly, eigenfunctions corresponding to distinct eigenvalues are not necessarily orthogonal with respect to the complex inner product $< f(x), g(x) >:= \int_0^L f(x)\bar{g}(x)\,dx$. However, we do have the biorthogonality relationship involving the eigenfunctions of the boundary value problem, Equation (8.1), and those of of the adjoint boundary value problem, Equation (8.9),

$$< u_p(x), v_q(x) >:= \int_0^L u_p(x)\bar{v}_q(x)\,dx = 0. \tag{8.10}$$

In turn, this provides us with the eigenfunction expansion

$$f(x) = \sum_{k=1}^{\infty} < f(x), v_k(x) > u_k(x), \tag{8.11}$$

where the series converges in the mean for $f(x) \in \mathcal{L}^2(0, L)$ [9, pp. 310-312].

We have already seen via Equations (8.7) and (8.8) that the modes naturally partition according to the parity of n. This fact is underscored by

Theorem 8.2.1. *The even/odd numbered modes are symmetric/antisymmetric, respectively, on the interval* $[0, L]$ *for all values of* σ*.*

Proof: Equation (8.3) may be recast as $u_n(x) = \cos\left(\frac{\nu\pi}{L}(x - \frac{L}{2}) + \frac{n\pi}{2}\right)$. Thus, if n is even/odd then $u_n(x)$ is a cosine/sine, respectively, centered at $x = \frac{L}{2}$. □

8.3 The Case of Real σ

In the case of real σ, the eigenstructure of the SL-BVP with an IBC defined by Equation (8.1) has been exhaustively treated in [88, pp. 90-98]. As a springboard for the study of the case of complex σ in the next section, we review here the highlights of those results.

When σ is real, the problem is self-adjoint so that the eigenvalues are real and the eigenfunctions can also be chosen to be real. Moreover, eigenfunctions corresponding to distinct eigenvalues are orthogonal with respect to the real inner product $< f(x), g(x) >:= \int_0^L f(x)g(x)\,dx$. Because of their very different behaviors, we treat the cases $\sigma \geq 0$ and $\sigma < 0$ separately. We will eventually see that, taken together, they display the characteristic behaviors exhibited in the general case of complex σ.

In what follows, we denote the dependence of the eigenvalues and eigenfunctions upon σ by $\lambda_n(\sigma) = (\frac{\nu(\sigma)\pi}{L})^2$ and $u_n(x;\sigma)$, respectively, for $n = 0, 1, \ldots$. The subscript n is chosen so that when $\sigma = 0$ they reduce to the corresponding values for the Neumann problem, $\delta_n(0) = 0 \Rightarrow \nu_n(0) = n$ and

$u_n(x;0) = N_n(x) := \cos(\frac{n\pi x}{L})$. Also, the Dirichlet problem has the same eigenvalues $\lambda_n(0)$ but with the restriction $n = 1, 2, \ldots$ and its corresponding eigenfunctions are denoted by $u_n(x;0) = D_n(x) := \sin(\frac{n\pi x}{L})$.

8.3.1 The Case $\sigma \geq 0$

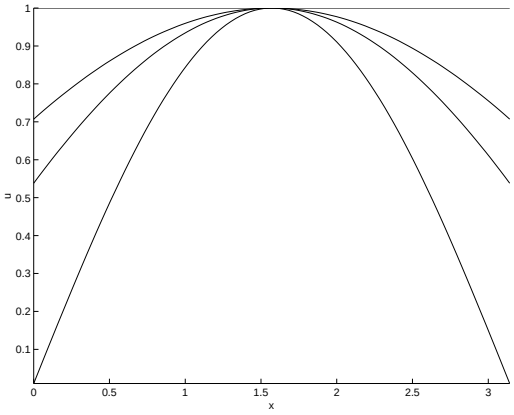

Figure 8.3: Mode Morphing ($n = 0,\ \theta = 0,\ L = \pi$)

The case of the radiation boundary condition ($\sigma > 0$) is by far the simplest in that the eigenvalues are not only real but are in fact all positive. Moreover, $n < \nu_n(\sigma) < n + 1$. It also possesses the simplest asymptotic behavior in that

$$\lim_{\sigma\to+\infty} \delta_n(\sigma) = \frac{\pi}{2} \Rightarrow \lim_{\sigma\to+\infty} \nu_n(\sigma) = n + 1,\ \lim_{\sigma\to+\infty} u_n(x;\sigma) = D_{n+1}(x). \quad (8.12)$$

That is, the Neumann mode $N_n(x)$ "morphs" analytically into the Dirichlet mode $D_{n+1}(x)$ as σ ranges from 0 to ∞. This is illustrated in Figure 8.3 which displays this homotopy between fundamental modes ($n = 0$) for $0 \leq \sigma \leq +\infty$.

8.3.2 The Case $\sigma < 0$

The case of the absorbing boundary condition ($\sigma < 0$) is more complicated in that the eigenvalues while still real are no longer all positive. However, for $n = 2, 3, \ldots$ we have $n - 1 < \nu_n(\sigma) < n$. These so-called IBC-Dirichlet modes possess the simple asymptotic behavior described by

$$\lim_{\sigma\to-\infty} \delta_n(\sigma) = -\frac{\pi}{2} \Rightarrow \lim_{\sigma\to-\infty} \nu_n(\sigma) = n - 1,\ \lim_{\sigma\to-\infty} u_n(x;\sigma) = -D_{n-1}(x). \quad (8.13)$$

That is, the Neumann mode $N_n(x)$ "morphs" analytically into the Dirichlet mode $-D_{n-1}(x)$ as σ ranges from 0 to $-\infty$. This is illustrated in Figure 8.4 which displays this homotopy between $N_2(x)$ and $-D_1(x)$ for $0 \geq \sigma \geq -\infty$.

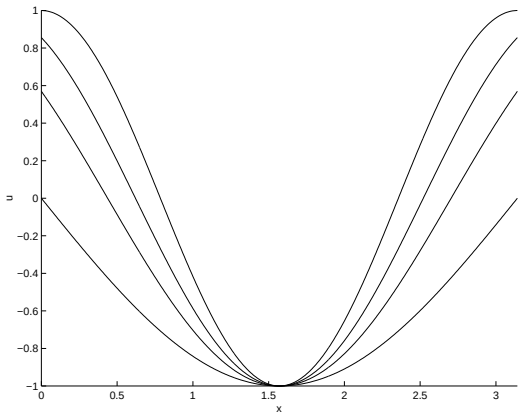

Figure 8.4: Mode Morphing ($n = 2,\ \theta = \pi,\ L = \pi$)

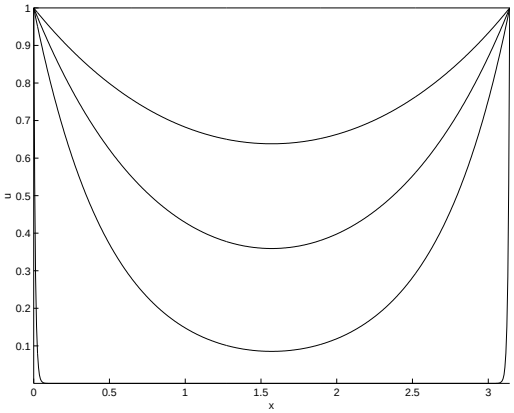

Figure 8.5: Missing Mode ($n = 0,\ \theta = \pi,\ L = \pi$)

This leaves open the case of the "missing modes" $n = 0, 1$. Since there are no Dirichlet modes for $n = -1, 0$ we clearly do not have the simple asymptotic behavior described by Equation (8.13). Thus we are confronted with the question: "What happens to the missing $n = 0, 1$ modes as $\sigma \to -\infty$?". The solution to the mystery of the missing modes naturally decomposes into two special cases each of which we now explore separately.

For $n = 0$, $\nu_0(\sigma)$ is pure imaginary and, consequently, $\lambda_0(\sigma)$ is negative. Specifically, for $\sigma \to -\infty$,

$$\delta_0(\sigma) \approx -\frac{\sigma L}{2} \cdot \imath \Rightarrow \nu_0(\sigma) \approx -\frac{\sigma L}{\pi} \cdot \imath \Rightarrow u_0(x;\sigma) \approx \cosh\left(-\sigma x + \frac{\sigma L}{2}\right). \quad (8.14)$$

This asymptotic expression for $u_0(x;\sigma)$ becomes unbounded as $\sigma \to -\infty$. However, if we first scale it by its value at an endpoint, $\cosh\left(\frac{\sigma L}{2}\right)$, we find that

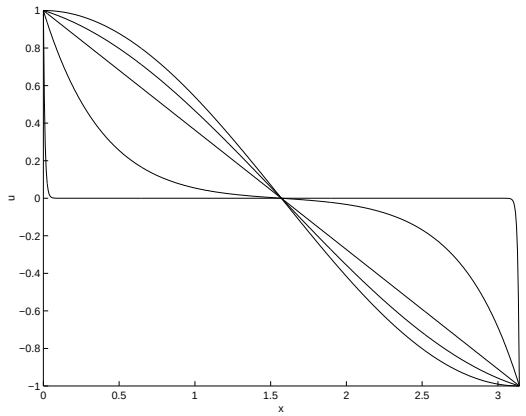

Figure 8.6: Missing Mode ($n = 1,\ \theta = \pi,\ L = \pi$)

this normalized mode approaches 1 at the two endpoints and 0 elsewhere. Such singular limiting behavior, necessary since this does not approach a Dirichlet mode, is on prominent display in Figure 8.5.

For $n = 1$, $\nu_1(\sigma)$ initially decreases along with σ until it vanishes when $\sigma = -\frac{2}{L}$. Specifically,

$$\lim_{\sigma \to -\frac{2}{L}} \delta_1(\sigma) = -\frac{\pi}{2} \cdot \imath \Rightarrow \lim_{\sigma \to -\frac{2}{L}} \nu_1(\sigma) = 0 \Rightarrow \lim_{\sigma \to -\frac{2}{L}} u_1(x;\sigma) = 0. \tag{8.15}$$

However, if we first scale $u_1(x;\sigma)$ by its value at the endpoint $x = 0$, $\cos(\delta)$, we find that this normalized mode approaches the straight line $u_1(x; -\frac{2}{L}) = 1 - \frac{2}{L} \cdot x$.

As σ continues to decrease we have, for $\sigma < -\frac{2}{L}$, pure imaginary $\delta_1(\sigma) + \frac{\pi}{2}$ thereby producing a $\nu_1(\sigma)$ which is also pure imaginary and, consequently, $\lambda_1(\sigma)$ becomes negative. Specifically, for $\sigma \to -\infty$,

$$\delta_1(\sigma) \approx -\frac{\pi}{2} - \frac{\sigma L}{2} \cdot \imath \Rightarrow \nu_1(\sigma) \approx -\frac{\sigma L}{\pi} \cdot \imath \Rightarrow u_1(x) \approx \imath \cdot \sinh\left(\sigma x - \frac{\sigma L}{2}\right). \tag{8.16}$$

This asymptotic expression for $u_1(x;\sigma)$ becomes unbounded as $\sigma \to -\infty$. However, if we first scale it by its value at the endpoint $x = 0$, $\imath \cdot \sinh(-\frac{\sigma L}{2})$, we find that this normalized mode approaches ± 1 at the left-/right-hand endpoint, respectively, and 0 elsewhere. The resulting unbounded derivative, necessary since this does not approach a Dirichlet mode, is evident in Figure 8.6.

8.4 The Case of Complex σ

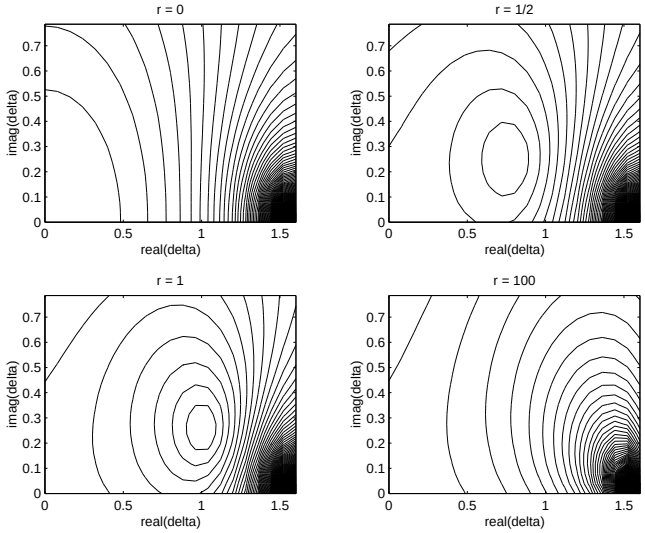

Figure 8.7: Modal Trajectories ($n = 0,\ \theta = \pi/4,\ L = \pi$)

In the case of complex σ, as previously noted, the SL-BVP defined by Equation (8.1) is non-self-adjoint and the eigenstructure is consequently complex. Defining the residual function of Equation (8.6) as

$$\rho_n(\delta;\sigma) = |(2\delta + n\pi)\tan(\delta) - \sigma L|, \tag{8.17}$$

we note that the sought-after eigenvalues are determined by its local minima. Next, define

$$\sigma = r \cdot e^{\imath\theta},\ \text{with } \theta \text{ fixed and } 0 \le r \le +\infty. \tag{8.18}$$

Figure 8.7, which is a contour plot of ρ_n, displays the resultant trajectory in the δ-plane for $n = 0$ as r varies with $\theta = \frac{\pi}{4}$. As occurred in the real case with $\sigma \ge 0$, δ varies from 0 to $\frac{\pi}{2}$ only now it makes an excursion into the complex plane rather than traveling along the real axis. The attendant complex mode morphing from $N_0(x)$ to $D_1(x)$ is made explicit by Figure 8.8.

Figure 8.9 displays the corresponding trajectories, this time in the ν-plane, for the the first four modes over the full range of values $0 \le \theta \le \pi$. As is evident from each of these plots, for some values of θ mode morphing occurs, i.e $\lambda_n(\sigma) \to \lambda_{n\pm1}(0)$, (IBC-Dirichlet modes) while for other values of θ we observe $|\lambda_n(\sigma)| \to \infty$ (missing modes). We are going to devote our remaining efforts to clarifying this asymptotic behavior.

In order to achieve this, we will require detailed knowledge of the properties of trajectories in the ν-plane. We commence with

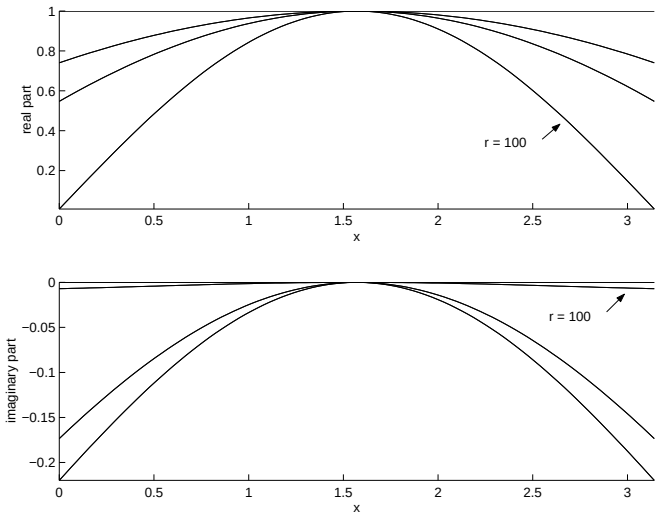

Figure 8.8: Mode Morphing ($n = 0,\ \theta = \pi/4,\ L = \pi$)

Theorem 8.4.1. *1. Let $\delta_n(r) = \delta_n^R(r) + \imath \cdot \delta_n^I(r)$ and $\nu_n(r) = \nu_n^R(r) + \imath \cdot \nu_n^I(r)$. Then, the trajectories $\delta_n(r)$ and $\nu_n(r)$ have the same slope.*

(a) If $n \neq 0$ then the trajectory $\nu_n(r)$ makes an angle θ measured counterclockwise from the real axis at $\nu_n(0) = n$.

(b) If $n = 0$ then the trajectory $\nu_0(r)$ makes an angle $\theta/2$ measured counterclockwise from the real axis at $\nu_0(0) = 0$.

2. As $r \to \infty$, either $\nu_n(r) \to n \pm 1$ or $|\nu_n(r)| \to \infty$.

(a) if $\nu_n(r) \to n \pm 1$ then the trajectory $\nu_n(r)$ makes an angle $\pi - \theta$ measured counterclockwise from the real axis at $\nu_n(\infty) = n \pm 1$.

(b) if $|\nu_n(r)| \to \infty$ then the trajectory $\nu_n(r)$ goes off to infinity at an angle $\theta - \frac{\pi}{2}$ measured counterclockwise from the real axis as $r \to \infty$.

Proof:

1. Since $\nu_n'(r) = \frac{2}{\pi} \cdot \delta_n'(r)$, both trajectories have slope $\delta_n^{I\prime}(r)/\delta_n^{R\prime}(r)$.

   (a) $r = 0 \Rightarrow \sigma = 0$ so that Equation (8.6) produces $\delta_n(0) = 0 \Rightarrow \nu_n(0) = n$. Substitution of Equation (8.18) into Equation (8.6) with subsequent differentiation with respect to r yields

$$\delta_n'(r) = \frac{Le^{\imath\theta}\cos^2(\delta_n(r))}{\sin(2\delta_n(r)) + 2\delta_n(r) + n\pi}. \tag{8.19}$$

   Thus, $\delta_n'(0) = \frac{Le^{\imath\theta}}{n\pi} \Rightarrow \tan\phi := \delta_n^{I\prime}(0)/\delta_n^{R\prime}(0) = \tan\theta \Rightarrow \phi = \theta$.

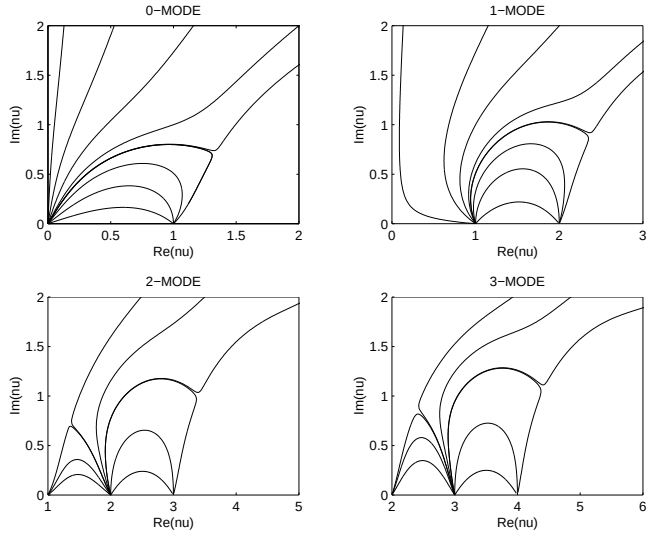

Figure 8.9: Modal Regions

(b) For $n = 0$, Equation (8.19) produces $\delta_0'(0) = \infty$ so that the slope $\tan\phi := \lim_{r\to 0} \delta_0^{I\prime}(r)/\delta_0^{R\prime}(r) = \lim_{r\to 0} \delta_0^I(r)/\delta_0^R(r)$ is indeterminate. However, by Equation (8.19),

$$\tan\phi = \lim_{r\to 0} \frac{Im[\frac{Le^{\imath\theta}}{4\delta_0(r)}]}{Re[\frac{Le^{\imath\theta}}{4\delta_0(r)}]} = \lim_{r\to 0} \frac{\delta_0^R \sin\theta - \delta_0^I \cos\theta}{\delta_0^R \cos\theta + \delta_0^I \sin\theta} = \frac{\tan\theta - \tan\phi}{1 + \tan\phi\tan\theta}.$$

Thus, $\tan\phi = \tan(\theta - \phi) \Rightarrow \phi = \theta/2$.

2. As $r = |\sigma| \to \infty$, Equation (8.6) clearly implies that either $\delta_n(r) \to \pm\frac{\pi}{2}$, in which case $\nu_n(r) \to n \pm 1$, or $|\delta_n(r)| \to \infty$, in which case $|\nu_n(r)| \to \infty$.

   (a) If $\delta_n(r) \to \pm\frac{\pi}{2}$ then $\nu_n(r) \to n \pm 1$ and $\delta_n'(r) \to 0$ by Equations (8.6) and (8.19), respectively. Thus, as $r \to \infty$, $\delta_n'(r) \to \epsilon_1 e^{\imath\phi}$ and $\delta_n(r) \to \pm\frac{\pi}{2} \pm \epsilon_2 e^{\imath\phi}$ where $\epsilon_1, \epsilon_2 \to 0$. Comparison of the arguments of both sides of Equation (8.19) reveals that $\phi = \theta + 2\phi \Rightarrow \phi = -\theta$.

   (b) If $|\delta_n(r)| \to \infty$ then $\tan(\delta_n(r)) \to \imath$. Inserting this into Equation (8.6) and equating real and imaginary parts produces $2\delta_n^R \to rL\sin(\theta)$ and $-2\delta_n^I \to rL\cos(\theta)$. Thus, $\frac{\delta_n^I(r)}{\delta_n^R(r)} \to -\cot(\theta) = \tan(\theta - \frac{\pi}{2})$. □

Returning now to Figure 8.9, note the following important structural features. For modes $n = 0$ and $n = 1$, there is a critical angle θ_n^- such that for $\theta < \theta_n^-$ we have the mode morphing $N_n(x) \mapsto D_{n+1}(x)$ while, for $\theta > \theta_n^-$, mode n is missing in the previously defined sense as $r \to \infty$. For all other

modes $n \geq 2$, there are two critical angles θ_n^- and θ_n^+. For $\theta < \theta_n^-$ we have the mode morphing $N_n(x) \mapsto D_{n+1}(x)$ and for $\theta > \theta_n^+$ we have the mode morphing $N_n(x) \mapsto -D_{n-1}(x)$ as $r \to \infty$. In the intermediate regime $\theta_n^- < \theta < \theta_n^+$, mode n is missing as $r \to \infty$.

Our next result concerns the trajectories at these critical angles.

Theorem 8.4.2. *1. The critical trajectories all possess a corner located in the δ-plane at the roots of the function*

$$\tau_n(\delta) := \sin(2\delta) + 2\delta + n\pi. \tag{8.20}$$

The smallest root with $Re(\delta_n^-) > 0$ corresponds to θ_n^- and the smallest root with $Re(\delta_n^+) < 0$ corresponds to θ_n^+.

2. All of these corners of the critical trajectories are 90°.

3. In the special case, $\theta = -\pi,\ n = 1$, the corner is located at $\delta = -\frac{\pi}{2}$ with a corresponding $\sigma = -\frac{2}{L}$.

Proof:

1. Clearly, there can be no transition from a bounded mode-morphing trajectory to the unbounded trajectory of a missing mode without a singularity exhibiting a corner. At such a corner, the derivative $\delta_n'(r)$ must either vanish or become unbounded. Inspection of Equation (8.19) reveals that the derivative does not vanish since $Im(\delta_n(r) > 0)$ for $r > 0$. Further perusal of Equation (8.19) shows that the derivative becomes unbounded if and only if $\delta_n(r)$ is located at a zero of the denominator, i.e. at a root of Equation (8.20). These critical values $\delta_n^\pm$ occur at branch points [67, pp. 404-408] of Equation (8.7) if n is even and of Equation (8.8) if n is odd. Observe that once $\delta_n^\pm$ is known then Equation (8.6) may be used to find the critical angle and modulus from $\sigma_n^\pm = r_n^\pm e^{\imath\theta_n^\pm}$.

2. The corner will be 90° if and only if $\mathcal{L} := \lim_{\epsilon\to 0^+} \frac{\delta_n'(r^\pm+\epsilon)}{\delta_n'(r^\pm-\epsilon)}$ is pure imaginary since, in that and only that case, the tangent vector is multiplied by a pure imaginary as we pass through the corner thereby producing the posited rotation by ±90°. But,

$$\mathcal{L} = \lim_{\epsilon\to 0^+} \frac{\cos^2(\delta_n(r_n^\pm+\epsilon))}{\cos^2(\delta_n(r_n^\pm-\epsilon))} \cdot \lim_{\epsilon\to 0^+} \frac{\sin(2\delta_n(r_n^\pm-\epsilon)) + 2\delta_n(r_n^\pm-\epsilon) + n\pi}{\sin(2\delta_n(r_n^\pm+\epsilon)) + 2\delta_n(r_n^\pm+\epsilon) + n\pi} =$$

$$\lim_{\epsilon\to 0^+} \frac{\delta_n'(r^\pm-\epsilon)}{\delta_n'(r^\pm+\epsilon)} \cdot \lim_{\epsilon\to 0^+} \frac{-2\cos(2\delta_n(r_n^\pm-\epsilon)) - 2}{+2\cos(2\delta_n(r_n^\pm-\epsilon)) + 2} = \frac{1}{\mathcal{L}} \cdot (-1),$$

by l'Hôpital's Rule. Thus, $\mathcal{L}^2 = -1 \Rightarrow \mathcal{L} = \pm\imath$.

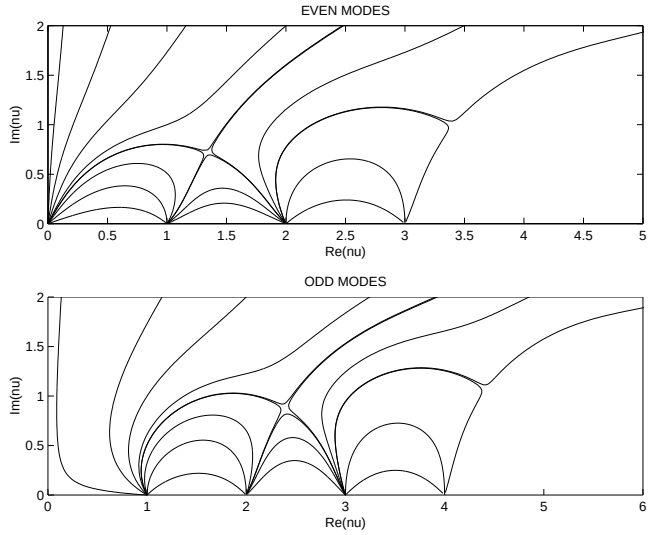

Figure 8.10: Modal Groups

3. Set $\theta = -\pi$ and $n = 1$. Then, since the eigenvalue is real, the corner on the critical trajectory occurs as it passes through $\nu_1 = 0 \Rightarrow \delta_1 = -\frac{\pi}{2}$. Thus, $\sigma L = \lim_{\delta \to -\pi/2}(2\delta + \pi) \cdot \tan(\delta) = -2$ by l'Hôpital's Rule. □

Returning once again to Figure 8.9, note that the corner on the critical trajectory corresponding to $\theta_n^{\pm}$ is a bifurcation point where one path leads to $n \mp 1$ and the other veers off to infinity at an angle of $\theta_n^{\pm} - \pi/2$ (Theorem 8.4.1, Part 2b). Turning attention to Figure 8.10 which is an amalgam of Figure 8.9, the top frame for the even numbered modes and the bottom frame for the odd numbered modes, observe that the boundaries of adjacent modal regions formed from these bifurcated trajectories align, the result in both cases being a corresponding partition of the ν-plane.

Furthermore, the trajectories corresponding to adjacent modes overlap but do not intersect in the sense that they never come in contact for the same value of σ. Specifically we have the following

Theorem 8.4.3. *1. A trajectory emanating from n never intersects a trajectory emanating from* $n \pm 1$ *for the same value of* σ.

2. A trajectory emanating from n intersects a trajectory emanating from $n \pm 2$ *for the same value of* σ *only at their common branch (bifurcation) point. In fact,* $\delta_n^+ = \delta_{n-2}^- - \pi$ *and* $\theta_n^+ = \theta_{n-2}^-$. *At the common branch point there is a modal deficiency and along the bifurcated trajectory there is modal ambiguity.*

Proof:

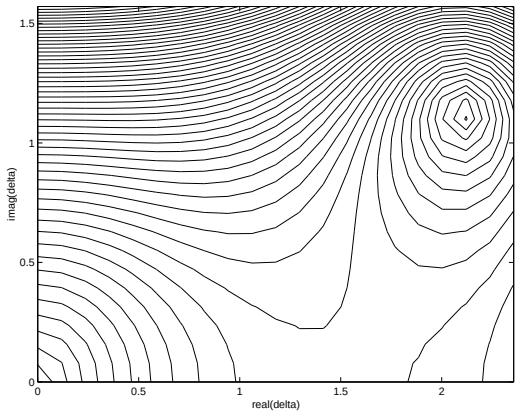

Figure 8.11: Branch Point ($n = 0$)

1. According to Equation (8.6), $\nu_n = \nu_{n+1}$ if and only if $\delta_n = \delta_{n+1} + \frac{\pi}{2}$ and $\tan(\delta_{n+1} + \frac{\pi}{2}) = \tan(\delta_{n+1})$. But, this would require that $-\cot(\delta_{n+1}) = \tan(\delta_{n+1})$ which is impossible.

2. From Equation (8.20), we have

$$\tau_{n-2}(\delta) = \sin(2(\delta - \pi)) + 2(\delta - \pi) + n\pi = \tau_n(\delta - \pi), \tag{8.21}$$

which implies that the roots of $\tau_n(\delta)$ are the roots of $\tau_{n-2}(\delta)$ shifted to the left by π. Thus, $\delta_n^+ = \delta_{n-2}^- - \pi$ and $\theta_n^+ = \theta_{n-2}^-$. Now, Equation (8.19) implies that

$$(\delta_{n-2}(r) - \pi)' = \frac{Le^{\imath\theta}\cos^2(\delta_{n-2}(r) - \pi)}{\sin(2(\delta_{n-2}(r) - \pi)) + 2(\delta_{n-2}(r) - \pi) + n\pi}, \tag{8.22}$$

so that $\delta_n(r)$ and $\delta_{n-2}(r) - \pi$ satisfy the same differential equation with different initial conditions. By the fundamental Existence and Uniqueness Theorem for ordinary differential equations [9, pp. 1-11], they can only intersect at a singularity and such an intersection is equivalent to $\nu_{n-2}(r) = \nu_n(r)$. At this common branch point, modes $n-2$ and n coalesce thereby producing a modal deficiency. Beyond the branch point, there is modal ambiguity in that it is not clear which mode to associate with which bifurcation branch. □

The modal deficiency and ambiguity established in the previous theorem must be taken into account when utilizing the eigenfunction expansion of Equation (8.11). Also, this theorem alleviates the need to calculate δ_n^+ and θ_n^+ since they are obtainable from δ_{n-2}^- and θ_{n-2}^-, respectively.

Figure 8.11 shows the level curves of $|\tau_0(\delta)|$ (see Equation (8.20)) where the branch point δ_0^- is on prominent display. We next study δ_n^- as n varies.

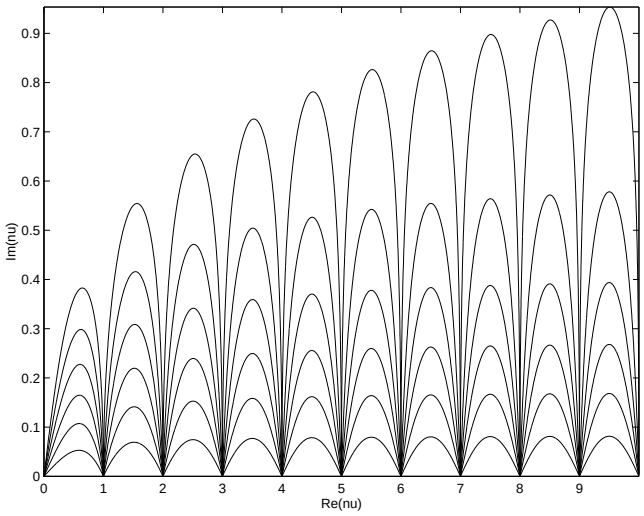

Figure 8.12: Modal Homotopy ($\nu_n : 0 \leq n \leq 9,\ \theta = m\pi/12 : 0 \leq m \leq 6,\ L = \pi$)

Theorem 8.4.4. *1. As $n \to \infty$, $\sigma_n^- \to [-\ln((3+2n)\pi) + \imath \cdot (n+3/2)\pi]/L$.*

2. For $0 \leq \theta \leq \frac{\pi}{2}$, all modes are IBC-Dirichlet modes (i.e. there are no missing modes).

Proof:

1. As $n \to \infty$, $Re(\delta_n^-) \to (\frac{3\pi}{4})^-$ and $\delta_n^{I\,-} := Im(\delta_n^-) \to +\infty$. Thus, $\tan(\delta_n^{I\,-}) \to \imath$ and, from $\tau_n(\delta_n^-) = 0$, $\delta_n^{I\,-} \to \frac{1}{2}\ln((3+2n)\pi)$. Solving for σ_n^- in Equation (8.6) yields $\sigma_n^- \to [-\ln((3+2n)\pi) + \imath \cdot (n+3/2)\pi]/L$.

2. Since $\theta_n^- := \arg \sigma_n^-$, we have $\theta_n^- = \tan^{-1}[-(n+3/2)\pi/\ln((3+2n)\pi)] \to \tan^{-1}(-\infty) = (\frac{\pi}{2})^+$. Therefore, all of the critical angles lie in the range $\frac{\pi}{2} < \theta_n^- \leq \pi$. □

8.4.1 The Case $Re(\sigma) \geq 0$

Because of the second part of Theorem 8.4.4, the asymptotic behavior for $Re(\sigma) \geq 0$ is especially simple. With reference to Figure 8.12, there is a complete modal homotopy from each of the Neumann modes to a corresponding Dirichlet mode. Specifically, $N_n(x) \mapsto D_{n+1}(x)$ for all n. This asymptotic behavior, illustrated by Figure 8.8 for $n = 0$ and $\theta = \pi/4$, is directly analogous to the case of σ real and positive except that now the homotopy passes through the complex plane.

8.4.2 The Case $Re(\sigma) < 0$

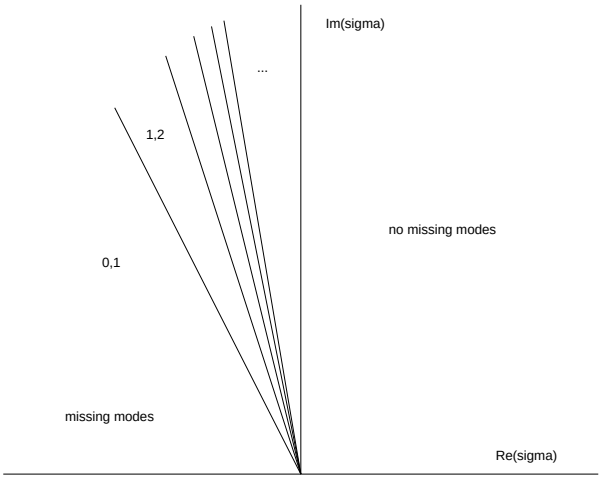

Figure 8.13: Missing Mode Zones

The asymptotic behavior for $Re(\sigma) < 0$, is directly analogous to the case of σ real and negative in that there are always two missing modes with the remainder being IBC-Dirichlet modes. However, which modes are missing is now determined by the value of θ. Specifically, if $\theta_n^- < \theta < \theta_{n-1}^-$ then modes n and $n+1$ will be missing. This is shown graphically in Figure 8.13. Table 8.1 lists many branch points δ_n^- together with their corresponding critical angles θ_n^-.

IBC-Dirichlet Modes

If $\theta < \theta_n^-$ then $N_n(x) \mapsto D_{n+1}(x)$ analogous to the case of the mode morphing displayed in the case of $Re(\sigma) \geq 0$. However, if $\theta > \theta_n^+ = \theta_{n-2}^-$ then $N_n(x) \mapsto -D_{n-1}(x)$ characteristic of the mode morphing displayed in the case of σ real and negative. This latter mode-morphing behavior is on display in Figure 8.14 for $n = 2$ and $\theta = 3\pi/4$.

Missing Modes

If $\theta_n^- < \theta < \theta_n^+ = \theta_{n-2}^-$ then mode n is missing. The resulting rightward procession of missing modes as θ is lowered from π to $\pi/2$ is shown in Figure 8.15. The missing modes for $\pi/2 < \theta < \pi$ exhibit a peculiar singular behavior as $r = |\sigma| \to \infty$.

Theorem 8.4.5. *For $\frac{\pi}{2} < \theta < \pi$, all missing modes oscillate between ± 1 at the endpoints and approach zero elsewhere.*

n	δ_n^-	θ_n^-
0	2.106196+1.125364$\imath$	.7150π
1	2.178042+1.384339$\imath$	.6500π
2	2.214676+1.551574$\imath$	.6172π
3	2.237591+1.676105$\imath$	.5970π
4	2.253497+1.775544$\imath$	.5832π
5	2.265277+1.858384$\imath$	.5730π
6	2.274400+1.929404$\imath$	.5653π
7	2.281699+1.991571$\imath$	.5591π
8	2.287689+2.046852$\imath$	.5541π
9	2.292704+2.096626$\imath$	.5499π
10	2.296970+2.141891$\imath$	.5464π
100	2.346069+3.229037$\imath$	.5074π
1,000	2.354804+4.373567$\imath$	.5010π
10,000	2.356019+5.524184$\imath$	.5001π

Table 8.1: Branch Points and Critical Angles

Proof: Simply let $|\delta = \delta_R + \imath \cdot \delta_I| \to \infty$ in Equation (8.3). At the endpoints, $u_n \to \pm(e^{\delta_I}/2) \cdot [\cos(\delta_R) - \imath \cdot \sin(\delta_R)]$ and normalization by $e^{\delta_I}/2$ reveals the oscillatory behavior at the endpoints as well the approach to zero for interior points. □

This oscillatory singular behavior is in evidence in Figures 8.16 (even numbered modes) and 8.17 (odd numbered modes).

8.5 Summary of Asymptotic Behavior

The bulk of this chapter has been devoted to exploring the asymptotic nature of the eigenstructure of the SL-BVP with an IBC, Equation (8.1), as $\sigma \to \infty$. Our main results may be summarized as follows (see Figure 8.2):

Theorem 8.5.1 (Asymptotic Behavior of SL-BVP/IBC Eigenstructure). *Consider the SL-BVP with an IBC described by Equation (8.1) with $\sigma(r) = re^{\imath\theta}$ for fixed θ and $0 \le r \le \infty$.*

1. *If $0 \le \theta \le \pi/2$ then $\lim_{r\to\infty} \lambda_n(\sigma) \to \lambda_{n+1}(0)$ and $\lim_{r\to\infty} u_n(x;\sigma) \to D_{n+1}(x)$ for all n.*

2. *If $\pi/2 < \theta \le \pi$ then there exists $n(\theta)$ such that*

   (a) *$\lim_{r\to\infty} \lambda_k(\sigma) \to \lambda_{k+1}(0)$ and $\lim_{r\to\infty} u_k(x;\sigma) \to D_{k+1}(x)$ for $k < n(\theta) - 1$,*

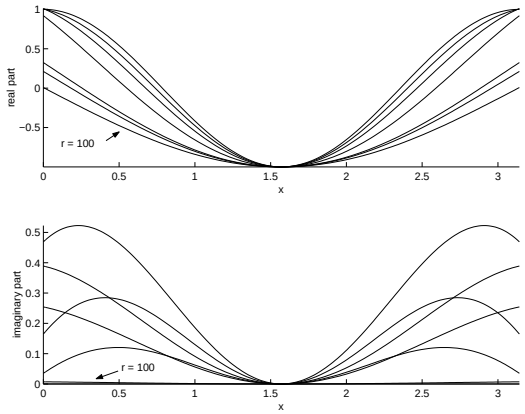

Figure 8.14: Mode Morphing ($n = 2,\ \theta = 3\pi/4,\ L = \pi$)

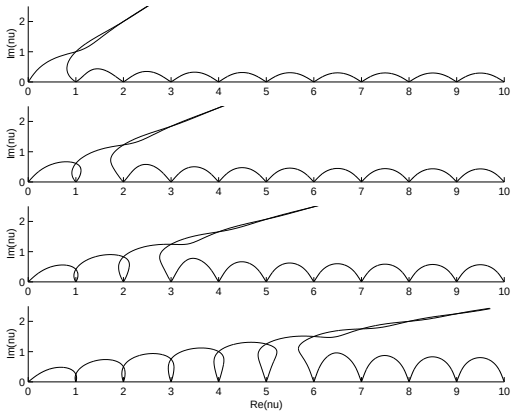

Figure 8.15: Shifting of Missing Modes ($\theta = .75\pi, .675\pi, .625\pi, .578\pi$)

(b) $\lim_{r\to\infty} \lambda_k(\sigma) \to \lambda_{k-1}(0)$ *and* $\lim_{r\to\infty} u_k(x;\sigma) \to -D_{k-1}(x)$ *for* $k > n(\theta)$,

(c) and $\lim_{r\to\infty} |\lambda_k(\sigma)| \to \infty$ *for* $k = n(\theta) - 1, n(\theta)$.

These observations are directly applicable to the rectangular waveguide [70, pp. 503-509].

Furthermore, these results lead naturally to the question of the corresponding asymptotic nature of the eigenstructure of the Laplacian on an equilateral triangle with an impedance boundary condition. The special cases of the radiation boundary condition (Chapter 6 [54]) and the absorbing boundary condition (Chapter 7 [55]) have already received exhaustive treatment. The one-dimensional results of the present chapter seem to indicate that these two special cases exhibit the full spectrum of possible asymptotic behavior as

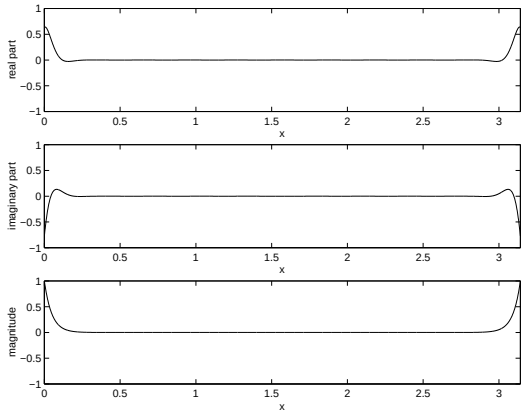

Figure 8.16: Even Missing Modes ($n = 0,\ \theta = 3\pi/4,\ L = \pi$)

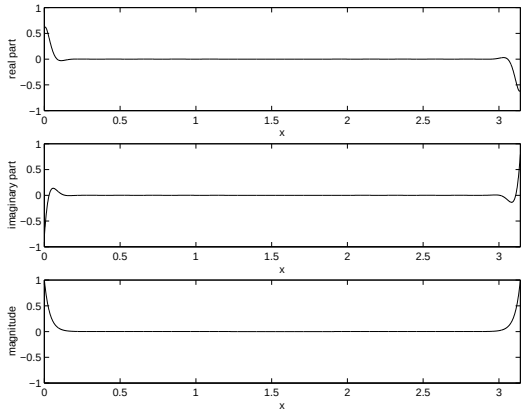

Figure 8.17: Odd Missing Modes ($n = 1,\ \theta = 3\pi/4,\ L = \pi$)

$\sigma \to \infty$. Chapter 9, *The Impedance Boundary Condition*, will address this problem.

8.6 Sturm and Liouville

Sturm-Liouville theory marked a watershed event in the development of differential equations. Up until that point, especially in the case of ordinary differential equations, the search for specific solution methods, either for classes of equations or for individual equations, had dominated [2]. Instead, Sturm and Liouville obtained information about the properties of the solutions directly from the differential equation itself [43].

In 1833, Sturm read a paper to the Académie des Sciences (Paris) on

Figure 8.18: Charles Sturm

Figure 8.19: Joseph Liouville

second-order linear differential equations which was followed, in 1836, by a pair of memoirs in the *Journal de Mathématiques Pures et Appliquées* (Liouville's Journal). These memoirs contained the first full treatment of the oscillation, comparison and separation theorems which were to bear his name as well as the genesis of the problem in heat conduction. The following year, 1837, Liouville and Sturm published a joint paper in the same journal where they proved the expansion theorem, namely that a large class of functions could be represented by a Fourier-type expansion in terms of the eigenfunctions. In 1836-1837, Liouville published a further series of papers significantly extending the theory of eigenfunction expansions [1, p. xv].

Taken together [24, p. 1230], the impact of these papers went well beyond their subject matter and extended to general linear and nonlinear differential equations and to analysis proper, including integral equations and functional analysis [93, p. ix]. Translations of portions of these fundamental papers are available in [6, p. 258-281] and they are discussed at length in [43, Chapter X].

8.6.1 Charles-François Sturm

Charles-François Sturm (1803-1855) was born in Geneva, Switzerland and studied Mathematics at Geneva Academy [23]. In 1823, he became private tutor to the youngest son of Madame de Staël at the Château de Coppet close to Geneva. He accompanied them to Paris for six months where he met Laplace, Poisson and Fourier. In 1824, he abandoned his teaching post and, in

1825, returned to Paris to pursue his scientific studies. In 1829, he published one of his most famous papers on the determination of the number of real roots of a polynomial on a given interval (Sturm's Theorem).

In 1830, he was appointed a professor at the Collège Rollin, became a French citizen in 1833 and was elected to the Académie des Sciences in 1836. See above for a description of his work on Sturm-Liouville boundary value problems of 1836-1837. He also made substantial contributions to infinitesimal geometry, projective geometry and the differential geometry of curves and surfaces. Additionally, he did important work in geometrical optics and helped make the first experimental determination of the speed of sound in water. In 1838, he began teaching at l'École Polytechnique and joined the Faculté des Sciences of Paris in 1840. Based on his lectures, a number of widely used texts were published posthumously. He died in Paris, aged 52, and his name was engraved on the Eiffel Tower.

8.6.2 Joseph Liouville

Joseph Liouville (1809-1882) was born in St.-Omer, Pas-de-Calais, France and studied Mathematics at the Collège St. Louis in Paris [43]. He entered l'École Polytechnique in 1825 and graduated in 1827. After some years as an assistant at various institutions, he was appointed Professor at l'École Polytechnique in 1838. He obtained a chair in Mathematics at the Collège de France in 1850 and a chair in mechanics at the Faculté des Sciences in 1857. In 1836, he founded *Journal de Mathématiques Pures et Appliquées* and, in 1846, the previously unpublished work of Évariste Galois appeared there.

He made fundamental contributions to number theory, complex analysis, differential geometry, topology, mathematical physics and astronomy. He was the first to prove the existence of transcendental numbers (Liouville numbers), proved that every bounded entire function must be constant (Liouville's Theorem) and showed that time evolution is measure preserving for a Hamiltonian system (another Liouville's Theorem). In Hamiltonian dynamics, he introduced the notion of action-angle variables as a description of completely integrable systems. He also introduced the subject of fractional calculus and investigated the general problem of integration of algebraic functions in finite terms. His work on Sturm-Liouville boundary value problems has been previously described. He died in Paris, aged 73.

Chapter 9

The Impedance Boundary Condition

A complete, direct, and elementary derivation of Lamé's formulas has previously been provided for the Dirichlet problem (Chapter 2 [51]) as well as the Neumann problem (Chapter 3 [52]). This was subsequently extended to the Robin problem with either a radiation boundary condition (Chapter 6 [54]) or an absorbing boundary condition (Chapter 7 [55]).

It is the express purpose of the present chapter to extend this previous work to the more difficult case of the Robin problem with an impedance boundary condition [68, p. 1366], [57]. The principal analytical difficulty that must be overcome is that, unlike the case of radiation/absorbing boundary conditions, the Robin problem is no longer self-adjoint with the consequence that the eigenvalues are now complex and the corresponding eigenfunctions are no longer mutually orthogonal.

We commence by employing separation of variables in Lamé's natural triangular coordinate system to derive the eigenvalues and eigenfunctions of the Robin problem with an impedance boundary condition (IBC). An important feature of this derivation is the decomposition into symmetric and antisymmetric modes (eigenfunctions). The problem is then reduced to the solution of a system of complex transcendental equations which we treat numerically using MATLAB [34, 64]. Surprisingly, all of the modes so determined (henceforth dubbed IBC modes) are expressible as combinations of complex sines and cosines (i.e. either real trigonometric or hyperbolic sines and cosines).

A natural homotopy between Lamé's Neumann modes and the IBC modes is exploited not only in the derivation of the modes but is also employed to shed light on the properties of these newly derived modes. Prominent among these considerations are rotational symmetry and modal degeneracy [53]. Completeness of the modes as well as their biorthogonality with those of the adjoint boundary value problem is also established.

This natural homotopy from Lamé's Neumann modes to the IBC modes possesses a bipartite structure. On the one hand, for certain modes the homotopy may be extended to approach Lamé's Dirichlet modes (the IBC-Dirichlet modes). On the other hand, the remaining modes do not approach Dirichlet modes (the missing modes). The determination of the precise nature of these latter eigenvalues together with that of their corresponding eigenfunctions is the primary focus of the present study.

9.1 Acoustic Waveguide

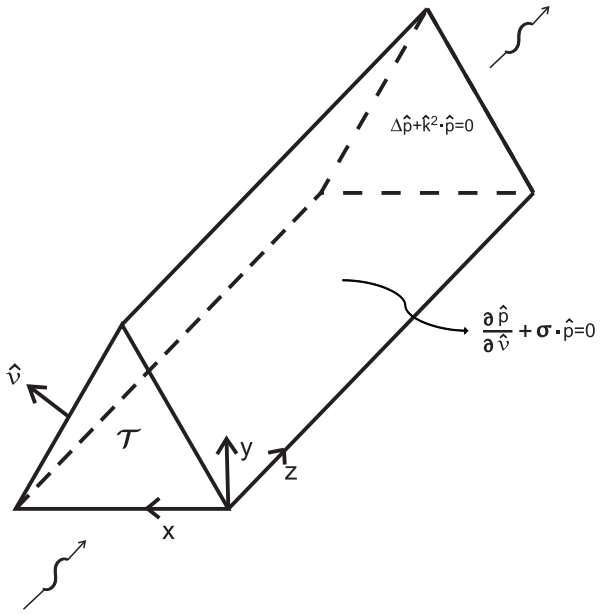

Figure 9.1: Equilateral Triangular Waveguide

Figure 9.1 illustrates the equilateral triangular acoustic waveguide with constant impedance walls which is the subject of the present paper. It may profitably be considered a generalization of the parallel plate waveguide considered in Chapter 8 [56]. A complex acoustic time-harmonic pressure wave of angular frequency ω is propagating in the z-direction [70, pp. 495-496]:

$$p(x, y, z, t) := \hat{p}(x, y) \cdot e^{\imath(\omega t - k_z z)}, \tag{9.1}$$

where the real physical acoustic pressure may be obtained as

$$P(x, y, z, t) = Re\{p(x, y, z, t)\}. \tag{9.2}$$

The axial propagation factor is $k_z := \sqrt{\left(\frac{\omega}{c}\right)^2 - \hat{k}^2}$ where c is the speed of sound and $\hat{k}^2$ is an eigenvalue determined by the Robin eigenproblem with impedance boundary condition:

$$\Delta\hat{p}(x,y) + \hat{k}^2\hat{p}(x,y) = 0,\ (x,y) \in \tau;\ \frac{\partial\hat{p}}{\partial\hat{\nu}}(x,y) + \sigma\hat{p}(x,y) = 0,\ (x,y) \in \partial\tau \quad (9.3)$$

where the eigenfunction $\hat{p}$ describes the transverse acoustic pressure distribution, Δ is the two-dimensional Laplacian, $\frac{\partial^2}{\partial x^2} + \frac{\partial^2}{\partial y^2}$, τ is the equilateral triangle shown in Figure 9.1, $\hat{\nu}$ is its outward pointing normal, and σ is a constant complex material parameter. In the above, $Re(k_z) > 0$ so that the acoustic wave propagates in the positive z direction as shown in Figure 9.1.

This same eigenproblem arises in the study of the vibrational modes of an elastic membrane stretched over an equilateral triangular boundary with sidewise displacement of the boundary supports [66, pp. 172-177]. The corresponding problem for electromagnetic waveguides leads to an eigenproblem for the vector Laplacian which cannot be decoupled componentwise for impedance walls as it can be for perfectly conducting walls [45, pp. 67-110], although approximate procedures have been developed [92].

The complex material parameter $\sigma = \sigma_R + \imath \cdot \sigma_I$ is related to the wall impedance which accounts for field penetration into the walls of the waveguide. σ_R is related to the acoustic reactance while σ_I is related to the acoustic resistance. For passive walls which absorb energy, we require that $\sigma_I > 0$. If $\sigma_R > 0$ then we have a mass/inductive impedance surface while if $\sigma_R < 0$ then we have a compliant/capacitive impedance surface. If $\sigma_R = 0$ then we have a purely resistive impedance surface. A perfectly rigid surface is described by $\sigma = 0$ and is called a hard boundary (Neumann boundary condition). A pressure release surface is described by $|\sigma| = \infty$ and is called a soft boundary (Dirichlet boundary condition). In the ensuing analysis, we will be particularly concerned with constructing homotopies in the complex σ-plane connecting hard and soft boundary problems with constant ratio of resistance to reactance.

Observe that in Equation (9.3) when $\sigma \to 0$ we recover the Neumann problem [52]. Thus, we may profitably view σ as a continuation parameter which provides a homotopy extending from this well understood problem to that of the impedance boundary condition. Throughout the ensuing development we will avail ourselves of this important observation. Furthermore, note that *if the normal derivative remains bounded* then $|\sigma| \to \infty$ yields the Dirichlet problem [51]. In that case, the homotopy may be further extended to lead from a Neumann mode to a corresponding Dirichlet mode.

The Robin eigenproblem described by Equation (9.3) is non-self-adjoint for complex values of σ. However, it is shown below that this problem reduces to the study of the solutions of a system of three complex transcendental equations. In what follows, we will derive and exhaustively study this system

of equations. The principal focus will be on what happens to the eigenstructure of the Neumann problem ($\sigma = 0$) as σ proceeds along rays emanating from the origin toward the point at infinity in the upper half of the complex plane.

We will find that, for the most part, there is the natural homotopy alluded to above connecting the Neumann modes to those of a corresponding Dirichlet problem (IBC-Dirichlet modes). However, we will show that, under appropriate conditions, there will be Neumann eigenvalues that have no Dirichlet counterpart. The determination of the precise nature of these latter eigenvalues together with that of their corresponding eigenfunctions ("missing modes") is the primary concern of the present investigation.

9.2 Symmetric/Antisymmetric Modes

We now commence with our original, complete, and elementary derivation by introducing the orthogonal coordinates (ξ, η) given by

$$\xi = u, \ \eta = v - w. \tag{9.4}$$

Equation (9.3) becomes

$$\frac{\partial^2 \hat{p}}{\partial \xi^2} + 3\frac{\partial^2 \hat{p}}{\partial \eta^2} + \hat{k}^2 \hat{p} = 0. \tag{9.5}$$

Hence, if we seek a separated solution of the form

$$f(\xi) \cdot g(\eta) \tag{9.6}$$

then we arrive at

$$f'' + \alpha^2 f = 0; \ g'' + \beta^2 g = 0; \ \alpha^2 + 3\beta^2 = \hat{k}^2. \tag{9.7}$$

Thus, there exist separated solutions of the form

$$f(u) \cdot g(v - w), \tag{9.8}$$

where f and g are (possibly complex) trigonometric functions.

Before proceeding any further, we will decompose the sought after eigenfunction into parts symmetric and antisymmetric about the altitude $v = w$ (see Figure 1.3)

$$\hat{p}(u, v, w) = \hat{p}_s(u, v, w) + \hat{p}_a(u, v, w), \tag{9.9}$$

where

$$\hat{p}_s(u, v, w) = \frac{\hat{p}(u, v, w) + \hat{p}(u, w, v)}{2}; \ \hat{p}_a(u, v, w) = \frac{\hat{p}(u, v, w) - \hat{p}(u, w, v)}{2}, \tag{9.10}$$

henceforth to be dubbed a symmetric/antisymmetric mode, respectively. We next take up the determination of $\hat{p}_s$ and $\hat{p}_a$.

As shown previously, a sum of three terms of the form of Equation (9.8) is required to solve the Robin problem, Equation (9.3). Hence, we make the Ansatz

$$\begin{aligned}\hat{p}_s &= \cos[\frac{\pi\lambda}{3r}(u+2r)-\delta_1]\cdot\cos[\frac{\pi(\mu-\nu)}{9r}(v-w)] \\ &+ \cos[\frac{\pi\mu}{3r}(u+2r)-\delta_2]\cdot\cos[\frac{\pi(\nu-\lambda)}{9r}(v-w)] \\ &+ \cos[\frac{\pi\nu}{3r}(u+2r)-\delta_3]\cdot\cos[\frac{\pi(\lambda-\mu)}{9r}(v-w)],\end{aligned} \tag{9.11}$$

$$\begin{aligned}\hat{p}_a &= \cos[\frac{\pi\lambda}{3r}(u+2r)-\delta_1]\cdot\sin[\frac{\pi(\mu-\nu)}{9r}(v-w)] \\ &+ \cos[\frac{\pi\mu}{3r}(u+2r)-\delta_2]\cdot\sin[\frac{\pi(\nu-\lambda)}{9r}(v-w)] \\ &+ \cos[\frac{\pi\nu}{3r}(u+2r)-\delta_3]\cdot\sin[\frac{\pi(\lambda-\mu)}{9r}(v-w)].\end{aligned} \tag{9.12}$$

with

$$\lambda+\mu+\nu=0, \tag{9.13}$$

and eigenvalue

$$\hat{k}^2=\frac{2}{27}(\frac{\pi}{r})^2[\lambda^2+\mu^2+\nu^2]=\frac{4}{27}(\frac{\pi}{r})^2[\mu^2+\mu\nu+\nu^2]. \tag{9.14}$$

As we shall see, the symmetric mode never vanishes identically while the antisymmetric mode may.

Careful perusal of Equations (9.11) and (9.12) now reveals that for $\delta_1 = \delta_2 = \delta_3 = 0$ they reduce to the symmetric/antisymmetric modes of the Neumann problem [52] while for $\delta_1 = \mp 3\pi/2,\ \delta_2 = \pm\pi/2,\ \delta_3 = \pm\pi/2$, or any cyclic permutation thereof, they reduce to the symmetric/antisymmetric modes of the Dirichlet problem [51]. Thus, our task amounts to finding values of $\lambda,\ \mu,\ \nu,\ \delta_1,\ \delta_2,\ \delta_3$ so that the Robin boundary condition is satisfied along the periphery of the equilateral triangle. These values are also to satisfy the constraint embodied by Equation (9.13).

Imposition of the Robin boundary condition along $u = r$ yields

$$\tan(\pi\lambda-\delta_1)=\frac{3\sigma r}{\pi\lambda},\ \tan(\pi\mu-\delta_2)=\frac{3\sigma r}{\pi\mu},\ \tan(\pi\nu-\delta_3)=\frac{3\sigma r}{\pi\nu}, \tag{9.15}$$

while imposition along $v = r$ yields

$$\tan(-\frac{\delta_2+\delta_3}{2})=\frac{3\sigma r}{\pi\lambda},\ \tan(-\frac{\delta_3+\delta_1}{2})=\frac{3\sigma r}{\pi\mu},\ \tan(-\frac{\delta_1+\delta_2}{2})=\frac{3\sigma r}{\pi\nu}. \tag{9.16}$$

By symmetry/antisymmetry, the boundary condition along $w = r$ will thereby be automatically satisfied.

Introducing the auxiliary variables, $L,\ M,\ N$, while collecting together these equations produces

$$\begin{aligned}
\tan(\pi\lambda - \delta_1) = \tan(-\frac{\delta_2+\delta_3}{2}) = \frac{3\sigma r}{\pi\lambda} = \tan L \quad &, \quad L := -\frac{\delta_2+\delta_3}{2} \\
\tan(\pi\mu - \delta_2) = \tan(-\frac{\delta_3+\delta_1}{2}) = \frac{3\sigma r}{\pi\mu} = \tan M \quad &, \quad M := -\frac{\delta_3+\delta_1}{2} \\
\tan(\pi\nu - \delta_3) = \tan(-\frac{\delta_1+\delta_2}{2}) = \frac{3\sigma r}{\pi\nu} = \tan N \quad &, \quad N := -\frac{\delta_1+\delta_2}{2}
\end{aligned} \tag{9.17}$$

and these six complex equations may in turn be reduced to the solution of the system of three complex (six real) transcendental equations for $L,\ M,\ N$

$$\begin{aligned}
[2L - M - N - (m+n)\pi] \cdot \tan L &= 3\sigma r, \\
[2M - N - L + m\pi] \cdot \tan M &= 3\sigma r, \\
[2N - L - M + n\pi] \cdot \tan N &= 3\sigma r,
\end{aligned} \tag{9.18}$$

where $m = 0, 1, 2, \ldots;\ n = m, m+1, \ldots$.

Once $L,\ M,\ N$ have been numerically approximated, e.g. using MATLAB [34, 64], the parameters of primary interest may then be determined as

$$\delta_1 = L - M - N;\ \delta_2 = -L + M - N;\ \delta_3 = -L - M + N, \tag{9.19}$$

and

$$\lambda = -\mu - \nu;\ \mu = \frac{2M - N - L}{\pi} + m;\ \nu = \frac{2N - L - M}{\pi} + n. \tag{9.20}$$

For future reference, when $m = n$ we have $M = N$, $\delta_2 = \delta_3$, $\mu = \nu$, and $2\pi\mu = \delta_2 - \delta_1 + 2m\pi$. Also, observe that the relations described by Equation (9.19) are invertible so that there is a one-to-one correspondence between (L, M, N) and $(\delta_1, \delta_2, \delta_3)$ while the transformation described by Equation (9.20) is singular so that different (L, M, N) may correspond to identical (λ, μ, ν).

Of particular interest is the limit $\sigma \to 0$, where we find that we may choose L, M, N so that each approaches 0, as do $\delta_1, \delta_2, \delta_3$, and, most significantly, $\lambda \to -(m+n), \mu \to m, \nu \to n$. In other words, we recover in this limit the Neumann modes, $N^{m,n}_{s,a}(x, y)$. Thus, we have constructed a homotopy extending from each IBC mode back to the Neumann mode with the same index (m, n) as $\sigma \to 0$. The behavior as $|\sigma| \to \infty$ is more subtle and will be addressed once we have established some of their basic properties.

9.3 Modal Properties

Certain properties of the IBC modes follow directly from Equations (9.11) and (9.12). However, these equations are identical to those for the Robin boundary condition with real σ (Chapters 6 & 7 [54, 55]) except that some quantities may now be complex. Thus, their proofs are formally identical to those of Chapters 6 & 7 [54, 55] and for that reason they are omitted here.

In what follows, it will be convenient to have the following alternative representations of our IBC modes:

$$\begin{aligned}
\hat{p}_s^{m,n} = \frac{1}{2} \quad \{ \quad & \cos[\frac{2\pi}{9r}(\lambda u + \mu v + \nu w + 3\lambda r) - \delta_1] \\
+ \quad & \cos[\frac{2\pi}{9r}(\nu u + \mu v + \lambda w + 3\nu r) - \delta_3] \\
+ \quad & \cos[\frac{2\pi}{9r}(\mu u + \nu v + \lambda w + 3\mu r) - \delta_2] \\
+ \quad & \cos[\frac{2\pi}{9r}(\mu u + \lambda v + \nu w + 3\mu r) - \delta_2] \\
+ \quad & \cos[\frac{2\pi}{9r}(\nu u + \lambda v + \mu w + 3\nu r) - \delta_3] \\
+ \quad & \cos[\frac{2\pi}{9r}(\lambda u + \nu v + \mu w + 3\lambda r) - \delta_1]\},
\end{aligned} \tag{9.21}$$

$$\begin{aligned}
\hat{p}_a^{m,n} = \frac{1}{2} \quad \{ \quad & \sin[\frac{2\pi}{9r}(\lambda u + \mu v + \nu w + 3\lambda r) - \delta_1] \\
- \quad & \sin[\frac{2\pi}{9r}(\nu u + \mu v + \lambda w + 3\nu r) - \delta_3] \\
+ \quad & \sin[\frac{2\pi}{9r}(\mu u + \nu v + \lambda w + 3\mu r) - \delta_2] \\
- \quad & \sin[\frac{2\pi}{9r}(\mu u + \lambda v + \nu w + 3\mu r) - \delta_2] \\
+ \quad & \sin[\frac{2\pi}{9r}(\nu u + \lambda v + \mu w + 3\nu r) - \delta_3] \\
- \quad & \sin[\frac{2\pi}{9r}(\lambda u + \nu v + \mu w + 3\lambda r) - \delta_1]\},
\end{aligned} \tag{9.22}$$

obtained from Equation (9.11) and Equation (9.12), respectively, by the application of appropriate trigonometric identities.

We may pare the collection of antisymmetric IBC modes through the following observation.

Theorem 9.3.1. *$\hat{p}_s^{m,n}$ never vanishes identically while $\hat{p}_a^{m,n}$ vanishes identically if and only if m=n.*

Hence, our reduced modal system is $\{\hat{p}_s^{m,n}\ (n \geq m \geq 0);\ \hat{p}_a^{m,n}\ (n > m \geq 0)\}$.

We next give the case $m = n$ further consideration. Recall that we have just determined that $\hat{p}_a^{m,m} \equiv 0$. Furthermore, in this case, we may combine the terms of Equation (9.21) to yield

$$\hat{p}_s^{m,m} = \cos[\frac{2\pi\mu}{3r}(r-u) - \delta_2] + \cos[\frac{2\pi\mu}{3r}(r-v) - \delta_2] + \cos[\frac{2\pi\mu}{3r}(r-w) - \delta_2], \tag{9.23}$$

which clearly illustrates that any permutation of (u, v, w) leaves $\hat{p}_s^{m,m}$ invariant. This is manifested geometrically in the invariance of $\hat{p}_s^{m,m}$ under a 120° rotation about the triangle center. This invariance will henceforth be termed rotational symmetry.

Moreover, the modes $\hat{p}_s^{m,m}$ are not the only ones that are rotationally symmetric.

Theorem 9.3.2. *$\hat{p}_s^{m,n}$ and $\hat{p}_a^{m,n}$ are rotationally symmetric if and only if $m \equiv n$ (mod 3).*

Subsequently, we will trace trajectories in complex (L, M, N)-space or, equivalently, in complex $(\delta_1, \delta_2, \delta_3)$- & (μ, ν)-spaces as the complex boundary parameter σ is varied. As shown in Figure 9.2, beginning with $\sigma = 0$

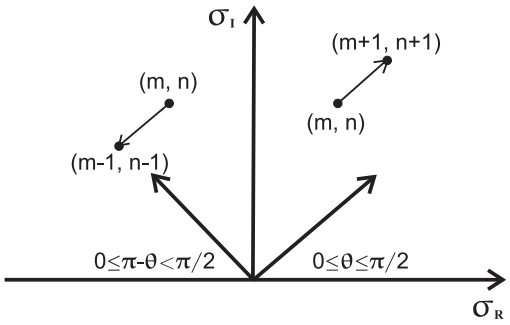

Figure 9.2: Complex Boundary Parameter

(the Neumann problem), we will allow σ to move along a ray inclined at an angle θ to the horizontal toward the point at infinity. We may then trace the trajectory of each Neumann eigenpair in order to determine whether it eventually approaches a Dirichlet eigenpair (in which case this will be called an IBC-Dirichlet mode) or migrates to infinity (in which case this will be called a "missing mode"). We will eventually find that these are the only two possible types of asymptotic behavior.

Before constructing a taxonomy of the asymptotic nature of the eigenstructure of our Robin problem with an IBC as $|\sigma| \to \infty$ (at which time, the mysterious icons on Figure 9.2 will become intelligible), it behooves us to first catalog some important additional properties of the eigenvalues and eigenfunctions of Equation (9.3).

We begin with the observation that, without loss of generality, we may restrict our attention to the case $Im(\sigma) \geq 0$ (corresponding to the physically realistic case of a passive impedance surface which absorbs energy) since, by taking complex conjugates in Equation (9.18), we find that $\sigma \mapsto \bar{\sigma} \Rightarrow (L, M, N) \mapsto (\bar{L}, \bar{M}, \bar{N}) \Rightarrow (\delta_1, \delta_2, \delta_3) \mapsto (\bar{\delta_1}, \bar{\delta_2}, \bar{\delta_3})$ & $(\lambda, \mu, \nu) \mapsto (\bar{\lambda}, \bar{\mu}, \bar{\nu})$. Thus, in the event that $Im(\sigma) < 0$, we can obtain trajectories in either (L, M, N)-space or $(\delta_1, \delta_2, \delta_3)$- & (μ, ν)-spaces by reflection about the real axis of the corresponding trajectories for $\bar{\sigma}$.

Furthermore, taking complex conjugates in Equation (9.3) itself reveals that $\sigma \mapsto \bar{\sigma} \Rightarrow \hat{k}^2 \mapsto \bar{\hat{k}}^2 =: \hat{l}^2,\ \hat{p}(x,y) \mapsto \bar{\hat{p}}(x,y) =: \hat{q}(x,y)$ where $\hat{l}^2$ and $\hat{q}(x,y)$ comprise the solution to the adjoint boundary value problem:

$$\Delta\hat{q}(x,y) + \hat{l}^2\hat{q}(x,y) = 0,\ (x,y) \in \tau;\ \frac{\partial\hat{q}}{\partial\hat{\nu}}(x,y) + \bar{\sigma}\hat{q}(x,y) = 0,\ (x,y) \in \partial\tau. \tag{9.24}$$

Since the Robin problem is non-self-adjoint for complex σ, the eigenvalues and eigenfunctions can be complex and, most importantly, eigenfunctions corresponding to distinct eigenvalues are not necessarily orthogonal with respect to the complex inner product $< f(x,y), g(x,y) >:= \int\int_\tau f(x,y)\bar{g}(x,y)\,dxdy$. However, we do have the biorthogonality relationship involving the eigenfunctions of the boundary value problem, Equation (9.3), and those of the adjoint boundary value problem, Equation (9.24):

$$< \hat{p}_i, \hat{q}_j > = < \hat{p}_i, \bar{\hat{p}}_j > = \int\int_\tau \hat{p}_i(x,y)\hat{p}_j(x,y)\,dxdy = 0\ (i \neq j). \tag{9.25}$$

In turn, this provides us with the (binormalized) eigenfunction expansion:

$$f(x,y) = \sum_{i=1}^{\infty} < f, \hat{q}_i > \hat{p}_i(x,y) = \sum_{i=1}^{\infty} < f, \bar{\hat{p}}_i > \hat{p}_i(x,y), \tag{9.26}$$

where the series converges in norm for $f(x,y) \in \mathcal{L}^2(\tau)$ [44, pp. 231-232].

9.4 The Case of Real σ

In the case of real σ (pure reactance), the eigenstructure of the Robin problem with an IBC defined by Equation (9.3) has been exhaustively treated

in Chapter 6 [54] for $\sigma > 0$ (pure mass reactance) and Chapter 7 [55] for $\sigma < 0$ (pure compliant reactance). As a springboard for the study of the case of complex σ in the next section, we review here the highlights of those results.

When σ is real, the problem is self-adjoint so that the eigenvalues are real and the eigenfunctions can also be chosen to be real. Moreover, eigenfunctions corresponding to distinct eigenvalues are orthogonal with respect to the real inner product $< f(x,y), g(x,y) >:= \int\int_\tau f(x,y)g(x,y)\,dxdy$. Because of their very different behaviors, we treat the cases $\sigma > 0$ and $\sigma < 0$ separately. We will eventually see that, taken together, they display the characteristic behaviors exhibited in the general case of complex σ.

In what follows, we denote the dependence of the eigenvalues and eigenfunctions upon σ by $\hat{k}^2_{m,n}(\sigma)$ and $\hat{p}^{m,n}_{s,a}(x,y;\sigma)$, respectively, with $n \geq m \geq 0$ for the symmetric modes and $n > m \geq 0$ for the antisymmetric modes. The indices m, n are chosen so that when $\sigma = 0$ the eigenpairs reduce to the corresponding values for the Neumann problem; specifically, $\hat{p}^{m,n}_{s,a}(x,y;0) = N^{m,n}_{s,a}(x,y)$ (Chapter 3 [52]). Also, the Dirichlet problem has the same eigenvalues $\hat{k}^2_{m,n}(0)$ but with the restriction $n \geq m > 0$ for the symmetric modes and $n > m > 0$ for the antisymmetric modes while its corresponding eigenfunctions are denoted by $D^{m,n}_{s,a}(x,y)$ (Chapter 2 [51]).

9.4.1 The Case $\sigma \geq 0$

The case of the pure mass reactance boundary condition ($\sigma > 0$) (Chapter 6 [54]) is by far the simplest in that the eigenvalues are not only real but are in fact all positive. It also possesses the simplest asymptotic behavior in that

$$\lim_{\sigma\to+\infty}(\mu,\nu)_{m,n}(\sigma) = (m+1, n+1);\ \lim_{\sigma\to+\infty}\hat{p}^{m,n}_{s,a}(x,y;\sigma) = D^{m+1,n+1}_{s,a}(x,y). \tag{9.27}$$

That is, the Neumann mode $N^{m,n}_{s,a}(x,y)$ "morphs" (analytically) into the Dirichlet mode $D^{m+1,n+1}_{s,a}(x,y)$ as σ ranges from 0 to $+\infty$.

9.4.2 The Case $\sigma < 0$

The case of the absorbing boundary condition ($\sigma < 0$) (Chapter 7 [55]) is more complicated in that the eigenvalues while still real are no longer all positive. However, for $m = 2, 3, \ldots$, these so-called IBC-Dirichlet modes possess the simple asymptotic behavior described by

$$\lim_{\sigma\to-\infty}(\mu,\nu)_{m,n}(\sigma) = (m-1, n-1);\ \lim_{\sigma\to-\infty}\hat{p}^{m,n}_{s,a}(x,y;\sigma) = -D^{m-1,n-1}_{s,a}(x,y). \tag{9.28}$$

That is, the Neumann mode $N^{m,n}_{s,a}(x,y)$ "morphs" (analytically) into the Dirichlet mode $-D^{m-1,n-1}_{s,a}(x,y)$ as σ ranges from 0 to $-\infty$.

This leaves open the case of the "missing modes" $m = 0, 1$. Since there are no Dirichlet modes for $m = -1, 0$ we clearly do not have the simple asymptotic behavior described by Equation (9.28). Thus we are confronted with the question: "What happens to the missing $m = 0, 1$ modes as $\sigma \to -\infty$?". The solution to the mystery of the missing modes naturally decomposes into four special cases each of which we now explore separately.

For $m = 0$, $n = 0$ and $\sigma < 0$, all the parameters of Section 9.2 become pure imaginary. Equation (9.11) for $\hat{p}_s^{0,0}(u, v, w)$ becomes unbounded as $\sigma \to -\infty$. However, if we first scale it by its value at a vertex, $\hat{p}_s^{0,0}(r, -2r, r)$, we find that this normalized mode approaches 1 at the three vertices and 0 elsewhere. Such singular limiting behavior along the boundary is necessary since this mode does not approach a Dirichlet mode.

For $m = 0$, $n \geq 1$ and $\sigma < 0$, μ becomes pure imaginary, and the remaining parameters of Section 9.2 become complex in such a way so as to guarantee that $\hat{k}^2$, $\hat{p}_s$ and $\hat{p}_a$ are real. For $\sigma = 0$, $\hat{k}^2$ is positive and, as σ is decreased, $\hat{k}^2$, likewise, decreases. When σ reaches a critical value, $\hat{\sigma}_n$, $\hat{k}^2(\hat{\sigma}_n) = 0$ and thereafter continues to decrease without bound. For $n = 1$, asymptotically, as $\sigma \to -\infty$, we have the limiting value $\hat{k}^2 \to -4\sigma^2$. Both $\hat{p}_s^{0,1}$ and $\hat{p}_a^{0,1}$ display prominent vertex singularities. For $n > 1$, asymptotically, as $\sigma \to -\infty$, we have the limiting value $\hat{k}^2 \to -\sigma^2 + \frac{4}{27}[\frac{\pi}{r}(n - \frac{3}{2})]^2$. Both $\hat{p}_s^{0,n}$ and $\hat{p}_a^{0,n}$ display prominent corner and edge singularities.

For $m = 1$, $n = 1$ and $0 > \sigma > \tilde{\sigma} := -1/r$, we have $\mu = \nu > 0$ and the relevant equations are those of Section 9.2 with $m = 1$ and $n = 1$. However, when $\sigma = \tilde{\sigma} = -2\sqrt{3} \approx -3.464$ with the normalization $h = 1$, we have $\mu = \nu = 0 \Rightarrow \hat{k}^2 = 0$. Also, as $\sigma \to \tilde{\sigma}$, we have $\hat{p}_s^{1,1}$ of Equation (9.11) approaches zero. However, if we normalize $\hat{p}_s^{1,1}$ so that its maximum value is one then it approaches the harmonic polynomial

$$\tilde{p}_s^{1,1} = 1 - \frac{2}{9r^3}[(r-u)^2(u+2r) + (r-v)^2(v+2r) + (r-w)^2(w+2r)]. \quad (9.29)$$

For $\sigma < \tilde{\sigma}$, all the parameters of Section 9.2 become complex. Asymptotically, as $\sigma \to -\infty$, we have the limiting value $\hat{k}^2 \to -\sigma^2$. Equation (9.11) for $\hat{p}_s^{1,1}(u, v, w)$ becomes unbounded as $\sigma \to -\infty$. However, if we first scale it by its value at a vertex, $\hat{p}_s^{1,1}(r, -2r, r)$, we find that this normalized mode approaches 1 at the three vertices and 0 in the interior. This results in prominent edge and corner singularities.

For $m = 1$, $n > 1$ and $0 > \sigma > \sigma_n^*$, we have $\mu > 0$ and the relevant equations are those of Section 9.2 with $m = 1$. However, as $\sigma \to \sigma_n^*$ we have $\mu \to 0$ For $\sigma < \sigma_n^*$, μ becomes pure imaginary, and the remaining parameters of Section 9.2 become complex in such a way so as to guarantee that $\hat{k}^2$, $\hat{p}_s$ and $\hat{p}_a$ are real. For $\sigma = 0$, $\hat{k}^2$ is positive and, as σ is decreased, $\hat{k}^2$, likewise, decreases. When σ reaches a critical value, $\hat{\sigma}_n < \sigma_n^*$, $\hat{k}^2(\hat{\sigma}_n) = 0$ and thereafter continues

to decrease without bound. Asymptotically, as $\sigma \to -\infty$, we have the limiting value $\hat{k}^2 \to -\sigma^2 + \frac{4}{27}[\frac{\pi}{r}(n-1)]^2$. Both $\hat{p}_s^{1,n}$ and $\hat{p}_a^{1,n}$ display prominent vertex and edge singularities.

9.5 The Case of Complex σ

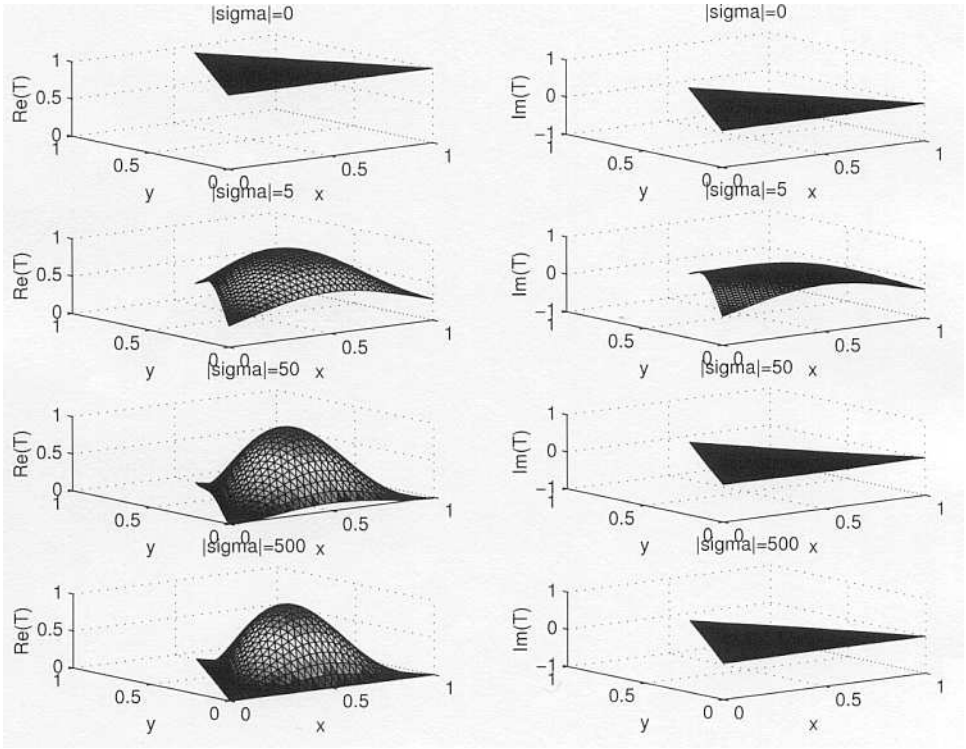

Figure 9.3: Mode Morphing: $(m,n) = (0,0),\ \theta = \pi/4$

In the case of complex σ, as previously noted, the Robin problem with IBC defined by Equation (9.3) is non-self-adjoint and the eigenstructure is consequently complex. Defining the mean-square residual function of Equation (9.18) as

$$\begin{aligned} R_{m,n}(L,M,N;\sigma) &= |[2L - M - N - (m+n)\pi] \cdot \tan(L) - 3\sigma r|^2, \\ &+ |[2M - N - L + m\pi] \cdot \tan(M) - 3\sigma r|^2 \\ &+ |[2N - L - M + n\pi] \cdot \tan(N) - 3\sigma r|^2, \end{aligned} \tag{9.30}$$

we note that the sought-after eigenvalues are determined by its local minima. Next, define

$$\sigma = \rho \cdot e^{\imath\theta}, \text{ with } \theta \text{ fixed and } 0 \le \rho \le +\infty. \tag{9.31}$$

The appropriate limiting behavior described in the previous section must be exhibited as $\theta \to 0^+$ (real $\sigma > 0$) and $\theta \to \pi^-$ (real $\sigma < 0$).

Figure 9.3 displays the resultant mode morphing for the fundamental mode $(m, n) = (0, 0)$ as ρ varies with $\theta = \frac{\pi}{4}$. As occurred in the real case with $\sigma \geq 0$, (μ, ν) varies from (m, n) to $(m+1, n+1)$ only now they make an excursion into the complex plane rather than traversing the real axis. The attendant complex mode morphing from $N_{0,0}(x, y)$ to $D_{1,1}(x, y)$ is made explicit by Figure 9.3.

As will be established below, mode morphings other than the $(m, n) \mapsto (m + 1, n + 1)$ homotopy of the previous example are possible. The possible homotopies are summarized in Table 9.1 together with their associated limiting parameter values.

(L, M, N)	(μ, ν)	$(\delta_1, \delta_2, \delta_3)$	$N_{m,n} \mapsto$
$(+\frac{\pi}{2}, -\frac{\pi}{2}, -\frac{\pi}{2})$	$(m-1, n-1)$	$(+\frac{3\pi}{2}, -\frac{\pi}{2}, -\frac{\pi}{2})$	$-D_{m-1,n-1}$
$(+\frac{\pi}{2}, -\frac{\pi}{2}, +\frac{\pi}{2})$	$(m-2, n+1)$	$(+\frac{\pi}{2}, -\frac{3\pi}{2}, +\frac{\pi}{2})$	$+D_{m-2,n+1}$
$(+\frac{\pi}{2}, +\frac{\pi}{2}, -\frac{\pi}{2})$	$(m+1, n-2)$	$(+\frac{\pi}{2}, +\frac{\pi}{2}, -\frac{3\pi}{2})$	$+D_{m+1,n-2}$
$(+\frac{\pi}{2}, +\frac{\pi}{2}, +\frac{\pi}{2})$	(m, n)	$(-\frac{\pi}{2}, -\frac{\pi}{2}, -\frac{\pi}{2})$	$-D_{m,n}$
$(-\frac{\pi}{2}, +\frac{\pi}{2}, +\frac{\pi}{2})$	$(m+1, n+1)$	$(-\frac{3\pi}{2}, +\frac{\pi}{2}, +\frac{\pi}{2})$	$+D_{m+1,n+1}$
$(-\frac{\pi}{2}, +\frac{\pi}{2}, -\frac{\pi}{2})$	$(m+2, n-1)$	$(-\frac{\pi}{2}, +\frac{3\pi}{2}, -\frac{\pi}{2})$	$-D_{m+2,n-1}$
$(-\frac{\pi}{2}, -\frac{\pi}{2}, +\frac{\pi}{2})$	$(m-1, n+2)$	$(-\frac{\pi}{2}, -\frac{\pi}{2}, +\frac{3\pi}{2})$	$-D_{m-1,n+2}$
$(-\frac{\pi}{2}, -\frac{\pi}{2}, -\frac{\pi}{2})$	(m, n)	$(+\frac{\pi}{2}, +\frac{\pi}{2}, +\frac{\pi}{2})$	$+D_{m,n}$

Table 9.1: Possible Modal Homotopies

However, before proceeding to a thorough treatment of the intricacies of the case of complex σ for the equilateral triangular acoustic waveguide, we first summarize, for purpose of comparison, what is known about the corresponding one-dimensional problem of the parallel-plate waveguide [56].

Theorem 9.5.1 (Asymptotic Behavior of SL-BVP/IBC Eigenstructure). *Consider the Sturm-Liouville boundary value problem (SL-BVP) with an IBC described by*

$$u''(x)+\lambda \cdot u(x) = 0,\ 0 < x < L;\ u'(0)-\sigma \cdot u(0) = 0,\ u'(L)+\sigma \cdot u(L) = 0, \quad (9.32)$$

with $\sigma(\rho) = \rho e^{\imath\theta}$ *for fixed* θ *and* $0 \leq \rho \leq \infty$.

1. *If* $0 \leq \theta \leq \pi/2$ *then* $\lim_{\rho\to\infty} \lambda_n(\sigma) \to \lambda_{n+1}(0)$ *and* $\lim_{\rho\to\infty} u_n(x;\sigma) \to D_{n+1}(x)$ *for all* n.

2. *If* $\pi/2 < \theta \leq \pi$ *then there exists* $n(\theta)$, *with* $\lim_{\theta\to\frac{\pi}{2}^+} n(\theta) = \infty$, *such that*

   (a) $\lim_{\rho\to\infty} \lambda_k(\sigma) \to \lambda_{k+1}(0)$ *and* $\lim_{\rho\to\infty} u_k(x;\sigma) \to D_{k+1}(x)$ *for* $k < n(\theta) - 1$,

(b) $\lim_{\rho\to\infty}\lambda_k(\sigma)\to\lambda_{k-1}(0)$ *and* $\lim_{\rho\to\infty}u_k(x;\sigma)\to -D_{k-1}(x)$ *for* $k > n(\theta)$,

(c) and $\lim_{\rho\to\infty}|\lambda_k(\sigma)|\to\infty$ *for* $k = n(\theta)-1, n(\theta)$.

Thus, there is a rightward procession of missing modes as θ is lowered from π to $\pi/2$. As we shall now discover, the two-dimensional case is much more involved.

We commence by defining three critical angles. We know from the above limiting cases that $N_{m-1,n-1}\mapsto D_{m,n}$ for $\theta\approx 0$. Define $\theta^-_{m,n}$ to be the smallest angle for which this is not the case. Likewise, we know that $N_{m+1,n+1}\mapsto -D_{m,n}$ for $\theta\approx\pi$. Define $\theta^+_{m,n}$ to be the largest angle for which this is not the case. If there is an intermediate angle where an additional modal exchange occurs then denote it by $\theta^*_{m,n}$. There is a modal ambiguity at each of these critical angles.

Due to the symmetric occurrence of m and n in Equation (9.18), we have $\mu_{m,m}(\sigma)=\nu_{m,m}(\sigma)$ for all values of σ. Thus, the main diagonal modes $\hat{p}^{m,m}_{s,a}(x,y;\sigma)$ possess an especially simple structure directly analogous to the one-dimensional case. Specifically, for $m\geq 1$, $\theta^-_{m,m}=\theta^+_{m,m}$ and

$$\begin{aligned} N_{m-1,m-1}\mapsto D_{m,m} \quad &;\quad \theta<\theta^{\pm}_{m,m},\\ N_{m+1,m+1}\mapsto -D_{m,m} \quad &;\quad \theta>\theta^{\pm}_{m,m}. \end{aligned} \tag{9.33}$$

Thus, there is a modal exchange at $\theta^{\pm}_{m,m}$. Alternatively, for $m>1$,

$$\begin{aligned} N_{m,m}\mapsto D_{m+1,m+1} \quad &;\quad \theta<\theta^{\pm}_{m+1,m+1},\\ N_{m,m}\mapsto -D_{m-1,m-1} \quad &;\quad \theta>\theta^{\pm}_{m-1,m-1}. \end{aligned} \tag{9.34}$$

Thus, $N_{m,m}$ becomes a missing mode for $\theta^{\pm}_{m+1,m+1}<\theta<\theta^{\pm}_{m-1,m-1}$. For $m=0$ or 1, $N_{m,m}\mapsto D_{m+1,m+1}$ for $\theta<\theta^{\pm}_{m+1,m+1}$ and becomes a missing mode for $\theta>\theta^{\pm}_{m+1,m+1}$.

Figure 9.4 displays the corresponding critical trajectories for the the first four main diagonal Dirichlet modes, the top frame for the odd numbered modes and the bottom frame for the even numbered modes. As is evident from both of these plots, for some values of θ mode morphing occurs, i.e $\mu_{m,m}(\sigma)\to\mu_{m\pm1,m\pm1}(0)$, (IBC-Dirichlet modes) while for other values of θ we observe $|\mu_{m,m}(\sigma)|\to\infty$ (missing modes). Note that the corner on the critical trajectory corresponding to $\theta^{\pm}_{m,m}$ is a bifurcation point where one path leads to (m,m) and the other veers off to infinity.

Our next result concerns the trajectories at these critical angles and is not confined to the special case $m=n$.

Theorem 9.5.2. *The critical trajectories all possess a branch (bifurcation) point in complex* (L,M,N)*-space located at a solution of the complex system*

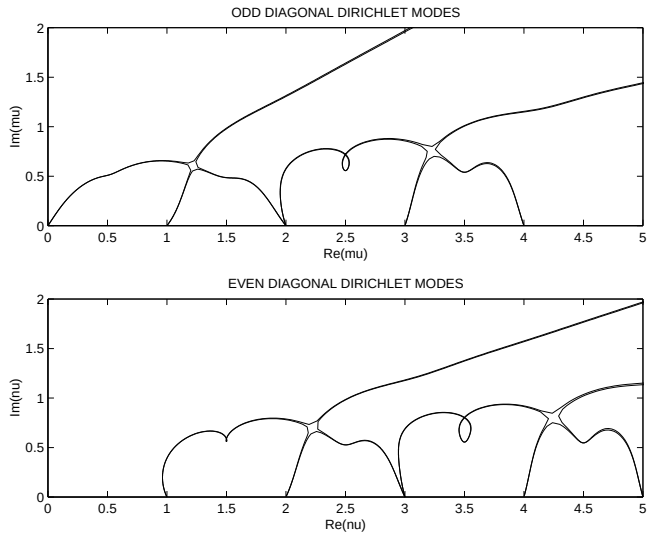

Figure 9.4: Main Diagonal Modal Groups

of equations:

$$\begin{aligned}(2L-M-N-(m+n)\pi)\cdot\tan L &= (2M-N-L+m\pi)\cdot\tan M,\\ (2L-M-N-(m+n)\pi)\cdot\tan L &= (2N-L-M+n\pi)\cdot\tan N,\\ \tan L\cdot\tan M\cdot\tan N\cdot(\mathcal{ABC}-\mathcal{A}-\mathcal{B}-\mathcal{C}-2) &= 0,\end{aligned}\tag{9.35}$$

where

$$\begin{aligned}\mathcal{A} &= 2+2\cdot(2L-M-N-(m+n)\pi)\cdot\csc(2L),\\ \mathcal{B} &= 2+2\cdot(2M-N-L+m\pi)\cdot\csc(2M),\\ \mathcal{C} &= 2+2\cdot(2N-L-M+n\pi)\cdot\csc(2N).\end{aligned}\tag{9.36}$$

At the common branch point shared by two neighboring modes there is modal deficiency and along the bifurcated trajectories there is modal ambiguity.

Proof: Differentiation of Equation (9.18) with respect to ρ produces the complex system of equations:

$$\begin{aligned}\mathcal{A}\tan L\cdot L'-\tan L\cdot M'-\tan L\cdot N' &= 3re^{\imath\theta},\\ -\tan M\cdot L'+\mathcal{B}\tan M\cdot M'-\tan M\cdot N' &= 3re^{\imath\theta},\\ -\tan N\cdot L'-\tan N\cdot M'+\mathcal{C}\tan N\cdot N' &= 3re^{\imath\theta}.\end{aligned}\tag{9.37}$$

The branch points of the critical trajectories in complex (L,M,N)-space will be located at those solutions of Equation (9.18) where (L',M',N') is indeterminate, i.e. where the determinant of the system described by Equation (9.37)

vanishes. Setting this determinant to zero yields the third equation of the system described by Equation (9.35) while elimination of $3\sigma r$ in Equation (9.18) yields the first two equations. At a common branch point, adjacent modes coalesce thereby producing a modal deficiency. Beyond the branch point, there is modal ambiguity in that it is not clear which mode to associate with which bifurcation branch. □

The modal deficiency and ambiguity identified in the previous theorem must be taken into account when utilizing the eigenfunction expansion of Equation (9.26). Once (L, M, N) has been determined by solving the system Equation (9.35), σ and *ipso facto* the critical angle θ may be determined from any of the three equations of the system described by Equation (9.18).

The critical angles $\theta^-_{m,n},\ \theta^*_{m,n},\ \theta^+_{m,n}$ $(0 \leq n - m \leq 6,\ 1 \leq m \leq 6)$ were calculated from minimization of the mean-square residual of the system described by Equation (9.35) and are summarized in Table 9.2. Observe that all of the critical angles lie in the range $\pi/2 < \theta < \pi$. We further note that $\lim_{m\to\infty} \theta^{\pm}_{m,m} = \frac{\pi}{2}^+$ which accounts for a northeastward procession of the two missing modes along the main diagonal as θ is lowered from π to $\pi/2$.

9.5.1 The Case $Re(\sigma) \geq 0$

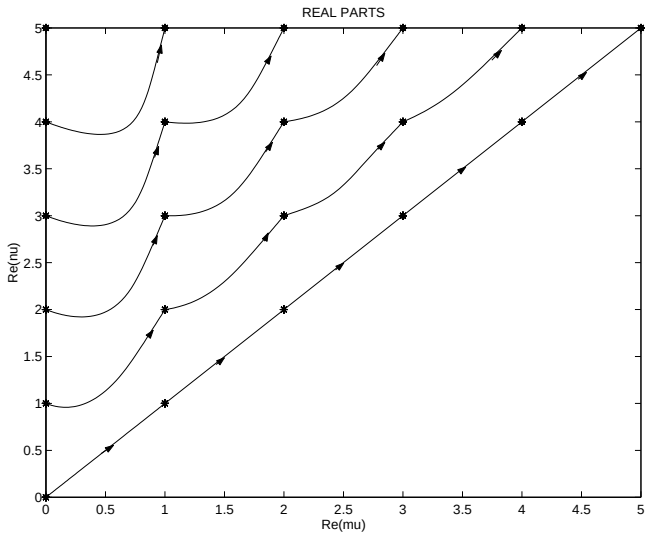

Figure 9.5: Modal Homotopies: $\theta = \pi/4$

The previous observation concerning critical angle bounds has the following important consequence.

Theorem 9.5.3. *For $0 \leq \theta \leq \frac{\pi}{2}$, all modes are IBC-Dirichlet modes (i.e. there are no missing modes).*

(m,n)	$\theta^-_{m,n}$	$\theta^*_{m,n}$	$\theta^+_{m,n}$
(1,1)	$.684206142\pi$	$-\,-\,-\,-\,-$	$.684206142\pi$
(2,2)	$.619166446\pi$	$-\,-\,-\,-\,-$	$.619166446\pi$
(3,3)	$.589143056\pi$	$-\,-\,-\,-\,-$	$.589143056\pi$
(4,4)	$.571704210\pi$	$-\,-\,-\,-\,-$	$.571704210\pi$
(5,5)	$.560241318\pi$	$-\,-\,-\,-\,-$	$.560241318\pi$
(6,6)	$.552098631\pi$	$-\,-\,-\,-\,-$	$.552098631\pi$
(1,2)	$.645011307\pi$	$.649882709\pi$	$.704097441\pi$
(2,3)	$.602065916\pi$	$.611505985\pi$	$.638710316\pi$
(3,4)	$.579505853\pi$	$.589698846\pi$	$.606359195\pi$
(4,5)	$.565487637\pi$	$.575403800\pi$	$.586755145\pi$
(5,6)	$.555881748\pi$	$.565238076\pi$	$.573512974\pi$
(6,7)	$.548862681\pi$	$.557607707\pi$	$.563929945\pi$
(1,3)	$.620807848\pi$	$.625093472\pi$	$.708807793\pi$
(2,4)	$.589725813\pi$	$.598167957\pi$	$.642902235\pi$
(3,5)	$.571974034\pi$	$.581563903\pi$	$.609975769\pi$
(4,6)	$.560387453\pi$	$.570077199\pi$	$.589904313\pi$
(5,7)	$.552186420\pi$	$.561591253\pi$	$.576291838\pi$
(6,8)	$.546054740\pi$	$.555038235\pi$	$.566412390\pi$
(1,4)	$.604161170\pi$	$.607651277\pi$	$.710931519\pi$
(2,5)	$.580326647\pi$	$.587470799\pi$	$.645011539\pi$
(3,6)	$.565893144\pi$	$.574368709\pi$	$.611908690\pi$
(4,7)	$.556111484\pi$	$.564957674\pi$	$.591654648\pi$
(5,8)	$.549005310\pi$	$.557805371\pi$	$.577879843\pi$
(6,9)	$.543589824\pi$	$.552158951\pi$	$.567860843\pi$
(1,5)	$.591916913\pi$	$.594771481\pi$	$.712104826\pi$
(2,6)	$.572891982\pi$	$.578927104\pi$	$.646269199\pi$
(3,7)	$.560862858\pi$	$.568273659\pi$	$.613114048\pi$
(4,8)	$.552465170\pi$	$.560407892\pi$	$.592779713\pi$
(5,9)	$.546232364\pi$	$.554298349\pi$	$.578923343\pi$
(6,10)	$.541405126\pi$	$.549389662\pi$	$.568828851\pi$
(1,6)	$.582485162\pi$	$.584855584\pi$	$.712829475\pi$
(2,7)	$.566843244\pi$	$.571985337\pi$	$.647091942\pi$
(3,8)	$.556621670\pi$	$.563112674\pi$	$.613931190\pi$
(4,9)	$.549312722\pi$	$.556423443\pi$	$.593561575\pi$
(5,10)	$.543789913\pi$	$.551137667\pi$	$.579662025\pi$
(6,11)	$.539452931\pi$	$.546829816\pi$	$.569523993\pi$
(1,7)	$.574969796\pi$	$.576969203\pi$	$.713310995\pi$
(2,8)	$.561813036\pi$	$.566240516\pi$	$.647664046\pi$
(3,9)	$.552990317\pi$	$.558706706\pi$	$.614516320\pi$
(4,10)	$.546555917\pi$	$.552933716\pi$	$.594133279\pi$
(5,11)	$.541619481\pi$	$.548308346\pi$	$.580210776\pi$
(6,12)	$.537696183\pi$	$.544494068\pi$	$.570046883\pi$

Table 9.2: Critical Angles

Proof: Since all of the critical angles lie in the indicated range, we have in particular that $\frac{\pi}{2} < \theta^-_{m,n} < \pi$. Thus, the range $0 \leq \theta \leq \frac{\pi}{2}$ is free of missing modes. □

Because of Theorem 9.5.3, the asymptotic behavior for $Re(\sigma) \geq 0$ is especially simple. With reference to Figure 9.5, there is a complete modal homotopy from each of the Neumann modes to a corresponding Dirichlet mode. Specifically, $N_{m,n}(x,y) \mapsto D_{m+1,n+1}(x,y)$ for all (m,n). This asymptotic behavior, illustrated by Figure 9.3 for $(m,n) = (0,0)$ and $\theta = \pi/4$, is directly analogous to the case of σ real and positive, as described in Section 9.4.1, except that now the homotopy passes through the complex plane.

9.5.2 The Case $Re(\sigma) < 0$

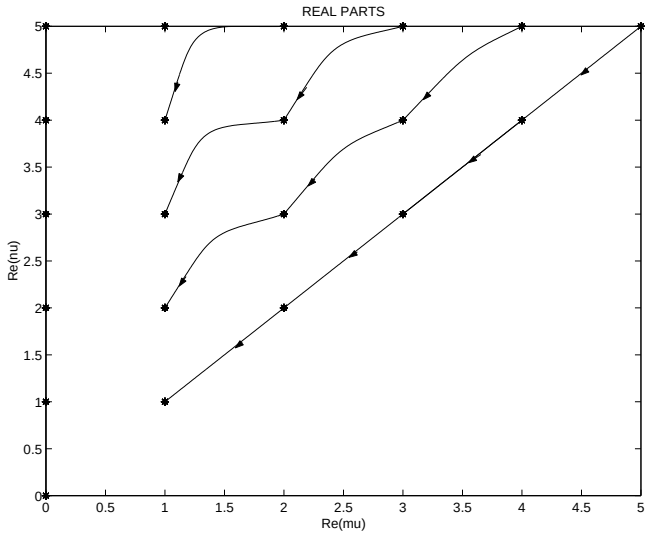

Figure 9.6: Modal Homotopies: $\theta = 11\pi/12$

For $\theta \to \pi^-$, the asymptotic behavior for $Re(\sigma) < 0$ is directly analogous to the case of σ real and negative, as described in Section 9.4.2. Thus, for (m,n) sufficiently close to the origin and for sufficiently large θ the situation obtains as is shown graphically in Figure 9.6. However the picture as seen in Figure 9.7, which displays the incoming homotopies for $1 \leq m,n \leq 5$, is much more complicated for arbitrary (m,n) and θ.

So as to bring order to this seemingly chaotic situation, we will avail ourselves of the following result.

Theorem 9.5.4. *The IBC modes $\hat{p}^{m,n}_{s,a}$ naturally partition themselves into three groups G_k, $k = (n-m)_{mod\ 3}$. All modal homotopies and exchanges are constrained to occur within a group.*

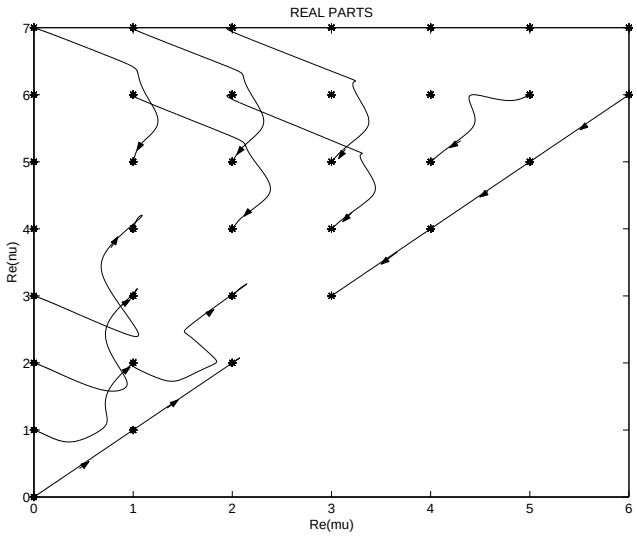

Figure 9.7: Modal Homotopies: $\theta = .6\pi$

Proof: In the system of equations embodied by Equation (9.18), make the change of variables

$$\begin{aligned} L &= \tilde{L} + n\pi - (n-m)\cdot\frac{\pi}{3}, \\ M &= \tilde{M} + (n-m)\cdot\frac{\pi}{3}, \\ N &= \tilde{N}, \end{aligned} \tag{9.38}$$

resulting in the transformed system

$$\begin{aligned} [2\tilde{L} - \tilde{M} - \tilde{N}]\cdot\tan\,(\tilde{L} - (\frac{n-m}{3})\cdot\pi) &= 3\sigma r, \\ [2\tilde{M} - \tilde{N} - \tilde{L}]\cdot\tan\,(\tilde{M} + (\frac{n-m}{3})\cdot\pi) &= 3\sigma r, \\ [2\tilde{N} - \tilde{L} - \tilde{M}]\cdot\tan\,\tilde{N} &= 3\sigma r. \end{aligned} \tag{9.39}$$

Thus, since $\tan z$ has period π, the IBC eigenstructure naturally partitions itself into the three groups $G_k,\ k = (n-m)_{mod\ 3}$. □

This result may be further refined. The permissible modal homotopies are restricted to $(L, M, N) :\ (0,0,0) \rightarrow (\pm\frac{\pi}{2}, \pm\frac{\pi}{2}, \pm\frac{\pi}{2})$. These possible homotopies are summarized in Table 9.1. Furthermore, the bottom three rows of that table are applicable only to the case of $m, n < 0$ and as such are of no interest in the present investigation. Thus, the relevant modal homotopies are confined to the top five rows of Table 9.1.

In order to further specify the nature of these modal homotopies, we must separately consider the cases: 1) $n - m = 0$, 2) $n - m = 1$ & 2, 3) $n - m = 3$,

4) $n - m > 3$. The first case has already been exhaustively treated above so that we now turn our attention to the remaining three cases.

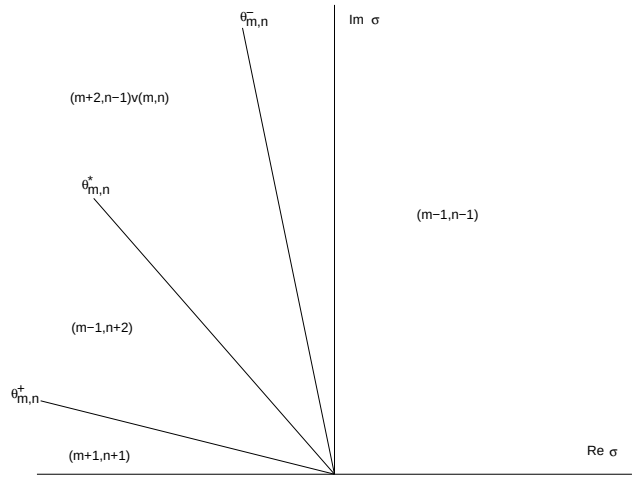

Figure 9.8: Modal Zones: $D_{m,n}$ $(n - m > 0)$

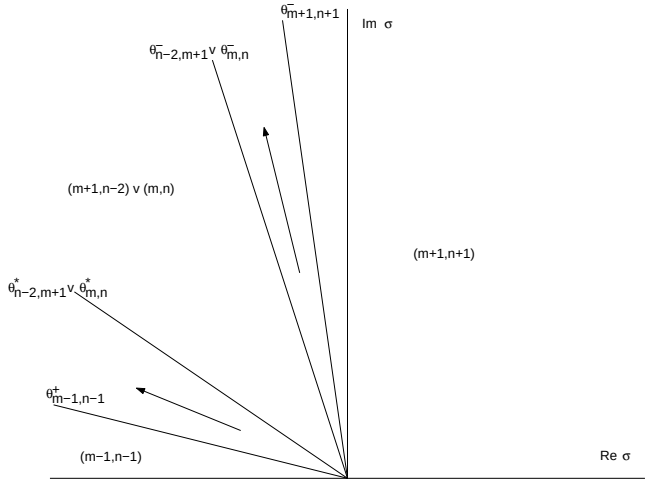

Figure 9.9: Modal Zones: $N_{m,n}$ $(0 < n - m \leq 3)$

For $n - m = 1$ & 2 and $m \geq 1$, we have (see Figure 9.8)

$$\begin{aligned} N_{m-1,n-1} &\mapsto D_{m,n} \quad ; \quad 0 \leq \theta < \theta^-_{m,n}, \\ N_{m+2,n-1} &\mapsto D_{m,n} \quad ; \quad \theta^-_{m,n} < \theta < \theta^*_{m,n}, \\ N_{m-1,n+2} &\mapsto D_{m,n} \quad ; \quad \theta^*_{m,n} < \theta < \theta^+_{m,n}, \\ N_{m+1,n+1} &\mapsto -D_{m,n} \quad ; \quad \theta^+_{m,n} < \theta \leq \pi. \end{aligned} \tag{9.40}$$

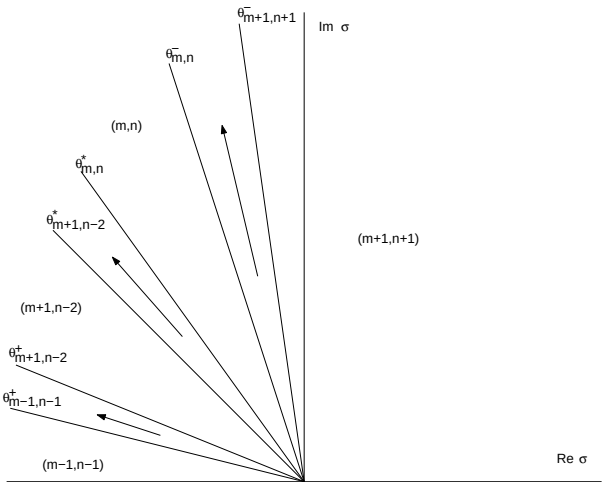

Figure 9.10: Modal Zones: $N_{m,n}$ $(n-m>3)$

Alternatively (see Figure 9.9), for $m>1$,

$$\begin{aligned} N_{m,n} &\mapsto D_{m+1,n+1} \quad ; \quad 0 \le \theta < \theta^-_{m+1,n+1}, \\ N_{m,n} &\mapsto D_{m+1,n-2} \quad ; \quad \theta^-_{n-2,m+1} < \theta < \theta^*_{n-2,m+1}, \\ N_{m,n} &\mapsto -D_{m-1,n-1} \quad ; \quad \theta^+_{m-1,n-1} < \theta \le \pi. \end{aligned} \tag{9.41}$$

$N_{m,n}$ becomes a missing mode for all other intermediate ranges of θ. For $m=0$, $N_{0,n=1\&2}$ becomes a missing mode also for the bottom two ranges of Equation (9.41). For $m=1$, $N_{1,3}$ becomes a missing mode also for the bottom range of Equation (9.41) while $N_{1,2}$ becomes a missing mode also for the bottom two ranges of Equation (9.41).

For $n-m=3$ and $m\ge 1$, we have (see Figure 9.8)

$$\begin{aligned} N_{m-1,n-1} &\mapsto D_{m,n} \quad ; \quad 0 \le \theta < \theta^-_{m,n}, \\ N_{m,n} &\mapsto -D_{m,n} \quad ; \quad \theta^-_{m,n} < \theta < \theta^*_{m,n}, \\ N_{m-1,n+2} &\mapsto D_{m,n} \quad ; \quad \theta^*_{m,n} < \theta < \theta^+_{m,n}, \\ N_{m+1,n+1} &\mapsto -D_{m,n} \quad ; \quad \theta^+_{m,n} < \theta \le \pi. \end{aligned} \tag{9.42}$$

Alternatively (see Figure 9.9), for $m>1$,

$$\begin{aligned} N_{m,n} &\mapsto D_{m+1,n+1} \quad ; \quad 0 \le \theta < \theta^-_{m+1,n+1}, \\ N_{m,n} &\mapsto -D_{m,n} \quad ; \quad \theta^-_{m,n} < \theta < \theta^*_{m,n}, \\ N_{m,n} &\mapsto -D_{m-1,n-1} \quad ; \quad \theta^+_{m-1,n-1} < \theta \le \pi. \end{aligned} \tag{9.43}$$

$N_{m,n}$ becomes a missing mode for all other intermediate ranges of θ. For $m=0$, $N_{0,3}$ becomes a missing mode also for the bottom two ranges of Equation (9.43).

For $m = 1$, $N_{1,4}$ becomes a missing mode also for the bottom range of Equation (9.43).

For $n - m > 3$ and $m \geq 1$, we have (see Figure 9.8)

$$\begin{aligned} N_{m-1,n-1} &\mapsto D_{m,n} \quad ; \quad 0 \leq \theta < \theta^{-}_{m,n}, \\ N_{m,n} &\mapsto -D_{m,n} \quad ; \quad \theta^{-}_{m,n} < \theta < \theta^{*}_{m,n}, \\ N_{m-1,n+2} &\mapsto D_{m,n} \quad ; \quad \theta^{*}_{m,n} < \theta < \theta^{+}_{m,n}, \\ N_{m+1,n+1} &\mapsto -D_{m,n} \quad ; \quad \theta^{+}_{m,n} < \theta \leq \pi. \end{aligned} \tag{9.44}$$

Alternatively (see Figure 9.10), for $m > 1$,

$$\begin{aligned} N_{m,n} &\mapsto D_{m+1,n+1} \quad ; \quad 0 \leq \theta < \theta^{-}_{m+1,n+1}, \\ N_{m,n} &\mapsto -D_{m,n} \quad ; \quad \theta^{-}_{m,n} < \theta < \theta^{*}_{m,n}, \\ N_{m,n} &\mapsto D_{m+1,n-2} \quad ; \quad \theta^{*}_{m+1,n-2} < \theta < \theta^{+}_{m+1,n-2}, \\ N_{m,n} &\mapsto -D_{m-1,n-1} \quad ; \quad \theta^{+}_{m-1,n-1} < \theta \leq \pi. \end{aligned} \tag{9.45}$$

$N_{m,n}$ becomes a missing mode for all other intermediate ranges of θ. For $m = 0$, $N_{0,n\geq 4}$ becomes a missing mode also for the two even ranges of Equation (9.45). For $m = 1$, $N_{1,n\geq 5}$ becomes a missing mode also for the bottom range of Equation (9.45).

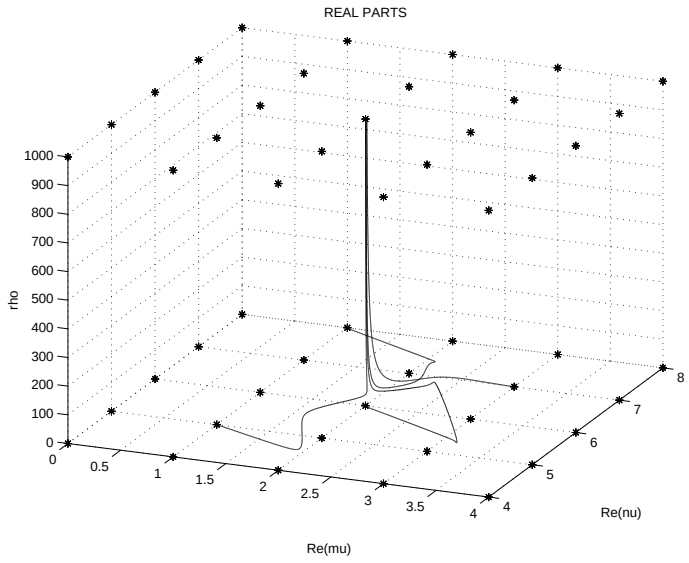

Figure 9.11: Homotopies Terminating At (2,6)-Mode

Figure 9.11 displays representative homotopies emanating from the neighboring modes $N_{1,5}$, $N_{2,6}$, $N_{1,8}$, and $N_{3,7}$ and terminating at $\pm D_{2,6}$ while Figure 9.12 shows the associated critical trajectories with corresponding branch points

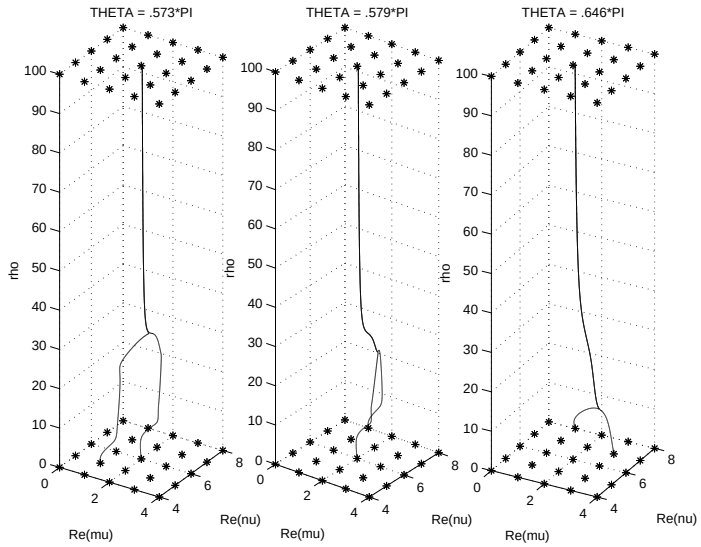

Figure 9.12: Branch Points for Homotopies Terminating At (2,6)-Mode

where modal exchange transpires. Figure 9.13 displays representative homotopies emanating from $N_{2,6}$ and terminating at the neighboring modes $D_{3,7}$, $-D_{2,6}$, $D_{3,4}$, and $-D_{1,5}$.

We conclude this section by making a final perusal of the critical angles of Table 9.2 where we observe the following patterns. Along vertical bands, m fixed, we have the inequalities

$$n_2 > n_1 \Rightarrow \theta^-_{m,n_2} < \theta^-_{m,n_1},\ \theta^*_{m,n_2} < \theta^*_{m,n_1},\ \theta^+_{m,n_2} > \theta^+_{m,n_1}, \tag{9.46}$$

and the limits

$$\lim_{n\to\infty} \theta^-_{m,n} = \frac{\pi}{2}^+ = \lim_{n\to\infty} \theta^*_{m,n},\ \lim_{n\to\infty} \theta^+_{m,n} = \pi^-. \tag{9.47}$$

Along diagonal bands, $n - m = k$ fixed, we have the inequalities

$$m_2 > m_1 \Rightarrow \theta^-_{m_2,m_2+k} < \theta^-_{m_1,m_1+k},\ \theta^*_{m_2,m_2+k} < \theta^*_{m_1,m_1+k},\ \theta^+_{m_2,m_2+k} < \theta^+_{m_1,m_1+k}, \tag{9.48}$$

and the limits

$$\lim_{m\to\infty} \theta^-_{m,m+k} = \lim_{m\to\infty} \theta^*_{m,m+k} = \lim_{m\to\infty} \theta^+_{m,m+k} = \frac{\pi}{2}^+. \tag{9.49}$$

Along horizontal bands, n fixed, we have the inequalities

$$m_2 > m_1 \Rightarrow \theta^-_{m_2,n} < \theta^-_{m_1,n},\ \theta^*_{m_2,n} < \theta^*_{m_1,n},\ \theta^+_{m_2,n} < \theta^+_{m_1,n}. \tag{9.50}$$

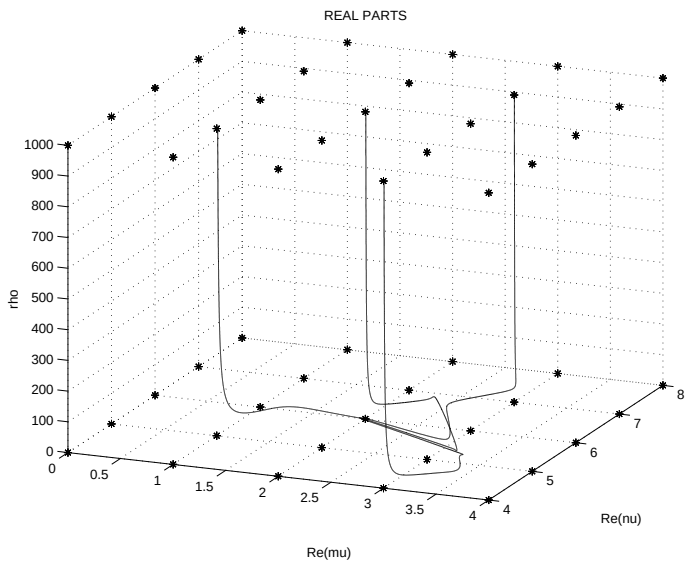

Figure 9.13: Homotopies Emanating From (2,6)-Mode

Along reverse-diagonal bands, $n+m=k$ fixed, we have the inequalities

$$m_2 > m_1 \Rightarrow \theta^-_{m_2,k-m_2} < \theta^-_{m_1,k-m_1},\ \theta^*_{m_2,k-m_2} > \theta^*_{m_1,k-m_1},\ \theta^+_{m_2,k-m_2} < \theta^+_{m_1,k-m_1}. \tag{9.51}$$

One immediate consequence of these observations is that the appropriate limiting homotopies are attained as the real σ-axis is approached. Furthermore, there are hidden patterns present in Figure 9.7. Specifically, with $k>0$, along:

- diagonals: $N_{m,n} \mapsto D_{m+1,n+1} \Rightarrow N_{m-k,n-k} \mapsto D_{m-k+1,n-k+1}$; $N_{m,n} \mapsto D_{m-1,n-1} \Rightarrow N_{m+k,n+k} \mapsto D_{m+k-1,n+k-1}$,
- verticals: $N_{m,n} \mapsto D_{m+1,n+1} \Rightarrow N_{m,n-k} \mapsto D_{m+1,n-k+1}$; $N_{m,n} \mapsto D_{m-1,n-1} \Rightarrow N_{m,n-k} \mapsto D_{m-1,n-k-1}$,
- reverse-diagonals: $N_{m,n} \mapsto D_{m+1,n+1} \Rightarrow N_{m-k,n+k} \mapsto D_{m-k+1,n+k+1}$; $N_{m,n} \mapsto D_{m-1,n-1} \Rightarrow N_{m+k,n-k} \mapsto D_{m+k-1,n-k-1}$,
- horizontals: $N_{m,n} \mapsto D_{m+1,n+1} \Rightarrow N_{m-k,n} \mapsto D_{m-k+1,n+1}$; $N_{m,n} \mapsto D_{m-1,n-1} \Rightarrow N_{m+k,n} \mapsto D_{m+k-1,n-1}$.

Lastly, the inequalities of Equations (9.46), (9.48), (9.50) and (9.51) imply:

Theorem 9.5.5. *The θ-ranges of Equations (9.41), (9.43) and (9.45) do not overlap.*

1. $0 < n-m < 3 \Rightarrow \theta^-_{m+1,n+1} < \theta^-_{n-2,m+1}$,

2. $0 < n - m < 3 \Rightarrow \theta^{*}_{n-2,m+1} < \theta^{+}_{m-1,n-1}$,

3. $\theta^{*}_{m,n} < \theta^{*}_{m+1,n-2}$,

4. $\theta^{+}_{m+1,n-2} < \theta^{+}_{m-1,n-1}$.

Proof:

1. $0 < n - m < 3 \Rightarrow \theta^{-}_{m+1,n+1} < \theta^{-}_{m+1,m+1} < \theta^{-}_{n-2,m+1}$,
2. $0 < n - m < 3 \Rightarrow \theta^{*}_{n-2,m+1} < \theta^{*}_{m-1,n-1} < \theta^{+}_{m-1,n-1}$,
3. $\theta^{*}_{m,n} < \theta^{*}_{m-1,n} < \theta^{*}_{m+1,n-2}$,
4. $\theta^{+}_{m+1,n-2} < \theta^{+}_{m+1,n+1} < \theta^{+}_{m-1,n-1}$. □

9.6 Spectral Properties

With reference to Equation (9.1), we express the axial wave number as

$$k_z^{m,n} := \sqrt{\left(\frac{\omega}{c}\right)^2 - \hat{k}^2_{m,n}} = \frac{2\pi}{\lambda_z^{m,n}} - \imath \cdot \pi\gamma_z^{m,n}, \tag{9.52}$$

with

$$\hat{k}^2_{m,n} = \left(\frac{4\pi}{3h}\right)^2 \cdot \chi^2_{m,n};\ \chi^2_{m,n} := \mu^2_{m,n} + \mu_{m,n}\nu_{m,n} + \nu^2_{m,n}, \tag{9.53}$$

where the axial wavelength of mode(s) (m, n) is $\lambda_z^{m,n}$ (so that its phase velocity is $c_z^{m,n} := \omega\lambda_z^{m,n}/2\pi$) and the pressure amplitude attenuates by a factor of e^{-1} in a distance of $1/\pi\gamma_z^{m,n}$ [70, pp. 496-497]. Thus, the propagation properties of the modes of the equilateral triangle hinge upon the structure of the spectral parameter $\chi^2_{m,n}$. The trajectory traced out in the complex χ^2-plane for each (m, n), $n \geq m \geq 0$, as σ varies from the origin to the point at infinity along a fixed direction in the complex plane, is termed a spectral curve.

Since $\hat{p}_s^{m,n}$ and $\hat{p}_a^{m,n}$ both correspond to the same spectral parameter $\chi^2_{m,n}$ given by Equation (9.53), it follows that all eigenvalues corresponding to $m \neq n$ have multiplicity equal to at least two. However, this modal degeneracy, as it is known in the engineering literature, extends also to the case $m = n$. Additional modal degeneracy is manifested in the intersection of spectral curves. For the Dirichlet and Neumann problems, number theoretic techniques permit a comprehensive treatment of such spectral multiplicity [53]. For the Robin problem, such techniques fail.

With $\sigma = \rho \cdot e^{\imath\theta}$, as $0 \leq \rho \leq \infty$ varies for fixed θ, trajectories are swept out in complex (L, M, N)-space and consequently in complex (μ, ν)-space. These modal trajectories have a direct bearing on the corresponding spectral curves.

Theorem 9.6.1 (Topological Structure of Spectral Curves). *Spectral curves corresponding to $\chi^2_{m_1,n_1}$ and $\chi^2_{m_2,n_2}$ with $(m_1,n_1) \neq (m_2,n_2)$ may touch or cross but may not coalesce.*

Proof: Because the only singularities which the complex transcendental functions appearing in the system Equation (9.18) possess are branch points, the associated modal trajectories are analytic functions of ρ except at these branch points. As such, the corresponding spectral curves, and *ipso facto* the related eigenfunctions, inherit this analyticity away from the branch points. Suppose, for the purpose of contradiction, that two spectral curves coincide on the interval (ρ_L, ρ_R) containing the point ρ^*. As we now show, the analytic dependence of $u(x,y;\rho)$ upon ρ precludes such a coalescence at $\rho = \rho^*$. To see this, let

$$\Delta u + k^2 u = 0,\ (x,y) \in \tau;\ \frac{\partial u}{\partial \nu} + \sigma u = 0,\ (x,y) \in \partial\tau. \tag{9.54}$$

Then

$$u(x,y;\rho) = u(x,y;\rho^*) + u'(x,y;\rho^*)\cdot(\rho-\rho^*) + u''(x,y;\rho^*)\cdot\frac{(\rho-\rho^*)^2}{2} + \cdots, \tag{9.55}$$

where $u' := \frac{\partial u}{\partial \rho}$ and each of the correction terms in the Taylor series is orthogonal to the eigenspace of $k^2(\rho^*)$. Each of the Taylor coefficients satisfies the boundary value problem

$$\begin{aligned} \Delta u^{(n)}(x,y;\rho^*) + k^2(\rho^*)u^{(n)}(x,y;\rho^*) = 0,\ (x,y) \in \tau, \\ \frac{\partial u^{(n)}}{\partial \nu}(x,y;\rho^*) + \sigma^* u^{(n)}(x,y;\rho^*) = -n u^{(n-1)}(x,y;\rho^*),\ (x,y) \in \partial\tau, \end{aligned} \tag{9.56}$$

which may be solved recursively and uniquely for $u', u'', \ldots, u^{(n)}, \ldots$ since they are each orthogonal to the eigenspace of k^2. Thus, $u(x,y;\rho)$ is uniquely determined and, consequently, such coalescence cannot transpire. □

This topological property of the spectral curves significantly simplifies the following treatment of biorthogonality and completeness of the IBC eigenfunctions given by Equations (9.11) and (9.12).

Theorem 9.6.2 (Biorthogonality of IBC Modes). *The collection of IBC modes $\{\hat{p}_s^{m,n}\ (n \geq m \geq 0);\ \hat{p}_a^{m,n}\ (n > m \geq 0)\}$ is biorthogonal.*

Proof: Eigenfunctions corresponding to distinct eigenvalues are guaranteed to satisfy the biorthogonality condition, Equation (9.25) [44, pp. 231-235]. Also, a symmetric mode and an antisymmetric mode automatically satisfy this same biorthogonality relation. However, as we discovered above,

the multiplicity of the eigenvalues given by Equation (9.14) is quite a complicated matter. Thus, we invoke the following continuity argument in order to confirm the biorthogonality of our collection of IBC eigenfunctions $\{\hat{p}_s^{m,n}\ (n \geq m \geq 0);\ \hat{p}_a^{m,n}\ (n > m \geq 0)\}$. Suppose that f and g are eigenfunctions of like parity that share an eigenvalue, $\hat{k}^2$, for some fixed value of $\sigma = \hat{\sigma}$. This corresponds to an intersection of two spectral curves. For σ in the neighborhood of $\hat{\sigma}$, the corresponding eigenvalues are distinct which guarantees that $\langle f, \bar{g} \rangle = \int\int_\tau fg\ dA = 0$. Thus, by continuity, $\langle f, \bar{g} \rangle = 0$ for $\sigma = \hat{\sigma}$ and biorthogonality of our full collection of IBC modes is assured. □

It is not *a priori* certain that the collection of eigenfunctions $\{\hat{p}_s^{m,n},\ \hat{p}_a^{m,n}\}$ is complete. For domains which are the Cartesian product of intervals in an orthogonal coordinate system, such as rectangles and annuli, completeness of the eigenfunctions formed from products of one-dimensional counterparts has been established [88, pp. 303-304]. Since the equilateral triangle is not such a domain, we must employ other devices in order to establish completeness.

Theorem 9.6.3 (Completeness of IBC Modes). *The collection of IBC modes* $\{\hat{p}_s^{m,n}\ (n \geq m \geq 0);\ \hat{p}_a^{m,n}\ (n > m \geq 0)\}$ *is complete.*

Proof: We will utilize an analytic continuation argument which hinges upon the previously established completeness of the Neumann modes [77]. The homotopy between the Neumann and IBC modes that we have established above guarantees a unique branch leading from each of the Neumann modes to its corresponding IBC mode in complex (μ, ν)-space. Likewise, for any $0 < \rho < \infty$ we may trace out a branch from any mode leading back to a Neumann mode as $\rho \to 0^+$. Suppose, for the sake of argument, that the collection of IBC modes constructed above is not complete for some $0 < \rho = \hat{\rho} < \infty$. Then, let $\hat{p}(x, y; \hat{\rho})$ be a mode that is not contained in our collection. Now, trace the branch of the corresponding spectral curve emanating from this point back to $\rho = 0$. Since we know that the collection of Neumann modes is complete, this branch must at some point, $\rho = \rho^*$, coalesce with a branch emanating from one of our IBC modes. However, the previously noted topological property of the modal trajectories precludes such a bifurcation point at $\rho = \rho^*$. Consequently, our collection of IBC modes is indeed complete. □

9.7 Morse and Feshbach

Methods of Theoretical Physics [67, 68], simply known as "Morse and Feshbach", is a classic tome of Mathematical Physics. Weighing in at 1,978 pages, it provides a magnificent summary of the application of classical Applied Mathematics to the problems of continuum physics. What began as a set of course notes by Morse for the "Methods of Theoretical Research" course at MIT

Figure 9.14: Philip Morse

Figure 9.15: Herman Feshbach

became a collaborative venture with his former doctoral student Feshbach (together with their graduate students) and, in 1953, was published in two parts after 16 years of labor. Three of its most notable features are its elaborate 3-D stereoscopic illustrations, its comprehensive treatment of Green's functions and eigenfunction expansions, and especially its elaborate discussion of the impedance boundary condition which is even further expounded upon in Morse and Ingard's *Theoretical Acoustics* [70].

9.7.1 Philip M. Morse

Philip McCord Morse (1903-1985), known as the father of operations research in the U.S., was born in Shreveport, Louisiana [65]. His family moved to Cleveland, Ohio shortly thereafter, where he spent his youth and graduated from the Case School of Applied Science in 1926 with a B.S. in physics. He earned his Ph.D. in physics from Princeton in 1929 with a thesis on the discharge of electricity through a low-pressure gas written under the supervision of Karl T. Compton. In that same year, he proposed the Morse potential function for diatomic molecules which is used to interpret vibrational spectra and also published the first American text on quantum mechanics with E. U. Condon. In 1930, he lectured on quantum mechanics at the famous University of Michigan summer school and then departed for Munich (where he did postgraduate research under Arnold Sommerfeld) and Cambridge as a Rockefeller International Fellow.

Upon his return to the United States in 1931, he joined the MIT Physics

Department. In 1936, he published his classic *Vibration and Sound* where he treated the wave properties of acoustic systems using the mathematical methods he had learned in his quantum mechanical studies. This work was eventually expanded into the 1968 treatise *Theoretical Acoustics* coauthored with K. U. Ingard. At this time, he also initiated a course entitled "Methods of Theoretical Research" whose class notes would eventually grow into the two-part *Methods of Theoretical Physics* (1953) previously described.

During World War II, he served as Director of the MIT Underwater Sound Project (1940-1942), where he developed a noisemaker that mimicked the sound of a ship well enough to thwart an acoustic mine, and as Director of the U.S. Naval Operations Research Group (1942-1946), where he played a vital role in the containment of the U-boat offensive which was destroying Atlantic and Mediterranean shipping at a catastrophic rate. For this work, he was awarded the Presidential Medal for Merit in 1946. An outgrowth of these wartime activities was his pioneering work in operations research. At MIT, he became the Director of the Operations Research Center and published *Methods of Operations Research* (1951) with G. K. Kimball as well as *Queues, Inventories and Maintenance* (1958) and *Library Effectiveness: A Systems Approach* (1968).

His other notable contributions included: cofounder of the MIT Acoustics Laboratory, first Director of the Brookhaven National Laboratory, founder and first Director the MIT Computation Center, author of *Thermal Physics* (1961) and Chairman of the advisory committee that supervised the preparation of the extremely influential *Handbook of Mathematical Functions* (1964) (a.k.a. Abramowitz and Stegun). He also served as President of the American Physical Society and the Acoustical Society of America as well as the board chair of the American Institute of Physics. He died in Concord, Massachusetts, aged 82.

9.7.2 Herman Feshbach

Herman Feshbach (1917-2000), who was known as one of the world's preeminent nuclear physicists, was born in New York City and graduated from the City College of New York in 1937 with an S.B. in physics [91]. He then went on to receive his Ph.D. in physics from MIT in 1942 for a thesis relating the properties of tritium to nuclear forces written under the supervision of Philip M. Morse. He was invited to stay at MIT after he received his doctorate and he remained on the physics faculty for more than 50 years. During this time, he served as Director of MIT's Center for Theoretical Physics (1967-1973) and Chairman of the Physics Department (1973-1983). His early papers were concerned with acoustic and electromagnetic scattering. His most widely known contribution to physics is the concept known as "Feshbach resonance" in quantum mechanics.

In addition to coauthoring the monumental *Methods of Theoretical Physics* (1953) with Morse, he also coauthored *Theoretical Nuclear Physics* (1974) with Amos de Shalit which is one of the classics in that field and wrote the sequel *Theoretical Nuclear Physics: Nuclear Reactions* (1992). Feshbach succeeded Morse as Chief Editor of *Annals of Physics* which they cofounded in 1957 as a reaction to what they viewed as the fragmentation of physics. He served as President of the American Physical Society (1980-1981) and the American Academy of Arts and Sciences (1982-1986). He was a member of the National Academy of Sciences (1969) and he was awarded the National Medal of Science (1986). He died of heart failure in Cambridge, Massachusetts, aged 83.

Chapter 10

Epilogue

The study of the eigenstructure of the equilateral triangle began with Lamé's pioneering paper of 1833 [39] and was further developed in his treatises on heat transfer [40] and elasticity [41]. Despite the fact that no further substantial progress was made on this problem until Pockels' treatise of 1891 [75], Grattan-Guinness [24, p. 1173] has severely criticized Lamé's extensive reliance on trigonometric functions. What he fails to recognize is that this direct trigonometric assault provides the most straightforward and elementary resolution of this important scientific problem available in the literature.

For example, the self-proclaimed elementary solution by Pinsky [73, 74] using reflection operators is opaque by comparison. (Incidentally, Cureton and Kuttler [14, p. 89] point out the misleading nature of Pinsky's expression for the eigenvalues while Helffer and Hoffmann-Ostenhof [33, p. 12] remark upon Pinsky's incorrect expression for the Dirichlet eigenfunctions.) Even more transparent approaches based upon harmonic analysis [27, pp. 107-109], group theory [5] and Lie groups [72] cannot compare with the simplicity and accessibility of Lamé's approach.

The only other truly elementary approach to the eigenstructure of the equilateral triangle has been provided by Práger [77] where he introduced the triangle-to-rectangle transformation. However, this approach is just as heavily dependent upon trigonometric expressions as is Lamé's. Moreover, unlike Lamé's analysis, the extensive reliance of Práger's analysis upon symmetry properties of the Laplacian renders it inapplicable to the practically most important case: the Robin problem. In addition, Lamé's analysis has been extended to the case of the basic elliptic equations on an equilateral triangle under a variety of nonhomogeneous boundary conditions [16].

In the foregoing, we have filled a prominent gap in the applied mathematical literature by providing a complete, direct, and elementary derivation of Lamé's formulas for the eigenfunctions of the equilateral triangle under Dirichlet and Neumann boundary conditions. In addition to its innate mathematical

interest, this problem is of practical interest as it relates to the calibration of numerical algorithms for approximating the eigenvalues of the Laplacian upon triangulated domains. Lamé's formulas have also been found useful in assessing the accuracy of the method of particular solutions for the Helmholtz equation [87].

In addition, we have established the orthonormality and completeness of this collection of eigenfunctions using the simplest of mathematical tools. The interested reader is referred to [89] where an unrelated orthogonal piecewise-polynomial basis is constructed for an arbitrary triangle. Furthermore, we have made an extensive investigation of the properties, especially the nodal/antinodal lines, of these modes. Also, the Green's function and Neumann function have been specified and related structures have been considered. The former have been applied to the reconstruction problem for elliptic voids [83].

An exhaustive classification of those polygonal domains possessing either a complete or a partial set of trigonometric eigenfunctions has been provided. These results were then extended to the case of a mixture of Dirichlet and Neumann boundary conditions. A gap in the engineering literature pertaining to modal degeneracy in equilateral triangular waveguides has also been filled.

Included was a complete elementary derivation of the extension of Lamé's formulas for the eigenfunctions of the equilateral triangle to Robin boundary conditions: the radiation, absorbing and impedance boundary conditions. The latter was preceded by an exhaustive exploration of the eigenstructure of the Sturm-Liouville boundary value problem with an impedance boundary condition. In addition, we have established the (bi)orthonormality and completeness of this collection of eigenfunctions using the simplest of mathematical tools. Furthermore, we have made an extensive investigation of the properties of the spectrum and modes. Also, the Robin function has been specified. The reader is invited to compare the simplicity of the present approach with that of Shanin [86] where functional equations of the Malyuzhenets type are employed.

Observe that the above described development for the Robin problem is inherently dependent upon the constancy of σ. If the eigenfunctions for variable σ were trigonometric then that would imply that the corresponding eigenfunctions for the problem with Dirichlet/Neumann conditions along two sides of the triangle and a Neumann/Dirichlet condition, respectively, along the third side were also trigonometric. This would violate theorems to the contrary established in Chapters 2 & 3 [51, 52].

Both the parallel plate and equilateral triangular acoustic waveguides have been considered. Extension to related acoustic resonators is also feasible [69]. The preceding is not directly applicable to electromagnetic waveguides with an impedance boundary as this involves the vector Laplacian rather than the scalar Laplacian [7], although approximate procedures have been developed [92]. However, Lamé's formulas have been used to design a biomimetic antenna

by deforming an equilateral triangle into the shape of a bat's ear [20].

Nuclear magnetic resonance (NMR) imaging is an important tool in the oil industry for measuring oil and brine content in saturated porous rocks. Most reservoir geometries contain sharp corners and triangles have consequently been employed in order to understand the multiphase behavior of porous rocks. One of the simplest geometries allowing more than one phase to form a stable configuration is an equilateral triangle and this problem has been successfully treated with the formulas of Lamé and McCartin [19].

The Laplace-Neumann eigenfunctions developed in Chapter 3 have recently found application in approximation theory [36]. Modified Fourier series built upon this basis, unlike Fourier series, converge pointwise at all points of continuity including the boundary. Convergence is typically quadratic in the interior and linear at the boundary. Since any triangle may be mapped affinely to any other triangle [62, p. 51], such a Laplace-Neumann expansion provides a natural generalization of modified Fourier series from the interval to arbitrary triangular domains.

The culmination of this seven year research program [51, 52, 53, 54, 55, 57, 58], focused on explicating and extending Lamé's trailblazing work, was the invitation from the World Scientific and Engineering Academy and Society (WSEAS) to present a Plenary Lecture at the First American Conference on Applied Mathematics held at Harvard University in March 2008. Corresponding survey papers detailing Lamé's formulas [59] and their extensions [60] appeared in the published Proceedings. What began as an attempt to make Lamé's work accessible to undergraduates has begun to bear fruit [15, 32].

Appendix A

Eigenstructure of the Discrete Laplacian

Lamé's formulas for the eigenvalues and eigenfunctions of the continuous Laplacian on an equilateral triangle under Dirichlet and Neumann boundary conditions are herein extended to the discrete Laplacian [61].

The eigenvalues and eigenfunctions of the continuous Laplacian on an equilateral triangle under Dirichlet and Neumann boundary conditions were first presented by G. Lamé [39, 40, 41] and then further explored by F. Pockels [75]. However, Lamé did not provide a complete derivation of his formulas but rather simply stated them and then proceeded to show that they satisfied the relevant equation and associated boundary conditions. A complete elementary derivation of his formulas was presented in Chapter 2 [51] for the Dirichlet problem and in Chapter 3 [52] for the Neumann problem.

It is the express purpose of the present appendix to provide the discrete counterparts to Lamé's formulas [61]. The motivation for the approach to be taken is as follows. It is well known that, for Dirichlet and Neumann boundary conditions, the eigenvectors of the discrete Laplacian on a square are simply the restriction of the eigenfunctions of the continuous Laplacian to the discrete set of grid points [35, pp. 281-285]. The corresponding eigenvalues are then calculated by applying the discrete Laplacian operator to these eigenvectors.

This naturally suggests the conjecture that the eigenvectors of the discrete Laplacian on an equilateral triangle under Dirichlet and Neumann boundary conditions are none other than the restriction of Lamé's eigenfunctions to the discrete set of grid points. The truth of this conjecture can be established by simply applying the discrete Laplacian operator to Lamé's formulas. The corresponding expression for the discrete eigenvalues is a direct byproduct of this procedure. Straightforward Taylor series expansions then yield a relation between the discrete and continuous spectra.

Armed with the above analysis of the eigenstructure of the continuous

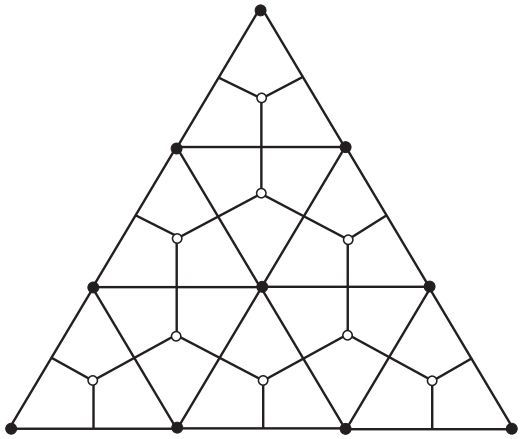

Figure A.1: Discrete Lattice

Laplacian, we now analyze the eigenstructure of the discrete Laplacian on the equilateral triangle. Specifically, we will consider the discrete triangular lattice of points denoted by solid dots in Figure A.1. We will employ the Control Region Approximation [49] to discretize the Laplacian on this lattice.

A.1 Dirichlet Problem

Consider the shaded hexagonal control region, D, surrounding the interior lattice point C in Figure A.2. and, using Equation (1.1), define

$$\phi_C = \phi(u, v, w), \tag{A.1}$$

$$\phi_E = \phi(u, v + \hat{h}\frac{\sqrt{3}}{2}, w - \hat{h}\frac{\sqrt{3}}{2}), \tag{A.2}$$

$$\phi_{NE} = \phi(u - \hat{h}\frac{\sqrt{3}}{2}, v + \hat{h}\frac{\sqrt{3}}{2}, w), \tag{A.3}$$

$$\phi_{NW} = \phi(u - \hat{h}\frac{\sqrt{3}}{2}, v, w + \hat{h}\frac{\sqrt{3}}{2}), \tag{A.4}$$

$$\phi_W = \phi(u, v - \hat{h}\frac{\sqrt{3}}{2}, w + \hat{h}\frac{\sqrt{3}}{2}), \tag{A.5}$$

$$\phi_{SW} = \phi(u + \hat{h}\frac{\sqrt{3}}{2}, v - \hat{h}\frac{\sqrt{3}}{2}, w), \tag{A.6}$$

$$\phi_{SE} = \phi(u + \hat{h}\frac{\sqrt{3}}{2}, v, w - \hat{h}\frac{\sqrt{3}}{2}), \tag{A.7}$$

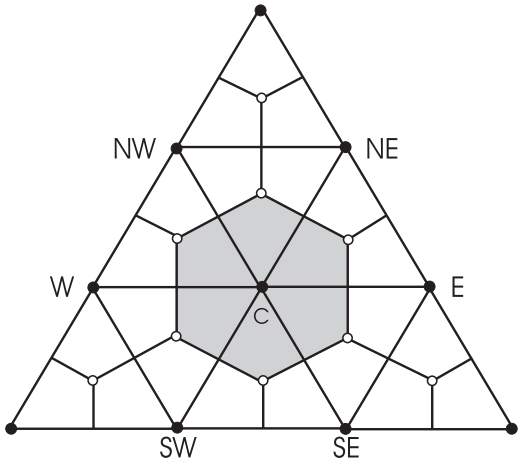

Figure A.2: Interior Control Region

where $\hat{h} := h/N$ is the edge length of the component triangles comprising the discrete lattice.

Integrating Equation (2.1) over the control region D and applying the Divergence Theorem produces

$$\oint_{\partial D} \frac{\partial \phi}{\partial \nu}\, d\sigma + k^2 \int\int_D \phi\, dA = 0, \tag{A.8}$$

where σ denotes arc length around the periphery of D.

Approximating the integrals in Equation (A.8) as described in [49] and denoting the eigenvalue of the resulting discrete operator by $\hat{k}$ yields

$$(\phi_E + \phi_{NE} + \phi_{NW} + \phi_W + \phi_{SW} + \phi_{SE} - 6\phi_C) \cdot \frac{1}{\sqrt{3}} + \hat{k}^2 \phi_C \cdot \hat{h}^2 \frac{\sqrt{3}}{2} = 0, \tag{A.9}$$

which may be rearranged as

$$\mathcal{L}[\phi] := \frac{2}{3\hat{h}^2} \cdot (\phi_E + \phi_{NE} + \phi_{NW} + \phi_W + \phi_{SW} + \phi_{SE} - 6\phi_C) = -\hat{k}^2 \phi_C. \tag{A.10}$$

Next, denote by $\vec{\phi}$ the vector obtained by evaluating either Equation (2.30) or Equation (2.31) on the discrete lattice. This vector automatically satisfies the Dirichlet boundary condition on $\partial\tau$. Applying the interior discrete operator $\mathcal{L}$, defined by Equation (A.10), to $\vec{\phi}$ and invoking appropriate trigonometric identities leads directly to

$$\hat{k}^2 = \frac{4}{3\hat{h}^2} \cdot \left\{ 3 - \cos\left[\frac{\sqrt{3}\pi\hat{h}}{9r} \cdot (m-l) \right] - \cos\left[\frac{\sqrt{3}\pi\hat{h}}{9r} \cdot (n-l) \right] - \cos\left[\frac{\sqrt{3}\pi\hat{h}}{9r} \cdot (m-n) \right] \right\}. \tag{A.11}$$

Now, applying Taylor series and the identity $l + m + n = 0$ establishes an important relationship between the Dirichlet spectra of the discrete and continuous Laplacians on the equilateral triangle:

$$\hat{k}^2_{m,n} = k^2_{m,n} - \left(\frac{\pi^2}{27r^2}\right)^2 (m^4+2m^3n+3m^2n^2+2mn^3+n^4)\cdot\hat{h}^2+O(\hat{h}^4). \quad \text{(A.12)}$$

The corresponding system of linearly independent Dirichlet eigenvectors is

$$\{\vec{\phi}^{m,n}_s \ (N \geq 3 : \ N-2 \geq n \geq 1, \ \min(n, N-1-n) \geq m \geq 1);$$
$$\vec{\phi}^{m,n}_a \ (N \geq 4 : \ N-2 \geq n \geq 2, \ \min(n-1, N-1-n) \geq m \geq 1)\}. \quad \text{(A.13)}$$

A.2 Neumann Problem

Let $\vec{\psi}$ denote the vector obtained by evaluating either Equation (3.22) or Equation (3.23) on the discrete lattice. Applying the interior discrete operator $\mathcal{L}$, defined by

$$\mathcal{L}[\psi] := \frac{2}{3\hat{h}^2}\cdot(\psi_E+\psi_{NE}+\psi_{NW}+\psi_W+\psi_{SW}+\psi_{SE}-6\psi_C) = -\hat{k}^2\psi_C, \quad \text{(A.14)}$$

to $\vec{\psi}$ and invoking appropriate trigonometric identities once again leads directly to Equation (A.11) for $\hat{k}^2$.

However, this vector does not automatically satisfy the Neumann boundary condition on $\partial\tau$. Unlike the case of the Dirichlet boundary condition, the Neumann boundary condition requires special treatment which we next provide.

Consider the shaded control regions of Figure A.3 surrounding the lattice points along the edges of τ, exclusive of the vertices. Along the bottom/right/left edges, application of the Control Region Approximation [49] yields

$$\mathcal{L}_1[\psi] := \frac{2}{3\hat{h}^2}\cdot(\psi_E+2\psi_{NE}+2\psi_{NW}+\psi_W-6\psi_C) = -\hat{k}^2\psi_C, \quad \text{(A.15)}$$

$$\mathcal{L}_2[\psi] := \frac{2}{3\hat{h}^2}\cdot(\psi_{NW}+2\psi_W+2\psi_{SW}+\psi_{SE}-6\psi_C) = -\hat{k}^2\psi_C, \quad \text{(A.16)}$$

$$\mathcal{L}_3[\psi] := \frac{2}{3\hat{h}^2}\cdot(2\psi_E+\psi_{NE}+\psi_{SW}+2\psi_{SE}-6\psi_C) = -\hat{k}^2\psi_C, \quad \text{(A.17)}$$

respectively.

However, by Corollary 4.1.1, we have the following symmetry relations along the bottom/right/left edges:

$$\psi_{SE} = \psi_{NE}; \ \psi_{SW} = \psi_{NW}, \quad \text{(A.18)}$$

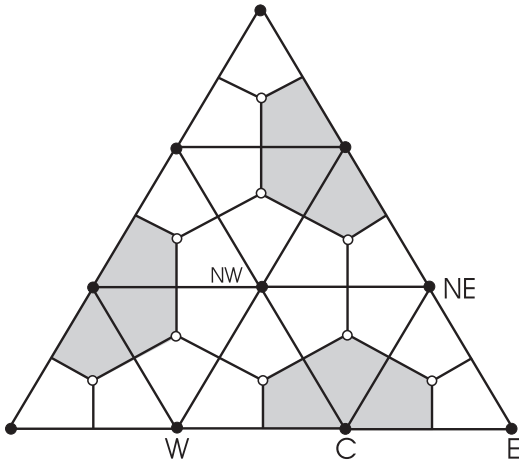

Figure A.3: Edge Control Regions

$$\psi_E = \psi_{SW};\ \psi_{NE} = \psi_W, \tag{A.19}$$

$$\psi_{NW} = \psi_E;\ \psi_W = \psi_E, \tag{A.20}$$

respectively.

Substitution of Equation (A.18/A.19/A.20) into Equation (A.14) (already known to lead to Equation (A.11) for $\hat{k}^2$) produces Equation (A.15/A.16/A.17), respectively. Thus, $\vec{\psi}$ satisfies the Neumann boundary condition along the edges of τ, exclusive of the vertices of τ.

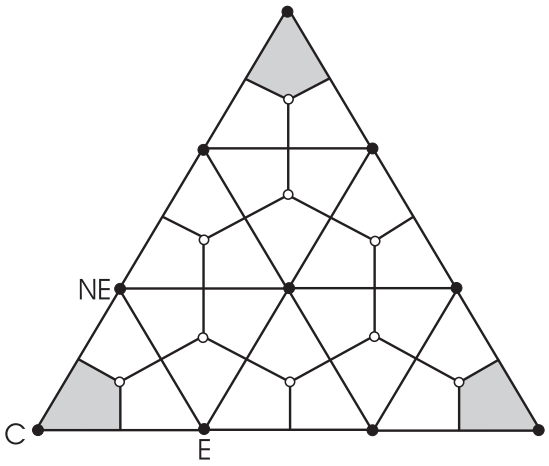

Figure A.4: Vertex Control Regions

Next, consider the shaded control regions of Figure A.4 surrounding the three lattice points at the vertices of τ. At the right/top/left vertex, applica-

tion of the Control Region Approximation [49] yields

$$\mathcal{L}_{1,2}[\psi] := \frac{2}{3\hat{h}^2} \cdot (3\psi_{NW} + 3\psi_W - 6\psi_C) = -\hat{k}^2\psi_C, \tag{A.21}$$

$$\mathcal{L}_{2,3}[\psi] := \frac{2}{3\hat{h}^2} \cdot (3\psi_{SW} + 3\psi_{SE} - 6\psi_C) = -\hat{k}^2\psi_C, \tag{A.22}$$

$$\mathcal{L}_{3,1}[\psi] := \frac{2}{3\hat{h}^2} \cdot (3\psi_E + 3\psi_{NE} - 6\psi_C) = -\hat{k}^2\psi_C, \tag{A.23}$$

respectively.

However, by Corollary 4.1.1, we have the following symmetry relations at the right/top/left vertex:

$$\psi_E = \psi_{SW} = \psi_{NW};\ \psi_{SE} = \psi_{NE} = \psi_W, \tag{A.24}$$

$$\psi_{NE} = \psi_W = \psi_{SE};\ \psi_{NW} = \psi_E = \psi_{SW}, \tag{A.25}$$

$$\psi_W = \psi_{SE} = \psi_{NE};\ \psi_{SW} = \psi_{NW} = \psi_E, \tag{A.26}$$

respectively.

Substitution of Equation (A.24/A.25/A.26) into Equation (A.14) (already known to lead to Equation (A.11) for $\hat{k}^2$) produces Equation (A.21/A.22/A.23), respectively. Thus, $\vec{\psi}$ also satisfies the Neumann boundary condition at the vertices of τ.

Hence, Equation (A.11) provides the spectrum of the discrete Laplacian under both Dirichlet and Neumann boundary conditions. Consequently, Equation (A.12) also provides the relationship between the Neumann spectra of the discrete and continuous Laplacians on the equilateral triangle.

The corresponding system of linearly independent Neumann eigenvectors is, for $N \geq 1$,

$$\begin{aligned} &\{\vec{\psi}_s^{m,n}\ (N \geq n \geq 0,\ \min(n, N-n) \geq m \geq 0); \\ &\vec{\psi}_a^{m,n}\ (\ N \geq n \geq 1,\ \min(n-1, N-n) \geq m \geq 0)\}. \end{aligned} \tag{A.27}$$

A.3 Robin Problem

In the foregoing, Lamé's formulas for the eigenvalues and eigenfunctions of the continuous Laplacian on an equilateral triangle under Dirichlet and Neumann boundary conditions [59] were extended to the discrete Laplacian. This was accomplished by establishing that the discrete eigenvectors are none other than the restriction of the continuous eigenfunctions to the discrete lattice of Figure A.1. In turn, this led directly to an explicit expression for the discrete eigenvalues and an associated relationship between them and their continuous

counterparts. The discrete problem may also be studied by prolongation from the equilateral triangle to an appropriately sized rectangle [78].

Unfortunately, these interesting results do not extend to the Robin boundary condition [60]. (Recall that the Robin boundary condition subsumes as special cases the radiation [54], the absorbing [55] and the impedance [57] boundary conditions.) It is impossible to define a discrete boundary operator with the usual stencil that is consistent with the Robin boundary condition and which leads to the same expression upon application to the restriction of the continuous eigenfunctions to the discrete lattice as that obtained by applying the discrete interior operator, $\mathcal{L}$, as was possible for the Dirichlet and Neumann boundary conditions. (Try it!)

The situation is even more acute in that the same situation obtains for even the one-dimensional Sturm-Liouville boundary value problem [56]. I.e., the device employed in the present paper works admirably for the Dirichlet and Neumann boundary conditions yet fails miserably for the Robin boundary condition. This makes it less surprising that difficulties arise in the two-dimensional boundary value problem considered in the present appendix.

A.4 Francis B. Hildebrand

Figure A.5: Francis Hildebrand

Francis Begnaud Hildebrand (1915-2002) was born and raised in Washing-

ton, PA and died in Wellesley, MA, aged 87 [85, 91]. He received his Bachelor's degree in 1936 and his Master's degree in 1938, both in Mathematics, from Washington and Jefferson College. (He received an honorary doctorate from W&J in 1969.) He then received his Ph.D. from Massachusetts Institute of Technology in 1940 for the thesis *The Solution by Polynomial Approximation of Singular Integral Equations Arising in Static Field Theory* under the supervision of Prescott Durand Crout. He was appointed to the MIT faculty the same year and stayed there for his entire 44 year career. His research focused on topics in Applied Mathematics such as the numerical solution of integral equations and the theory of elasticity. During World War II, he worked for two years at MIT's Radiation Laboratory which spearheaded the U.S. effort to develop microwave radar. He was best known for his pioneering textbooks: *Advanced Calculus for Engineers* (1948) which became *Advanced Calculus for Applications* (1964), *Methods of Applied Mathematics* (1952), and *Introduction to Numerical Analysis* (1956/1987). This trilogy helped to shape a whole generation of American Applied Mathematicians (the present author included!). His book *Finite Difference Equations and Simulations* (1968) [35] contains the relationship between the continuous and discrete spectrum of the Laplacian which was the inspiration for the present appendix. Outside of his academic life, he was an accomplished jazz musician and an enthusiast of early photography.

Bibliography

[1] W. O. Amrein, A. M. Hinz and D. B. Pearson (Editors), *Sturm-Liouville Theory: Past and Present*, Birkhäuser, Basel, 2005.

[2] T. Archibald, "Differential Equations: A Historical Overview to circa 1900" in *A History of Analysis*, H. N. Jahnke (Editor), American Mathematical Society, Providence, RI, 2003, pp. 325-353.

[3] P. Bachmann, *Die Lehre von der Kreistheilung*, B. G. Teubner, Leipzig, 1872.

[4] L. Bauer and E. L. Reiss, "Cutoff Wavenumbers and Modes of Hexagonal Waveguides", *SIAM Journal on Applied Mathematics*, Vol. 35, No. 3 (November 1978), pp. 508-514.

[5] P. H. Bérard, "Spectres et Groupes Cristallographiques I: Domaines Euclidiens", *Inventiones Mathematicae*, Vol. 58 (1980), pp. 179-199.

[6] G. Birkhoff, *A Source Book in Classical Analysis*, Harvard University Press, Cambridge, MA, 1973.

[7] F. E. Borgnis and C. H. Papas, "Electromagnetic Waveguides and Resonators", *Handbuch der Physik, Vol. XVI* (S. Flügge, Ed.), Springer-Verlag, Berlin, 1958, pp. 285-422.

[8] C. B. Boyer, *A History of Mathematics*, Wiley, New York, NY, 1968.

[9] E. A. Coddington and N. Levinson, *Theory of Ordinary Differential Equations*, McGraw-Hill, New York, NY, 1955.

[10] J. H. Conway and R. K. Guy, *The Book of Numbers*, Copernicus, New York, NY, 1996.

[11] R. Courant and D. Hilbert, *Methods of Mathematical Physics, Volume I*, Wiley-Interscience, New York, NY, 1953.

[12] R. Courant and D. Hilbert, *Methods of Mathematical Physics, Volume II*, Wiley-Interscience, New York, NY, 1962.

[13] S. H. Crandall and W.-Q. Zhu, "Wide Band Random Vibration of an Equilateral Triangular Plate", *Probabilistic Engineering Mechanics*, Vol. 1, No. 1 (1986), pp. 5-12.

[14] L. M. Cureton and J. R. Kuttler, "Eigenvalues of the Laplacian on Regular Polygons and Polygons Resulting from Their Dissection", *Journal of Sound and Vibration*, Vol. 220, No. 1 (1999), pp. 83-98.

[15] A. Damle and G. C. Peterson, "Understanding the Eigenstructure of Various Triangles", *SIAM Undergraduate Research Online*, Volume 3, Issue 1, `http://www.siam.org/students/siuro/vol3/S01061.pdf`, September 29, 2010, pp. 187-208.

[16] G. Dassios and A. S. Fokas, "The Basic Elliptic Equations in an Equilateral Triangle", *Royal Society of London, Series A*, Vol. 461, No. 2061 (2005), pp. 2721-2748.

[17] L. E. Dickson, *History of the Theory of Numbers, Volumes II-III*, Chelsea, New York, NY, 1952.

[18] G. F. Duff, *Partial Differential Equations*, University of Toronto Press, Toronto, 1956.

[19] J. Finjord, A. Hiorth, U. H. a Lad and S. M. Skjaeveland, "NMR for equilateral triangular geometry under conditions of surface relaxivity - analytical and random walk solution", *Transport in Porous Media*, Vol. 69, (2006), pp. 33-53.

[20] J. A. Flint, "A Biomimetic Antenna in the Shape of a Bat's Ear", *IEEE Antennas and Wireless Propagation Letters*, Vol. 5, Issue 1 (Dec. 2006), pp. 145-147.

[21] J. Fourier, *The Analytical Theory of Heat*, Dover, Mineola, NY, 1955.

[22] K. O. Friedrichs, *Perturbation of Spectra in Hilbert Space*, American Mathematical Society, Providence, RI, 1965.

[23] C. C. Gillispie, *Biographical Dictionary of Mathematicians, Volumes 1-4*, Charles Scribners' Sons, New York, NY, 1970-1991.

[24] I. Grattan-Guinness, *Convolutions in French Mathematics, 1800-1840*, Birkhäuser Verlag, Basel, 1990.

[25] J. Gray, *Möbius's Geometrical Mechanics*, Möbius and His Band, J. Fauvel et al. (eds.), Oxford University Press, New York, NY, 1993.

[26] B. Grünbaum and G. C. Shephard, *Tilings and Patterns*, W. H. Freeman and Co., New York, NY, 1987.

[27] D. Gurarie, *Symmetries and Laplacians: Introduction to Harmonic Analysis, Group Representations and Applications*, Dover, Mineola, NY, 2008.

[28] K. Gustafson and T. Abe, "The Third Boundary Condition - Was it Robin's?", *The Mathematical Intelligencer*, Vol. 20, No. 1 (1998), pp. 63-71.

[29] K. Gustafson and T. Abe, "(Victor) Gustave Robin: 1855-1897", *The Mathematical Intelligencer*, Vol. 20, No. 2 (1998), pp. 47-53.

[30] R. W. Hamming, *Digital Filters*, Second Edition, Prentice-Hall, Englewood Cliffs, NJ, 1983.

[31] G. H. Hardy and E. M. Wright, *An Introduction to the Theory of Numbers*, 3rd Edition, Oxford University Press, London, 1954.

[32] E. Healy, *Can One Hear the Shape of a Drum?*, University of Durham, `http://maths.dur.ac.uk/Ug/projects/library/PR4/0910/PR4_EmmaHealy.pdf`, April 29, 2010.

[33] B. Helffer and T. Hoffmann-Ostenhof, "Remarks on Two Notions of Spectral Minimal Partitions", *The Erwin Schrrödinger International Institute for Theoretical Physics*, ESI Preprint, No. 2194 (2009), November 11, 2009.

[34] D. J. Higham and N. J. Higham, *MATLAB Guide*, Society for Industrial and Applied Mathematics, Philadelphia, PA, 2000.

[35] F. B. Hildebrand, *Finite-Difference Equations and Simulations*, Prentice-Hall, Englewood Cliffs, NJ, 1968.

[36] D. Huybrechs, A. Iserles and S. Nørsett, "From High Oscillation to Rapid Approximation V: The Equilateral Triangle", *Cambridge Numerical Analysis Reports*, NA2009/04 (November 30, 2009).

[37] D. S. Jones, *Acoustic and Electromagnetic Waves*, Clarendon, Oxford, 1986.

[38] J. B. Keller, "The Scope of the Image Method", *Communications on Pure and Applied Mathematics*, Vol. VI, (1953), pp. 505-512.

[39] G. Lamé, "Mémoire sur la propagation de la chaleur dans les polyèdres", *Journal de l'École Polytechnique*, Vol. 22 (1833), pp. 194-251.

[40] G. Lamé, *Leçons sur la Théorie Analytique de la Chaleur*, Mallet-Bachelier, Paris, 1861.

[41] G. Lamé, *Leçons sur la Théorie Mathématique de l'Élasticité des Corps Solides*, Deuxième Édition, Gauthier-Villars, Paris, 1866.

[42] S. S. Lee and S. H. Crandall, "The Eigenmodes of an Equilateral Triangle", *Mélanges Offert à Th. Vogel*, B. Rybak, P. Janssens and M. Jessel (Editors), Université libre de Bruxelles, Bruxelles, 1978, pp. 255-268.

[43] J. Lützen, *Joseph Liouville (1809-1882), Master of Pure and Applied Mathematics*, Springer-Verlag, New York, NY, 1990.

[44] C. R. MacCluer, *Boundary Value Problems and Orthogonal Expansions: Physical Problems from a Sobolev Viewpoint*, IEEE Press, New York, NY, 1994.

[45] S. F. Mahmoud, *Electromagnetic Waveguides: Theory and Applications*, Peter Peregrinus Ltd., London, UK,1991.

[46] E. Makai, "Complete Orthogonal Systems of Eigenfunctions of Three Triangular Membranes", *Studia Scientiarum Mathematicarum Hungarica*, Vol. 5 (1970), pp. 51-62.

[47] J. C. Maxwell, *A Treatise on Electricity and Magnetism, Volume One*, Third Edition, Dover, New York, NY, 1954(1891).

[48] B. J. McCartin, "A Perturbation Procedure for Nearly Rectangular, Homogeneously Filled, Cylindrical Waveguides", *IEEE Microwave and Guided Wave Letters*, Vol. 6, pp. 354-356, (1996).

[49] B. J. McCartin, "Seven Deadly Sins of Numerical Computation", *American Mathematical Monthly*, 105 (10) (1998), 929-941.

[50] B. J. McCartin, "Modal Degeneracy in Square Waveguides", *Journal of the Acoustical Society of America*, Vol. 111, No. 1, Pt. 1, (Jan. 2002), pp. 49-52.

[51] B. J. McCartin, "Eigenstructure of the Equilateral Triangle, Part I: The Dirichlet Problem", *SIAM Review*, Vol. 45, No.2 (2003), pp. 267-287.

[52] B. J. McCartin, "Eigenstructure of the Equilateral Triangle, Part II: The Neumann Problem", *Mathematical Problems in Engineering*, Vol. 8, No.6 (2002), pp. 517-539.

[53] B. J. McCartin, "Modal Degeneracy in Equilateral Triangular Waveguides", *Journal of Electromagnetic Waves and Applications*, Vol. 16, No. 7 (2002), pp. 943-956.

[54] B. J. McCartin, "Eigenstructure of the Equilateral Triangle, Part III: The Robin Problem", *International Journal of Mathematics and Mathematical Sciences*, Vol. 2004, No. 16 (16 March 2004), pp. 807-825.

[55] B. J. McCartin, "Eigenstructure of the Equilateral Triangle, Part IV: The Absorbing Boundary Condition", *International Journal of Pure and Applied Mathematics*, Vol. 37, No. 3 (2007), pp. 395-422.

[56] B. J. McCartin, "On the Eigenstructure of a Sturm-Liouville Problem with an Impedance Boundary Condition", *Global Journal of Pure and Applied Mathematics*, Vol. 3, No. 1 (2007), pp. 63-82.

[57] B. J. McCartin, "Eigenstructure of the Equilateral Triangle, Part V: The Impedance Boundary Condition", *Applied Mathematical Sciences*, Vol. 2, 2008, no. 44, pp. 2187-2217.

[58] B. J. McCartin, "On Polygonal Domains with Trigonometric Eigenfunctions of the Laplacian under Dirichlet or Neumann Boundary Conditions", *Applied Mathematical Sciences*, Vol. 2, 2008, no. 58, pp. 2891-2901.

[59] B. J. McCartin, "Spectral Structure of the Equilateral Triangle I: Lamé's Formulas", *Recent Advances in Applied Mathematics (Proceedings of the American Conference on Applied Mathematics)*, WSEAS, 2008, pp. 195-200.

[60] B. J. McCartin, "Spectral Structure of the Equilateral Triangle II: Beyond Lamé's Formulas", *Recent Advances in Applied Mathematics (Proceedings of the American Conference on Applied Mathematics)*, WSEAS, 2008, pp. 201-208.

[61] B. J. McCartin, "Eigenstructure of the Discrete Laplacian on the Equilateral Triangle: The Dirichlet & Neumann Problems", *Applied Mathematical Sciences*, Vol. 4, 2010, no. 53, pp. 2633-2646.

[62] B. J. McCartin, *Mysteries of the Equilateral Triangle*, Hikari, 2010.

[63] B. J. McCartin, *Lore & Lure of the Laplacian*, Hikari, 2012.

[64] C. B. Moler, *Numerical Computing with MATLAB*, Society for Industrial and Applied Mathematics, Philadelphia, PA, 2004.

[65] P. M. Morse, *In at the Beginnings: A Physicist's Life*, MIT Press, Cambridge, MA, 1977.

[66] P. M. Morse, *Vibration and Sound*, Acoustical Society of America, Melville, NY, 1976.

[67] P. M. Morse and H. Feshbach, *Methods of Theoretical Physics, Part I*, McGraw-Hill, New York, NY, 1953.

[68] P. M. Morse and H. Feshbach, *Methods of Theoretical Physics, Part II*, McGraw-Hill, New York, NY, 1953.

[69] P. M. Morse and K. U. Ingard, "Linear Acoustic Theory", *Handbuch der Physik, Vol. XI/1, Acoustics I*, S. Flügge (ed.), Springer-Verlag, 1961.

[70] P. M. Morse and K. U. Ingard, *Theoretical Acoustics*, McGraw-Hill, New York, NY, 1968.

[71] J. J. O'Connor and E. F. Robertson, *The MacTutor History of Mathematics*, `http://www-history.mcs.st-andrews.ac.uk/Biographies/`, 2010.

[72] J. Patera and A. Zaratsyan, "Discrete and Continuous Sine Transform Generalized to Semisimple Lie Groups of Rank Two", *Journal of Mathematical Physics*, Vol. 47, No. 4 (2006), 043512, 22 pages.

[73] M. A. Pinsky, "The Eigenvalues of an Equilateral Triangle", *SIAM Journal on Mathematical Analysis*, Vol. 11, No. 5 (1980), pp. 819-827.

[74] M. A. Pinsky, "Completeness of the Eigenfunctions of the Equilateral Triangle", *SIAM Journal on Mathematical Analysis*, Vol. 16, No. 4 (1985), pp. 848-851.

[75] F. Pockels, *Über die partielle Differentialgleichung* $\Delta u + k^2 u = 0$, B. G. Teubner, Leipzig, 1891.

[76] G. Pólya, "A Note on the Principal Frequency of a Triangular Membrane", *Quarterly of Applied Mathematics*, Vol. VIII, No. 4 (1951), p. 386.

[77] M. Práger, "Eigenvalues and Eigenfunctions of the Laplace Operator on an Equilateral Triangle", *Applications of Mathematics*, Vol. 43, No. 4 (1998), pp. 311-320.

[78] M. Práger, "Eigenvalues and Eigenfunctions of the Laplace Operator on an Equilateral Triangle for the Discrete Case", *Applications of Mathematics*, Vol. 46, No. 3 (2001), pp. 231-239.

[79] Lord Rayleigh, *The Theory of Sound*, Second Edition, Dover, Mineola, NY, 1877(1894).

[80] C. Reid, *Courant*, Springer-Verlag, New York, NY, 1996.

[81] C. Reid, *Hilbert*, Springer-Verlag, New York, NY, 1996.

[82] G. F. Roach, *Green's Functions*, 2nd Edition, Cambridge University Press, London, 1982.

[83] A. Scalia and M. A. Sumbatyan, "Green's Function Technique and Global Optimization in Reconstruction of Elliptic Objects in the Regular Triangle", *Applied Mathematics*, Vol. 2 (2011), pp. 294-302.

[84] S. A. Schelkunoff, *Electromagnetic Waves*, Van Nostrand, Princeton, NJ, 1943.

[85] J. Segel (Editor), *Recountings: Conversations with MIT Mathematicians*, A K Peters, Natick, MA, 2009.

[86] A. V. Shanin, "Excitation of a Wave Field in a Triangular Domain with Impedance Boundary Conditions", *Journal of Mathematical Sciences*, Vol. 102, No. 4 (2000), pp. 4328-4338.

[87] G. E. Sneddon and W. W. Read, "The Method of Particular Solutions for the Helmholtz Equation", *ANZIAM Journal*, 46 (E) (2005), pp. C544-C557.

[88] W. A. Strauss, *Partial Differential Equations: An Introduction*, Wiley, New York, NY, 1992.

[89] J. Sun, "Orthogonal Piecewise-Polynomial Basis on an Arbitrary Domain and Its Applications", *Journal of Computational Mathematics*, Vol. 19, No. 1 (2001), pp. 55-66.

[90] M. D. Waller, *Chladni Figures: A Study in Symmetry*, G. Bell and Sons, London, 1961.

[91] Wikipedia, *The Free Encyclopedia*, `http://en.wikipedia.org/wiki/`, 2010.

[92] G. M. Wysin, "Electromagnetic Modes in Dielectric Equilateral Triangle Resonators", *J. Optical Society of America B*, Vol. 23, No. 8 (2006), pp. 1586-1599.

[93] A. Zettl, *Sturm-Liouville Theory*, American Mathematical Society, Providence, RI, 2005.

Index